REMOTE SENSING OF ALPINE FOREST STRUCTURAL ATTRIBUTES

Dissertation
zur
Erlangung der naturwissenschaftlichen Doktorwürde
(Dr. sc. nat.)
vorgelegt der
Mathematisch-naturwissenschaftlichen Fakultät
der
Universität Zürich

von
Parviz Fatehi
aus
Iran

Promotionskomitee
Prof. Dr. Michael E. Schaepman (Vorsitz)
Dr. Mathias Kneubühler (Leitung der Dissertation)

Zürich, 2016

Mathematisch-naturwissenschaftliche Fakultät
der Universität Zürich

Dissertation
Remote Sensing of Alpine Forest Structural Attributes

Author:
Parviz Fatehi

Remote Sensing Laboratories
Department of Geography
University of Zurich

Winterthurerstrasse 190
CH-8057 Zurich
Switzerland
http://www.geo.uzh.ch/en/units/rsl/

Abstract

Forests play a crucial role in many aspects such as the conservation of biodiversity, wood and non-wood supply, soil protection, water balance, wildlife habitat, climate change studies, and the global carbon cycle. Accordingly, forests require comprehensive assessments for their reliable utilization, management and protection at various spatial scales ranging from the individual tree level to the global scale. For this purpose, the structure and function, which both are used to characterize a forest ecosystem, are investigated. Remote Sensing (RS) imagery, obtained from either active or passive systems, provides a fundamental opportunity to quantify, map, and monitor forest ecosystems. This thesis focuses on obtaining forest attributes from RS data. Different approaches coupled with different types of RS data are employed to map ecosystem properties and estimate forest attributes over a complex landscape with a structurally heterogeneous forested area.

The performance of two methods, i.e., a discrete and a continuous field (CF) mapping approach to map vegetation (i.e., grassland and forest) aboveground biomass (AGB) was tested. To achieve this, Airborne Prism Experiment (APEX) data and in-situ measurements were acquired over the Swiss National Park (SNP). The proposed CF mapping approach showed a reasonable accuracy in estimating vegetation AGB due to its capability to involve sub-pixel information and hence outperformed the discrete approach. This thesis investigates the capability of imaging stereoscopy (IS) data to empirically predict and map forest structural attributes such as canopy closure, basal area, and timber volume in a mixed and multi-layered forest. Findings reveal a strong relationship between canopy closure and APEX derived metrics. In addition, findings show promising results to estimate basal area and timber volume as well. Furthermore, in this thesis we implemented a methodology to estimate the most challenging forest structural attribute, i.e., tree density (TD), and a forest functional attribute, i.e., forest productivity based on an integration of Airborne Laser Scanning (ALS) and IS data. The results show a large underestimation of ALS derived TD for small trees. Larger trees were predicted with higher accuracy. Beside faced limitations in predicting TD, this thesis concludes that the combined application of ALS and IS data offers an efficient alternative to provide relevant information to gain understanding on

dependencies between structural and functional attributes at plot and landscape scales in a protected area.

Zusammenfassung

Wälder spielen in vielen Bereichen eine entscheidende Rolle, unter anderem zum Schutz der Biodiversität, der Versorgung mit Holz- und nichthölzernen Produkten, im Bereich des Bodenschutzes und des Wasserhaushaltes, als Lebensraum für Wildtiere, und nicht zuletzt für Studien zum Klimawandel und dem globalen Kohlenstoffkreislauf. Folglich ist es notwendig, Wälder sowohl hinsichtlich ihrer Nutzbarkeit und Bewirtschaftung als auch im Hinblick auf ihren Schutz zu beurteilen. Diese Beurteilung muss hierbei auf unterschiedlichen räumlichen Skalen, vom Einzelbaum bis auf globale Ebene, durchgeführt werden. Zu diesem Zweck werden sowohl die Struktur als auch die Funktion von Wäldern untersucht, da sie für eine Charakterisierung von Waldökosystemen häufig verwendet werden. Fernerkundungsbilder von aktiven als auch passiven Fernerkundungssystemen bieten in diesem Zusammenhang eine einzigartige Möglichkeit für die Quantifizierung, Kartierung und Überwachung von Waldökosystemen. Die vorliegende Arbeit widmet sich der Erfassung von Waldeigenschaften mittels Fernerkundungsdaten. Verschiedene Methoden werden mit unterschiedlichen Fernerkundungsdaten kombiniert, um Waldeigenschaften in einer sehr komplexen Landschaftstopographie mit heterogenen Waldstrukturen abzuleiten und zu kartieren.

Zuerst wird auf die Qualität zweier Kartierungsmethoden zur Schätzung der oberirdischen Vegetation-Biomasse (OVB) von Grasland und Wald eingegangen: der diskreten und der *continuous field* (CF) Methode. Für diesen Zweck wurden Bilddaten des abbildenden Spektrometers APEX (Airborne Prism Experiment) und entsprechende Referenzmessungen im Schweizer Nationalpark (SNP) erhoben. Im Gegensatz zur diskreten Methode konnten hierbei mit der CF-Methode durch die Nutzung der Sub-Pixel Informationen gute Ergebnisse bei der Schätzung der OVB erzielt werden. Zudem wird die Eignung von abbildender Spektropskopie zur empirischen Schätzung und Kartierung von Waldstruktureigenschaften, wie z.B. Kronenschluss, Bestandesgrundfläche und Holzvolumen in einem mehrschichtigen Mischwald untersucht. Es wurde sowohl ein starker Zusammenhang zwischen Kronenschluss und den von APEX-Daten abgeleiteten Maßen nachgewiesen, als auch vielversprechende Ergebnisse für die Schätzung der Bestandsgrundfläche und des Holzvolumens erzielt. Darüber hinaus wird in dieser Arbeit eine Methodik basierend

auf der Kombination von flugzeuggestützten Laser-Scanning (ALS) und abbildenden Spektroskopie Daten zur Schätzung einer strukturellen und einer funktionalen Waldeigenschaft vorgestellt. Diese Eigenschaften umfassen die Baumdichte (BD), die am schwierigsten zu bestimmende Waldstruktureigenschaft, und die Produktivität des Waldes. Die Ergebnisse zeigen eine grosse Unterschätzung der ALS basierten BD für kleine Bäume. Die BD in Beständen mit grösseren Bäumen konnte jedoch mit höherer Genauigkeit bestimmt werden. Trotz der Einschränkungen bei der Schätzung der BD lässt sich aus den Ergebnissen schliessen, dass die kombinierte Anwendung von ALS und abbildenden Spektroskopie Daten eine Alternative bei der Generierung von relevanten Informationen für das Verständnis von klein- und grossräumlichen Abhängigkeiten zwischen strukturellen und funktionalen Waldeigenschaften darstellt.

Table of contents

List of Abbreviations

AGB	Aboveground Biomass
APAR	Absorbed Photosynthetically Active Radiation
ALS	Airborne Laser Scanning
APEX	Airborne Prism Experiment
AVIRIS	Airborne Visible/Infrared Imaging Sensor
AUC	Area Under Curve
ABA	Area-based Approach
ATCOR	Atmospheric Correction
BD	Band Depth
BA	Basal Area
BRDF	Bidirectional Reflectance Distribution Function
BEF	Biomass Expansion Factor
CC	Canopy Closure
CHM	Canopy Height Model
CF	Continuous Field
CR	Continuum Removal
DBH	Diameter at Breast Height
DGPS	Differential Global Positioning System
DEM	Digital Elevation Model
DSM	Digital Surface Model
DTM	Digital Terrain Model
EO	Earth Observation
EVI	Enhanced Vegetation Index
ENVI	Environment for Visualizing Images
FAO	Food and Agriculture Organization
FP	Forest Productivity
GIS	Geographical Information System
GPP	Gross Primary Production
HCRF	Hemispherical Conical Reflectance Factor
IS	Imaging Spectroscopy
ITD	Individual Tree Detection
IUCN	International Union for the Conservation of Nature
LCT	Land Cover Type
LAI	Leaf Area Index
LOOCV	Leave-one-out Cross Validation
LSM	Linear Spectral Mixture
LM	Local Maxima
LUT	Look-up Table

MS	Multispectral
MODIS	Moderate Resolution Imaging Spectroradiometer
NIR	Near Infrared
NBDI	Normalized Band Depth Index
BDR	Band Depth Ratio
NDVI	Normalized Difference Vegetation Index
PARGE	Parametric Geocoding
PVI	Perpendicular Vegetation Index
RTM	Radiative Transfer Model
REP	Red-edge Position
rRMSE	Relative Root Mean Square Error
RS	Remote Sensing
RMSE	Root Mean Square Error
SAVI2	Second Soil-Adjusted Vegetation Index
SWIR	Shortwave Infrared
SNR	Signal to Noise Ratio
SR	Simple Ratio
SD	Standard Deviation
SNP	Swiss National Park
SAR	Synthetic Aperture Radar
3D	Three-dimensional
TD	Tree Density
VIF	Variance Inflation Factor
URPP-GCB	University Research Priority Programme Global Change and Biodiversity
VI	Vegetation Index
Visible	VIS
WD	Wood Density

1

Introduction

1.1 Background

"We can look forward to the translations of these capabilities of space vehicles and associated remote sensors into a variety of applications programs."

— E. M. Riseley, 1967

The Food and Agriculture Organization of the United Nations (FAO) reported that forests cover 31 percent of terrestrial ecosystems [1], which contain 45% of the word's terrestrial carbon [2]. Forests contribute to the economic development of many countries. It is estimated that approximately 410 million people are directly dependent on forests for subsistence and income, and that 1.6 billion people rely on forest goods and services for some part of their livelihood [3]. In addition, forests play a crucial role in many aspects such as the conservation of biodiversity [4], [5], wood and non-wood supply [6], soil protection [7], [8], water balance [9], [10], wildlife habitat [11], [12], climate change studies [13], and the global carbon cycle [14]–[16]. Accordingly, forests require comprehensive assessments for their reliable utilization, management and protection at various spatial scales ranging from the individual tree level to the global scale [1], [17]. In response to this need, forest resources have been managed by foresters for a long time and have received a great deal of attention not only from forest communities but also from the public. Sustainable forest management aims to reconcile the economic, ecological, social and cultural functions of forests with the preservation of their structural and ecological characteristics for the benefit of current and future generations [6], [18].

Forest inventories have been used in order to capture forest characteristics and follow their developments. These support activities at both the operational level (i.e., harvest planning, road layout, and regeneration treatment) and the strategic level (i.e., provide data for long term forest management plans and support a multitude of decisions relevant to forest protection and wildlife management) [19]. The traditional way to implement forest inventory is based on field sample plots. Field measurements fail to allow wall-to-wall mapping of forest attributes. The combination of field inventories and remote sensing (RS) data, e.g., satellite, airborne, or terrestrial laser scanning data, provides a possibility to scale up the field data to generate spatial maps of parameters of interest at regional or national scale and can make field-based inventories more efficient

[20]. Beside the advances in image processing approaches, the widespread availability of RS data made it relatively possible to a huge number of users to employ such data to address their issue [21]. In forest studies, RS data have been proven effective to characterize homogenous forest ecosystems.

This thesis focuses on obtaining forest attributes from RS data. Different approaches coupled with different types of RS data are tested to map landscape and forest attributes of a complex landscape with a structurally heterogeneous forested area, which was selected as study area.

The introduction section gives a general overview on the importance of forests and forest management. Forest structure definition and the approaches to obtain forest structural information are addressed in section 1.2. Two conceptual methods to map ecosystem attributes are presented in section 1.3. The following section (1.4) specifies the objectives and research questions. Finally, section 1.5 provides the structure of the thesis.

1.2 Different approaches to forest structure characterization

Forest ecosystems are complex, diverse, and dynamic. In general, three components – composition, function, and structure – are used to characterize a forest ecosystem [22]. Composition is expressed as the number of species (species diversity) or genetic diversity (i.e., how many genes and pieces of genetic information are present in a forest) [23], [24]. Forest function simply refers to what a forest does and the interaction among both biotic and a biotic forest components [25]. In general, it reflects the economical, biological, and social products of a forested area; for example, gain of carbon through photosynthesis (productivity), timber production, energy exchange with atmosphere, soil and water conservation. Forest structure indicates the spatial arrangement, vertically and horizontally, of vegetation components of a particular forested area [26].

These components are often closely correlated to each other; for example, a structural attribute, like biomass, is also an indicator of a functional attribute such as productivity [7]. Species composition and their abundance can also be an indicator of structural attributes such as canopy closure or canopy layering. Therefore, McElhinny et al. (2005) [5] suggested that to define structure in an unambiguous way, structural, functional and composition attributes can be integrated into a single category simply called forest structural attributes [5]. A wide variety of structural attributes has been used

to characterize forest structure (cf. McElhinny et al. [5] and Franklin et al. [22]). Among these, tree diameter at breast height (DBH), height, canopy closure, tree density, basal area, timber volume, and biomass, are the most commonly used by literature for determining forest structure [23], [27]–[30].

1.2.1 Traditional approach

Forest inventories can provide forest structural attributes based on field measurements [31]–[33]. Kangas et al. [34] defined an inventory as a system for measuring the extent, quantity, composition, and condition of forests. In other words, forest inventories attempt to characterize a forested area by estimating forest structural attributes [29], [35]–[37], obtaining information on forest tree species [30], [38], and more recently determining the forest functioning mechanisms [12], [39]–[41]. It is practically impossible to obtain full inventory coverage of a large area on the ground [42], therefore, forest experts measure the relevant attributes in some randomly selected sample plots (with relatively small size of e.g., 0.1 ha), which are distributed over the whole forested area. Then, the structural attributes of the entire forest are estimated by multiplying the measured values by the total forest area [43].

Although field surveys are the most accurate way to collect forest structural attributes [44]–[46], taking field measurements is time and labor intensive, and often difficult to implement for remote areas. In practice, non-observation of sample plots can usually happen due to inaccessibility [47]. In addition, field sampling is spatially restricted since it covers only a small part of a given area [48]. Furthermore, high temporal resolution sampling is challenging for larger areas (e.g. regional or national scales) [49], [50]. Consequently, many studies conclude that it is crucial to use auxiliary data to enhance the estimation of forest structural parameters and to generate spatial explicit information [32], [51], [52].

Remote sensing (RS) approaches have become a realistic way to estimate forest ecosystem attributes in recent decades [53]–[56]. RS data can provide a synoptic view of a large area at a wide range of spatial and temporal resolutions [57], which in turn, offers the opportunity to generate wall-to-wall maps of forest attributes in combination with field data [58].

1.2.2 Remote sensing approach

Remote sensing has been defined as the science of acquiring information about an object without being in contact with it [59]. Two types of RS systems are often employed, being passive and active sensors. Passive optical sensors capture the reflected or emitted electromagnetic energy from the Earth's surfaces [60]. In contrast, active systems both generate and record the energy at a given wavelength. Both passive and active systems have been widely used to predict forest structural attributes [61]. The rapid progress of RS instruments provides scientists with a great opportunity for a variety of terrestrial ecosystem applications [62]. Therefore, the need to evaluate the capability of a new generation of sensors is of critical importance [63]. This thesis investigates the use of two promising techniques i.e., imaging spectroscopy (IS) and airborne laser scanning (ALS) data to estimate forest attributes [64], [65] including accuracy assessment of the applied methods.

1.2.2.1 Imaging spectroscopy

Imaging spectrometers function as a passive sensor, being able to capture a wide range of the electromagnetic radiation coming from the Earth surface. According to Schaepman et al. [66], Imaging Spectroscopy (IS) is "the simultaneous acquisition of spatially co-registered images, in many narrow, spectrally contiguous bands between 400 nm and 2500 nm, measured in calibrated radiance units, from a remotely operated platform". Compared to multispectral (MS) data, the high capability of IS sensors to measure detailed spectral information make them a preferred choice in many fields, including forest characterization [67]. The spectral reflectance contains information related to bio-chemical and structural properties of vegetation canopy.

The estimation of vegetation properties using optical data, in general, is based on determining a link between spectral information captured by the sensor and vegetation metrics of interest. IS data have been successfully utilized for forest structural estimation [61], [68]–[71]. More research on the potential of IS data for forest characterization is necessary to prepare the remote sensing community for future, space-borne, imaging spectrometers such as EnMap [72].

Two main approaches exist in order to estimate forest structural attributes from IS data: i) physical-based approaches, and ii) empirical approaches [73]. Physical-based approaches use leaf and canopy radiative transfer models (RTM) to model canopy

reflectance [74]. The spectral variation of canopy reflectance is simulated as a function of viewing and illumination geometry, as well as canopy, leaf and soil background characteristics [72]. To estimate the forest structural and biochemical properties the canopy reflectance models need to be inverted [75]. The main advantages of physical-based approaches are their general applicability to different sites, different acquisition configurations and, importantly, the necessity of no or only a few field sample points [76]. However, RTM parameterization requires many input parameters, which are not often readily available, especially for structurally heterogeneous forests with multiple canopy layers [77]. Further, the procedure is computationally intense and is suffering from the ill-posedness of model inversion (i.e., several sets of input can generate similar spectra) [78], thus limiting its applicability for large areas [79].

Empirical approaches employ a statistical relationship between in-situ measured reference and RS data [80]. Typically, either original spectral bands or mathematical transformation of spectral bands (e.g., vegetation indices (VIs)) are defined and then linked to the variable of interest based on a fitting function [81]. Empirical approaches strongly rely on the assumption that variations in forest attributes affect the spectral reflectance of a forest and can be modeled by a parametric or a non-parametric regression [82]. Empirical approaches for forest structural estimation are commonly developed using *in-situ* measured reference data at stand, plot, or individual tree level (e.g., canopy closure, timber volume, basal area, biomass). These reference data, also called dependent variables, are afterwards combined with spectral bands or VIs data (i.e., independent variables) to derive empirical models that finally allow estimating forest structural attributes for the entire study area [80].

Forest structural variables have been successfully retrieved from IS data by i) considering original spectral bands, ii) computing all possible two-band combinations of e.g., normalized difference vegetation indices (NDVI) type [83], [84], iii) narrow simple ratio (SR) vegetation indices [69], [85], [86], iv) narrow-band normalized difference water indices (NDWI) [87], v) red-edge position (REP) analysis, or vi) band depth analysis [46], [88],. Due to their ease of implementation and efficiency, empirical approaches based on VIs are by far the most common and largest group of forest structural attributes estimation methods [81], [89]–[91]. However, the empirical approaches have to be developed based on extensive field work to collect *in-situ* data [73], [92]. Another drawback of these approaches is the non-transferability of results from one area to another [84], [93], [94].

1.2.2.2 Airborne laser scanning

Airborne Laser Scanning (ALS) is an active remote sensing technology that emits pulses of laser energy towards the Earth surface [95] and measures the distance from the sensor to the target, based on the two-way return time of emitted laser pulses over a region of interest [96]. The position of the sensor is precisely recorded by a differential global positioning system (DGPS). The aircraft's orientation is obtained from an inertial measurement unit (IMU) [19]. Consequently, by having the precise orientation and position of the laser, ALS can provide the three-dimensional (3D) position of points, called point cloud, from which it is possible to obtain a digital terrain model (DTM), a digital surface model (DSM), and information on the vertical and horizontal structure of forest canopies [97]. ALS systems can be categorized as either discrete return systems or full waveform systems. A discrete return system records one (e.g., first or last), two (e.g., first and last), or multi- (e.g., five) returns for each pulse [98]. In the case of a full waveform system, the returned signal is completely digitized [99]. Footprint size (i.e., small footprints with 0.2-3 m of diameter or large footprints with tens of meters of diameter) is another criteria to classify ALS systems [100]. The ALS data have been extensively used as a promising source to model forest structural attributes [70], [101]

Approaches to model forest structural attributes from ALS are typically grouped into two categories: i) area-based approach (ABA) and ii) individual tree detection (ITD) approach [102]. The ABA approach is based on developing an empirical relationship between forest structural attributes (e.g., tree height, basal area) and ALS metrics within pre-defined areas such as field plots [103]. The ABA approach is now commonly applied in operational forestry applications [104]. However, it relies on extensive *in-situ* data (i.e., for model training and validation) and is site specific [105].

The ITD approach, in general, uses either the ALS point cloud data or a canopy height model (CHM) to identify individual trees [102], [104], [106]. Afterwards, the structural attributes of forests at the individual tree scale can be estimated using allometric equations [107]. One disadvantage of this approach is that the inaccuracy of tree detection can introduce a considerable systematic error in forest structure estimation. Estimating forest structural attributes, e.g., timber volume, from ALS data using the ITD approach requires several steps [108]: first, detecting the trees, using either a CHM or point clouds, covering the area of interest (e.g., over a plot or a stand); second, linking the detected trees derived from ALS data to the known trees observed on field plots; third, fitting an empirical model (e.g., a statistical model) to regress field-measured

attributes (e.g. tree volume) against ALS metrics derived for the detected trees (e.g., maximum height, percentage of first pulses); fourth, implementing the fitted model for all detected trees within the field plots or the stand; finally, summing up the predicted volumes at tree scale in order to calculate the mean or total volume at plot or stand scale. Usually, only trees occupying the upper part of the forest canopy are correctly identified. Depending on the rate of commission error (the number of falsely detected trees) and undetected trees present in the lower part of the forest canopy (omission error), the implementation of the empirical model developed in step 3 can introduce a huge uncertainty (bias) in tree volume estimation. Furthermore, this approach requires ALS data with higher point density compared to the ABA approach. The ITD approach has not yet been widely applied in practice. Hence, there is a need to assess its capability to estimate forest structural attributes (e.g., tree density).

1.2.2.3 Vegetation and structural mapping strategy

Conceptually, two approaches, namely the *discrete* approach and *the continuous field* (CF) approach, can be used to map ecosystems based on RS data [85], [109].

The discrete approach follows Boolean logic in labeling every single pixel and represents one class only for each pixel [110]–[112]. This approach assumes that the image pixel is completely occupied by one thematic class and discrete hard boundaries are separating classes. Alpine ecosystems are characterized as a highly heterogeneous landscape. These include often a complex combination of vegetation, soil, rock and snow cover [113]. Pre-dominant land cover types (LCTs) are spatially heterogeneous within and between classes. For example, vegetation cover (i.e., forest and grassland) shows a gradient with change in elevation. It is basically a transition from dense closed forest to the treeline and finally ending up with alpine grassland. A small-scale pattern of all land-cover types such as tree, grassland, rock, soil and snow can be observed at the same time across a small change in elevation. RS data face a challenge to cope with such a high heterogeneity. The mapping of ecological components in such an environment with the presence of broad ecotones, i.e., areas of transition in which components grade into each other across complex geomorphic, edaphic, and hydrologic gradients, is challenging and difficult [114]. Hence, applying a discrete strategy in such complex landscape may not be able to realistically reflect gradients within ecosystem components [109].

The CF approach has been developed based on the fact that the changes in a natural landscape are following a gradient trend [115]. It simply assumes that pixels can contain different LCTs, and thus are a mixture of different spectral information [112],

[116]. The presence (abundance) of each ecosystem component (i.e., LCTs) is computed within each pixel. The CF mapping approach is a promising alternative for representing the spatial and temporal distribution and potential changes of terrestrial ecosystems in highly heterogeneous alpine environments.

1.3 Research context

According to Thenkabail [63], [68], IS data contain spectral information that allow accurate quantification of forest structural attributes. A majority of studies in this field have employed VIs to estimate a number of forest attributes. VIs are intended to enhance sensitivity to specific vegetation properties, while minimizing the effects of soil background, illumination and view angles, as well as atmospheric disturbance [92]. Such VIs have been traditionally developed for broad- spectral band sensors [81]. Broad-band VIs use average spectral information over a wide spectral range, leading to loss of crucial information available in specific narrow-bands [111]. Furthermore, it has been shown that broad-band VIs can suffer from saturation once a certain level of canopy cover or leaf area index (LAI) [117] is reached. Using IS data to generate narrow-band VIs can mitigate such drawbacks of broad-band VIs [117]. A number of studies have used narrow-band VIs as proxies to predict forest structural attributes. Schlerf et al. [69], for example, found a significant linear relationship between forest LAI and crown volume using a narrow-band perpendicular vegetation index (PVI) with HyMap data over highly managed and relatively homogenous Norway spruce (*Picea abies*). Cho et al. [61] selected a homogenous (in terms of in DBH, height, tree density and species) and dense beech (*Fagus sylvatica*) stand to test the relationship between reflectance factors derived from HyMap data and forest structural attributes including mean DBH, mean tree height and tree density. They reported that the new VIs, generated from contrasting spectral regions around the red-edge shoulder (756-820 nm) and the water absorption feature centered at 1200 nm (1172-1320 nm), showed higher correlation with structural variables compared with the standard vegetation indices derived from near-infrared and visible reflectance. Previous studies have mostly focused on IS data being used on managed and relatively homogenous forested areas, while this thesis concentrates on their potential for forest structural attributes estimation in a highly heterogeneous, protected alpine ecosystem, i.e., the Swiss National Park (SNP).

Canopy spectral reflectance varies with canopy structure, leaf properties, and soil background proportion [17]. This variation may result in challenges in using VIs to assess forest structural attributes. This is particularly true in an alpine environment, where vegetation complexity, spatial variability, diversity, and dynamics are at their highest level. Therefore, there is a crucial need to evaluate the potential of IS data in a complex natural environment and to develop new combinations of narrow-band VIs aiming to cope with heterogeneity, to compensate for disturbing background effects, and finally to enable improved linkage of spectral features to natural vegetation structural attributes.

In this thesis, the capacity of narrow-band VIs, continuum removal (CR) techniques and band depth analysis to retrieve vegetation biomass (forest and grassland AGB), forest canopy cover, forest basal area, forest timber volume and forest productivity are investigated. The study area is the Swiss National Park (SNP), which is a heterogeneous alpine ecosystem comprising natural forests of different coniferous tree species, with variation in their composition and abundance. The SNP has been protected since 1914 and represents an area where human impact is strictly controlled [118]. For various reasons the application of IS and ALS data to estimate structural attributes in an unmanaged and protected forest, such as in the SNP, proved to be difficult and highly challenging. Noormets et al [39] showed that unmanaged forests contain about 50% higher C stocks than managed forests. Paillet et al [119] found that tree basal area is significantly higher in an unmanaged forest. Higher structural diversity for unmanaged forests has been reported by Latifi et al. [120]. All these findings have an effect on increased heterogeneity, which in turn makes the estimation of forest structural attributes based on RS data more challenging. Promising results to predict forest structural attributes have been achieved by using IS data in relatively homogenous and monoculture forests. It is, however, recommended to investigate the applicability of IS data in natural mixed forests [61], [69].

Application of ALS data to characterize forest structural attributes has increased over the past decade [19], [107], [121], [122]. Despite the capability to directly predict tree height [123] and canopy cover [124] from ALS data, researchers face difficulties to accurately estimate tree density using ALS data [125], [126]. Tree density (TD), the number of trees per unit area, is a significant structural component of forest ecosystems. TD plays a crucial role to study forest succession dynamics [127], forest productivity [128], and to assess spatio-temporal patterns in tree mortality [129]. Therefore, TD estimation has attracted the most attention especially in non-commercial forests and protected areas, such as the SNP. The accuracy of TD estimation using either ITD or ABA approaches from ALS data varies largely among studies, ranging from 30% to 90% [130],

[131]. Tree detection approaches basically assume that each tree has a distinct boundary with no overlap between adjacent crowns [132], and tree location is identified as a point or a pixel containing the highest height value of the point cloud compared to other pixels in a specific neighborhood [133]. These assumptions hold in flat terrain, in tree plantations, and in homogenous stands in terms of species and tree size. Consequently, TD for structurally less complex forest distributed over relatively flat areas has been estimated with high accuracy [134], [135]. Pretzsch (2014) [136] indicated that mixed-species and structurally heterogeneous forests are well explored in their favorable ecological, socio-economical functions and services compared to pure forest stands, but still poorly understood in their structure and functions. Technically, there is a lack of knowledge on the capability of ALS data used to estimate TD in a natural unmanaged multi-story forested area. Consequently, we aim to combine the ALS and IS data to investigate the assessment of structural and functional properties of forested area in the SNP.

1.4 Research questions

The main objective of the present thesis is to explore the contribution of remotely sensed data to estimate and map forest structural/functional attributes in a complex natural environment. IS and ALS data were acquired in a highly protected, heterogeneous alpine environment (the Swiss National Park, previously described in Section 1.3). The following research questions are addressed:

- How can remotely sensed data capture the heterogeneity of an alpine ecosystem and what are the accuracies of retrieved ecosystem variables?
- Can forest structural attributes be estimated based on IS data in a heterogeneous, alpine forest area?
- What is the capability of ALS and IS data integration to map *structural and functional properties* in a heterogeneous, alpine forest area?

1.5 Structure of the thesis

This thesis consists of five chapters as follows:

Chapter 1 contains a general introduction and provides a definition of forest structure. This Chapter introduces the approaches to estimate and to map forest structural attributes. The research questions and the structure of thesis also are presented.

Chapter 2 is based on a first-authored peer-reviewed scientific paper (Fatehi et al., 2015) published in *IEEE Journal of Selected Topics in Applied Earth Observations and Remote Sensing*. It describes a new concept to generate continuous fields (CF) maps of grassland and forest aboveground biomass (AGB) in an alpine environment. It also discusses the potential of the CF mapping approach and compares it with a discrete approach to map grassland and forest areas. The publication is self-contained in terms of structure and content.

Chapter 3 consists of a first-authored peer-reviewed scientific paper (Fatehi et al., 2015) published in the *MDPI Remote Sensing* journal. The paper describes the capability of Imaging Spectroscopy (IS) data to map forest structural attributes such as canopy closure, basal area, and timber volume in a highly heterogonous alpine-forested area. The publication is self-contained in terms of structure and content.

Chapter 4 is based on a first-authored peer-reviewed scientific paper (Fatehi et al., 2016) submitted to *Forest ecology and management*. This Chapter describes an approach using Airborne Laser Scanning (ALS) and Imaging Spectroscopy (IS) data to quantify and assess patterns of tree density (TD) and forest productivity in the Swiss National Park (SNP). The publication is self-contained in both structure and content.

Chapter 5 summarizes and synthesizes the major findings of chapters 2-4, provides concluding remarks and an outlook to the thesis.

References

[1] FAO, “Global forest resources assessment 2010,” Rome, 2010.

[2] E. Romijn, C. B. Lantican, M. Herold, E. Lindquist, R. Ochieng, A. Wijaya, D. Murdiyarso, and L. Verchot, “Assessing change in national forest monitoring capacities of 99 tropical countries,” *For. Ecol. Manage.*, vol. 352, pp. 109–123, 2015.

[3] M. Köhl, R. Lasco, M. Cifuentes, Ö. Jonsson, K. T. Korhonen, P. Mundhenk, J. de Jesus Navar, and G. Stinson, “Changes in forest production, biomass and carbon: Results from the 2015 UN FAO Global Forest Resource Assessment,” *For. Ecol. Manage.*, vol. 352, pp. 21–34, 2015.

[4] D. Morales-Hidalgo, S. N. Oswalt, and E. Somanathan, “Status and trends in global primary forest, protected areas, and areas designated for conservation of biodiversity from the Global Forest Resources Assessment 2015,” *For. Ecol. Manage.*, vol. 352, pp. 68–77, 2015.

[5] C. McElhinny, P. Gibbons, C. Brack, and J. Bauhus, "Forest and woodland stand structural complexity: Its definition and measurement," *For. Ecol. Manage.*, vol. 218, no. 1–3, pp. 1–24, 2005.

[6] C. de Wasseige and P. Defourny, "Remote sensing of selective logging impact for tropical forest management," *For. Ecol. Manage.*, vol. 188, no. 1–3, pp. 161–173, Feb. 2004.

[7] C. Eisfelder, C. Kuenzer, and S. Dech, "Derivation of biomass information for semi-arid areas using remote-sensing data," *Int. J. Remote Sens.*, vol. 33, no. February 2015, pp. 2937–2984, 2012.

[8] S. Miura, M. Amacher, T. Hofer, J. San-Miguel-Ayanz, Ernawati, and R. Thackway, "Protective functions and ecosystem services of global forests in the past quarter-century," *For. Ecol. Manage.*, vol. 352, pp. 35–46, 2015.

[9] V. R. Kane, J. A. Lutz, C. Alina Cansler, N. A. Povak, D. J. Churchill, D. F. Smith, J. T. Kane, and M. P. North, "Water balance and topography predict fire and forest structure patterns," *For. Ecol. Manage.*, vol. 338, pp. 1–13, 2015.

[10] E. Dufrêne, H. Davi, C. François, G. Le Maire, V. Le Dantec, and A. Granier, "Modelling carbon and water cycles in a beech forest," *Ecol. Model.*, vol. 185, no. 2–4, pp. 407–436, Jul. 2005.

[11] P. Hyde, R. Dubayah, B. Peterson, J. B. Blair, M. Hofton, C. Hunsaker, R. Knox, and W. Walker, "Mapping forest structure for wildlife habitat analysis using waveform lidar: Validation of montane ecosystems," *Remote Sens. Environ.*, vol. 96, no. 3–4, pp. 427–437, Jun. 2005.

[12] T. M. Fearer, S. P. Prisley, D. F. Stauffer, and P. D. Keyser, "A method for integrating the Breeding Bird Survey and Forest Inventory and Analysis databases to evaluate forest bird-habitat relationships at multiple spatial scales," *For. Ecol. Manage.*, vol. 243, no. 1, pp. 128–143, 2007.

[13] S. A. Soenen, D. R. Peddle, C. A. Coburn, R. J. Hall, and F. G. Hall, "Canopy Reflectance Model Inversion in Multiple For ward Mode : Forest Str uctural Information Retrieval fr om Solution Set Distributions," *Photogramm. Eng. Remote Sens.*, vol. 75, no. 4, pp. 361–374, 2009.

[14] J. B. Bradford, R. a. Birdsey, L. a. Joyce, and M. G. Ryan, "Tree age, disturbance history, and carbon stocks and fluxes in subalpine Rocky Mountain forests," *Glob. Chang. Biol.*, vol. 14, no. 12, pp. 2882–2897, Dec. 2008.

[15] C. Loehle, C. Idso, and T. Bently Wigley, "Physiological and ecological factors influencing recent trends in United States forest health responses to climate change," *For. Ecol. Manage.*, vol. 363, pp. 179–189, 2016.

[16] J. S. Kimball, a. R. Keyser, S. W. Running, and S. S. Saatchi, "Regional assessment of boreal forest productivity using an ecological process model and remote sensing parameter maps," *Tree Physiol.*, vol. 20, no. 11, pp. 761–775, Jun. 2000.

[17] D. S. Boyd and F. M. Danson, "Satellite remote sensing of forest resources: three decades of research development," *Prog. Phys. Geogr.*, vol. 29, no. 1, pp. 1–26, Jan. 2005.

[18] K. G. MacDicken, P. Sola, J. E. Hall, C. Sabogal, M. Tadoum, and C. de Wasseige, "Global progress toward sustainable forest management," *For. Ecol. Manage.*, vol. 352, pp. 47–56, 2015.

[19] M. A. Wulder, C. W. Bater, N. C. Coops, T. Hilker, and J. C. White, "The role of LiDAR in sustainable forest management," *For. Chron.*, vol. 84, no. 6, pp. 807–826, 2008.

[20] C. Ginzler and M. Hobi, "Countrywide Stereo-Image Matching for Updating Digital Surface Models in the Framework of the Swiss National Forest Inventory," *Remote Sens.*, vol. 7, no. 4, pp. 4343–4370, 2015.

[21] K. S. Fassnacht, W. B. Cohen, and T. A. Spies, "Key issues in making and using satellite-based maps in ecology: A primer," *For. Ecol. Manage.*, vol. 222, no. 1–3, pp. 167–181, 2006.

[22] J. F. Franklin, D. C. Shaw, K. Bible, J. Chen, T. A. Spies, R. Van Pelt, A. B. Carey, D. A. Thornburgh, D. R. Berg, D. B. Lindenmayer, M. E. Harmon, and W. S. Keeton, "Disturbances and structural development of natural forest ecosystems with silvicultural implications, using Douglas-fir forests as an example," *For. Ecol. Manage.*, vol. 155, no. 1, pp. 399–423, 2002.

[23] A. Haywood, A. Mellor, and C. Stone, "A strategic forest inventory for public land in Victoria, Australia," *For. Ecol. Manage.*, vol. 367, pp. 86–96, 2016.

[24] J. Cavender-Bares, J. E. Meireles, J. J. Couture, M. Kaproth, C. C. Kingdon, A. Singh, S. P. Serbin, A. Center, E. Zuniga, G. Pilz, and P. A. Townsend, "Associations of leaf spectra with genetic and phylogenetic variation in oaks: prospects for remote detection of biodiversity," *Remote Sens.*, vol. 7, no. 1–x manuscripts, pp. 1–26, 2016.

[25] J. N. Stone and J. L. Porter, "What is Forest Stand Structure and How to Measure lt ? Need for Better Descriptions," *Northwest Sci.*, vol. 72, no. 2, pp. 25–26, 1998.

[26] L. Wallace, A. Lucieer, Z. Malenovský, D. Turner, and P. Vopěnka, "Assessment of Forest Structure Using Two UAV Techniques: A Comparison of Airborne Laser Scanning and Structure from Motion (SfM) Point Clouds," *Forests*, vol. 7, no. 3, p. 62, 2016.

[27] H. Latifi, "Characterizing forest structure by means of remote sensing: A review," in *Remote Sensing - Advanced Techniques and Platforms*, INTECH Open Access Publisher, 2012, pp. 3–28.

[28] K. L. O'Hara, "Multiaged forest stands for protection forests: concepts and applications," *For. Snow Landsc. Res.*, vol. 80, no. 1, pp. 45–55, 2006.

[29] K. D. Brosofske, R. E. Froese, M. J. Falkowski, and A. Banskota, "A Review of Methods for Mapping and Prediction of Inventory Attributes for Operational Forest Management," *For. Sci.*, vol. 60, no. 4, pp. 733–756, 2014.

[30] F. Zellweger, V. Braunisch, A. Baltensweiler, and K. Bollmann, "Remotely sensed forest structural complexity predicts multi species occurrence at the landscape scale," *For. Ecol. Manage.*, vol. 307, pp. 303–312, Nov. 2013.

[31] A. Van Laar and A. Akca, *Forest mensuration*. Springer Science & business Media, 2007.

[32] R. E. McRoberts, E. O. Tomppo, A. O. Finley, and J. Heikkinen, "Estimating areal means and variances of forest attributes using the k-Nearest Neighbors technique and satellite imagery," *Remote Sens. Environ.*, vol. 111, pp. 466–480, 2007.

[33] J. Hyyppä, H. Hyyppä, M. Inkinen, M. Engdahl, S. Linko, and Y.-H. Zhu, "Accuracy comparison of various remote sensing data sources in the retrieval of forest stand attributes," *For. Ecol. Manage.*, vol. 128, no. 1–2, pp. 109–120, Mar. 2000.

[34] A. Kangas and M. Maltamo, *Forest Inventory Methodology and Applications*. Springer, 2006.

[35] M. Immitzer, C. Stepper, S. Böck, C. Straub, and C. Atzberger, "Use of WorldView-2 stereo imagery and National Forest Inventory data for wall-to-wall mapping of growing stock," *For. Ecol. Manage.*, vol. 359, pp. 232–246, 2016.

[36] L. T. Waser, C. Fischer, Z. Wang, and C. Ginzler, "Wall-to-Wall Forest Mapping Based on Digital Surface Models from Image-Based Point Clouds and a NFI Forest Definition," *Forests*, vol. 6, no. 12. Multidisciplinary Digital Publishing Institute, pp. 4510–4528, 11-Dec-2015.

[37] R. E. McRoberts, G. C. Liknes, and G. M. Domke, "Using a remote sensing-based, percent tree cover map to enhance forest inventory estimation," *For. Ecol. Manage.*, vol. 331, pp. 12–18, Nov. 2014.

[38] E. Lindberg, J. Holmgren, K. Olofsson, J. Wallerman, and H. Olsson, "Estimation of Tree Lists from Airborne Laser Scanning Using Tree Model Clustering and k-MSN Imputation," *Remote Sens.*, vol. 5, no. 4, pp. 1932–1955, Apr. 2013.

[39] A. Noormets, D. Epron, J. C. Domec, S. G. McNulty, T. Fox, G. Sun, and J. S. King, "Effects of forest management on productivity and carbon sequestration: A review and hypothesis," *For. Ecol. Manage.*, vol. 355, pp. 124–140, Jun. 2015.

[40] S. Stagakis, N. Markos, T. Vanikiotis, A. Tzotsos, O. Sykioti, and Kyparissis, "sCASE: A primary productivity monitoring system for the forests of North Pindus National Park (Epirus, Greece)," *Eur. J. Remote Sens.*, pp. 223–243, 2015.

[41] B. Konôpka, J. Pajtík, K. Noguchi, and M. Lukac, "Replacing Norway spruce with European beech: A comparison of biomass and net primary production patterns in young stands," *For. Ecol. Manage.*, vol. 302, pp. 185–192, Aug. 2013.

[42] S. A. Hall, I. C. Burke, D. O. Box, M. R. Kaufmann, and J. M. Stoker, "Estimating stand structure using discrete-return lidar: an example from low density, fire prone ponderosa pine forests," *For. Ecol. Manage.*, vol. 208, no. 1–3, pp. 189–209, Apr. 2005.

[43] M. Katoh and F. a. Gougeon, "Improving the Precision of Tree Counting by Combining Tree Detection with Crown Delineation and Classification on Homogeneity Guided Smoothed High Resolution (50 cm) Multispectral Airborne Digital Data," *Remote Sens.*, vol. 4, no. 12, pp. 1411–1424, May 2012.

[44] D. Lu, "The potential and challenge of remote sensing-based biomass estimation," *Int. J. Remote Sens.*, vol. 27, no. 7, pp. 1297–1328, Apr. 2006.

[45] M. T. Gebreslasie, F. B. Ahmed, and J. a. N. van Aardt, "Predicting forest structural attributes using ancillary data and ASTER satellite data," *Int. J. Appl. Earth Obs.*

Geoinf., vol. 12, pp. S23–S26, Feb. 2010.

[46] P. Fatehi, A. Damm, M. E. Schaepman, and M. Kneubühler, "Estimation of alpine forest structural variables from imaging spectrometer data," *Remote Sens.*, vol. 7, no. 12, pp. 16315–16338, 2015.

[47] M. Köhl, S. Magnussen, and M. Marchetti, *Sampling Methods, Remote Sensing and GIS Multiresource Forest Inventory*. Springer Berlin Heidelberg, 2006.

[48] T. Ota, O. S. Ahmed, S. E. Franklin, M. A. Wulder, T. Kajisa, N. Mizoue, S. Yoshida, G. Takao, Y. Hirata, N. Furuya, T. Sano, S. Heng, and M. Vuthy, "Estimation of Airborne Lidar-Derived Tropical Forest Canopy Height Using Landsat Time Series in Cambodia," *Remote Sens.*, vol. 6, no. 11, pp. 10750–10772, Nov. 2014.

[49] J. Q. Chambers, G. P. Asner, D. C. Morton, L. O. Anderson, S. S. Saatchi, F. D. B. Espírito-Santo, M. Palace, and C. Souza, "Regional ecosystem structure and function: ecological insights from remote sensing of tropical forests," *Trends Ecol. Evol.*, vol. 22, no. 8, pp. 414–423, 2007.

[50] M. García, D. Riaño, E. Chuvieco, and F. M. Danson, "Estimating biomass carbon stocks for a Mediterranean forest in central Spain using LiDAR height and intensity data," *Remote Sens. Environ.*, vol. 114, no. 4, pp. 816–830, Apr. 2010.

[51] R. E. McRoberts, G. R. Holden, M. D. Nelson, G. C. Liknes, and D. D. Gormanson, "Using satellite imagery as ancillary data for increasing the precision of estimates for the Forest Inventory and Analysis program of the USDA Forest Service," *Can. J. For. Res.*, vol. 35, no. 12, pp. 2968–2980, 2005.

[52] T. W. Crowther, H. B. Glick, K. R. Covey, C. Bettigole, D. S. Maynard, S. M. Thomas, J. R. Smith, G. Hintler, M. C. Duguid, G. Amatulli, M.-N. Tuanmu, W. Jetz, C. Salas, C. Stam, D. Piotto, R. Tavani, S. Green, G. Bruce, S. J. Williams, S. K. Wiser, M. O. Huber, G. M. Hengeveld, G.-J. Nabuurs, E. Tikhonova, P. Borchardt, C.-F. Li, L. W. Powrie, M. Fischer, A. Hemp, J. Homeier, P. Cho, A. C. Vibrans, P. M. Umunay, S. L. Piao, C. W. Rowe, M. S. Ashton, P. R. Crane, and M. A. Bradford, "Mapping tree density at a global scale," *Nature*, Sep. 2015.

[53] M. Maltamo, K. Eerikäinen, J. Pitkänen, J. Hyyppä, and M. Vehmas, "Estimation of timber volume and stem density based on scanning laser altimetry and expected tree size distribution functions," *Remote Sens. Environ.*, vol. 90, no. 3, pp. 319–330, Apr. 2004.

[54] S. Nink, J. Hill, H. Buddenbaum, J. Stoffels, T. Sachtleber, and J. Langshausen, "Assessing the suitability of future multi- and hyperspectral satellite systems for mapping the spatial distribution of norway spruce timber volume," *Remote Sens.*, vol. 7, no. 9, pp. 12009–12040, 2015.

[55] T. D. Mzinyane, J. Van Aardt, and F. Ahmed, "Estimation of Merchantable Volume of Eucalyptus Clones Based on Leaf-Level Hyperspectral Data," *IEEE J. Sel. Top. Appl. Earth Obs. Remote Sens.*, vol. 8, no. 6, pp. 3095–3106, 2015.

[56] D. Gatziolis, J. S. Fried, and V. S. Monleon, "Challenges to estimating tree height via LiDAR in closed-canopy forests: A parable from Western Oregon," *For. Sci.*, vol. 56, no. 2, pp. 139–155, 2010.

[57] M. E. Jakubauskas and K. P. Price, "Empirical Relationships between Structural and Spectral Factors of Yellowstone Lodgepole Pine Forests," *Photogramm. Eng. Remote Sens.*, vol. 63, no. 1, pp. 1375–1381, 1997.

[58] P. Hyde, R. Dubayah, W. Walker, J. B. Blair, M. Hofton, and C. Hunsaker, "Mapping forest structure for wildlife habitat analysis using multi-sensor (LiDAR, SAR/InSAR, ETM+, Quickbird) synergy," *Remote Sens. Environ.*, vol. 102, pp. 63–73, 2006.

[59] T. M. Lillesand and R. W. Kiefer, *Remote sensing and image interpretation*. New York: Willy & Sons, 1994.

[60] S. G. Zolkos, S. J. Goetz, and R. Dubayah, "A meta-analysis of terrestrial aboveground biomass estimation using lidar remote sensing," *Remote Sens. Environ.*, vol. 128, pp. 289–298, Jan. 2013.

[61] M. A. Cho, A. K. Skidmore, and I. Sobhan, "Mapping beech (Fagus sylvatica L.) forest structure with airborne hyperspectral imagery," *Int. J. Appl. Earth Obs. Geoinf.*, vol. 11, no. 3, pp. 201–211, Jun. 2009.

[62] J. Hyyppä, H. Hyyppä, D. Leckie, F. Gougeon, X. Yu, and M. Maltamo, "Review of methods of small-footprint airborne laser scanning for extracting forest inventory data in boreal forests," *Int. J. Remote Sens.*, vol. 29, no. 5, pp. 1339–1366, Mar. 2008.

[63] P. S. Thenkabail, E. A. Enclona, M. S. Ashton, C. Legg, and M. J. De Dieu, "Hyperion, IKONOS, ALI, and ETM+ sensors in the study of African rainforests," *Remote Sens. Environ.*, vol. 90, no. 1, pp. 23–43, Mar. 2004.

[64] M. A. Higgins, G. P. Asner, R. E. Martin, D. E. Knapp, C. Anderson, T. Kennedy-Bowdoin, R. Saenz, A. Aguilar, and S. Joseph Wright, "Linking imaging spectroscopy and LiDAR with floristic composition and forest structure in Panama," *Remote Sens. Environ.*, vol. 154, pp. 358–367, May 2014.

[65] H. Andersen, S. E. Reutebuch, and R. J. Mcgaughey, "Active remote sensing," in *Computer Applications in Sustainable Forest Management*, G. Shao and K. M. Reynolda, Eds. Springer Netherlands, 2006, pp. 43–66.

[66] M. E. Schaepman, S. L. Ustin, A. J. Plaza, T. H. Painter, J. Verrelst, and S. Liang, "Earth system science related imaging spectroscopy—An assessment," *Remote Sens. Environ.*, vol. 113, pp. S123–S137, Sep. 2009.

[67] H. Buddenbaum, O. Stern, B. Paschmionka, E. Hass, T. Gattung, J. Stoffels, J. Hill, and W. Werner, "Using VNIR and SWIR field imaging spectroscopy for drought stress monitoring of beech seedlings," *Int. J. Remote Sens.*, vol. 36, no. 18, pp. 4590–4605, 2015.

[68] P. S. Thenkabail, E. A. Enclona, M. S. Ashton, and B. Van Der Meer, "Accuracy assessments of hyperspectral waveband performance for vegetation analysis applications," *Remote Sens. Environ.*, vol. 91, no. 3–4, pp. 354–376, Jun. 2004.

[69] M. Schlerf, C. Atzberger, and J. Hill, "Remote sensing of forest biophysical variables using HyMap imaging spectrometer data," *Remote Sens. Environ.*, vol. 95, no. 2, pp. 177–194, Mar. 2005.

[70] H. Latifi, F. Fassnacht, and B. Koch, "Forest structure modeling with combined airborne hyperspectral and LiDAR data," *Remote Sens. Environ.*, vol. 121, pp. 10–25,

Jun. 2012.

[71] A. A. Mohammedshum and L. Kooistra, "Mapping tree distribution and LAI in peatlands using field methods and imaging spectroscopy : a case study for the Haaksbergerveen , the Netherlands," *Int. J. Remote Sens.*, vol. 36, no. 18, pp. 4535–4549, 2015.

[72] C. Atzberger, R. Darvishzadeh, M. Immitzer, M. Schlerf, A. Skidmore, and G. le Maire, "Comparative analysis of different retrieval methods for mapping grassland leaf area index using airborne imaging spectroscopy," *Int. J. Appl. Earth Obs. Geoinf.*, vol. 43, pp. 1–13, 2015.

[73] M. Schlerf and C. Atzberger, "Inversion of a forest reflectance model to estimate structural canopy variables from hyperspectral remote sensing data," *Remote Sens. Environ.*, vol. 100, no. 3, pp. 281–294, Feb. 2006.

[74] F. D. Schneider, R. Leiterer, F. Morsdorf, J. Gastellu-etchegorry, N. Lauret, N. Pfeifer, and M. E. Schaepman, "Simulating imaging spectrometer data: 3D forest modeling based on LiDAR and in situ data," *Remote Sens. Environ.*, vol. 152, pp. 235–250, Sep. 2014.

[75] R. Zurita-Milla, V. C. E. Laurent, and J. A. E. van Gijsel, "Visualizing the ill-posedness of the inversion of a canopy radiative transfer model: A case study for Sentinel-2," *Int. J. Appl. Earth Obs. Geoinf.*, vol. 43, pp. 7–18, 2015.

[76] F. Gascon, J.-P. Gastellu-Etchegorry, M.-J. Lefevre-Fonollosa, and E. Dufrene, "Retrieval of forest biophysical variables by inverting a 3-D radiative transfer model and using high and very high resolution imagery," *Int. J. Remote Sens.*, vol. 25, no. 24, pp. 5601–5616, Dec. 2004.

[77] A. Viña, A. A. Gitelson, A. L. Nguy-robertson, and Y. Peng, "Comparison of different vegetation indices for the remote assessment of green leaf area index of crops," *Remote Sens. Environ.*, vol. 115, no. 12, pp. 3468–3478, 2011.

[78] R. Darvishzadeh, C. Atzberger, A. Skidmore, and M. Schlerf, "Mapping grassland leaf area index with airborne hyperspectral imagery: A comparison study of statistical approaches and inversion of radiative transfer models," *ISPRS J. Photogramm. Remote Sens.*, vol. 66, no. 6, pp. 894–906, Nov. 2011.

[79] S. A. Soenen, D. R. Peddle, R. J. Hall, C. A. Coburn, and F. G. Hall, "Estimating aboveground forest biomass from canopy reflectance model inversion in mountainous terrain," *Remote Sens. Environ.*, vol. 114, no. 7, pp. 1325–1337, Jul. 2010.

[80] L. Ji, B. K. Wylie, D. R. Nossov, B. Peterson, M. P. Waldrop, J. W. McFarland, J. Rover, and T. N. Hollingsworth, "Estimating aboveground biomass in interior Alaska with Landsat data and field measurements," *Int. J. Appl. Earth Obs. Geoinf.*, vol. 18, pp. 451–461, Aug. 2012.

[81] J. Verrelst, G. Camps-Valls, J. Muñoz-Marí, J. P. Rivera, F. Veroustraete, J. G. P. W. Clevers, and J. Moreno, "Optical remote sensing and the retrieval of terrestrial vegetation bio-geophysical properties – A review," *ISPRS J. Photogramm. Remote Sens.*, vol. 108, pp. 273–290, Oct. 2015.

[82] P. Holmgren and T. Thuresson, “Satellite remote sensing for forestry planning—A review,” *Scand. J. For. Res.*, vol. 13, no. February 2015, pp. 90–110, 1998.

[83] A. Psomas, M. Kneubühler, S. Huber, and K. Itten, “Hyperspectral remote sensing for estimating aboveground biomass,” *Int. J. Remote Sens.*, vol. 32, no. 24, pp. 9007–9031, 2011.

[84] G. Le Maire, C. Francois, K. Soudani, D. Berveiller, J. Pontailler, N. Breda, H. Genet, H. Davi, and E. Dufrene, “Calibration and validation of hyperspectral indices for the estimation of broadleaved forest leaf chlorophyll content, leaf mass per area, leaf area index and leaf canopy biomass,” *Remote Sens. Environ.*, vol. 112, no. 10, pp. 3846–3864, Oct. 2008.

[85] P. Fatehi, A. Damm, A. Schweiger, M. E. Schaepman, and M. Kneubühler, “Mapping Alpine Aboveground Biomass From Imaging Spectrometer Data : A Comparison of Two Approaches,” *IEEE J. Sel. Top. Appl. Earth Obs. Remote Sens.*, vol. 8, no. 6, pp. 3123–3139, 2015.

[86] M. A. Cho and A. K. Skidmore, “Hyperspectral predictors for monitoring biomass production in Mediterranean mountain grasslands: Majella National Park, Italy,” *Int. J. Remote Sens.*, vol. 30, no. 2, pp. 499–515, Jan. 2009.

[87] A. Swatantran, R. Dubayah, D. Roberts, M. Hofton, and J. B. Blair, “Mapping biomass and stress in the Sierra Nevada using lidar and hyperspectral data fusion,” *Remote Sens. Environ.*, vol. 115, no. 11, pp. 2917–2930, Nov. 2011.

[88] O. Mutanga and A. K. Skidmore, “Hyperspectral band depth analysis for a better estimation of grass biomass (Cenchrus ciliaris) measured under controlled laboratory conditions,” *Int. J. Appl. Earth Obs. Geoinf.*, vol. 5, no. 2, pp. 87–96, May 2004.

[89] F. E. Fassnacht, F. Hartig, H. Latifi, C. Berger, J. Hernández, P. Corvalán, and B. Koch, “Importance of sample size , data type and prediction method for remote sensing-based estimations of aboveground forest biomass,” *Remote Sens. Environ.*, vol. 154, pp. 102–114, 2014.

[90] S. L. Powell, W. B. Cohen, S. P. Healey, R. E. Kennedy, G. G. Moisen, K. B. Pierce, and J. L. Ohmann, “Quantification of live aboveground forest biomass dynamics with Landsat time-series and field inventory data: A comparison of empirical modeling approaches,” *Remote Sens. Environ.*, vol. 114, no. 5, pp. 1053–1068, May 2010.

[91] J. Heiskanen, “Estimating aboveground tree biomass and leaf area index in a mountain birch forest using ASTER satellite data,” *Int. J. Remote Sens.*, vol. 27, no. 6, pp. 1135–1158, Mar. 2006.

[92] G. Omer, O. Mutanga, E. Abdel-Rahman, and E. Adam, “Empirical Prediction of Leaf Area Index (LAI) of Endangered Tree Species in Intact and Fragmented Indigenous Forests Ecosystems Using WorldView-2 Data and Two Robust Machine Learning Algorithms,” *Remote Sens.*, vol. 8, no. 4, pp. 1–26, 2016.

[93] J. Defibaugh y Chávez and J. A. Tullis, “Deciduous Forest Structure Estimated with LIDAR-Optimized Spectral Remote Sensing,” *Remote Sens.*, vol. 5, no. 1, pp. 155–182, Jan. 2013.

[94] M. Kalacska, G. a. Sanchez-Azofeifa, B. Rivard, T. Caelli, H. P. White, and J. C. Calvo-Alvarado, "Ecological fingerprinting of ecosystem succession: Estimating secondary tropical dry forest structure and diversity using imaging spectroscopy," *Remote Sens. Environ.*, vol. 108, no. 1, pp. 82–96, May 2007.

[95] W. Wagner, M. Hollaus, C. Briese, and V. Ducic, "3D vegetation mapping using small-footprint full-waveform airborne laser scanners," *Int. J. Remote Sens.*, vol. 29, no. 5, pp. 1433–1452, 2008.

[96] E. Næsset, T. Gobakken, J. Holmgren, H. Hyyppä, J. Hyyppä, M. Maltamo, M. Nilsson, H. Olsson, Å. Persson, and U. Söderman, "Laser scanning of forest resources: the nordic experience," *Scand. J. For. Res.*, vol. 19, no. 6, pp. 482–499, Dec. 2004.

[97] D. Stojanova, P. Panov, V. Gjorgjioski, A. Kobler, and S. Džeroski, "Estimating vegetation height and canopy cover from remotely sensed data with machine learning," *Ecol. Inform.*, vol. 5, no. 4, pp. 256–266, Jul. 2010.

[98] K. Lim, P. Treitz, K. Baldwin, I. Morrison, and J. Green, "Lidar remote sensing of biophysical properties of tolerant northern hardwood forests," *Can. J. Remote Sens.*, vol. 29, no. 5, pp. 658–678, Oct. 2003.

[99] J. B. Drake, R. O. Dubayah, D. B. Clark, R. G. Knox, J. B. Blair, M. A. Hofton, R. L. Chazdon, J. F. Weishampel, and S. Prince, "Estimation of tropical forest structural characteristics using large-footprint lidar," *Remote Sens. Environ.*, vol. 79, no. 2–3, pp. 305–319, Feb. 2002.

[100] X. Yu, P. Litkey, J. Hyyppä, M. Holopainen, and M. Vastaranta, "Assessment of Low Density Full-Waveform Airborne Laser Scanning for Individual Tree Detection and Tree Species Classification," *Forests*, vol. 5, no. 5, pp. 1011–1031, 2014.

[101] H. Latifi, A. Nothdurft, and B. Koch, "Non-parametric prediction and mapping of standing timber volume and biomass in a temperate forest: application of multiple optical/LiDAR-derived predictors," *Forestry*, vol. 83, no. 4, pp. 395–407, Jul. 2010.

[102] J. Hyyppä, X. Yu, H. Hyyppä, M. Vastaranta, M. Holopainen, A. Kukko, H. Kaartinen, A. Jaakkola, M. Vaaja, J. Koskinen, and P. Alho, "Advances in Forest Inventory Using Airborne Laser Scanning," *Remote Sens.*, vol. 4, no. 12, pp. 1190–1207, May 2012.

[103] E. Næsset, "Determination of mean tree height of forest stands using airborne laser scanner data," *ISPRS J. Photogramm. Remote Sens.*, vol. 52, no. 2, pp. 49–56, 1997.

[104] P. Tompalski, N. C. Coops, J. C. White, and M. A. Wulder, "Enriching ALS-Derived Area-Based Estimates of Volume through Tree-Level Downscaling," *Forests*, vol. 6, no. 8, pp. 2608–2630, 2015.

[105] S. D. Roberts, T. J. Dean, D. L. Evans, J. W. McCombs, R. L. Harrington, and P. a. Glass, "Estimating individual tree leaf area in loblolly pine plantations using LiDAR-derived measurements of height and crown dimensions," *For. Ecol. Manage.*, vol. 213, no. 1–3, pp. 54–70, 2005.

[106] J. Vauhkonen, L. Ene, S. Gupta, J. Heinzel, J. Holmgren, J. Pitkanen, S. Solberg, Y. Wang, H. Weinacker, K. M. Hauglin, V. Lien, P. Packalen, T. Gobakken, B. Koch, E. Naesset, T. Tokola, and M. Maltamo, "Comparative testing of single-tree detection algorithms under different types of forest," *Forestry*, vol. 85, no. 1, pp. 27–40, 2012.

[107] D. Jaskierniak, G. Kuczera, R. Benyon, and L. Wallace, "Using tree detection algorithms to predict stand sapwood area, basal area and stocking density in Eucalyptus regnans forest," *Remote Sens.*, vol. 7, no. 6, pp. 7298–7323, 2015.

[108] M. Maltamo, E. Næsset, and J. Vauhkonen, *Forestry applications of airborne laser scanning: concepts and case studies*. Dordrecht: Springer, 2014.

[109] M. Kneubühler, A. Damm, A. Schweiger, A. C. Risch, M. Schütz, and M. E. Schaepman, "Continuous Fields From Imaging Spectrometer Data for Ecosystem Parameter Mapping and Their Potential for Animal Habitat Assessment in Alpine Regions," *IEEE J. Sel. Top. Appl. Earth Obs. Remote Sens.*, vol. 7, no. 6, pp. 2600–2610, 2014.

[110] S. M. De Jong, E. J. Pebesma, and B. Lacaze, "Above-ground biomass assessment of Mediterranean forests using airborne imaging spectrometry: the DAIS Peyne experiment," *Int. J. Remote Sens.*, vol. 24, no. 7, pp. 1505–1520, Jan. 2003.

[111] M. A. Cho, A. K. Skidmore, F. Corsi, S. E. van Wieren, and I. Sobhan, "Estimation of green grass/herb biomass from airborne hyperspectral imagery using spectral indices and partial least squares regression," *Int. J. Appl. Earth Obs. Geoinf.*, vol. 9, no. 4, pp. 414–424, Dec. 2007.

[112] D. Rocchini, G. M. Foody, H. Nagendra, C. Ricotta, M. Anand, K. S. He, V. Amici, B. Kleinschmit, M. Förster, S. Schmidtlein, H. Feilhauer, A. Ghisla, M. Metz, and M. Neteler, "Uncertainty in ecosystem mapping by remote sensing," *Comput. Geosci.*, vol. 50, pp. 128–135, May 2013.

[113] J. Gehrig-Fasel, A. Guisan, and N. E. Zimmermann, "Tree line shifts in the Swiss Alps: Climate change or land abandonment?," *J. Veg. Sci.*, vol. 18, no. 4, pp. 571–582, 2007.

[114] P. A. Townsend and S. J. Walsh, "Remote Sensing of Forested Wetlands : Application of Multitemporal and Multispectral Satellite Imagery to Determine Plant Community Composition and Structure in Southeastern Stable URL : http://www.jstor.org/stable/20051167 and sensing of forested wetland," *Plant Ecol.*, vol. 157, no. 2, pp. 129–149, 2001.

[115] R. S. DeFries, C. B. Field, I. Fung, C. O. Justice, S. Los, P. a. Matson, E. Matthews, H. a. Mooney, C. S. Potter, K. Prentice, P. J. Sellers, J. R. G. Townshend, C. J. Tucker, S. L. Ustin, and P. M. Vitousek, "Mapping the land surface for global atmosphere-biosphere models: Toward continuous distributions of vegetation's functional properties," *J. Geophys. Res.*, vol. 100, no. D10, p. 20867, 1995.

[116] D. Rocchini, "While Boolean sets non-gently rip: A theoretical framework on fuzzy sets for mapping landscape patterns," *Ecol. Complex.*, vol. 7, no. 1, pp. 125–129, Mar. 2010.

[117] O. Mutanga and A. K. Skidmore, "Narrow band vegetation indices overcome the saturation problem in biomass estimation," *Int. J. Remote Sens.*, vol. 25, no. 19, pp. 3999–4014, Oct. 2004.

[118] A. C. Risch, M. F. Jurgensen, D. S. Page-Dumroese, O. Wildi, and M. Schütz, "Long-term development of above-and below-ground carbon stocks following land-use change in subalpine ecosystems of the Swiss National Park," *J. For.*, vol. 1602, pp. 1590–1602, 2008.

[119] Y. Paillet, C. Pernot, V. Boulanger, N. Debaive, M. Fuhr, O. Gilg, and F. Gosselin, "Quantifying the recovery of old-growth attributes in forest reserves: A first reference for France," *For. Ecol. Manage.*, vol. 346, pp. 51–64, Jun. 2015.

[120] H. Latifi, F. E. Fassnacht, J. Müller, A. Tharani, S. Dech, and M. Heurich, "Forest inventories by LiDAR data : A comparison of single tree segmentation and metric-based methods for inventories of a heterogeneous temperate forest," *Int. J. Appl. Earth Obs. Geoinf.*, vol. 42, pp. 162–174, 2015.

[121] E. Lindberg, J. Holmgren, K. Olofsson, J. Wallerman, and H. Olsson, "Estimation of tree lists from airborne laser scanning by combining single-tree and area-based methods," *Int. J. Remote Sens.*, vol. 31, no. 5, SI, pp. 1175–1192, 2010.

[122] M. A. Lefsky, W. B. Cohen, S. A. Acker, G. G. Parker, T. A. Spies, and D. Harding, "Lidar Remote Sensing of the Canopy Structure and Biophysical Properties of Douglas-Fir Western Hemlock Forests," *Remote Sens. Environ.*, vol. 70, no. 3, pp. 339–361, Dec. 1999.

[123] M. O. Hunter, M. Keller, D. Victoria, and D. C. Morton, "Tree height and tropical forest biomass estimation," *Biogeosciences*, vol. 10, no. 12, pp. 8385–8399, 2013.

[124] D. Moeser, J. Roubinek, P. Schleppi, F. Morsdorf, and T. Jonas, "Canopy closure, LAI and radiation transfer from airborne LiDAR synthetic images," *Agric. For. Meteorol.*, vol. 197, pp. 158–168, Oct. 2014.

[125] E. Næsset and K.-O. Bjerknes, "Estimating tree heights and number of stems in young forest stands using airborne laser scanner data," *Remote Sens. Environ.*, vol. 78, no. 3, pp. 328–340, Dec. 2001.

[126] M. Heurich, "Automatic recognition and measurement of single trees based on data from airborne laser scanning over the richly structured natural forests of the Bavarian Forest National Park," *For. Ecol. Manage.*, vol. 255, no. 7, pp. 2416–2433, Apr. 2008.

[127] R. S. Capers, R. L. Chazdon, A. R. Brenes, and B. V. Alvarado, "Successional dynamics of woody seedling communities in wet tropical secondary forests," *J. Ecol.*, vol. 93, no. 6, pp. 1071–1084, 2005.

[128] D. K. Bolton, N. C. Coops, and M. A. Wulder, "Measuring forest structure along productivity gradients in the Canadian boreal with small-footprint Lidar," *Environ. Monit. Assess.*, vol. 185, pp. 6617–6634, 2013.

[129] G. J. Sproull, M. Adamus, M. Bukowski, T. Krzyżanowski, J. Szewczyk, J. Statwick, and J. Szwagrzyk, "Tree and stand-level patterns and predictors of Norway spruce mortality caused by bark beetle infestation in the Tatra Mountains," *For. Ecol. Manage.*, vol. 354, pp. 261–271, 2015.

[130] H. Kaartinen, J. Hyyppä, X. Yu, M. Vastaranta, H. Hyyppä, A. Kukko, M. Holopainen, C. Heipke, M. Hirschmugl, F. Morsdorf, E. Næsset, J. Pitkänen, S. C. Popescu, S. Solberg, B. M. Wolf, and J.-C. Wu, "An International Comparison of Individual Tree Detection and Extraction Using Airborne Laser Scanning," *Remote Sens.*, vol. 4, no. 12, pp. 950–974, Mar. 2012.

[131] J. Pitkänen, M. Maltamo, J. Hyyppä, and X. Yu, "Adaptive Methods for Individual Tree

Detection on Airborne Laser Based Canopy Height Model," in *Proceedings of ISPRS Workshop Laser-Scanners for Forest and Landscape Assessment*, 2004, pp. 187–191.

[132] C. Song, M. B. Dickinson, L. Su, S. Zhang, and D. Yaussey, "Estimating average tree crown size using spatial information from Ikonos and QuickBird images: Across-sensor and across-site comparisons," *Remote Sens. Environ.*, vol. 114, no. 5, pp. 1099–1107, May 2010.

[133] B. Koch, U. Heyder, and H. Weinacker, "Detection of Individual Tree Crowns in Airborne Lidar Data," *Photogramm. Eng. Remote Sens.*, vol. 72, no. 4, pp. 357–363, Apr. 2006.

[134] S. G. Tesfamichael, F. Ahmed, J. a. N. van Aardt, and F. Blakeway, "A semi-variogram approach for estimating stems per hectare in Eucalyptus grandis plantations using discrete-return lidar height data," *For. Ecol. Manage.*, vol. 258, no. 7, pp. 1188–1199, Sep. 2009.

[135] D. Leckie, "Stand delineation and composition estimation using semi-automated individual tree crown analysis," *Remote Sens. Environ.*, vol. 85, no. 3, pp. 355–369, May 2003.

[136] H. Pretzsch, "Canopy space filling and tree crown morphology in mixed-species stands compared with monocultures," *For. Ecol. Manage.*, vol. 327, pp. 251–264, Sep. 2014.

2

Mapping Alpine Aboveground Biomass from Imaging Spectrometer Data: a Comparison of Two Approaches

This chapter has been published as:

Fatehi, P., Damm, A., Schweiger, A-K., Schaepman, M.E., & Kneubühler, M. (2015). Mapping Alpine aboveground biomass from imaging spectrometer data: a comparison of two approaches. IEEE Journal of Selected Topics in Applied Earth Observations and Remote Sensing, 8 (6), 3123-3139.

Abstract

Aboveground biomass (AGB) of terrestrial ecosystems is an important constraint of global change and productivity models and used to assess carbon stocks and thus the contribution of vegetated ecosystems to the global carbon cycle. Although an indispensable and important requirement for decision makers, coherent and accurate estimates of grassland and forest AGB especially in complex environments are still lacking. In this study we aim to assess the capability of two strategies to map grassland and forest AGB in a complex alpine ecosystem, i.e., using a *discrete* as well as a *continuous field* (CF) mapping approach based on imaging spectroscopy (IS) data. *In-situ* measurements of grassland and forest AGB were acquired in the Swiss National Park (SNP) to calibrate empirical models and to validate AGB retrievals. The selection of robust empirical models considered all potential two narrow-band combinations of the Simple Ratio (SR) and the Normalized Difference Vegetation Index (NDVI) generated from Airborne Prism Experiment (APEX) IS data and *in-situ* measurements. We found a narrow-band SR including spectral bands from the short wave infrared (SWIR) (1689 nm) and near infrared (NIR) (851 nm) as the best regression models to estimate grassland AGB. Forest AGB showed highest correlation with a SR generated from two spectral bands in the SWIR (1498 nm, 2112 nm). The applied accuracy assessment revealed good results for estimated grassland AGB using the discrete mapping approach (R^2 of 0.65, mean RMSE of 0.91 $t.ha^{-1}$, and mean relative RMSE of 26%). The CF mapping approach produced a higher R^2 (R^2 = 0.94), and decreased the mean RMSE and the mean relative RMSE to 0.55 $t.ha^{-1}$ and 15%, respectively. For forest, the discrete approach predicted AGB with a R^2 value of 0.64, a mean RMSE of 67.8 $t.ha^{-1}$, and a mean relative RMSE of 25%. The CF mapping approach improved the accuracy of forest AGB estimation with R^2 = 0.85, mean RMSE = 55.85 $t.ha^{-1}$, and mean relative RMSE = 21%. Our results indicate that, in general, both mapping approaches are capable to accurately map grassland and forest AGB in complex environments using IS data, while the CF based approach yielded higher accuracies due to its capability to incorporate sub-pixel information (abundances) of different land cover types.

Authors' contributions: PF, AD, MES, MK designed the study and developed the methodology. PF and A-KS collected the data. PF and AD performed the analysis. All authors wrote the manuscript.

2.1 Introduction

The Aboveground biomass (AGB) of terrestrial ecosystems is an important constraint of dynamic global vegetation models to assess carbon stocks and feedbacks of vegetation with the global carbon cycle [1]. Further, quantitative maps of AGB are an important input to support forest and landscape management [2], [3], to understand deforestation impact on carbon release and global warming [4], to assess productivity of forested areas in relation to forest composition [5] and in view of specific forest management practices [1], [6]. Since AGB is an indicator for quantity and quality of forage, it is considered relevant information to study animal ecology, i.e., herbivore behaviors [7] and grazing intensities [8], [9]. Further, grassland biomass has a high potential to become flammable during an extended dry season [10], and therefore accurate AGB estimates are relevant input for fire risk assessment [11] and carbon cycle modeling.

Different approaches have been applied to estimate AGB including i) geographical information systems (GIS) based modeling parameterized with various environmental data [4], [12], ii) *in-situ* observations [3], or iii) remote sensing (RS) based assessments [13], [14], [2]. A GIS-based approach provides a platform to apply a mathematical model to employ all parameters, (i.e., forest inventory data, vegetation distribution map, digital elevation model (DEM), soil inventory data, soil distribution map) that potentially affect the available biomass (see Deng et al. [12] and Lu [15] for more details). This implies that identifying relevant data as well as underlying assumptions directly impact the performance of a GIS-based approach. Further, input data with reasonable quality and accuracy are often not available, limiting the applicability for timely biomass estimates [15].

In-situ observational approaches based on field surveys are the most accurate way to collect biomass data [15], but required in-situ measurements are often limited in their spatial and temporal resolution [16]. Furthermore, in-situ sampling is expensive and time consuming, and often not transferrable to large and/or remote areas.

Various studies discuss the estimation of biomass using RS data [17]. RS provides the advantage of spatially explicit mapping of vegetation biomass with reasonable accuracy [18], repeatedly over large and remote areas [19]. As such, it reduces time and human effort compared to field observations. Two predominant approaches to estimate vegetation properties (e.g., chlorophyll, LAI, biomass) from imaging spectrometer data are i) physical-based approaches, and ii) empirical approaches. Physical-based approaches use leaf and canopy radiative transfer models (RTM), to identify the spectral/directional

variation of canopy reflectance [20]. The inversion of an RTM allows to predict vegetation properties. However, RTM parameterization requires many input parameters [21], [22]. The procedure is computationally intense, thus limiting its applicability for large areas for biomass estimation [23]. Empirical approaches for biomass estimation are commonly developed using *in-situ* measured reference data at stand, plot, or individual tree level (e.g., canopy closure, canopy height, tree diameter at breast height (DBH)). These reference data are combined with RS data to derive empirical models that finally allow estimating vegetation biomass for the entire study area [14]. Two conceptual approaches can be distinguished, i.e., the *direct* and the *indirect* approach [24]. The direct approach relates top-of canopy reflectance or transformed data values (e.g., vegetation indices, principle components or tasseled cap components) and biomass using statistical techniques (e.g., linear regression, multiple regression analysis or partial least squares regression) [25]. Indirect approaches combine various vegetation variables derived from RS data (e.g., tree height, DBH, or crown closure) considering mechanistic relations to model biomass [26]. The direct approach is commonly applied for estimating biomass from spectroscopy data. Various studies successfully demonstrated the extraction of biochemical and biophysical information from imaging spectrometer (IS) data by using original spectral bands, computing all possible two-band combinations of normalized difference vegetation indices (NDVI type) [2], [27], red-edge position (REP), narrow simple ratio (SR) vegetation indices [28], [29], band depth analysis [30], narrow-band normalized difference water indices (NDWI) [31] or multispectral data by mostly computing broad-band vegetation indices (VI) [19], [32], [33].

Independent of the method used to estimate biomass; it remains a challenge to map realistic representations of biomass gradients across landscapes. In this context, two main approaches are used most frequently, namely the *discrete* approach and the *continuous field* (CF) approach. The discrete approach follows Boolean logic in labeling every single pixel and represents one class only for each pixel [25], [34], [35]. The thematic classes are mutually exclusive, with discrete boundaries separating these classes. However, this assumption does not realistically reflect gradients within vegetation types [36] where vegetation classes vary gradually over the landscape or pixels may belong to two or more classes (sub-pixel mixture of different vegetation types) [37]. The effect of mixed pixels is especially important in complex landscapes such as alpine environments, where a given pixel can represent e.g., trees mixed with grass and non-vegetated surfaces (i.e., soil/rock or snow). Many studies have attempted to produce better representations of the true complexity of ecosystem parameters by suggesting to i) consider the amount of shadow

and bare soil in biomass mapping [32], ii) apply spectral mixture analysis to demonstrate habitats vary in space in a continuous fashion [35] or iii) apply fuzzy set theory [38], [39], [40]. CF approaches provide the ability to deal with mixed pixels and to represent the distribution of vegetation biomass accurately also in complex landscapes. The CF mapping approach was introduced by DeFries et al. [37] and was found to better represent the spatial distribution of biomass in terrestrial ecosystems [41].

The aim of this study is to evaluate the capability of IS data for estimating AGB in a heterogeneous alpine ecosystem and comparing the performance of a CF map approach and a discrete approach to map AGB in a complex landscape. The specific objectives of this study are to i) derive an empirical model to map grassland and forest AGB from IS data; ii) apply a CF mapping approach to represent gradients of biomass at landscape level; iii) validate resulting maps with reference data obtained in grasslands and forest; iv) discuss the capability of the two mapping approaches (i.e., discrete and CF mapping approach).

2.2 Study area and Data

2.2.1 Study area

The study area is located in the Swiss National Park (SNP), situated in the southeastern part of Switzerland (Fig. 2. 1). As an IUCN (International Union for the Conservation of Nature) category Ia nature reserve (strict nature reserve), the SNP represents an area where human impact is strictly controlled and limited since its foundation in 1914 [42]. The SNP therefore offers a great potential to study ecosystem processes and to gain a better understanding of how natural areas function. The SNP covers an area of 170 km^2. While 50% are covered with vegetation (forest and grassland), the remaining area consists of rock and soil surfaces. Dominant tree species are mountain pine (*Pinus montana* Miller), Swiss stone pine (*Pinus cembra* L.), and larch (*Larix decidua* L.), while scope pine (*Pinus sylvestris* L.) and Norway spruce (*Picea abies* (L.) Karst) are associated species and spatially less important [42]. In the Trupchun Valley (Val Trupchun), our main study area within the SNP, larch is the dominant tree, whereas Norway spruce and Swiss stone pine are associated species.

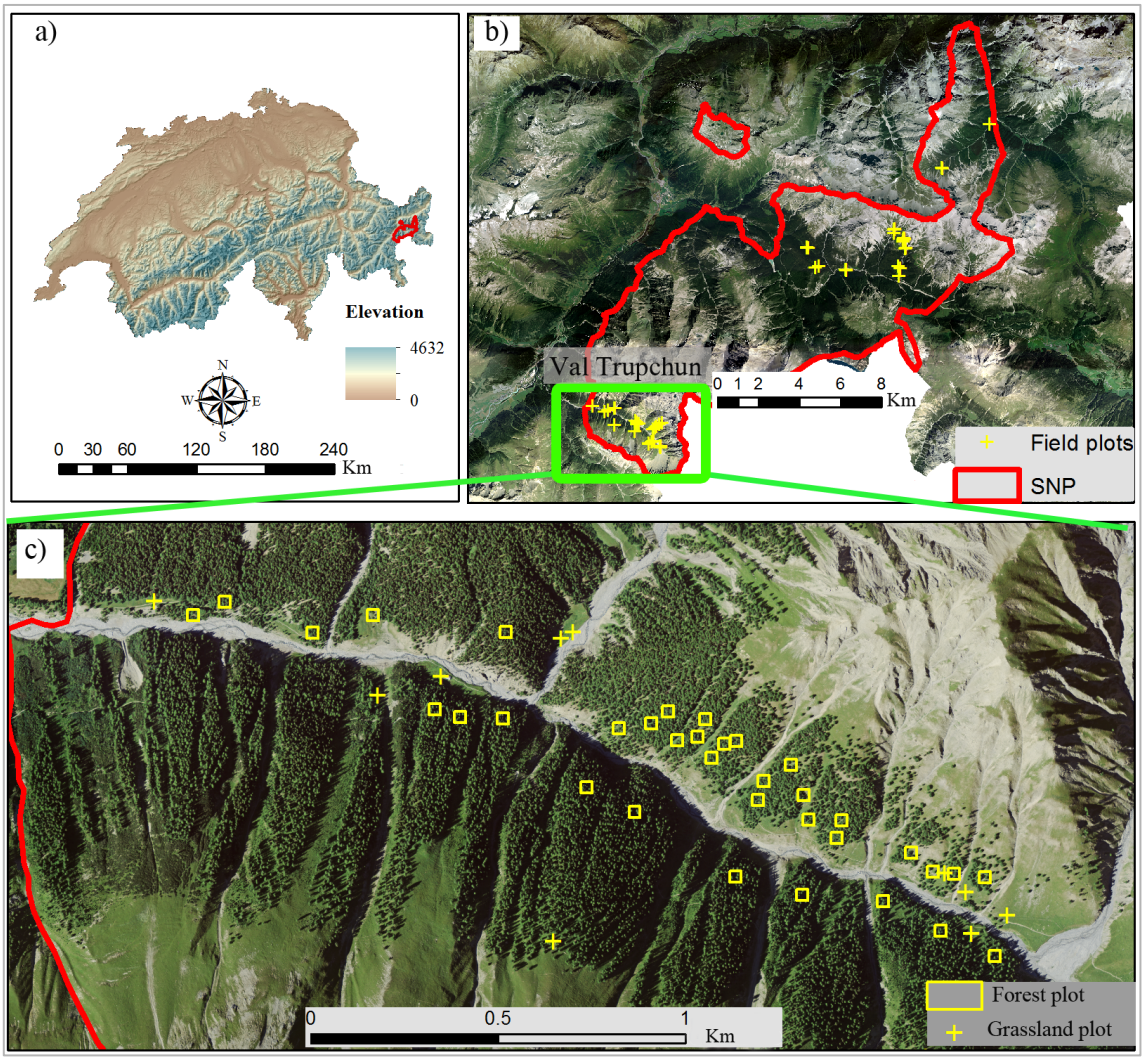

Fig. 2. 1. Study area and field plots. a): location of the SNP in Switzerland (red shape); a digital elevation model is used as background (source: swisstopo). b): distribution of field plots (yellow crosses) in the SNP (red shape). C): distribution of forest field plots (yellow squares) and grassland field plots (yellow crosses) in the Val Trupchun; a true color image is used as background (source: swisstopo).

The SNP covers an alpine landscape, with an elevation ranging from 1350 m to 3170 m above sea level (a.s.l.). The climate of the region is dry and harsh with an average annual temperature of 0.9 °C ± 0.5 °C (mean ± SD) and average annual precipitation of 744 mm ± 160 mm (2008–2012, recorded at the park's weather station Buffalora at 1977 m a.s.l. [43]).

2.2.2 Field data

Several Field reference data were collected for grassland in summer 2010 (26 June) at the exact time of the Airborne Prism Experiment (APEX) overpasses and for forest in summer 2012 (20 June to 10 July). For the grassland, 51 field reference plots distributed

over the area of the SNP and capturing a large range of productivity, exposure and plant species compositions were investigated. The field plots were 6 m x 6 m in size and homogenous in species composition and cover. At the day of APEX IS data takes, grass was cut in a 1 m x 1 m subplot in the center of each plot, immediately sealed into plastic bags, and weighted the same day to determine biomass (fresh weight). A differential global positioning system (DGPS) providing an accuracy better than 1 m was used to record the position of each field plot.

In a second field campaign carried out in June 2012, aboveground biomass of the forested parts of the SNP in the Trupchun Valley was measured. Sample plots with a size of 30 m x 30 m were identified by applying a stratified random sampling while excluding protected areas that were not accessible. Identified plots represent most of the present tree species and possible ranges of their properties, i.e., canopy cover, density, and species composition. In each of the 35 plots, species type, DBH, and tree height were measured, while only trees with a DBH greater than 5 cm were considered [44]. For each plot, the height of five trees, including the tree closest to a corner of each plot and the largest tree in terms of DBH were measured using a Haga altimeter (Haga GmbH and Co. KG, Nuremberg, Germany) [45]. The Haga altimeter is an instrument, which uses trigonometric principles to measure tree height. As the measurement of tree height is relatively time consuming, it can usually only be undertaken on a limited number of trees (subsample). The height of non-measured trees is often based on predictions obtained using a model estimated from the subsample of heights. The most common model is a height curve, indicating the relationship between tree height and DBH (called height–DBH function) [46]. To generate the species-specific height–DBH function the measured trees were classified into three groups according to their species. Using the height–DBH function, the heights of all trees were estimated per plot. To obtain the aboveground tree biomass of each plot, the volume of the trees was estimated as a function of the DBH and tree height. AGB was finally calculated as function of tree volume (V) in m^3, wood density (WD) in kg $m^{-3}$and a unit less biomass expansion factor (BEF) as described in literature according to [47]:

$$AGB = V \times WD \times BEF \quad (1)$$

We used values of 460, 400, 400 (kg m^{-3}) for the WD of larch, Swiss stone pine and Norway spruce [5], [6]. For BEF we used a value of 1.61 for the whole study area as suggested by [48]. Tree AGB was then summed up to estimate the AGB of the respective plot.

2.2.3 APEX imaging spectrometer data

The Airborne Prism Experiment (APEX) is an airborne dispersive pushbroom imaging spectrometer [49]. **Table 2. 1** presents an overview of APEX instrument characteristics for the SNP data acquisitions.

Table 2. 1

APEX instrument characteristics the SNP data acquisition.

	Spectral Performance	
	VNIR	SWIR
Spectral range	375–983 nm	991–2500 nm
Spectral bands (unbinned configuration)	335	198
Spectral bands (binned configuration) after removal of noisy bands	110	175
Spectral sampling interval	0.45–7.5 nm	5–10 nm
Spectral resolution (FWHM)	0.7–9.7 nm	6.2–12 nm
	Spatial Performance	
Spatial pixels (across track)	1000	
Field of view (FOV)	28°	
Instantaneous field of view (IFOV)	0.028°	
Spatial sampling interval (across track)	1.5-2.4 m (depending on surface height)	

The entire SNP was recorded with APEX at a flight height of 6500 m a.s.l., resulting in 2 m average pixel size, under cloud free conditions on 26 June 2010 between 9:30 am - 11:30 am UTC. The sun zenith angle varied between 31.8° and 28.1° and the sun azimuth angle between 127.5° and 1391.1°. Image acquisition started two hours prior to solar noon and concluded at solar noon. Four adjacent APEX flight lines (FL) were used in this study. The data sets were geometrically corrected using a parametric geocoding approach (PARGE) [50]. An evaluation of the resulting geometric accuracy using 15 ground control points revealed a total uncertainty of 3.2 m ± 1.4 m, corresponding to a total pixel shift of 1.3-1.9 pixels ± 0.5-0.8 pixel. Atmospheric correction of the APEX data sets was performed using ATCOR-4 [51], which is based on pre-calculated look-up tables (LUT) generated with the atmospheric radiative transfer code MODTRAN-5. Defining an atmosphere type and an aerosol model (here we assumed mid-latitude summer and a rural aerosol model) in combination with image based estimates of atmospheric water vapor and visibility allows the pixel-wise selection of LUT entries to compensate for atmospheric effects and to derive top-of-canopy hemispherical conical reflectance factor (HCRF) data (for terminology see [52]). Spectral reference data of various land cover types were collected during the APEX 2010 data acquisition using an ASD field spectrometer (PANalytics, Boulder) for subsequent IS data validation. The radiometric performance of the APEX data sets was evaluated using three *in-situ* surface reflectance measurements of homogeneous targets

(i.e., asphalt, gravel, grassland), revealing an average RMSE of 15% considering the entire wavelength range (data not shown). Subsequent analysis was based on mosaicked HCRF data. A comparison of HCRF values extracted from sample plots located in the overlapping region of two adjacent APEX flight lines showed differences in measured HCRF values. We therefore considered HCRF values and related ground information of sample plots located in the overlapping region of two flight lines as an independent set of measurements. This assumption increased the number of grassland reference plots from 51 to 84 and from 35 to 63 for the forest.

2.3 Methods

2.3.1 Vegetation Indices

The Vegetation indices (VIs) are widely used to estimate biophysical vegetation properties, i.e., biomass [32], [33], [53], [54], LAI [22], [27], [55], canopy closure [56], [57], or stand volume [58], [28]. The Simple Ratio (SR) and the Normalized Difference Vegetation Index (NDVI) are among the most common VIs to estimate biophysical properties of vegetation [28], [29], [59]. The concepts of SR and NDVI indices are usually based on the contrast between two spectral bands. Traditional SR and NDVI are computed to take advantage of strong chlorophyll absorption in the red region and strong reflectance in the near-infrared region because of internal mesophyll structure of healthy green leaves. In our study we used the following general mathematical descriptions of spectral ratio [see (2)] and normalized difference [see (3)] to generate VIs:

$$SR = \rho_1 / \rho_2 \quad (2)$$

$$NDVI = (\rho_1-\rho_2) / (\rho_1+\rho_2) \quad (3)$$

where ρ_1 and ρ_2 are reflectance values at distinct wavelengths.

While at the cost of physical explanation and subject to potential pseudo-correlations, several studies have shown that instead of the traditional red – NIR band combinations new combinations of two narrow bands over the entire wavelength range from 350–2500 nm can enhance the estimation power of VIs [28]. By eliminating spectral bands located in the water vapor absorption regions at 1335 nm to 1490 nm and at 1780 nm to 1990 nm from our analysis, 193 APEX bands were used to compute narrow-band VIs (both SR and NDVI) for all possible combinations (37,249 different combinations). The subsequent identification of suitable VIs that can effectively predict biomass is a critical step. A common approach to distinguish the best narrow-band VIs is based on the calculation of a linear regression between each band combination and vegetation biomass, and a

subsequent selection of band combinations with the highest predictive power regarding the target variable (i.e., biomass) [45], [2], [59]. The selection of VIs based on this approach typically considers different criteria: i) statistical measures, e.g., R^2 or RMSE describing the correlation between target variable and VIs must be above or below a certain threshold (here we used a R^2 threshold of 0.3 with a confidence level of 95%); ii) band combinations identified must be in plausible wavelength ranges to enable causality; iii) bands incorporated in calculating VIs must exceed a minimum spectral distance to avoid multi-collinearity (here we defined a minimum spectral distance of 10 nm to account for the maximum spectral sampling interval of APEX in the SWIR); iv) the band combinations must be in a "hot-spot area" (spectral range) showing a pattern of high correlation, which helps to avoid selecting single (random) band combinations with high R^2 in the 2D correlogram. The set of identified VIs was then incorporated in subsequent statistical analysis (see next section).

2.3.2 Regression Analysis

Empirical models are efficient tools to relate *in-situ* and remote sensing data [55]. Regression analysis is commonly applied to derive relationships between a dependent variable that is complex or expensive to measure and an independent variable or predictor, which is relatively easy to measure [55].

Such empirical approaches rely on rigorous data quality since measurement errors can determine artificial relationships. We hence applied a standard deviation outlier labeling method, i.e., the 3SD method [60] to identify sample plots with exceptional values compared to the other sample plots and to exclude them from further analysis. The applied method labeled two grassland plots as outliers. Since normal data distribution is another requirement in regression analysis, we applied the Shapiro-Wilk test ($p > 0.05$), developed to analyze small sample sizes (≤ 50 observations), to test our field data for normality [45]. The Shapiro-Wilk test revealed that both grassland AGB ($W = 0.961$, $p = 0.105$) and forest AGB ($W = 0.972$, $p = 0.509$) were normally distributed. To reduce uncertainty related to spatial mis-registration of the IS data set, average reflectance values of grassland from IS data were extracted for each field plot using a 2x2 pixels window. The window size for forest plots was set to 15x15 pixels.

A linear regression analysis using the APEX HCRF data and *in-situ* measured AGB values was performed to predict the relationships between AGB as the dependent variable, and the set of identified VIs as the independent variables (i.e., potential narrow-band SR and NDVI types, which were selected based on the criteria presented in the previous section).

We applied a stepwise linear regression method to select significant variables [61] using the SPSS 20.0 statistical package (IBM Crop. 2011). The probability of F was used as a criterion to include ($F < 0.05$) or to remove ($F > 0.10$) an independent variable in the stepwise multiple linear regression [62]. The statistical parameters R^2, *RMSE*, *variance inflation factor* (VIF) and *model simplicity* were used to select the best-fitting model [63]. The VIF indicates multicollinearity among variables and potential overfitting of the model [64], [65]. It is commonly accepted that a VIF value above 10 is indicative of multicollinearity [66], [63]. For both grassland and forest approximately 70% of all sample data (i.e., 54 plots of grassland and 45 plots of forest) were randomly assigned to the calibration data set, and 30% (i.e., 26 plots of grassland and 18 plots of forest) to the validation data set [34].

2.3.3 AGB mapping: discrete approach

The best calibration model suggested after the statistical analysis was applied to APEX IS data to predict grassland and forest AGB separately on a per-pixel basis. Typically, the selected model is inverted to generate the AGB map over large areas of corresponding land-cover types (i.e., grassland, forest). Boolean logic was applied to classify predominant land-cover types in discrete classes. Since there were no reference data for all land-cover types, a narrow-band NDVI (using spectral bands at 665 nm and 831 nm) in combination with thresholds was applied to separate grassland, forested areas, and non-vegetated areas (snow and soil/rock) [29]. The thresholds, i.e., defining minimum and maximum NDVI value per class, were empirically obtained considering the class affiliation of our reference plots. Because forest and grassland NDVI thresholds overlapped slightly with increasing heterogeneity (i.e., in the tree line region), the forest boundary map was manually updated by visual interpretation of a digital aerial photograph acquired in 2006 with 20 cm spatial resolution. As a result, individual masks for non-vegetated areas, grassland and forest, were created. The masks were used to delineate the three classes in the APEX data sets. Forest and grassland calibration models were then inverted class wise to predict AGB from APEX data, resulting in two individual discrete AGB maps of grassland and forested areas.

2.3.4 AGB mapping: CF mapping approach

A CF map representing AGB was calculated as function of sub-pixel vegetation cover and the thematic AGB maps of predominant land cover types (LCT). A linear spectral mixture (LSM) model was applied to generate abundance maps of predominant LCT in the

study area (i.e., forest, grassland, soil/rock and snow), while the selection of these LCT was justified by field surveys. The LSM approach assumes that the reflectance signal of a given pixel can be approximated as a linear combination of pure spectra, called *endmembers*, representative for existing LCT's within the pixel [67], [68]. Endmember spectra were selected from the image considering aerial photography and field knowledge to identify areas purely representing one surface type. To minimize uncertainties in resulting abundance estimates caused by the omission of surface heterogeneity, we selected several pixels in a closer area and calculated the endmember spectra as an average of these spectra. Abundances of all endmembers were estimated using a constraint LSM approach, summing the individual endmember abundances to unity while allowing abundances to lie below 0 or above 1 [36], [69]. Kneubühler et al. [36] demonstrated that the combination of quantitative ecosystem parameters (i.e., forest and grassland AGB) and LCT abundance information is the key input to generate CF maps (Fig. 2. 2). Three critical steps were performed before combining all input data. Firstly, the LCT abundance values were rescaled between 0 and 1. Secondly, the grassland and forest AGB thematic maps were generated by employing the respective calibration models and APEX IS data sets. Thirdly, the rescaled LCT abundance maps were multiplied with the corresponding thematic AGB maps separately. It is obvious that thematic AGB values for snow and soil/rock LCT are equal to zero. The final integration of the individual AGB maps into a combined product resulted in a map of CF values of AGB [36]. The workflow of the methodology to generate both discrete and CF maps of AGB in the study area is presented in Fig. 2. 2.

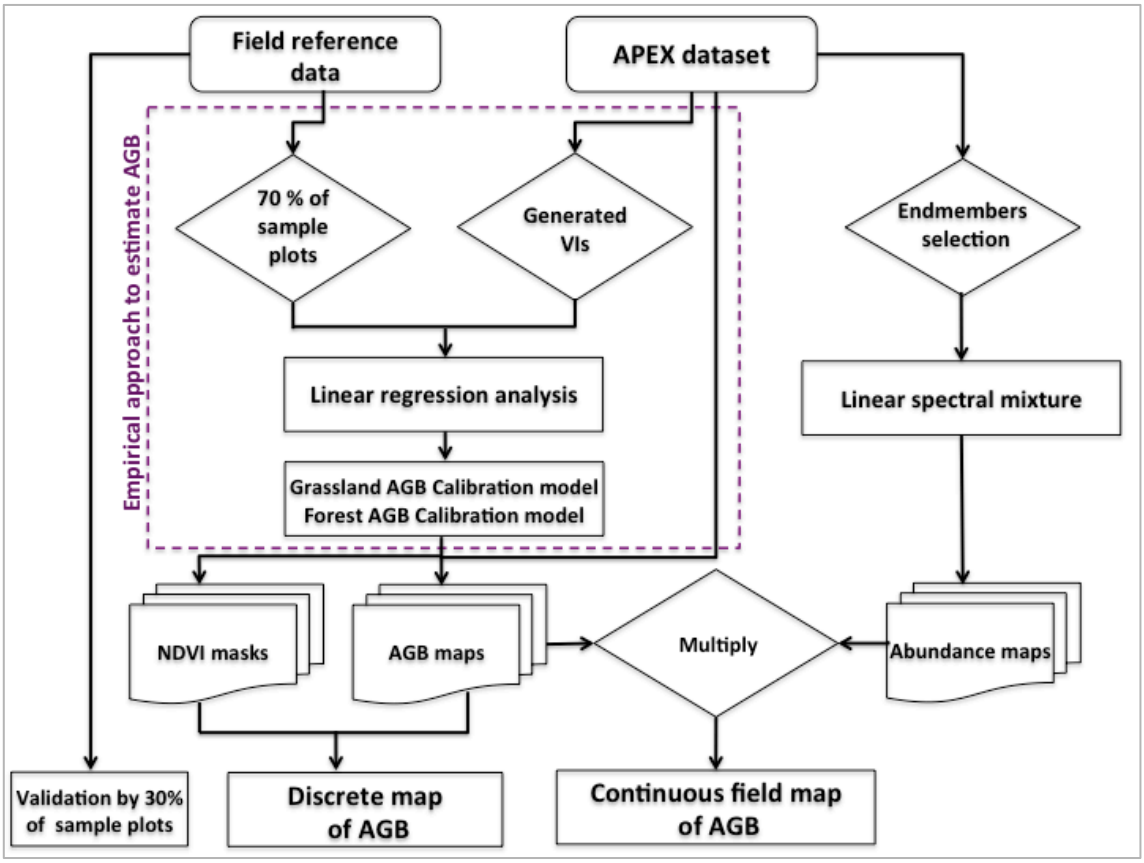

Fig. 2. 2. Flowchart illustrating the approach to generate discrete and continuous field AGB maps.

2.3.5 Validation

The validation of resulting AGB maps of both the discrete and the CF approach was performed on an independent validation dataset (i.e., 26 plots for grassland and 18 plots for forest). Forest AGB was measured in a small valley of the SNP called Val Trupchun. For the validation of grassland AGB, we consequently selected only those grass validation plots that are located in the Val Trupchun area of the SNP (n=13). The accuracy of the generated maps was quantified using the root mean square error (RMSE) and mean relative RMSE (rRMSE [%]) according to [70]–[73].

$$RMSE = \sqrt{\frac{\sum_{i=1}^{n}(\hat{y}_i - y_i)^2}{n}} \quad (4)$$

$$rRMSE = \frac{RMSE}{\bar{y}} \times 100 \quad (5)$$

where $\hat{y}_i$ is the estimated biomass, y_i is the measured biomass, n is the number of observations and $\bar{y}$ is the mean of the observed biomass. Because of the limited number

of reference plots, we applied a leave-one-out cross validation (LOOCV) according to [14] providing an unbiased estimation of the prediction error [18].

2.4 Results

2.4.1 In-situ AGB measurements

Total AGB obtained from field measurements ranged from 56 t.ha^{-1} to 521 t.ha^{-1} for forest and 0.2 t.ha^{-1} to 8.62 t.ha^{-1} for grassland (**Table 2. 2**). These value ranges represent almost the full range of AGB values reported elsewhere for alpine areas [74], [75]. The mean AGB for grassland was 3.43 t.ha^{-1} and corresponds to results reported in other grassland studies [74], [76]. For forest, we observed a mean AGB of 294 t.ha^{-1}, which is in agreement with results reported in the Swiss National Forest Inventory [75]. Grassland AGB showed a larger variability than forest AGB (**Table 2. 2**). This can be attributed to the distribution of grass plots over the entire SNP area, while forest plots were located only in the Trupchun Valley,a small part of the SNP.

Table 2. 2

Statistical overview of AGB for grassland and forest in the SNP obtained from field measurements (n = number of field plots, SD = standard deviation, CV = coefficient of variation).

Vegetation type	Mean [t.ha^{-1}]	Minimum [t.ha^{-1}]	Maximum [t.ha^{-1}]	SD [t.ha^{-1}]	CV [%]
Grassland (n = 49)	3.43	0.20	8.62	2.06	60
Forest (n = 35)	294	56	521	121	41

In-situ measured AGB for forest and grassland as used for model calibration and data validation are shown in **Table 2. 3**.

Table 2. 3

Descriptive statistics of grassland and forest AGB model calibration and validation plots (SD = standard deviation, n = number of observations).

Category	Calibration (n=54)				Validation (n=26)			
Grassland[a]	Mean	Max	Min	SD	Mean	Max	Min	SD
[t.ha^{-1}]	3.5	8.6	0.2	2	3.5	8.6	0.6	2.2
	Calibration (n=45)				Validation (n=18)			
Forest	Mean	Max	Min	SD	Mean	Max	Min	SD
[t.ha^{-1}]	292	521	56	125	281	490	62	122

[a] Four outlier plots (with considering the overlapping issue) were eliminated.

2.4.2 Empirical model to derive grassland AGB

We applied an empirical approach to derive grassland AGB from APEX IS data and tested all possible two-band combinations of SR and NDVI type VIs. The individual performances of the VIs were visualized in 2D correlation plots (correlograms). Correlograms represent the coefficients of determination (R^2) of individual linear

regression models relating APEX derived VIs and in-situ measured grassland AGB (Fig. 2. 3).

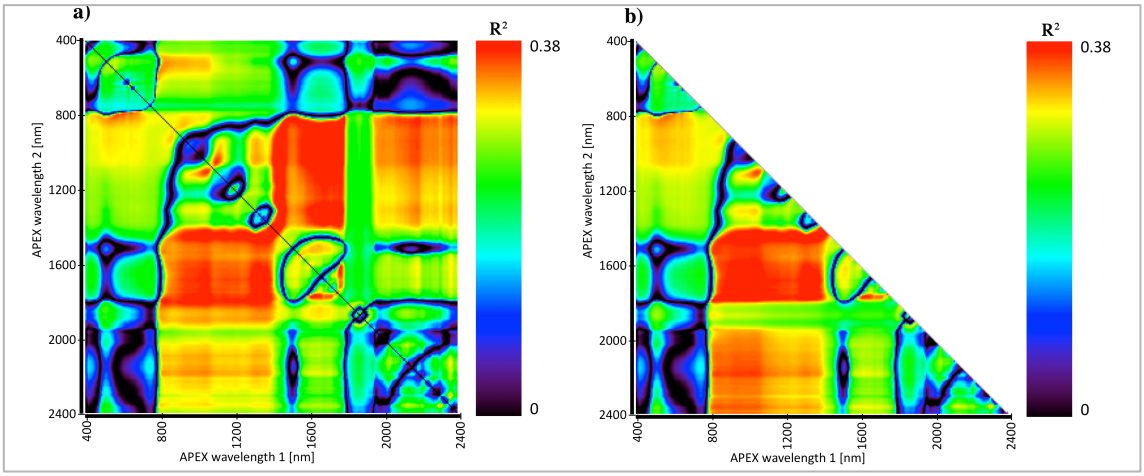

Fig. 2. 3. Correlograms showing the coefficient of determination (R^2) between simple ratio (SR) (a) and NDVI type (b) VIs for all two-band combinations and grassland AGB. For NDVI type VIs the matrix is symmetrical, hence the combinations below the diagonal line are shown only. For SR type VIs the matrix is non-symmetrical, especially in the NIR region. Therefore, the whole matrix is presented.

Based on the correlograms, we identified potential band combinations and wavelength regions showing high sensitivity to variations of grassland AGB. Sensitive band combinations are located in i) the visible (VIS) in combination with the red-edge spectral region, ii) the red-edge in combination with the near-infrared (NIR) and shortwave infrared (SWIR), and iii) the NIR in combination with the NIR or the SWIR. Because the NDVI can be considered as a linear combination of the SR, both NDVI and SR show similar patterns for grassland AGB. Identified wavelength regions are in agreement with previous studies suggesting optimal combinations in the red-edge region [30], [77], [54], the NIR, and the SWIR spectral region [22], [2], [78].

The selection of the most sensitive VIs as input for the stepwise multiple linear regression analysis considered a set of selection criteria (Section III.A) and resulted in 62 candidates for the SR and 160 candidates for the NDVI. **Table 2. 4** shows that the stepwise regression analysis has selected five different models. However, four models (i.e., model 2, model 3, model 4, and model 5) have not fulfilled the statistical collinearity requirement with VIF values greater than 10 [63]. This indicates that the stepwise multiple regression did not improve the model performance.

Table 2. 4

Selected models for grassland AGB estimation based on stepwise multiple regression analysis. (R = reflectance at specific wavelength, VIF = variance inflation factor).

Model	Variables	R^2	RMSE [$t.ha^{-1}$]	VIF
1	SR (R_{1689}/R_{851})	0.38	1.49	1.00
2	SR (R_{1689}/R_{851}) NDVI (R_{741}, R_{2260})	0.45	1.49	46.52 46.52
3	SR (R_{1689}/R_{851}) NDVI (R_{741}, R_{2260}) NDVI (R_{1199}, R_{2232})	0.51	1.41	68.38 173.27 45.47
4	SR (R_{1689}/R_{851}) NDVI (R_{741}, R_{2260}) NDVI (R_{1199}, R_{2232}) NDVI (R_{888}, R_{895})	0.55	1.36	77.38 173.32 49.85 1.98
5	SR (R_{1689}/R_{851}) NDVI (R_{741}, R_{2260}) NDVI (R_{1199}, R_{2232}) NDVI (R_{888}, R_{895}) SR (R_{1762}/R_{1627})	0.60	1.28	78.17 177.96 75.75 3.25 8.26

Table 2. 5 summarizes the results of the simple regression analysis and provides a set of quality criteria (i.e., R^2, RMSE, VIF and model simplicity) for identifying the best global model (considering all plots distributed in all flight lines (FL)). For estimating grassland AGB, the best model is a SR type VI and includes a water absorption band in the SWIR (1689 nm) and a spectral band from the NIR (851 nm), showing a negative relationship between the SR and AGB. Furthermore, the identified VI was calibrated for all individual FL to provide FL-specific calibration models for subsequent uncertainty assessments (Fig. 2. 4). All calibration models were statistically significant (*p-value <0.001*). Some FL-specific calibration models (FL4, FL6) showed an improved model fit compared to the global model.

Table 2. 5

Best performing calibration models to estimate grassland AGB based on a simple ratio (SR) narrow-band combination using spectral bands at 1689 nm and 851 nm (Y: AGB [$t.ha^{-1}$], x: SR, n = number of observations, global= all plots, FL 4 = flight line 4, FL 5 = flight line 5, FL 6 = flight line 6, FL7 = flight line 7).

Site	n	Calibration model	R^2	RMSE [$t.ha^{-1}$]
Global	54	Y = -6.18x + 8.28	0.38	1.49
FL4	6	Y= -7.82x + 10.65	0.60	1.49
FL5	17	Y =-6.86x + 8.84	0.41	1.63
FL6	18	Y = -6.69x + 8.82	0.46	1.38
FL7	13	Y = -6.98x + 8.13	0.32	1.28

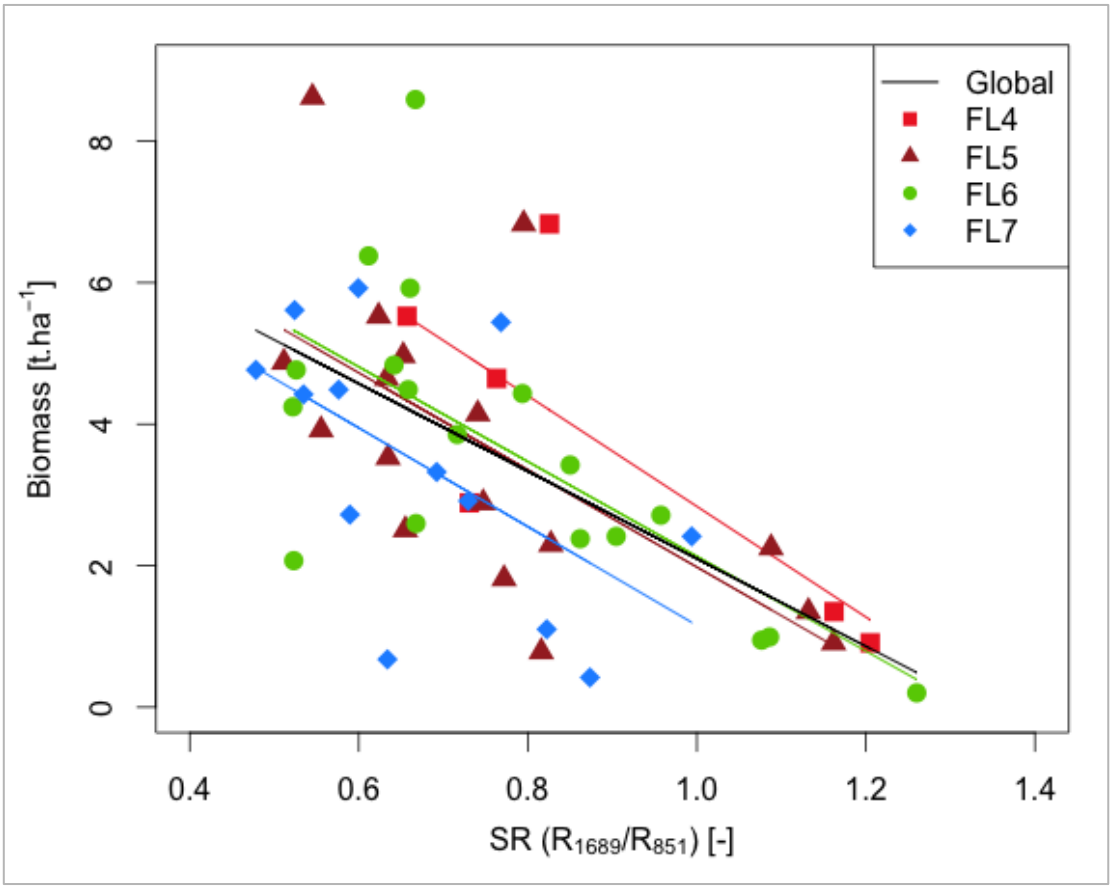

Fig. 2. 4. Relationship between the selected narrow-band Simple ratio and measured grassland AGB for all plots (global model as black line) and each flight line (colored lines). Statistics of regression lines are given in Table 2. 5**.** (FL 4 = flight line 4, FL 5 = flight line 5, FL 6 = flight line 6, FL7 = flight line 7, R = reflectance at 1689 and 851 nm).

2.4.3 Empirical model to derive Forest AGB

Similar to the approach applied for grassland AGB estimates, we derived regression models to estimate forest AGB from APEX IS data. **Fig. 2. 5** illustrates the relationships between forest AGB and all possible two-band combinations for SR and NDVI type VIs. Again, the sensitivity pattern for both VI types was similar. The wavelength regions with highest R^2 between VI and forest AGB are located in i) the red-edge and the NIR in combination with the VIS, ii) the red-edge and NIR in combination with the SWIR, and iii) the SWIR in combination with the SWIR or the VIS.

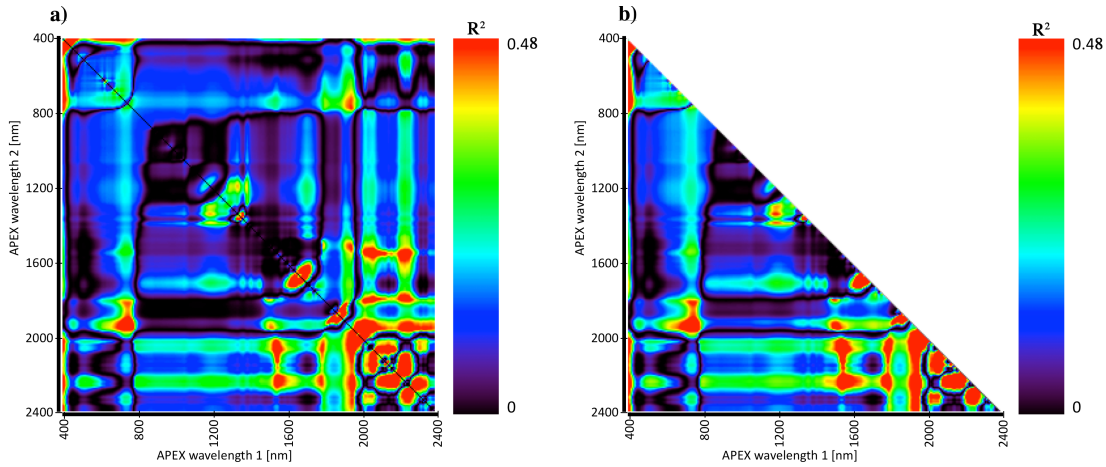

Fig. 2. 5. Correlograms showing the coefficient of determination (R^2) between simple ratio (SR) (a) and NDVI type (b) VIs for all two-band combinations and forest AGB. For NDVI type VIs the matrix is symmetrical, hence the combinations below the diagonal line are shown only. For SR type VIs the matrix is non-symmetrical, especially in the 1600-2000 nm region. Therefore the whole matrix is presented.

The selection of the most sensitive regression model followed the same procedure as described for grassland AGB. 25 candidates for the SR and 35 candidates for the NDVI were used to estimate forest AGB using stepwise multiple regression analysis. Three different models were selected (**Table 2. 6**), while the VIF value is relatively high (VIF > 10) for model 2 and model 3. Consequently, the stepwise multiple regression did not reveal an improved model performance.

Table 2. 6

Selected models for forest AGB estimation based on stepwise multiple regression analysis. (R = reflectance at specific wavelength, VIF = variance inflation factor).

Model	Variables	R^2	RMSE [t.ha^{-1}]	VIF
1	SR (R_{1498}/R_{2112})	0.45	97.28	1.00
2	SR (R_{1498}/R_{2112}) SR (R_{1698}/R_{1636})	0.50	87.71	12.52 12.52
3	SR (R_{1498}/R_{2112}) SR (R_{1698}/R_{1636}) SR (R_{2286}/R_{2169})	0.55	83.44	12.46 4.97 21.06

The best simple regression models to estimate forest AGB for all plots and FLs (global model) and for the individual FLs are shown in **Table 2. 7**. All calibration models were statistically significant (*p-value <0.001*). Only the individual calibration model for FL5 showed a higher performance to estimate forest AGB compared to the global model.

Table 2. 7

Best performing calibration models to estimate forest AGB based on a SR narrow-band combination using spectral bands at 1498 nm and 2112 nm (Y: AGB [t.ha^{-1}], x: SR, n = number of observations, global = all plots, FL 5 = flight line 5, FL 6 = flight line 6, FL7 = flight line 7).

Site	n	Calibration model	R^2	RMSE [t.ha^{-1}]
Global	45	Y = 693.61x - 901.53	0.45	97.28
FL5	9	Y = 889.73x - 1199.6	0.72	73.45
FL6	25	Y = 952.12x - 1343.9	0.43	100.23
FL7	11	Y = 617.88x - 787.55	0.34	110.11

The final calibration model for estimating forest AGB is a SR type VI employing the spectral bands at 1498 nm and 2112 nm and showing a positive correlation with forest AGB (Fig. 2. 6). It is important to note that the linear relationship is strongly affected by two sample plots located in FL7 with moderate AGB (around 250 t.ha-1) but relatively high SR values. For both grassland and forest AGB estimations, NDVI type VIs did not lead to improved model fits.

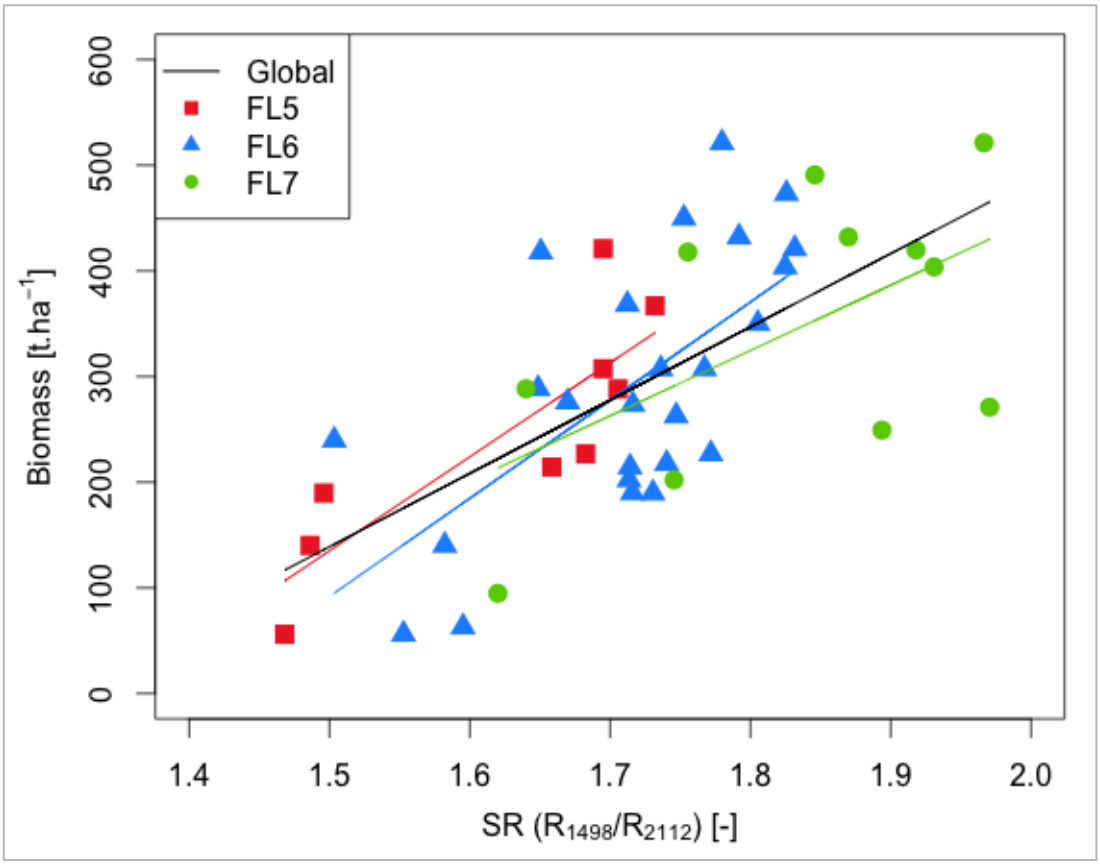

Fig. 2. 6. Relationship between narrow-band SR and measured forest AGB for all plots (global model as black line) and each flight line (colored lines). Statistics of regression lines are given in Table 2. 7.. (FL 5 = flight line 5, FL 6 = flight line 6, FL7 = flight line 7, R = reflectance at 1498 and 2112 nm).

2.4.4 Fractional abundances of predominant land cover types

AGB mapping using the CF approach relies on the accuracy of estimated fractional abundance maps of involved LCTs. The applied LSM approach is based on image endmembers (Fig. 2. 7) and was applied for each flight line separately.

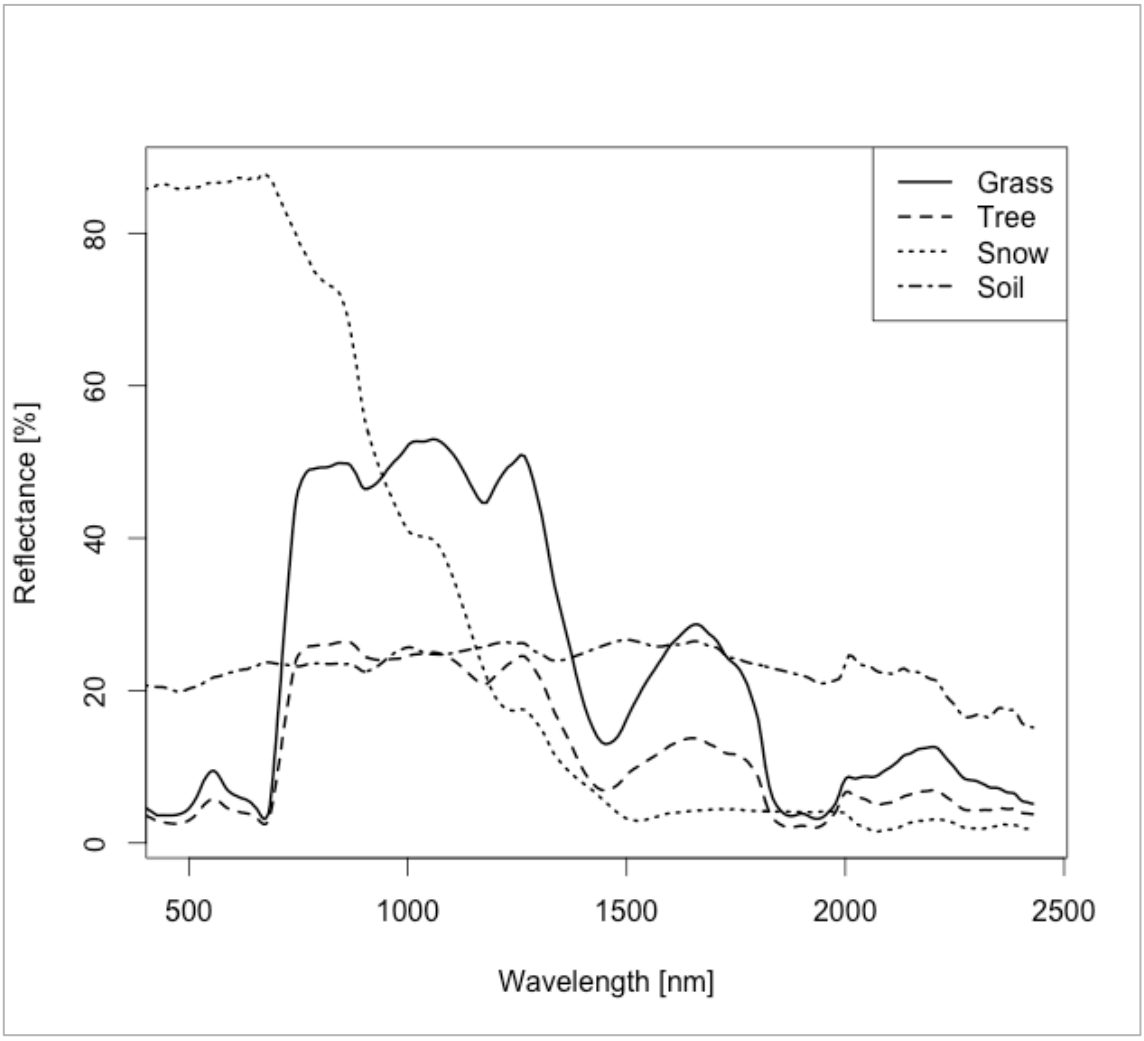

Fig. 2. 7. Image based endmember spectra extracted from flight line 6.

In absence of quantitative reference information, we qualitatively assessed the accuracy of retrieved abundance maps considering the grassland and forest reference plots (Fig. 2. 8). As expected, fractional abundances of grass are dominant in grass plots (Fig. 2. 8-left). Some grass plots show a notable fraction of soil, likely caused by heterogeneity of these plots in terms of canopy closure. Further, three grass plots were placed in the vicinity of forested areas and show confusion with forest abundances. This demonstrates that even with reasonable distance between grass plots and forest (i.e., more than 10 m) multiple scattering effects can determine interferences between grass

and forest reflectance. Highest forest abundances were observed in forest plots (Fig. 2. 8-right). The fractional amounts of snow and soil are almost zero, but grass reaches abundances above zero. This is due to the low density of the forest plots where forest mixes spatially with other LCT, mainly grass. This qualitative performance assessment provides evidence on the suitability of the LSM approach to differentiate fractional abundances of predominant LCT.

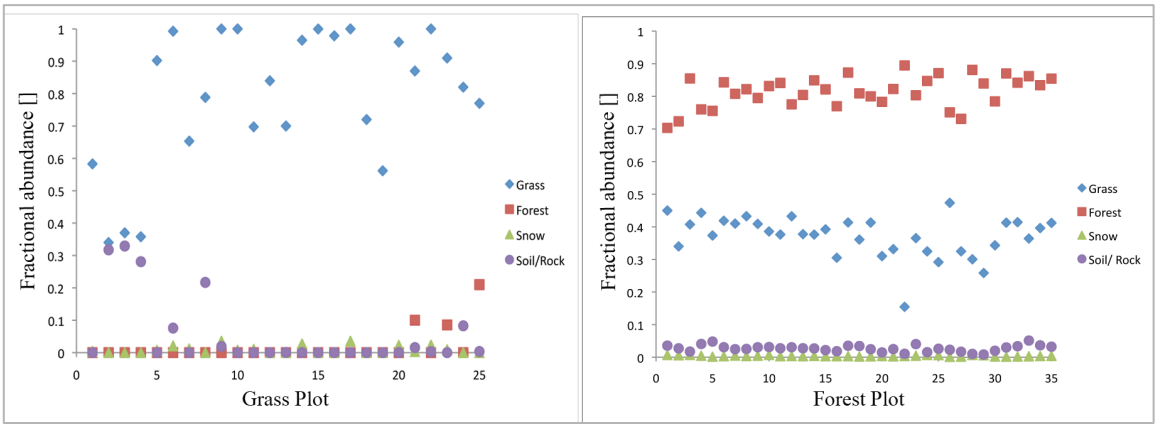

Fig. 2. 8. Variation of LSM derived abundance estimates for in-situ reference grassland and forest plots. Left: grassland plots. Right: forest plots.

Beside the qualitative assessment, we quantitatively assessed the accuracy of the LSM result using the overall residual error (RMSE) provided by the LSM approach [36]. Mean RMSE values for the individual LCTs confirmed the good performance of the LSM approach. Forested areas show a RMSE of 1.17% reflectance (SD=0.6% reflectance), grassland of 1.14% reflectance (SD=0.6 reflectance), snow of 1.07% reflectance (SD=0.4% reflectance), and soil/rock of 0.92% reflectance (SD=0.59% reflectance).

2.4.5 Grassland and forest AGB maps

Global calibration models for forest and grass AGB (Tables **Table 2. 5** and **Table 2. 7**) were used to generate a discrete pixel-based map of total AGB (Fig. 2. 9(b)). The AGB representation based on the CF mapping approach is shown in Fig. 2. 9(c). For both approaches, green colors indicate grassland AGB and blue to white colors represent forest AGB. The average AGB derived from the discrete approach is 123 t.ha^{-1}, while the CF approach revealed 115 t.ha^{-1}. For forested areas and grassland, AGB values of 260 t.ha^{-1} and 3.04 t.ha^{-1} could be obtained with the discrete approach while the CF approach reveals AGB values of 234 t.ha^{-1} and 2.86 t.ha^{-1}. It must be noted that the distribution of both forest and grassland AGB follows an elevation gradient. Further, the discrete approach results in

hard boundaries between LCTs (Fig. 2. 9(b)). In contrast, the CF mapping approach better represents the heterogeneity within and between classes and shows subtle gradients of AGB due to the usage of sub-pixel information of respective LCT abundances.

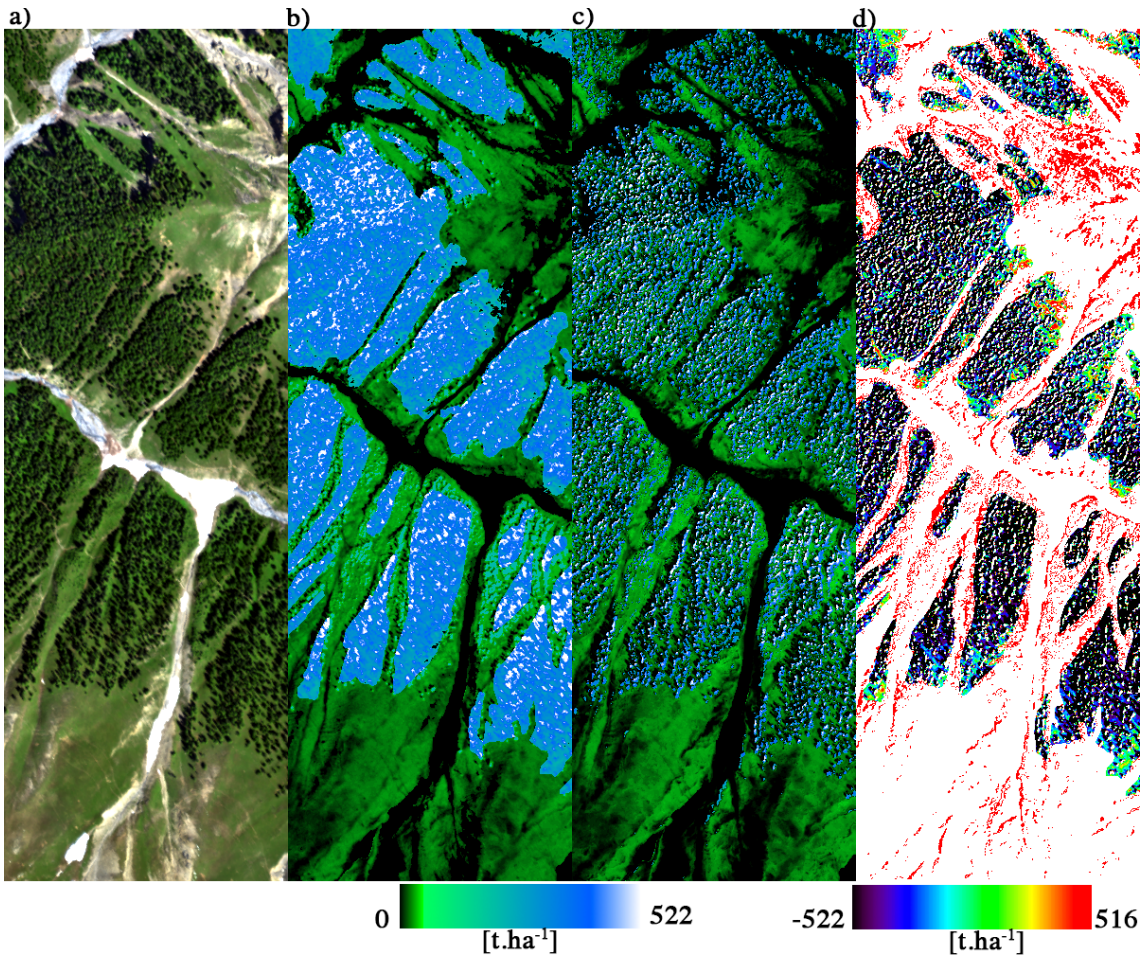

Fig. 2. 9. Total AGB derived from APEX IS data based on the discrete and the CF mapping approach. Study site represented as true color composite (a), the AGB map based on the discrete approach (b), the AGB map based on the CF mapping approach (c), and the spatial difference map between the two approaches (d).

Spatial differences between the discrete and the CF approach are shown in Fig. 2. 9(d). The magnitude of differences follows a gradient pattern: extreme differences appear at low elevations and decrease with increasing elevation. Extreme spatial differences appear as well around the tree line. Further, a positive correlation between forest abundance and spatial differences could be observed. Both grass and soil/rock abundance maps show a negative correlation with the difference map.

The quantitative validation of APEX derived AGB maps was based on a comparison with *in-situ* measured AGB values by applying a LOOCV approach that allows detecting and accounting for outliers [28], [59], [79]. After applying the LOOCV, we could identify one

field plot showing exceptional values for both vegetation land-cover types (i.e., forest and grassland). These plots were excluded from further validation.

In general, the accuracy of estimated AGB is higher for grassland compared to forests (**Table 2. 8**). The discrete mapping approach shows a good agreement of APEX derived and *in-situ* measured grassland AGB with a R^2 of 0.65, a mean RMSE of 0.91 t.ha^{-1}, and a mrRMSE of 26%. The CF mapping approach results in an even higher accuracy with a R^2 of 0.94, a RMSE of 0.55 t.ha^{-1}, and a mrRMSE of 15% (Fig. 2. 10). For forest AGB, the discrete approach predicted forest AGB with a R^2 of 0.64, a mean RMSE (mRMSE) of 67.8 t.ha^{-1}, and a mean relative RMSE (mrRMSE) of 25%. The CF mapping approach again improved the performance with resulting in a R^2 of 0.85, a mean RMSE of 55.85 t.ha^{-1}, and a mrRMSE of 21% (Fig. 2. 11).

Table 2. 8

Performance of the discrete and the CF mapping approaches to estimate forest and grassland AGB (mean coefficient of determination (R^2 ± SD), mean root mean square error (mRMSE ± SD), mean relative root mean square error of prediction (mrRMSE% ± SD).

Grassland (n=12)			
Method	R^2	mRMSE [t.ha^{-1}]	mrRMSE [%]
Discrete approach	0.65 ± 0.05	0.91 ± 0.05	26 ± 1.42
CF mapping	0.94 ± 0.03	0.55 ± 0.04	15 ± 1.04
Forest (n=17)			
Method	R^2	mRMSE [t.ha^{-1}]	mrRMSE [%]
Discrete approach	0.64 ± 0.05	67.80 ± 2.56	25 ± 0.95
CF mapping	0.85 ± 0.02	55.85 ± 2.15	21 ± 0.79

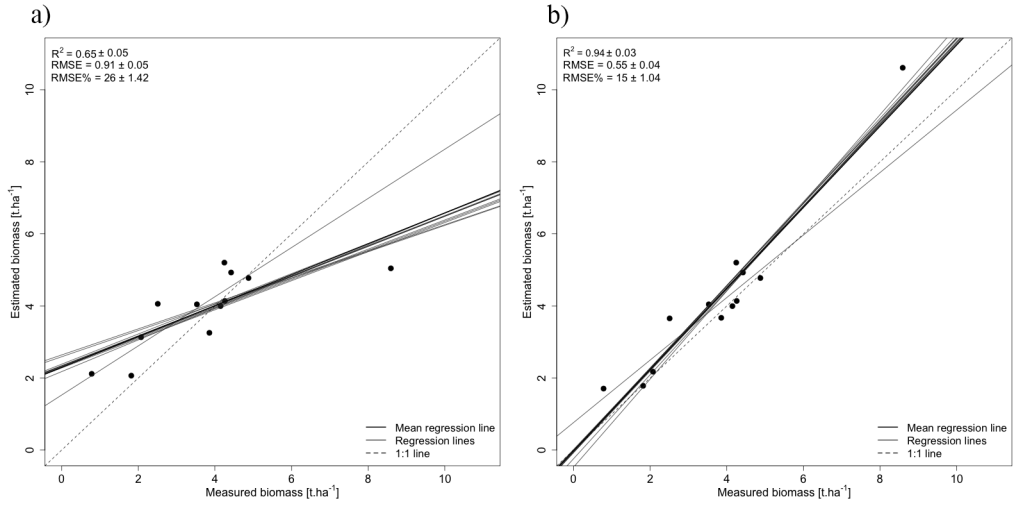

Fig. 2. 10. Agreement of APEX derived grassland AGB with in-situ data. AGB based on the discrete approach (a) and the CF mapping approach (b). Coefficient of determination (R^2 ± SD), root mean square error (RMSE ± SD), relative root mean square error of prediction (RMSE%) are shown.

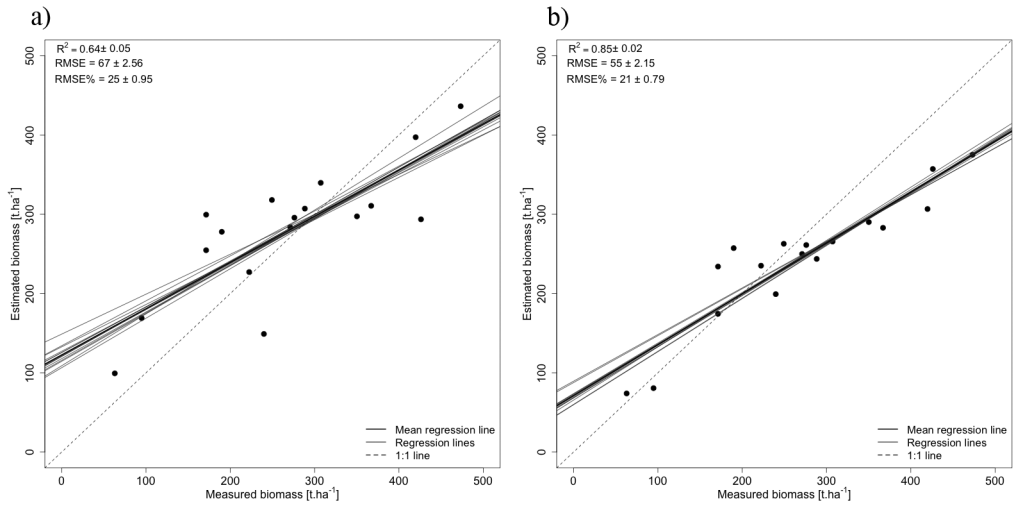

Fig. 2. 11. Agreement of APEX derived forest AGB with in-situ data. AGB based on the discrete approach (a) and the CF mapping approach (b). Coefficient of determination (R^2 ± SD), root mean square error (RMSE ± SD), relative root mean square error of prediction (RMSE%) are shown.

The discrete approach yielded lower accuracies compared to the CF approach for both grassland and forest. For both cases, the discrete approach tends to overestimate low AGB values, while high AGB values were underestimated (Fig. 2. 10(a)). The CF based AGB estimate shows a slight overestimation for high grassland AGB values (Fig. 2. 10(b)) but an underestimation for dense forest (Fig. 2. 11(b)). Further, mean grassland AGB using the discrete and the CF mapping approach considering validation data were 3.8 ± 1.06 $t.ha^{-1}$, and 4.2 ± 2.3 $t.ha^{-1}$, respectively. Compared with the mean value of the reference data (i.e., 3.75 ± 1.9 $t.ha^{-1}$) the CF mapping as well as the discrete approach both showed an overestimation of grassland AGB. Forest mean AGB values obtained with the discrete and the CF mapping approach considering validation data were 279 ± 83 $t.ha^{-1}$, and 245 ± 79 $t.ha^{-1}$, respectively. Considering again the mean AGB of our validation data (i.e. 269 ± 114 $t.ha^{-1}$) the CF mapping approach shows underestimation and the discrete approach an overestimation of forest AGB.

2.4.6 Assessment of Directional Effects on the AGB Retrieval

A comparison of HCRF spectra corresponding to the same sample plots but extracted from two adjacent APEX flight lines revealed differences in HRCF values. These differences can be attributed to surface anisotropy effects [34], [80] and remaining topographic effects after the atmospheric compensation. To evaluate potential uncertainties in retrieved AGB maps due to surface anisotropy, we investigated AGB differences along a transect in the overlapping region of two adjacent APEX data sets. Fig. 2. 12 shows the

agreement of grassland AGB values (extracted from the discrete AGB map) derived from the two APEX flight lines over the same area. Corresponding view angles per target depend on the actual location with respect to the sensors field of view and range between +/- 7-14° off-nadir.

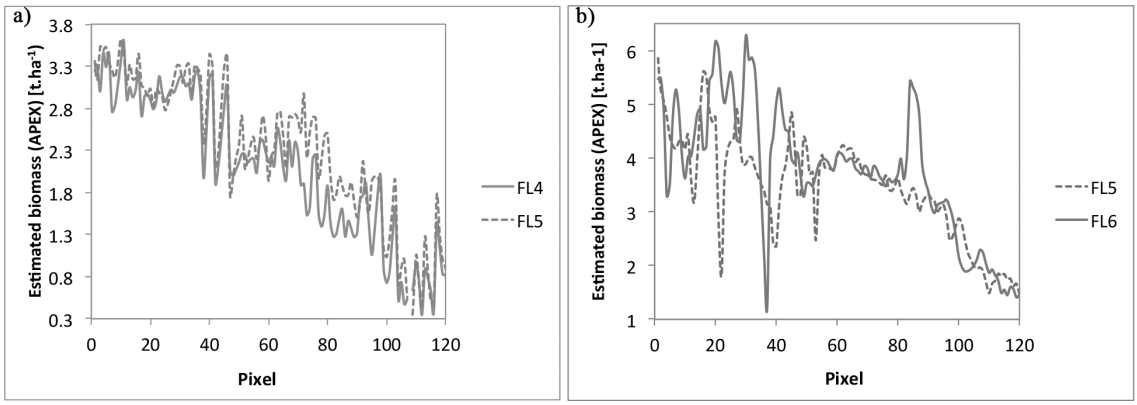

Fig. 2. 12. Estimated discrete grassland AGB extracted from an overlapping region of APEX flight line 4 and flight line 5 (a), and of flight line 5 and flight line 6 (b), respectively (FL 4 = flight line 4, FL 5 = flight line 5, FL 6 = flight line 6).

In general, a good agreement (R^2 = 0.90) between grassland AGB values in the overlapping regions mainly covered with grass was found (Fig. 2. 12(a)). In areas with a higher abundance of trees, uncertainties between two observations with contrasting viewing angles increase, resulting in a R^2 of 0.7 (Fig. 2. 12(b)). In addition to more pronounced anisotropy effects in forested areas, the decrease of agreement can be superimposed by the weaker performance of the forest AGB model compared to the grassland model. With increasing abundances of trees the uncertainty of the total AGB map increases. The AGB differences for grassland, forest, and total AGB between the two flight lines in the overlapping region are 0.1 $t.ha^{-1}$ (grassland), 1.9 $t.ha^{-1}$ (forest) and 2.6 $t.ha^{-1}$ (total AGB) for the discrete approach, and 0.3 $t.ha^{-1}$ (grassland), 0.5 $t.ha^{-1}$ (forest), 1.2 $t.ha^{-1}$ (total AGB) for the CF approach, respectively.

2.5 Discussion

2.5.1 Biomass estimation using empirical approaches and IS data

Empirical approaches are frequently applied in optical remote sensing to estimate biomass of vegetated ecosystems. The retrieval of volumetric vegetation parameters from optical data suffers from intrinsic limitations, e.g., being not transferable from one site to another [9], or missing causality of light interaction with vegetation surfaces. With the

careful consideration of crucial factors, we could partly compensate for these influential factors. This allowed us to successfully apply an empirical approach for obtaining AGB of a heterogeneous ecosystem and to finally evaluate the performance of a discrete and continuous mapping approach. AGB estimates obtained for forest ecosystems are comparable or even better than results reported elsewhere: A recent paper [14] summarized studies that use optical remote sensing for forest AGB estimation and reported accuracy ranges for the R^2 of 0.50-0.70 and for the RMSE of 30-60 $t.ha^{-1}$. Other studies using IS report AGB retrieval accuracies with a R^2 ranging between 0.36 – 0.65 [64], [25], [81], [82], [28], [31], [83]. As demonstrated in **Table 2. 8**, the R^2 obtained by our discrete approach is within reported accuracy ranges for optical data, while the CF mapping approach outperformed the accuracy of forest AGB estimates with a R^2 of 0.84 and a relative RMSE of 21%.

For grasslands, the performance of our discrete approach lies also in the accuracy range indicated in various studies (e.g., [29], [18], [79], [84]), but was below the accuracy of other studies using field spectroscopy data [30], [77], [85], IS data [2], or multispectral data [32], [60], [62], [86]. Again, the CF approach yielded better performance in estimating grassland AGB compared to the discrete approach. The accuracy of the CF approach corresponds to the one reported by [2] for a semi-natural grassland habitat in the central part of Switzerland (R^2 = 0.86 and relative RMSE = 30%).

It must be acknowledged that optical data tend to saturate with higher amounts of biomass. Although also our approach tends to underestimate AGB, we found a good sensitivity to map biomass with optical data in an alpine environment. This can be explained by the lower amount of biomass due to harsh environmental conditions in combination with the relatively early data acquisition for such high alpine test sites, where the phenological cycle starts late in the year [36].

For the grassland, we found a band combination that incorporates the SWIR and NIR spectral regions as most sensitive index. Mechanistically, the index contrasts a spectral region affected by vegetation water content (SWIR band at 1689 nm) [87] against a highly reflective part in the NIR (851 nm) with almost maximum scattering and no absorption dominating factors. Such a band combination has previously been reported to be applicable for estimating photosynthetically active and non-active vegetation, as well as AGB [88]. Other authors reported similar results when estimating grassland AGB [2], [78], [84] or grassland LAI [22], [59], [89]. Ustin et al. [88], for example, suggest that an accurate estimation of grassland and forest AGB requires the full spectrum including the SWIR. In contrast, [18] indicate that indices using wavelengths in the SWIR region are not

better than the traditional indices using red and NIR wavelengths for estimating fresh grassland AGB of agricultural crops. A possible explanation why we found the SWIR spectral region as most important is related to the composition of our study area: The SNP is a strictly protected area without any management. AGB is consequently a mixture of dry plant material from past years (dry plant residues) and fresh AGB. Since dry plant materials show largest variability in the SWIR region [90], we likely found the SWIR as highly sensitive for grassland AGB.

As illustrated in **Fig. 2. 5** observed variation patterns of R^2 for forest differ from patterns found for grassland. For the forest correlograms it is worth to note that spectral bands in the SWIR part of the spectrum seem to be crucial for the estimation of forest AGB. These findings are in line with previous studies reporting optimal band combinations of NIR and VIS [28], [72], [91], NIR and SWIR [45], [19], [92], as well as SWIR and SWIR [45], [28], [93]. Furthermore, high correlations between the SWIR region or SWIR band combinations and forest AGB using IS data [81], [28], [31], [25] and multispectral optical data [72], [19], [92] have been reported frequently. The reflectance behavior of forest canopies in the SWIR is strongly affected by canopy water content, canopy biochemical properties such as cellulose, lignin and protein [94], and shadowing [92]. Forest AGB is directly related to these parameters, and as a consequence, indirectly to the SWIR reflectance and absorption of the spectrum [84].

Irrespective of the used model, surface anisotropy likely affects the retrieval of vegetation variables since surface reflectances vary with changing observation angles even if data were corrected for atmospheric distortions. Reference plots used for model calibration must be distributed across the entire view angle range to account for potential anisotropy effects. In our case, reference plots did not span the entire range of observation angles as the accessibility to some sites was limited, causing uncertainties of up to 1-2 %.

2.5.2 CF vs discrete mapping of AGB in heterogeneous environment

We tested two approaches that allow representing environmental variables across various land cover types in a heterogeneous alpine environment. Results of the discrete approach for grassland and forest AGB are in line with previous studies using *in-situ* field spectrometer data and airborne IS data to estimate grassland AGB [29], [18], [79], [84]. However, the discrete approach tends to overestimate low AGB and underestimates high AGB (Fig. 2. 10(a) and Fig. 2. 11(a)), a well-known issue called 'local bias' [45]. The local bias effect has been well addressed in previous studies and was attributed to non-linear relationships between spectral indices and AGB [45], [55], [90], [15], [14]. It has its origin

in the saturation of reflectance data in dense and multi-layered vegetation canopies with complex understory and soil components, especially where the forest canopies are not closed [45]. The CF mapping approach allows compensating for the local bias effect by isolating the vegetation and understory components. In result, estimated AGB values were closer to the 1:1 line (Fig. 2. 10(b), and Fig. 2. 11(b)). However, the CF approach tends to slightly overestimate grassland AGB estimates for high AGB levels (Fig. 2. 10(b)), likely caused by multiple scattering effects of trees in close vicinity of the respective grass reference plot. Nevertheless, our results indicate that the CF mapping approach can reduce the main source of uncertainties when grassland and forest AGB are estimated by incorporating fractional abundances of dominant LCT and isolating vegetation proportion in a given pixel.

The successful implementation of a CF mapping approach relies on the capability of the applied spectral mixture analysis to provide high quality maps of fractional abundances of dominant LCT. Our results show that with increasing surface heterogeneity, the mixture of spectral reflectance of different endmembers is non-linear [95] due to multiple scattering between the involved land-cover types [96]. Separating fractional amounts of present LCT remains challenging and determines the success of the presented CF approach over highly complex landscapes.

2.6 Conclusion

We evaluated the capability of a discrete and a continuous mapping approach to represent the distribution of AGB across a heterogeneous alpine environment. Although both approaches are generally capable to map grassland and forest AGB, the CF mapping approach shows several advantages including better capability to incorporate heterogeneity effects caused by changing understory or varying soil background. In this context, the results using linear spectral mixture approaches are considered as more helpful, since the CF mapping approach relies on accurate abundance estimates of predominant LCT. Further, results of this study provide evidence that the concept of continuous fields allow successful representations of ecosystem parameters in complex environments.

Effects of surface anisotropy, topography, or time lags between data acquisitions are important aspects impacting the accuracy of AGB retrieval using IS data and need to be further elaborated in the future. The consideration of dry plant material in spectral mixture analysis and subsequent AGB retrievals will lead to further improvements of AGB estimates, including an update of AGB semantics depending on ecosystem services

definition. Applying empirical approaches to estimate vegetation properties (i.e., biochemical and biophysical quantities) from remotely sensed data have some well-known drawbacks: models are i) sensor specific, ii) specific to the dataset used for calibration, and iii) rely on extensive *in-situ* data [15], [45], [28], [22]. However, empirical approaches have seen a more widespread use due to their ease of implementation [97], [98]. In our paper the main objective was to examine the capability of a CF mapping approach to generate an AGB map compared to a discrete approach (traditional approach) in a complex environment rather than introducing a global calibration model to estimate AGB. The choice of a calibration model might not yet present the best possible solution in term of transferability, since we used the same calibration model to test the suitability of both approaches. Nevertheless, it was considered sufficiently accurate for our purpose. We are aware of the fact that vegetation biomass estimation is challenged by its dependence on phenological stages. To take into account seasonal variability, the multi-temporal acquisition of data and related ground truth is crucial. Consequently, the development of phenology-independent calibration models may be possible. Besides phenology, the development of species- or plant functional types-specific calibration models for biomass estimation needs consideration as well. In this study, we measured an extensive range of biomass for both grassland and forested areas to capture its full variability in the study area. However, the SNP is the only national park in the Alps that has been categorized by IUCN as a strict nature reserve, which corresponds to the highest protection level. We were limited in our activities by legal limitations imposed by the park authorities. The possibility to collect a richer temporal dataset, including species and plant functional types would provide a major benefit to improve the predictive power of biomass estimations. In conclusion, further research is needed to test the capability of the CF mapping approach to assess ecosystem properties, both in combination with other approaches (e.g., physical-based approaches), as well as in different environments.

Acknowledgements

The authors would like to thank the Swiss National Park staff for collecting grassland biomass in-situ data, and for providing logistic support during field campaigns. We are grateful to numerous colleagues at the Remote Sensing Laboratories (RSL) of the University of Zürich who supported our fieldwork. The contribution of MES is supported by the University Research Priority Program on 'Global Change and Biodiversity' (URPP GCB). We also thank the University of Kurdistan for financial support. We wish to thank

the editor and three anonymous referees for their detailed reviews that substantially improved the content of this paper.

References

[1] J. E. Luther, R. A. Fournier, D. E. Piercey, L. Guindon, and R. J. Hall, "Biomass mapping using forest type and structure derived from Landsat TM imagery," Int. J. Appl. Earth Obs. Geoinf., vol. 8, no. 3, pp. 173–187, Sep. 2006.

[2] A. Psomas, M. Kneubühler, S. Huber, and K. Itten, "Hyperspectral remote sensing for estimating aboveground biomass," Int. J. Remote Sens., vol. 32, no. 24, pp. 9007–9031, 2011.

[3] S. Tuominen, K. Eerikäinen, A. Schibalski, M. Haakan, and A. Lehtonen, "Mapping biomass variables with a multi-source forest inventory technique," Silva Fenica, vol. 44, no. 1, pp. 109–119, 2010.

[4] M. V. Gil, D. Blanco, M. T. Carballo, and L. F. Calvo, "Carbon stock estimates for forests in the Castilla y León region, Spain. A GIS based method for evaluating spatial distribution of residual biomass for bio-energy," Biomass and Bioenergy, vol. 35, no. 1, pp. 243–252, Jan. 2011.

[5] S. Etzold, N. K. Ruehr, R. Zweifel, M. Dobbertin, A. Zingg, P. Pluess, R. Häsler, W. Eugster, and N. Buchmann, "The Carbon Balance of Two Contrasting Mountain Forest Ecosystems in Switzerland: Similar Annual Trends, but Seasonal Differences," Ecosystems, vol. 14, no. 8, pp. 1289–1309, Sep. 2011.

[6] IPCC, "Good practice guidance for land use, land-use change and forestry," 2003.

[7] D. Minjie, G. Qingzhu, W. Yunfan, L. Yue, G. Yaqi, G. Zhabu, Y. Liu, and X. Qin, "Biomass estimation of alpine grasslands under different grazing intensities using spectral vegetation indices," Can. J. Remote Sens., vol. 37, no. 4, pp. 413–421, 2011.

[8] D. L. Peterson, K. P. Price, and E. a. Martinko, "Investigating Grazing Intensity and Range Condition of Grasslands in Northeastern Kansas Using Landsat Thematic Mapper Data," Geocarto Int., vol. 17, no. 4, pp. 15–26, Dec. 2002.

[9] A. Schweiger, A. C. Risch, A. Damm, M. Kneubühler, R. Haller, M. E. Schaepman, and M. Schütz, "Using imaging spectroscopy to predict aboveground plant biomass in alpine grasslands grazed by large ungulates," J. Veg. Sci., vol. 26, pp. 175–190, 2015.

[10] J. Boone Kauffman, D. L. Cummings, and D. E. Ward, "Relationships of Fire, Biomass and Nutrient Dynamics along a Vegetation Gradient in the Brazilian Cerrado," J. Ecol., vol. 82, no. 3, pp. 519–531, 1994.

[11] J. Verbesselt, B. Somers, J. van Aardt, I. Jonckheere, and P. Coppin, "Monitoring herbaceous biomass and water content with SPOT VEGETATION time-series to improve

fire risk assessment in savanna ecosystems," Remote Sens. Environ., vol. 101, no. 3, pp. 399–414, Apr. 2006.

[12] S. Deng, Y. Shi, Y. Jin, and L. Wang, "A GIS-based approach for quantifying and mapping carbon sink and stock values of forest ecosystem: A case study," Energy Procedia, vol. 5, pp. 1535–1545, Jan. 2011.

[13] L. Ji, B. K. Wylie, D. R. Nossov, B. Peterson, M. P. Waldrop, J. W. McFarland, J. Rover, and T. N. Hollingsworth, "Estimating aboveground biomass in interior Alaska with Landsat data and field measurements," Int. J. Appl. Earth Obs. Geoinf., vol. 18, pp. 451–461, Aug. 2012.

[14] S. G. Zolkos, S. J. Goetz, and R. Dubayah, "A meta-analysis of terrestrial aboveground biomass estimation using lidar remote sensing," Remote Sens. Environ., vol. 128, pp. 289–298, Jan. 2013.

[15] D. Lu, "The potential and challenge of remote sensing-based biomass estimation," Int. J. Remote Sens., vol. 27, no. 7, pp. 1297–1328, Apr. 2006.

[16] K. T. Vashum and S. Jayakumar, "Methods to Estimate Above-Ground Biomass and Carbon Stock in Natural Forests - A Review," J. Ecosyst. Ecography, vol. 02, no. 04, 2012.

[17] R. Houghton, K. Lawrence, J. Hackler, and S. Brown, "The spatial distribution of forest biomass in the Brazilian Amazon: a comparison of estimates," Glob. Chang. Biol., vol. 7, no. 7, pp. 731–746, 2001.

[18] J. Clevers, G. Van der Heijden, S. Verzakov, and M. E. Schaepman, "Estimating grassland biomass using SVM band shaving of hyperspectral data," Photogramm. Eng. Remote Sens., vol. 73, no. 10, pp. 1141–1148, 2007.

[19] D. Lu, P. Mausel, E. Brondízio, and E. Moran, "Relationships between forest stand parameters and Landsat TM spectral responses in the Brazilian Amazon Basin," For. Ecol. Manage., vol. 198, no. 1–3, pp. 149–167, Aug. 2004.

[20] F. D. Schneider, R. Leiterer, F. Morsdorf, J. Gastellu-etchegorry, N. Lauret, N. Pfeifer, and M. E. Schaepman, "Simulating imaging spectrometer data: 3D forest modeling based on LiDAR and in situ data," Remote Sens. Environ., vol. 152, pp. 235–250, Sep. 2014.

[21] A. Viña, A. A. Gitelson, A. L. Nguy-robertson, and Y. Peng, "Comparison of different vegetation indices for the remote assessment of green leaf area index of crops," Remote Sens. Environ., vol. 115, no. 12, pp. 3468–3478, 2011.

[22] R. Darvishzadeh, C. Atzberger, A. Skidmore, and M. Schlerf, "Mapping grassland leaf area index with airborne hyperspectral imagery: A comparison study of statistical approaches and inversion of radiative transfer models," ISPRS J. Photogramm. Remote Sens., vol. 66, no. 6, pp. 894–906, Nov. 2011.

[23] S. A. Soenen, D. R. Peddle, R. J. Hall, C. A. Coburn, and F. G. Hall, "Estimating aboveground forest biomass from canopy reflectance model inversion in mountainous terrain," Remote Sens. Environ., vol. 114, no. 7, pp. 1325–1337, Jul. 2010.

[24] B. Koch, "Status and future of laser scanning, synthetic aperture radar and hyperspectral remote sensing data for forest biomass assessment," ISPRS J. Photogramm. Remote Sens., vol. 65, no. 6, pp. 581–590, Nov. 2010.

[25] S. M. De Jong, E. J. Pebesma, and B. Lacaze, "Above-ground biomass assessment of Mediterranean forests using airborne imaging spectrometry: the DAIS Peyne experiment," Int. J. Remote Sens., vol. 24, no. 7, pp. 1505–1520, Jan. 2003.

[26] R. J. Hall, R. S. Skakun, E. J. Arsenault, and B. S. Case, "Modeling forest stand structure attributes using Landsat ETM+ data: Application to mapping of aboveground biomass and stand volume," For. Ecol. Manage., vol. 225, no. 1–3, pp. 378–390, Apr. 2006.

[27] G. Lemaire, C. Francois, K. Soudani, D. Berveiller, J. Pontailler, N. Breda, H. Genet, H. Davi, and E. Dufrene, "Calibration and validation of hyperspectral indices for the estimation of broadleaved forest leaf chlorophyll content, leaf mass per area, leaf area index and leaf canopy biomass," Remote Sens. Environ., vol. 112, no. 10, pp. 3846–3864, Oct. 2008.

[28] M. A. Cho and A. K. Skidmore, "Hyperspectral predictors for monitoring biomass production in Mediterranean mountain grasslands: Majella National Park, Italy," Int. J. Remote Sens., vol. 30, no. 2, pp. 499–515, Jan. 2009.

[29] M. Schlerf, C. Atzberger, and J. Hill, "Remote sensing of forest biophysical variables using HyMap imaging spectrometer data," Remote Sens. Environ., vol. 95, no. 2, pp. 177–194, Mar. 2005.

[30] O. Mutanga and A. K. Skidmore, "Hyperspectral band depth analysis for a better estimation of grass biomass (Cenchrus ciliaris) measured under controlled laboratory conditions," Int. J. Appl. Earth Obs. Geoinf., vol. 5, no. 2, pp. 87–96, May 2004.

[31] A. Swatantran, R. Dubayah, D. Roberts, M. Hofton, and J. B. Blair, "Mapping biomass and stress in the Sierra Nevada using lidar and hyperspectral data fusion," Remote Sens. Environ., vol. 115, no. 11, pp. 2917–2930, Nov. 2011.

[32] T. Calvão and J. M. Palmeirim, "Mapping Mediterranean scrub with satellite imagery: biomass estimation and spectral behaviour," Int. J. Remote Sens., vol. 25, no. 16, pp. 3113–3126, Aug. 2004.

[33] G. . Devagiri, S. Money, S. Singh, V. . Dadhawal, P. Patil, A. Khaple, A. S. Devakumar, and S. Hubballi, "Assessment of above ground biomass and carbon pool in different vegetation types of south western part of Karnataka, India using spectral modeling," Trop. Ecol., vol. 54, no. 2, pp. 149–165, 2013.

[34] M. A. Cho, A. K. Skidmore, F. Corsi, S. E. van Wieren, and I. Sobhan, "Estimation of green grass/herb biomass from airborne hyperspectral imagery using spectral indices and

partial least squares regression," Int. J. Appl. Earth Obs. Geoinf., vol. 9, no. 4, pp. 414–424, Dec. 2007.

[35] D. Rocchini, G. M. Foody, H. Nagendra, C. Ricotta, M. Anand, K. S. He, V. Amici, B. Kleinschmit, M. Förster, S. Schmidtlein, H. Feilhauer, A. Ghisla, M. Metz, and M. Neteler, "Uncertainty in ecosystem mapping by remote sensing," Comput. Geosci., May 2012.

[36] M. Kneubühler, A. Damm, A. Schweiger, A. C. Risch, M. Schütz, and M. E. Schaepman, "Continuous Fields From Imaging Spectrometer Data for Ecosystem Parameter Mapping and Their Potential for Animal Habitat Assessment in Alpine Regions," IEEE J. Sel. Top. Appl. Earth Obs. Remote Sens., vol. 7, no. 6, pp. 2600–2610, 2014.

[37] R. S. DeFries, C. B. Field, I. Fung, C. O. Justice, S. Los, P. a. Matson, E. Matthews, H. a. Mooney, C. S. Potter, K. Prentice, P. J. Sellers, J. R. G. Townshend, C. J. Tucker, S. L. Ustin, and P. M. Vitousek, "Mapping the land surface for global atmosphere-biosphere models: Toward continuous distributions of vegetation's functional properties," J. Geophys. Res., vol. 100, no. D10, p. 20867, 1995.

[38] G. M. Foody, "Fuzzy modelling of vegetation from remotely sensed imagery," Ecol. Modell., vol. 85, no. 1, pp. 3–12, Feb. 1996.

[39] F. Maselli, C. Conese, T. De Filippis, and S. Norcini, "Estimation of forest parameters through fuzzy classification of TM data," IEEE Trans. Geosci. Remote Sens., vol. 33, no. 1, pp. 77–84, 1995.

[40] D. Rocchini, "While Boolean sets non-gently rip: A theoretical framework on fuzzy sets for mapping landscape patterns," Ecol. Complex., vol. 7, no. 1, pp. 125–129, Mar. 2010.

[41] R. Fernandes, R. Fraser, R. Latifovic, J. Cihlar, J. Beaubien, and Y. Du, "Approaches to fractional land cover and continuous field mapping: A comparative assessment over the BOREAS study region," Remote Sens. Environ., vol. 89, no. 2, pp. 234–251, Jan. 2004.

[42] A. C. Risch, L. M. Nagel, S. Martin, B. O. KrÜsi, F. Kienast, and H. Bugmman, "Structure and Long-Term Development of Subalpine Pinus montana Miller and Pinus cembra L. Forests in the Central European Alps," Forstwissenschaftliches Cent., vol. 122, no. 4, pp. 219–230, 2003.

[43] MeteoSwiss, "IDAweb. The data portal of MeteoSwiss for research and teaching.," http://www.meteoschweiz.admin.ch/web/de/services/datenportal/idaweb.html. accessed, 2013.

[44] A. Leboeuf, A. Beaudoin, R. Fournier, L. Guindon, J. Luther, and M. Lambert, "A shadow fraction method for mapping biomass of northern boreal black spruce forests using QuickBird imagery," Remote Sens. Environ., vol. 110, no. 4, pp. 488–500, Oct. 2007.

[45] M. A. Cho, A. K. Skidmore, and I. Sobhan, "Mapping beech (Fagus sylvatica L.) forest structure with airborne hyperspectral imagery," Int. J. Appl. Earth Obs. Geoinf., vol. 11, no. 3, pp. 201–211, Jun. 2009.

[46] S. Huang, S. J. Titus, and D. P. Wiens, “Comparison of nonlinear height-diameter functions for major Alberta tree species,” Can. J. For. Res., vol. 22, pp. 1297–1304, 1992.

[47] X. Wei, “Biomass Estimation: A Remote Sensing Approach,” Geogr. Compass, vol. 4, no. 11, pp. 1635–1647, Nov. 2010.

[48] E. Thürig and S. Schmid, “Jährliche CO 2 -Flüsse im Wald: Berechnungsmethode für das Treibhausgasinventar | Annual CO 2 fluxes in forests: calculation method for the Greenhouse Gas Inventory,” Schweizerische Zeitschrift fur Forstwes., vol. 159, no. 2, pp. 31–38, Feb. 2008.

[49] M. E. Schaepman, M. Jehle, A. Hueni, P. D’Odorico, A. Damm, J. Weyermann, F. D. Schneider, V. Laurent, C. Popp, F. C. Seidel, K. Lenhard, P. Gege, C. Küchler, J. Brazile, P. Kohler, L. De Vos, K. Meuleman, R. Meynart, D. Schläpfer, M. Kneubühler, and K. I. Itten, “Advanced radiometry measurements and Earth science applications with the Airborne Prism Experiment (APEX,” Remote Sens. Environ., vol. 158, pp. 207–219, 2015.

[50] D. Schläpfer and R. Richter, “Geo-atmospheric processing of airborne imaging spectrometry data. Part 1: Parametric orthorectification,” Int. J. Remote Sens., vol. 23, no. 13, pp. 2609–2630, Jan. 2002.

[51] R. Richter and D. Schläpfer, “Geo-atmospheric processing of airborne imaging spectrometry data. Part 2: Atmospheric/topographic correction,” Int. J. Remote Sens., vol. 23, no. 13, pp. 2631–2649, Jan. 2002.

[52] G. Schaepman-Strub, M. E. Schaepman, T. H. Painter, S. Dangel, and J. V. Martonchik, “Reflectance quantities in optical remote sensing—definitions and case studies,” Remote Sens. Environ., vol. 103, no. 1, pp. 27–42, Jul. 2006.

[53] M. Shen, A. Tang, J. Klein, P. Zhang, S. Gu, A. Shimono, and J. Chen, “Estimation of aboveground biomass using in situ hyperspectral measurements in five major grassland ecosystems on the Tibetan Plateau,” J. Plant Ecol., vol. 1, no. 4, pp. 247–257, Nov. 2008.

[54] P. M. Hansen and J. K. Schjoerring, “Reflectance measurement of canopy biomass and nitrogen status in wheat crops using normalized difference vegetation indices and partial least squares regression,” Remote Sens. Environ., vol. 86, no. 4, pp. 542–553, Aug. 2003.

[55] W. B. Cohen, T. K. Maiersperger, S. T. Gower, and D. P. Turner, “An improved strategy for regression of biophysical variables and Landsat ETM+ data,” Remote Sens. Environ., vol. 84, pp. 561–571, 2003.

[56] V. Torontow and D. King, “Forest complexity modelling and mapping with remote sensing and topographic data: a comparison of three methods,” Can. J. Remote Sens., vol. 37, no. 4, pp. 387–402, 2011.

[57] M. Poulain, M. Peña, A. Schmidt, H. Schmidt, and A. Schulte, “Relationships between forest variables and remote sensing data in a Nothofagus pumilio forest,” Geocarto Int., vol. 25, no. 1, pp. 25–43, Feb. 2010.

[58] M. T. Gebreslasie, F. B. Ahmed, and J. a. N. van Aardt, "Predicting forest structural attributes using ancillary data and ASTER satellite data," Int. J. Appl. Earth Obs. Geoinf., vol. 12, pp. S23–S26, Feb. 2010.

[59] R. Darvishzadeh, C. Atzberger, A. K. A. Skidmore, and A. A. Abkar, "Leaf Area Index derivation from hyperspectral vegetation indices and the red edge position," Int. J. Remote Sens., vol. 30, no. 23, pp. 6199–6218, 2009.

[60] Y. Xie, Z. Sha, M. Yu, Y. Bai, and L. Zhang, "A comparison of two models with Landsat data for estimating above ground grassland biomass in Inner Mongolia, China," Ecol. Modell., vol. 220, no. 15, pp. 1810–1818, Aug. 2009.

[61] S. R. Freitas, M. C. S. Mello, and C. B. M. Cruz, "Relationships between forest structure and vegetation indices in Atlantic Rainforest," For. Ecol. Manage., vol. 218, no. 1–3, pp. 353–362, Oct. 2005.

[62] S. Ullah, Y. Si, M. Schlerf, A. K. Skidmore, M. Shafique, and I. A. Iqbal, "Estimation of grassland biomass and nitrogen using MERIS data," Int. J. Appl. Earth Obs. Geoinf., vol. 19, pp. 196–204, Oct. 2012.

[63] S. Eckert, "Improved Forest Biomass and Carbon Estimations Using Texture Measures from WorldView-2 Satellite Data," Remote Sens., vol. 4, no. 4, pp. 810–829, Mar. 2012.

[64] J. Anderson, L. Plourde, M. Martin, B. Braswell, M. Smith, R. Dubayah, M. Hofton, and J. Blair, "Integrating waveform lidar with hyperspectral imagery for inventory of a northern temperate forest," Remote Sens. Environ., vol. 112, no. 4, pp. 1856–1870, Apr. 2008.

[65] L. Willemen, P. H. Verburg, L. Hein, and M. E. F. van Mensvoort, "Spatial characterization of landscape functions," Landsc. Urban Plan., vol. 88, no. 1, pp. 34–43, Oct. 2008.

[66] M. García, D. Riaño, E. Chuvieco, and F. M. Danson, "Estimating biomass carbon stocks for a Mediterranean forest in central Spain using LiDAR height and intensity data," Remote Sens. Environ., vol. 114, no. 4, pp. 816–830, Apr. 2010.

[67] J. B. Adams, M. O. Smith, and P. E. Johnson, "Spectral mixture modeling: A new analysis of rock and soil types at the Viking Lander 1 Site," J. Geophys. Res., vol. 91, no. B8, p. 8098, 1986.

[68] J. W. Boardman, F. A. Kruse, and R. O. Green, "Mapping target signatures via partial unmixing of AVIRIS data," in Summaries of the fifth annual JPL airborne geoscience workshop geoscience workshop, 1995, no. 23, pp. 23–26.

[69] F. Van Der Meer and S. M. De Jong, "Improving the results of spectral unmixing of Landsat Thematic Mapper imagery by enhancing the orthogonality of end-members," Int. J. Remote Sens., vol. 21, no. 15, pp. 2781–2797, Jan. 2000.

[70] J. Heiskanen, “Estimating aboveground tree biomass and leaf area index in a mountain birch forest using ASTER satellite data,” Int. J. Remote Sens., vol. 27, no. 6, pp. 1135–1158, Mar. 2006.

[71] A. Kangas and M. Maltamo, Forest Inventory Methodology and Applications. Springer, 2006, p. 362.

[72] H. Latifi, F. Fassnacht, and B. Koch, “Forest structure modeling with combined airborne hyperspectral and LiDAR data,” Remote Sens. Environ., vol. 121, pp. 10–25, Jun. 2012.

[73] H. Gallaun, G. Zanchi, G.-J. Nabuurs, G. Hengeveld, M. Schardt, and P. J. Verkerk, “EU-wide maps of growing stock and above-ground biomass in forests based on remote sensing and field measurements,” For. Ecol. Manage., vol. 260, no. 3, pp. 252–261, Jun. 2010.

[74] A. Stampfli and M. Zeiter, “Plant species decline due to abandonment of meadows cannot easily be reversed by mowing. A case study from the southern Alps,” J. Veg. Sci., vol. 10, pp. 151–164, 1999.

[75] P. Brassel and H. Lischke, “Swiss national forest inventory: methods and models of the second assessment,” WSL Swiss Fed. Res. instute, p. 312, 2001.

[76] F. Schläpfer, A. B. Pfisterer, and B. Schmid, “Non-random species extinction and plant production: implications for ecosystem functioning,” J. Appl. Ecol., vol. 42, no. 1, pp. 13–24, Feb. 2005.

[77] O. Mutanga and A. K. Skidmore, “Narrow band vegetation indices overcome the saturation problem in biomass estimation,” Int. J. Remote Sens., vol. 25, no. 19, pp. 3999–4014, Oct. 2004.

[78] R. Geerken, N. Batikha, D. Celis, and E. DePauw, “Differentiation of rangeland vegetation and assessment of its status: field investigations and MODIS and SPOT VEGETATION data analyses,” Int. J. Remote Sens., vol. 26, no. 20, pp. 4499–4526, Oct. 2005.

[79] H. Ren and G. Zhou, “Estimating senesced biomass of desert steppe in Inner Mongolia using field spectrometric data,” Agric. For. Meteorol., vol. 161, pp. 66–71, Aug. 2012.

[80] J. Weyermann, A. Damm, M. Kneubühler, and M. E. Schaepman, “Correction of reflectance anisotropy effects of vegetation on airborne spectroscopy data and derived products,” IEEE Trans. Geosci. Remote Sens. Remote Sens., vol. 52, no. January 2014, pp. 616–627, 2014.

[81] M. L. Clark, D. A. Roberts, J. J. Ewel, and D. B. Clark, “Estimation of tropical rain forest aboveground biomass with small-footprint lidar and hyperspectral sensors,” Remote Sens. Environ., vol. 115, no. 11, pp. 2931–2942, Nov. 2011.

[82] M. a. Lefsky, W. B. Cohen, and T. a. Spies, "An evaluation of alternate remote sensing products for forest inventory, monitoring, and mapping of Douglas-fir forests in western Oregon," Can. J. For. Res., vol. 31, no. 1, pp. 78–87, 2001.

[83] G. Vaglio Laurin, Q. Chen, J. A. Lindsell, D. A. Coomes, F. Del Frate, L. Guerriero, F. Pirotti, and R. Valentini, "Above ground biomass estimation in an African tropical forest with lidar and hyperspectral data," ISPRS J. Photogramm. Remote Sens., vol. 89, pp. 49–58, Mar. 2014.

[84] I. Numata, D. Roberts, O. Chadwick, J. Schimel, L. Galvao, and J. Soares, "Evaluation of hyperspectral data for pasture estimate in the Brazilian Amazon using field and imaging spectrometers," Remote Sens. Environ., vol. 112, no. 4, pp. 1569–1583, Apr. 2008.

[85] J. Chen, S. Gu, M. Shen, Y. Tang, and B. Matsushita, "Estimating aboveground biomass of grassland having a high canopy cover: an exploratory analysis of in situ hyperspectral data," Int. J. Remote Sens., vol. 30, no. 24, pp. 6497–6517, 2009.

[86] T. F. Porter, C. Chen, J. A. Long, R. L. Lawrence, and B. F. Sowell, "Estimating biomass on CRP pastureland: A comparison of remote sensing techniques," Biomass and Bioenergy, Feb. 2014.

[87] J. Verrelst, M. E. Schaepman, B. Koetz, and M. Kneubühler, "Angular sensitivity analysis of vegetation indices derived from CHRIS/PROBA data," Remote Sens. Environ., vol. 112, no. 5, pp. 2341–2353, May 2008.

[88] S. L. Ustin, D. a. Roberts, J. a. Gamon, G. P. Asner, and R. O. Green, "Using Imaging Spectroscopy to Study Ecosystem Processes and Properties," Bioscience, vol. 54, no. 6, p. 523, 2004.

[89] K.-S. Lee, W. B. Cohen, R. E. Kennedy, T. K. Maiersperger, and S. T. Gower, "Hyperspectral versus multispectral data for estimating leaf area index in four different biomes," Remote Sens. Environ., vol. 91, no. 3–4, pp. 508–520, Jun. 2004.

[90] G. P. Asner, "Biophysical and Biochemical Sources of Variability in Canopy Reflectance," Remote Sens. Environ., vol. 64, no. 3, pp. 234–253, Jun. 1998.

[91] H. Latifi, A. Nothdurft, and B. Koch, "Non-parametric prediction and mapping of standing timber volume and biomass in a temperate forest: application of multiple optical/LiDAR-derived predictors," Forestry, vol. 83, no. 4, pp. 395–407, Jul. 2010.

[92] P. Roy and S. A. Ravan, "Biomass estimation using satellite remote sensing data — An investigation on possible approaches for natural forest," J. Biosci., vol. 21, no. 4, pp. 535–561, 1996.

[93] A. Langner, H. Samejima, R. C. Ong, J. Titin, and K. Kitayama, "Integration of carbon conservation into sustainable forest management using high resolution satellite imagery: A case study in Sabah, Malaysian Borneo," Int. J. Appl. Earth Obs. Geoinf., vol. 18, pp. 305–312, Aug. 2012.

[94] R. F. Kokaly, G. P. Asner, S. V. Ollinger, M. E. Martin, and C. A. Wessman, "Characterizing canopy biochemistry from imaging spectroscopy and its application to ecosystem studies," Remote Sens. Environ., vol. 113, pp. S78–S91, Sep. 2009.

[95] Z. Gong, T. Cui, and H. Gong, "Estimating wetland vegetation abundance based on spectral mixture analysis: a comparison between LSMA and FCM classification methods," Int. J. Remote Sens., vol. 35, no. 1, pp. 189–203, Jan. 2014.

[96] C. Wessman, C. Bateson, and T. Benning, "Detecting fire and grazing patterns in tallgrass prairie using spectral mixture analysis," Ecol. Appl., vol. 7, no. 2, pp. 493–511, 1997.

[97] A. Viña and A. Gitelson, "Sensitivity to foliar anthocyanin content of vegetation indices using green reflectance," Geosci. Remote Sens. Lett., vol. 8, no. 3, pp. 463–467, 2011.

[98] F. E. Fassnacht, F. Hartig, H. Latifi, C. Berger, J. Hernández, P. Corvalán, and B. Koch, "Importance of sample size , data type and prediction method for remote sensing-based estimations of aboveground forest biomass," Remote Sens. Environ., vol. 154, pp. 102–114, 2014.

3

Estimation of Alpine Forest Structural Variables from Imaging Spectrometer Data

This chapter has been published as:

Fatehi, P., Damm, A., Schaepman, M.E., & Kneubühler, M. (2015). Estimation of alpine forest structural variables from imaging spectrometer data. Remote Sensing, 7(12), 16315-16338.

Abstract

Spatial information of forest structural variables is crucial for sustainable forest management planning, forest monitoring, and the assessment of forest ecosystem productivity. We investigate a complex alpine forest ecosystem located in the Swiss National Park (SNP) and apply empirical models to retrieve the structural variables *canopy closure*, *basal area*, and *timber volume* at plot scale. We used imaging spectrometer (IS) data from the Airborne Prism EXperiment (APEX) in combination with *in-situ* measurements of forest structural variables to develop empirical models. These models are based on simple and stepwise multiple regressions, while all potential two narrow-band combinations of the Simple Ratio (SR), the Normalized Difference Vegetation Index (NDVI), the perpendicular vegetation index (PVI), the second soil-adjusted vegetation index (SAVI2), and band depth indices were tested. The accuracy of the estimated structural attributes was evaluated using a leave-one-out cross-validation technique. Using stepwise multiple regression models, we obtained a moderate to good accuracy when estimating *canopy closure* (R^2=0.81, rRMSE=10%), *basal area* (R^2=0.68, rRMSE=20%), and *timber volume* (R^2=0.73, rRMSE=22%). We discuss the reliability of empirical approaches for estimates of canopy structural parameters considering the causality of light interaction and surface information.

Authors' contributions: PF, AD, MES, MK designed the study and developed the methodology. PF collected the data. PF performed the analysis. All authors wrote the manuscript.

3.1 Introduction

Forest inventories seek to enumerate trees over a defined area and to gain forest structural attributes, such as volume, basal area, canopy cover, stem density, diameter at breast height (DBH) and maximum height at individual tree, plot, stand, regional, national, and global scale [1]. Structural attributes are crucial to determine information facilitating the management of forest ecosystems [2], [3], to modify silvicultural practices [4], [5], to quantify deforestation impacts on the carbon cycle and related impacts for global warming [6], and to assess productivity of forested areas in relation to forest composition [7] as well as in view of specific forest management practices [4], [5]. Further, accurate estimates of structural variables are practical indicators for determining forest evolutionary history [8], monitoring forest sustainability [9], assessing insect infestation susceptibility [10], [11], study wildlife management and biodiversity [12], as well as forest water flux modeling [13]. Accordingly, there is an increasing need to generate accurate information regarding forest structural dynamics [14].

Traditionally, forest structure data have been collected by means of field surveys [15]. Field surveys are the most accurate way to collect forest structural data [16], [17], but require *in-situ* measurements that are generally limited to a small area (plot area). Consequently, they do not provide continuous spatial and temporal information on forest structure variables across scales [18]. Furthermore, sampling is expensive, time consuming, and not applicable to large or remote areas [19], [20]. Therefore, remote sensing (RS) data, acquired from either airborne or space-borne platforms, have been taken into consideration as a practical means to estimate forest attributes at different scales [21], [22]. RS provides the advantage of spatially explicit mapping of forest attributes [23], repeatedly over large and remote areas [24].

RS systems to measure forest structural attributes include two main categories: i) active sensors, such as synthetic aperture radar (SAR) or light detection and ranging (LiDAR), and ii) passive optical sensors [25], [26]. Active RS bears the potential to capture the vertical structure information and three-dimensional shape of forest canopies; therefore, many studies have demonstrated that active RS, i.e., LiDAR, is a promising alternative to map forest structural attributes [26]–[29]. However, acquiring wall to wall coverage of LiDAR data is extremely costly, both in monetary and computational terms [14], [30], [31]. Moreover, LiDAR data processing requires specific skills, knowledge, algorithms and software [16], [32]. Complex canopy structure and topography effects (i.e., steep slopes or rough topography) can also impose uncertainties to retrieval of structural

parameters from LiDAR data [33], [34]. Tree height is often underestimated due to the low probability of laser pulses to intercept the top layer of a tree [35]. Dense understory vegetation layers further lead to a low probability of ground terrain determination (digital terrain model overestimation) [36]. Lean trees, which are found most often in steep slope, can cause errors due to a two-dimensional offset between tree base and top of the tree. Furthermore, LiDAR returns in steep slopes may be erroneously assigned to vegetation [37]. All these issues limit the operational use of this technology in forest structural estimation. Approaches employing SAR data can suffer from saturation effects in complex and dense forest [26], [38].

Passive optical sensors, comprising both multispectral (MS) and imaging spectroscopy (IS) sensors, have been widely used for mapping various plant traits of forest canopies, including biochemical properties and structural attributes [7], [39]. The estimation of vegetation properties using optical RS is based on determining a link between spectral information contained in a data set and vegetation metrics of interest. Various studies demonstrate that this relationship can be successfully modeled to estimate, for example, forest and grassland aboveground biomass (AGB) [40], [41], and to measure plant functional traits using imaging spectrometer data [42]–[45].

Thenkabail et al, [46], [47] indicated that IS data contain spectral information that allow quantifying characteristics of forest canopies. However, since optical sensors mainly capture information from the upper part of a vegetation canopy, developing a relationship between spectral reflectance and forest structural variables is a challenge [48], [49]. Moreover, reflected solar radiation is subject to mutual shadowing effects [50], bidirectional reflectance distribution function (BRDF) effects [51], variable atmospheric conditions, and instrument characteristics [52]. Despite these drawbacks, it has been widely attempted to derive forest properties at canopy scale from optical RS data using either physically-based approaches or empirical approaches [52].

Physical-based approaches use leaf and canopy radiative transfer models (RTM) to simulate the spectral properties of canopy reflectance based on structural, biochemical, and forest background attributes [44], [53]. The RTM needs to be adapted for different sensors and acquisition geometries [44] and can subsequently be inverted to retrieve forest properties. However, the procedure is computationally intense, and is suffering from the ill-posedness of model inversion [54], [55], thus limiting its applicability for large areas [56]. Empirical approaches employ a statistical relationship between in-situ measured reference and RS data [49].

Empirical approaches strongly rely on the assumption that variations in forest variables affect the spectral reflectance of a forest and can be modeled by simple relationships [57]. Structural variables have been successfully retrieved from IS data by considering original spectral bands, computing all possible two-band combinations of, e.g., normalized difference vegetation indices (NDVI) type [58], [59], red-edge position (REP), narrow simple ratio (SR) vegetation indices [60], [61], band depth analysis [62], narrow-band normalized difference water indices (NDWI) [31], or from MS data by mostly either employing original spectral bands or computing broad-band vegetation indices (VI) [63]–[65]. As an example, Schlerf et al. [61] used HyMap data of highly managed and relatively homogenous Norway spruce (*Picea abies*) stands and reported significant linear relationships between forest leaf area index (LAI) and crown volume with a narrow-band perpendicular vegetation index (PVI). Cho et al. [39] tested the relationship between reflectance factors derived from HyMap data and forest structural attributes including mean DBH, mean tree height and tree density in a homogenous (i.e. homogeneous in DBH, height, tree density and species) and closed canopy beech (*Fagus sylvatica*) stand. They conclude that their new vegetation indices, generated from contrasting spectral regions around the red-edge shoulder (756-820 nm) and the water absorption feature centered at 1200 nm (1172-1320 nm), showed higher correlation with structural variables compared with the standard vegetation indices derived from near-infrared and visible reflectance. Latifi et al. [66] have noted that the original bands of HyMap data located in the green and near-infrared parts of the spectrum contain useful information correlated to structural variables in a temperate forest site in Germany. All these studies suggest that the usage of narrow- band vegetation indices generated from the whole spectrum (350-2500 nm) offers a strategy to overcome the saturation problem at high canopy cover or LAI [67].

Relationships between vegetation indices and important stand characteristics are rarely documented [19]. Furthermore, since empirical relationships are at the cost of causality, their transferability is reduced and the usage of obtained results requires specific attention. We, consequently aim to demonstrate the capability of IS data to empirically map structural attributes and to discuss the reliability of such approaches. We selected a heterogeneous alpine ecosystem comprising a natural forest including different tree species at varying proportions to empirically retrieve the forest structural attributes canopy closure, basal area, and volume from IS data. We tested various data analysis methods such as continuum removal (CR) and band depth analysis introduced by Kokaly and Clark [68] that were proposed to enhance spectral absorption features, to compensate

disturbing background reflectance, and to enable improved linkage of spectral features to vegetation structural properties [69]–[71].

3.2 Method

3.2.1 Study area

The study was conducted in the Trupchun valley (Val Trupchun) within the Swiss National Park (SNP), located in the southeastern part of Switzerland (Fig. 3. 1). Val Trupchun covers an area of 22 km2 and the elevation ranges from 1775 to 3145 meter above sea level (a.s.l.) [72]. Based on climate data recorded by MeteoSwiss at the SNP's weather station, Buffalora at 1977 m a.sl., the climate of the SNP is dry and harsh with an average annual precipitation of 744 mm ± 160 mm (mean ± standard deviation (SD)) and an average annual temperature of 0.9 °C ± 0.5 °C [73]. The study site is a heterogeneous alpine landscape with a rough topography and steep slopes. The forest is classified as boreal type forests with European larch (*Larix decidua* L.) as a dominant tree. The Norway spruce (*Picea abies* (L.) Karst) and Swiss stone pine (*Pinus cembra* L.) are associated species [40]. The Norway spruce is present at lower altitude, whereas the Swiss stone pine occurs at high altitude. The trees are approximately 250 years old and have been strictly protected and unmanaged since 1914 [74].

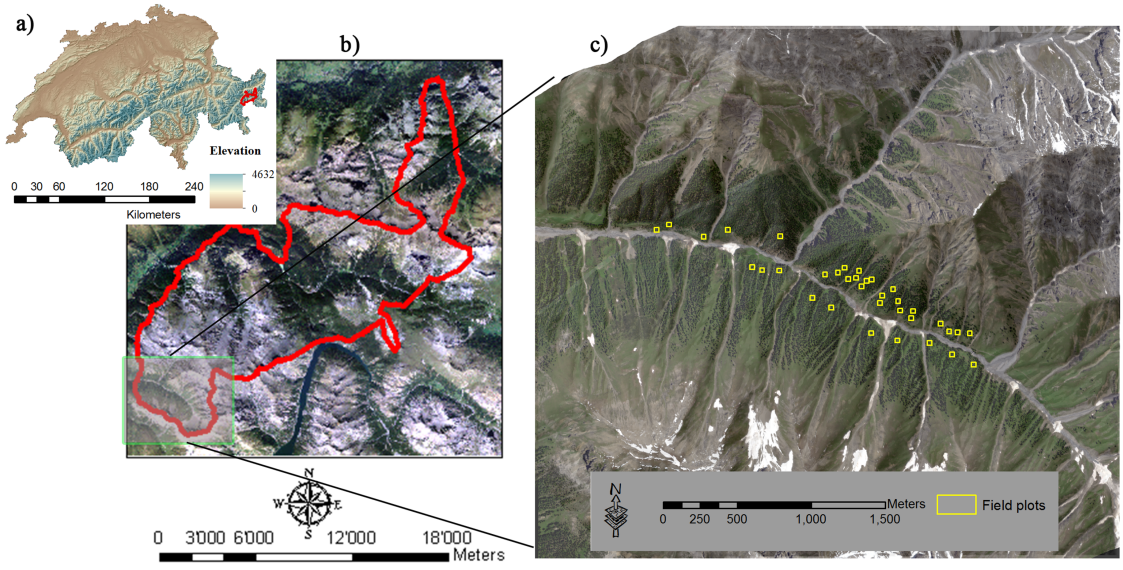

Fig. 3. 1. Study area and location of field plots. (a) Location of the SNP in Switzerland (red line) with digital elevation model as background (source: swisstopo http://www.swisstopo.admin.ch). (b) Location of Val Trupchun (green box) within the SNP; a true color image is used as background (source: swisstopo). (c) Location of field plots (yellow boxes) in Val Trupchun; an APEX true color image is used as background.

3.2.2 Field data

Field reference data of forest structural variables were collected in June 2012 in the Trupchun valley of the SNP. 35 Sample plots with a size of 30 m x 30 m were identified by applying a stratified random sampling, and excluding protected areas that were not accessible. Identified plots represent most of the present tree species and possible ranges of their properties, i.e., canopy cover, density, and species composition. A differential global positioning system (DGPS) providing an accuracy better than 1 m was used to record the geographic position of the four corners of the field plots. Within each plot, tree species, DBH, and tree height were measured, while only trees having a DBH (DBH measured at 1.3 m above the ground surface) greater than 5 cm were considered [75]. Basal area (BA), i.e., the cross-sectional areas of a tree stem measured at 1.3 m above ground [76], was estimated according to (Eq.1):

$$BA = \sum \frac{\pi (DBH)^2}{4} \times \frac{10000}{Plot} \quad (1)$$

where BA is the estimated basal area (m^2/ha), DBH is the diameter of a tree stem (m), and $Plot$ is the area of the field plot (m^2).

Height was measured for five randomly selected trees within each plot. A Haga hypsometer (Haga GmbH and Co. KG, Nuremberg, Germany) [39] was used to measure the height of the largest tree in term of DBH and the trees located at the four corners of each plot. It should be noted that we had no a-priori information in term of DBH, height, and species type about the distribution of trees within each randomly selected plot. Meaning that each tree has an equal probability of being selected from the respective population. To increase the selection chance of large trees (in term of DBH), which are highly contribute to various forest structural properties, i.e., stand height, stand timber volume, stand biomass, and canopy cover, the height of a tree with the largest DBH in each sample plot was also measured. In total, the heights of 175 trees were measured in the study area. A type specific height-DBH function was developed while considering tree species, DBH, and the measured height [77]. According to tree species, the corresponding type specific height-DBH function was then applied to estimate the height of the unmeasured trees. The volume of the trees was calculated as a function of the measured DBH and estimated tree height. Tree volume was summed up to estimate the volume of the respective plot.

Canopy closure (CC) is defined as the percentage of ground within 30m×30m, covered by the vertical projection of the overlying trees' crown [21]. The CC was visually estimated using a digital aerial photograph acquired in 2006 with 25 cm spatial resolution.

It is important to mention that there was a two-year time lag between field reference data collection and imaging spectrometer data acquisition and also a four-year time lag between aerial photograph and imaging spectrometer data acquisition. However, the newest reference available providing a sub-meter resolution were aerial photographs from 2006. Since the average tree ring width increase is 3mm/year [78], a stem growth of less than 1 cm/year can be expected and canopy cover change from 2006-2010 is assumed to be negligible. Further, the SNP is a protected area without any human activity and no occurrence of significant natural disturbance (i.e., fire, windstorm or bark beetle attack) is reported in Val Trupchun after 2006 or even before that time, thus, we assumed that the forest structure attributes remain relatively constant during this period [13], [49].

3.2.3 APEX imaging spectrometer data

Airborne Prism EXperiment (APEX) imaging spectrometer data were used in this study. APEX is an airborne pushbroom device with 1000 imaging pixels across track and covers a swath width of 1.5 km to 5 km (depending on flight altitude) with a field of view (FOV) of 28° [43]. The spectral wavelength range of 372-2500 nm is recorded by a Visible/Near Infrared (VNIR), and a Shortwave Infrared (SWIR) detector. The spectral resolution (FWHM) ranges between 0.7 and 9.7 nm for the VNIR and between 6.2 and 12 nm for the SWIR detector. After removal of noisy bands, an APEX data cube contains 285 spectral bands.

APEX data over the SNP were acquired on 26 June 2010 under cloud free condition and with a 2 m pixel size. The acquisition time was close to solar noon. The sun zenith and azimuth angle ranged between 31.8° and 28.1° and between 127.5° and 139.1°. A parametric geocoding approach (PARGE) using 15 ground control points with Swiss national coordinate system (CH 1903 LV03) was applied to the data [79], resulting in a geometric accuracy of 3.2 m ± 1.4 m. This corresponds to a total pixel shift of 1.3-1.9 pixels ± 0.5-0.8 pixel. Measured APEX radiance data were atmospherically corrected using an atmospheric and topographic correction approach for rugged terrain (ATCOR-4) [80]. ATCOR-4 comprises the atmospheric radiative transfer code MODTRAN-5 [81] to pre-calculated look-up tables (LUT) of atmospheric variables. We set the atmosphere type and the aerosol model to mid-latitude summer and a rural aerosol model. These settings in addition to image based estimates of atmospheric water vapor and visibility provided by the pixel-wise selection of LUT entries allowed to compensate for atmospheric effects and to determine top-of-canopy hemispherical conical reflectance factor (HCRF) data (for terminology see [82]).

3.2.4 Vegetation indices

3.2.4.1 Narrow-band vegetation indices

Vegetation indices (VIs) are widely used to estimate biophysical vegetation properties, i.e., biomass [40], [83], LAI [55], [59], canopy closure [84], [85], or stand volume [17], [61]. In this study we used two main categories of vegetation indices; ratio-based and soil-based indices. The Simple Ratio (SR) and the Normalized Difference Vegetation Index (NDVI) (both ratio-based indices), as well as the PVI and the second soil-adjusted vegetation index (SAVI2) (both soil-based indices) were proposed by previous studies to estimate biophysical properties of vegetation. We calculated SR [86], NDVI [87], PVI [88], and SAVI2 [89] as:

$$SR = \frac{\rho_1}{\rho_2} \tag{2}$$

$$NDVI = \frac{(\rho_1 - \rho_2)}{(\rho_1 + \rho_2)} \tag{3}$$

$$PVI = \frac{\rho_1 - a\rho_2 - b}{\sqrt{1 + a^2}} \tag{4}$$

$$SAVI2 = \frac{\rho_1}{\rho_2 + \left(b/a\right)} \tag{5}$$

where ρ_1 and ρ_2 are reflectance values at distinct wavelengths, a and b are the soil line coefficient.

Previous studies have shown that the narrow-band indices can provide significant improvement as compared to broadband indices for estimating vegetation structural variables [39], [61], [67] . Consequently, we only focused on narrow-band indices.

3.2.4.2 Band depth indices

Band depth indices generated from continuum-removed spectra were used to estimate structural properties. This approach has shown its capability to improve the performance of structural variable estimation [62], [71]. Based on previous research, the continuum removal was applied to four regions of the spectrum, ranging from the VIS to the SWIR part (**Table 3. 1**). The selected region in VIS is affected by chlorophyll absorption, whereas the NIR [62] and SWIR regions are mainly affected by water, lignin, and cellulose absorption [68]. The inversion of the reflectance factors was applied on SWIR1 and SWIR2

using equation (6). This procedure was necessary to reshape the concave form of the spectrum to a convex form in order to calculate band depth indices [71].

$$\rho_{inverse} = 1 - \rho_i \tag{6}$$

where $\rho_{inverse}$ is the inverse reflectance factor at band *i* and ρ_i is the original reflectance factor at band *i*.

Table 3. 1

Start, end, and center points of selected spectral regions for continuum removal and subsequent calculation of band depth indices (VIS = visible domain, NIR = near-infrared, SWIR = shortwave infrared).

Spectral domain	Location of the selected wavelength		
	Start of spectral region analysis (nm)	Center of spectral region analysis (nm)	End of spectral region analysis (nm)
VIS	653	678	724
NIR	1113	1179	1286
SWIR1	1600	1707	1784
SWIR2	2090	2211	2252

Band depth indices including band depth (BD), normalized band depth ratio (BDR), normalized band depth index (NBDI), the area under curve (AUC) of a continuum removed spectrum, as well as the Area under continuum-removed curve Normalized to the Chlorophyll absorption Band depth (ANCB) [90], were implemented. They were calculated according to the following equations:

$$R' = {R}/{R_c} \tag{7}$$

$$BD = 1 - R' \tag{8}$$

$$BDR = {BD}/{BD_c} \tag{9}$$

$$NBDI = {BD - BD_c}/{BD + BD_c} \tag{10}$$

$$AUC = \frac{1}{2}\sum_{j=1}^{n-1}(\lambda_{i+1} - \lambda_i)(BD_{i+1} - BD_i) \tag{11}$$

$$ANCB = {AUC}/{BD_c} \tag{12}$$

where R' is the continuum removed spectrum, *R* is the original reflectance value, *Rc* is the reflectance value of the continuum line [68], BDC is the band depth at the band center, λ_{i+1} and λ_i are wavelengths of the *i* and *i* + 1 bands, $BD_i + 1$ and BD_i are band depths at the *i* and *i* + 1 bands, *n* is the number of used spectral bands.

3.2.5 Correlograms

In order to identify sensitive wavelength regions to predict forest structural attributes a 2D correlation plot (correlogram) was calculated for all possible band combinations of SR, NDVI, SAVI2, and PVI type. These correlograms represent the coefficients of determination (R^2) of the individual linear regression models relating APEX derived VIs and *in-situ* measurements of each target variable (*i.e.*, canopy closure, basal area, and forest volume) [39]. The spectral bands with strong water absorption features at 1335–1490 nm and at 1780–1990 nm were excluded from further analysis. Therefore, 193 APEX spectral bands were used to generate correlograms, allowing to compute 37,249 different narrow-band combinations. The optimal band combination was selected based on R^2 (*i.e.*, we used an R^2 threshold of 0.5 with a confidence level of 95%), considering multi-collinearity issues, causality explanations, and focusing on "hot-spot areas" (spectral range) [40]. The selected band combinations were then used in regression analysis.

3.2.6 Regression analysis

Regression analysis is an empirical approach to determine the relationships among variables, i.e., dependent and independent variables (or predictors). In remote sensing literature regression analysis has seen a widespread use due to its ease of implementation and efficiency [91]. We used simple and stepwise multiple regression to predict forest structural attributes from APEX IS metrics. An implemented standard deviation outlier labeling method, i.e., the 3SD method [92], identified one field plot as an outlier that was removed from further analysis. Normality distribution of dependent variables is an important assumption associated with regression [39]. The Shapiro-Wilk test indicated that the BA ($W = 0.975$, $p = 0.579$), volume ($W = 0.974$, $p = 0.566$), and CC ($W = 0.965$, $p = 0.328$) followed a normal distribution ($p > 0.05$). A 15 × 15 pixels window (30 m × 30 m) was used to extract average reflectance values corresponding to each field plot from APEX IS data.

Stepwise multiple regression was run in two phases. First, we performed a stepwise multiple regression with optimal narrow-band indices to predict their performance to estimate structural variables. Afterwards, we ran the stepwise multiple regression with optimal narrow-band *and* band depth indices together to assess the influence of the band depth indices on the performance of the model [65]. The SPSS 20.0 package (IBM Crop. 2011) was used for statistical analysis. The probability of F was employed as a criterion to include ($F < 0.05$) or to remove ($F > 0.10$), an independent variable in the regression

analysis [70]. The best model was selected by comparing R^2, *RMSE*, and *variance inflation factor* (VIF). The acceptable VIF value was set to smaller than 10 to avoid multi-collinearity among variables and potential over-fitting of the model [93].

3.2.7 Validation

The results were tested by comparing the estimated forest structural attributes with the actual measurements obtained from field inventory. Because of the limited number of field plots, a leave-one-out cross-validation technique (LOOCV) was used to evaluate the accuracy of the estimated structural attribute [49]. The root mean square error (RMSE) and mean relative RMSE (rRMSE (%)) according to [1,66] were employed to quantify the reliability of the predictions.

$$RMSE = \sqrt{\frac{\sum_{i=1}^{n}(\hat{y}_i - y_i)^2}{n}} \tag{13}$$

$$rRMSE = \frac{RMSE}{\bar{y}} \times 100 \tag{14}$$

where $\hat{y}_i$ is the estimated basal area or canopy closure or volume, y_i is the measured basal area or canopy closure or volume, n is the number of observations and $\bar{y}$ is the mean of the measured variable (basal area or canopy closure or volume). The LOOCV has the advantage of providing an unbiased estimation of the prediction error [23]. In addition, we evaluated the performance of selected models using a bootstrapping approach with 5000 replications. The bootstrapping approach enables to increase the robustness of a model where the number of field plots is limited [94,95]. Three metrics, *i.e.*, the mean of R^2 ± one SD, the mean of RMSE ± one SD, and the mean rRMSE ± one SD were calculated to assess the model fit and predictive performance. The uncertainty was quantified at the 95% confidence interval.

3.3 Results

3.3.1 In-Situ Forest Structural Measurements

Descriptive statistics of the *in-situ* data are shown in **Table 3. 2.** The measured volume ranged between 77.6 m^3/ha and 807 m^3/ha. The average volume was 421.7 ± 181.7 m^3/ha, roughly representing the full range of volume values reported elsewhere for alpine areas [96,97]. The mean basal area was 42.5 ± 16 m^2/ ha and the canopy closure ranged

between 22% and 85% with an average of 61% ± 15.3%. Our findings are in line with results reported in other studies performed in the SNP [74,98].

Table 3. 2

Forest structural characteristics derived from reference data in the study area (DBH = diameter at breast height, SD = standard deviation, CV = coefficient of variation).

Parameter	Mean	Minimum	Maximum	SD	CV (%)
Mean DBH (cm)	31.9	18.62	53.5	9	28
Mean height (m)	16	10.8	22.7	2.9	18
Basal area (m^2/ha)	42.5	8.8	74	16	37
Volume (m^3/ha)	421.7	77.6	807	181.7	43
Canopy closure (%)	61	22	85	15.3	25

3.3.2 Empirical models to estimate structural variables

3.3.2.1 Canopy closure

We calculated correlograms representing the coefficients of determination (R^2) of individual linear regression models relating APEX derived VIs and in-situ measured CC for all possible two-band combinations of SR, NDVI, PVI, and SAVI2 type. Based on these correlograms, we identified potential band combinations and wavelength regions showing high sensitivity to variations of forest canopy closure (**Fig. S3. 1**).

In general, similar patterns in terms of sensitive wavelengths combinations are observed for SR and NDVI (**Fig. S3. 1**(a) and (b)). Sensitive combinations are mainly located in the shortwave infrared (SWIR). PVI type VIs shows a different pattern and higher R^2 compared to SR, NDVI, and SAVI2. Potential band combinations for PVI type VIs are located in (i) the VIS part in combination with NIR and SWIR, (ii) the red-edge region in combination with red wavelengths, and (iii) the SWIR part in combination with the NIR or the SWIR.

Table S3. 1 provides the results of the selection of candidate VIs derived from 2D correlograms based on a set of criteria introduced in the method section. The generated VIs obtained different results. The maximum R^2 values were 0.61, 0.62, 0.65, and 0.76 using NDVI, SR, SAVI2, and PVI, respectively. This indicates that a PVI type index generated from red-edge and NIR regions (883 and 763 nm) provided more information to estimate canopy cover than other categories of VIs (SR, NDVI, and SAVI2 type). The NIR and red-edge regions (895 and 754 nm) again were found suitable to estimate canopy closure using a SAVI2 type index (R^2 = 0.65). For SR and NDVI type VIs, spectral wavelengths with highest R^2 are located at 2204 and 2253 nm.

In a second step of the regression analysis, a stepwise multiple regression was applied considering all narrowband SR, NDVI, SAVI2, PVI type VIs that performed best. These are

listed in **Table S3. 1** in addition to selected band depth indices (*i.e.*, BD, BDR, NBDI, AUC, and ANCB) as independent variables to test whether band depth indices improve the prediction performance. As shown in **Table 3. 3**, using the stepwise multiple regression increased the R^2 to 0.90. The best performing stepwise multiple regression model has fulfilled the statistical collinearity requirement with the VIF values <10 [93]. This model uses band depth indices generated from the NIR and SWIR2 regions as well as an SR narrow-band VI employing wavelengths from the SWIR (2204 nm, 2253 nm) region. The corresponding wavelengths for each regression variable are summarized in **Table 3. 3**. The two models, *i.e.*, the simple and stepwise multiple regression models, were tested for significance using analysis of variance (ANOVA) at 5% significance level. The obtained *p* value (p = 0.0005) indicates that there is a statistically significant difference between the two models. In conclusion, the combination of band depth indices and an SR index increases the reliability of the prediction model for canopy closure compared to a model based on a single PVI type index. Consequently, stepwise multiple regression improved the model performance.

Table 3. 3

Best performing simple and stepwise multiple regression models to estimate canopy closure.

Variable	Model	Wavelength (nm)	R^2	VIF
Canopy closure	Y= −0.305 × PVI + 124.57	888, 763	0.76	1
	Y= −1372.12 × BDR_NIR − 214.91 × BDR_SWIR2 + 5.33 × AUC_NIR-317.35 × SR + 469.79	**BDR_NIR: 1257**	**0.90**	**1.42**
		BDR_SWIR2: 2176		**1.01**
		AUC: 1113-1286		**2.95**
		SR: 2253, 2204		**3.40**

The final stepwise multiple regression model presented in **Table 3. 3** was applied to the entire APEX data set to generate the canopy closure map (Fig. 3. 2). The estimated values range from 0% to 90% with an average of 56% ± 15%.

The relationship between measured and estimated canopy closure obtained by applying a LOOCV approach is depicted in Fig. 3. 3. The model employing a single variable (i.e., a PVI type index) gained reasonable results (R^2 = 0.60, RMSE = 9.34, and rRMSE =15%). Predicted values showed a good agreement with high canopy closure values (CC>60%). However, this relationship is weak for low and medium canopy closure values of 20-60% (Fig. 3. 3a). The result indicate that PVI generated from red-edge wavelengths shows a high sensitivity to denser canopy closure, and thus low sensitivity to open

canopies.

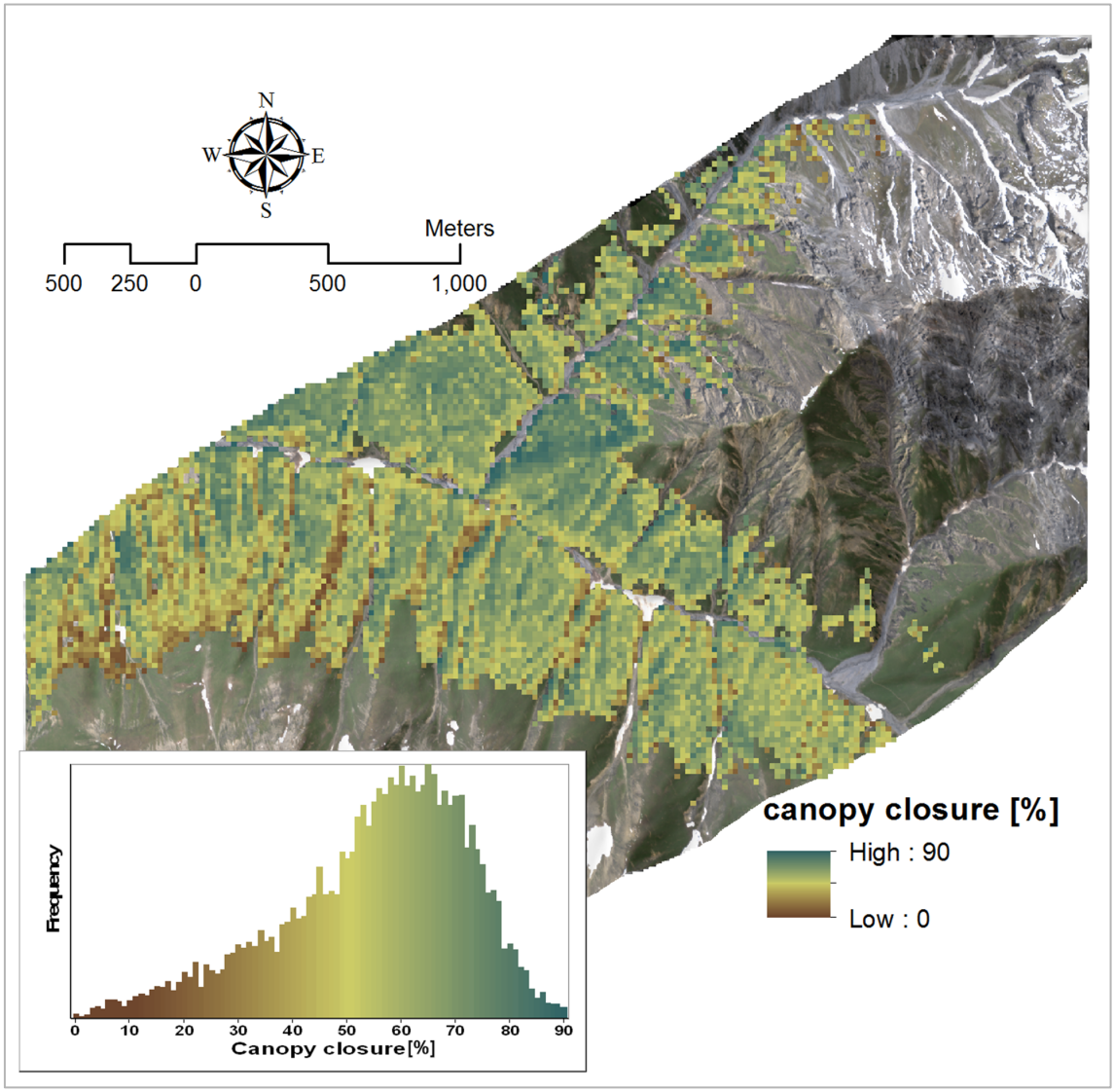

Fig. 3. 2. APEX derived forest canopy closure; an APEX true color composite is used as background.

The stepwise multiple regression model yielded higher accuracy with an R^2 of 0.81, and a rRMSE of 10% (Fig. 3. 3b). This model significantly increased the R^2 and reduced the relative RMSE error. **Table S3. 2**, Fig. S3. 2 and Fig. S3. 3 illustrate the obtained mean values and distribution of R^2, RMSE, and rRMSE generated from the bootstrapping approach, yielding slightly better results compared to cross validation approach (i.e., R^2 of 0.82 and a rRMSE of 10%). As it can be seen in Fig. 3. 3b the combination of band depth indices and a SR type index substantially improved prediction power, especially for low and medium canopy closure (20-60%). This indicates that the selected VI and band depth indices are highly sensitive to canopy closure and can minimize disturbing effects such as soil background, atmospheric, and sun–target-sensor geometry effects [91].

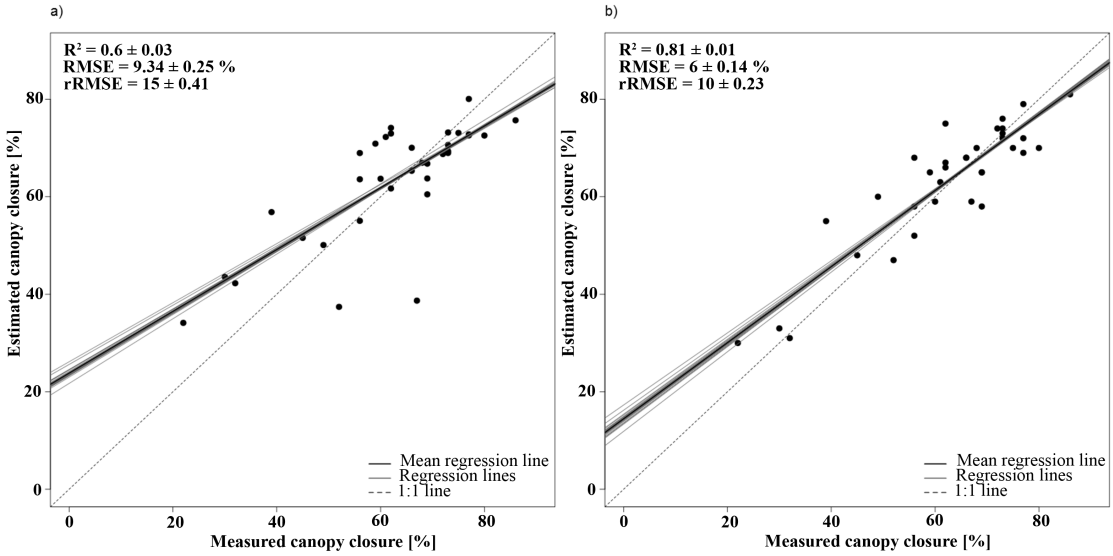

Fig. 3. 3. Agreement of estimated canopy closure with in-situ data; (a) simple regression model based on a PVI index; (b) stepwise multiple regression model based on band depth indices and a SR type index. The corresponding wavelengths of the indices are given in Table 3. 3. Coefficient of determination (R^2 ± SD), root mean square error (RMSE ± SD), and relative root mean square error of prediction (rRMSE ± SD) are shown.

3.3.2.2 Basal area

The maximum R^2 obtained from the correlation plots for basal area considering SR, NDVI, and PVI is almost identical ($R^2 > 0.60$). The pattern of variation in R^2 is similar for SR and NDNI type VIs (Fig. S3. 4(a) and (b)). In addition, these figures show that the narrow-band combinations generated mainly from narrow portions of the SWIR can explain variability in basal area most effectively. Contrary to SR and NDVI type VIs, the PVI and SAVI2 type VIs (Fig. S3. 4(c) and (d)) resulted in different correlograms in terms of sensitive wavelengths. Fig. S3. 4 shows that a large portion of the spectrum could potentially be used to predict basal area. Sensitive combinations are mainly generated from i) the VIS part in combination with NIR and SWIR parts, ii) the red-edge region in combination with NIR wavelengths, and iii) a combination of NIR wavelengths themselves or together with the SWIR part. Interestingly, the highest variability explained by SAVI2 type indices ($R^2 = 0.44$) is significantly smaller than the highest R^2 for SR, NDVI, and PVI (0.69, 0.69, 0.64).

The optimal narrowband VIs derived from 2D correlograms to predict basal area are presented in **Table S3. 3**. An SR type index that can be calculated from the SWIR (2385 nm, 1993 nm), and a NDVI type index located in the SWIR (1993 nm, 2391 nm) contained most information to estimate the basal area. The stepwise multiple regression using all optimal VIs did not improve model performance (data not shown). Several studies have reported a

strong correlation between the SWIR domain and basal area [10], [11], [65], [92]. The SWIR region is highly affected by canopy water content [50], canopy biochemical properties like cellulose, lignin and protein [93], and shadowing [94]. Forest structural attributes such as basal area are related to the addressed variables. Our results show that the selected VIs from the SWIR region are best correlated to basal area (Table S3).

Stepwise multiple regression was subsequently performed to assess the joint usage of optimal narrow-band VIs and band depth indices to predict basal area. As is evident from **Table 3. 4**, the best performing stepwise multiple regression model (including a SR type VI and a normalized band depth index (NBDI) obtained a higher R^2 compared to the best performing simple linear model. The result of an ANOVA test ($p = 0.017$) indicated a statistically significant difference between the two models at 5% significance level. The significant wavelengths in both the simple and the stepwise multiple regression model are located in the SWIR part of the spectrum. For forest basal area estimation NDVI, PVI, and SAVI2 type indices did not lead to improved model fits.

Table 3. 4

Best performing simple and stepwise multiple regression models to predict basal area.

Variable	Model	Wavelength (nm)	R^2	VIF
Basal area	Y=-252.01*SR+220.32	2385, 1993	0.63	1
	Y=-265.2*SR-115.99*NBDI_SWIR1+241.269	**NBDI_SWIR1: 1698** **SR: 2385, 1993**	**0.72**	**1.02** **1.02**

The basal area thematic map was generated by employing the stepwise multiple regression model and the APEX IS data set (Fig. 3. 4). The estimated values ranged from 0 to 75 m^2/ha with an average of 42 ± 17 m^2/ha.

The relationship between measured and estimated basal area obtained by applying a LOOCV approach is illustrated in Fig. 3. 5. The simple linear model yielded an R^2 value of 0.60, a RMSE value of 9 m^2/ha, and a rRMSE value of 23% (Fig. 3. 5a). The stepwise multiple regression model produced a higher R^2 (R^2 = 0.68), and decreased the RMSE and the rRMSE values to 8 m^2/ha and 20%. This result is in line with the findings of Mutanga & Skidmore [62], who concluded that the use of stepwise multiple regression using band depth information improved structural parameter estimation (biomass). The suitability of band depth indices to assess vegetation structural attributes has been indicated by previous studies [52], [69], [90], [95], [96].

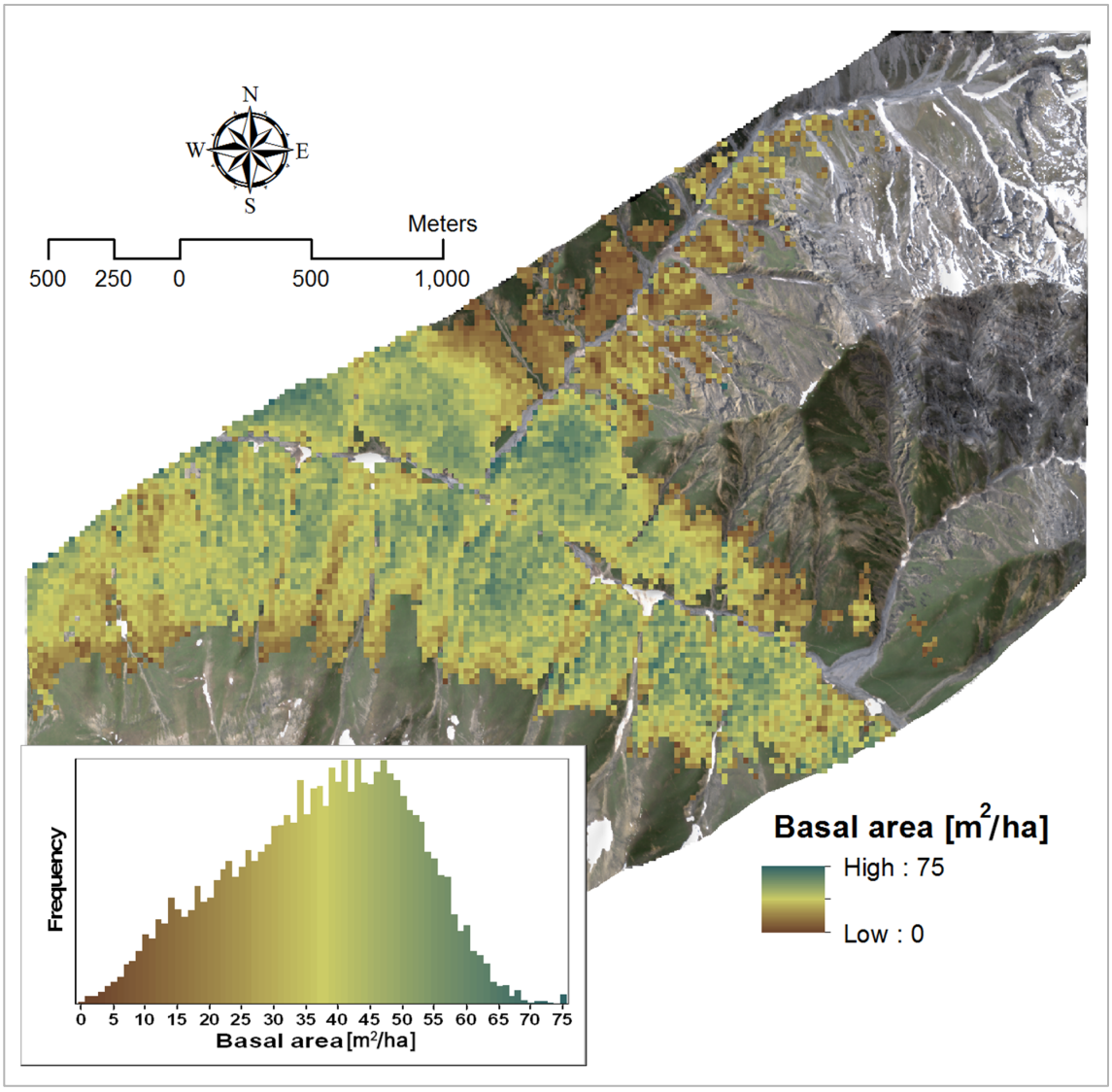

Fig. 3. 4. Predicted map of forest basal area in Val Trupchun; an APEX true color composite is used as background.

As can be observed from Fig. 3. 5(a) and (b), the linear relationship between estimated and measured basal area is stronger for the stepwise multiple regression model than for the simple model. In fact, for the simple model, the trend line is closer to power form (non-linear) than to a linear relationship in a way that applying an exponential model would increase the model performance (R^2 = 0.63). The bootstrapping approach (**Table S3. 4**, Fig. S3. 5 Fig. S3. 6) confirms the statistics of the leave-one-out cross validation approach and yielded a R^2 of 0.68 and a rRMSE of 20%.

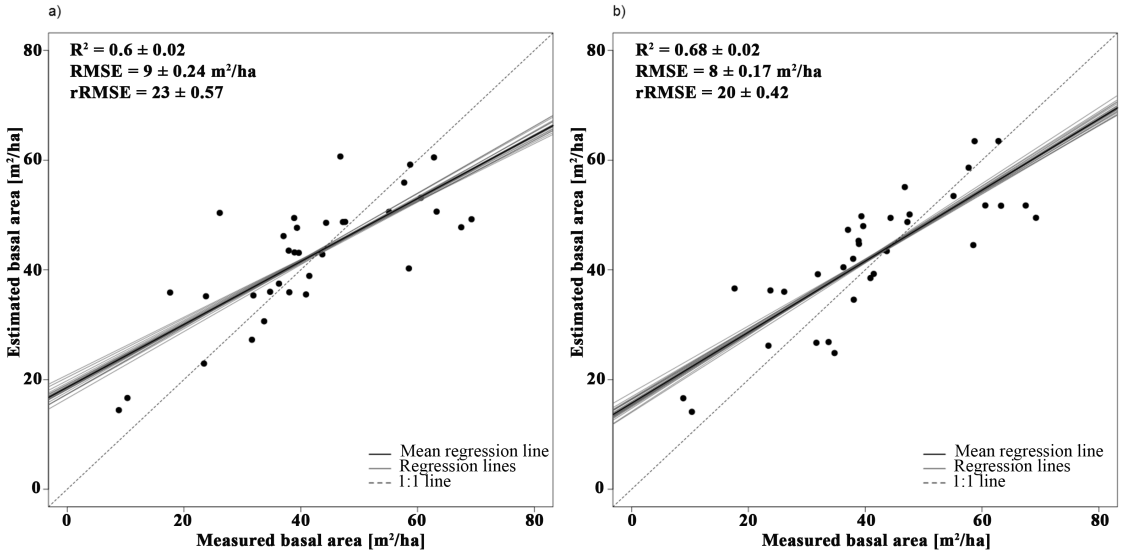

Fig. 3. 5. Agreement of estimated basal area with in-situ data; (a) simple regression model based on a SR index; (b) stepwise multiple regression model based on a band depth index and a SR type index. The corresponding wavelengths of the indices are given in Table 3. 4. Coefficient of determination (R^2 ± SD), root mean square error (RMSE ± SD), and relative root mean square error of prediction (rRMSE ± SD) are shown.

3.3.2.3 Volume

Considering all potential band combinations for SR, NDVI, PVI and SAVI2 type indices for forest volume, the strength of relationship increased from the VIS to the SWIR for all generated VIs (Fig. S3. 7). Maximum R^2 was higher for SR, NDVI, and PVI type indices compared to SAVI2. The similar sensitive spectral region to predict volume using SR and NDVI type indices observed and mainly located in the SWIR (Fig. S3. 7 (a) and (b)). These two types of VIs are functionally similar and thus contain the same information [97]. In addition to the SWIR region, parts of the VIS and NIR regions showed sensitivity to predict volume using PVI and SAVI2 type indices (Fig. S3. 7(c) and (d)).

Table S3. 5 lists the best narrow-band VIs derived from 2D correlograms based on a set of criteria introduced in the method section to estimate volume. The maximum R^2 value varied from 0.61, 0.61, 0.64, to 0.38 using the SR, NDVI, PVI, and SAVI2. A PVI type index located in the SWIR (1993 nm and 2091 nm) provided more information to estimate forest volume than the other categories of VIs (i.e., SR, NDVI, and SAVI2 type). The predictive performance of a SR and a NDVI type index (1993 nm and 2385 nm), both with R^2 = 0.61, was slightly lower than in the case of PVI. **Table S3. 5** indicates the suitability of the SWIR region for forest volume estimation. Our findings correspond with Schlerf et al. [61], who reported highest correlations of narrow-band indices with forest crown volume in wavelengths related to water absorption features in the SWIR. In contrast, Cho et al. [39]

found that VIs based on the contrast between reflectance values in the red-edge shoulder of the spectrum and in water absorption features are related to forest structural attributes. The relationship between the SWIR spectral information and forest volume has been reported elsewhere [7], [85]. However, some study reported red and near-infrared spectral bands as good predictors to estimate forest volume [17]. A stepwise multiple regression analysis on all optimal VIs listed in **Table S3. 5** did not improve the model performance (data not shown).

The combined use of optimal narrow-band VIs and band depth indices was assessed to predict forest volume using a stepwise multiple regression. It is evident from **Table 3. 5** that the stepwise multiple regression model (including a PVI type VI and a NBDI index) obtained a higher R^2 compared to the best performing simple linear model. The result of an ANOVA test ($p = 0.024$) indicated a statistically significant difference between the two models at 5% significance level. The significant wavelengths in both the simple and the stepwise multiple regression model are located in the SWIR part of the spectrum. From our results, it appears that the band depth indices have a high potential for an improved estimation of forest volume and forest structure attributes in general. This might be due to the capability of such indices to minimize effects of external influences, such as atmospheric water vapor, soil background [71] and BRDF effects [68].

Table 3. 5

Best performing simple and stepwise multiple regression models to estimate volume.

Variable	Model	Wavelength (nm)	R2	VIF
Volume	Y=3.27*PVI+59.79	1993, 2091	0.64	-
	Y=- 2052.02*NBDI_SWIR1+3.33*PVI +185.91	**NBDI_SWIR1: 1698 PVI: 1993, 2091**	**0.72**	**1.03 1.03**

The volume thematic map generated from APEX IS data is shown in Fig. 3. 6. The average estimated forest volume was 431 ± 149 m^3/ha. Fig. 3. 7 illustrates the agreement between measured and estimated forest volume for the simple and the stepwise multiple regression model. The simple model explained 68% of variability in volume estimation (R^2 = 0.68, RMSE = 101 m^3/ha, and rRMSE = 24) based on a PVI type index involving wavelengths at 1993 nm and 2091 nm. The stepwise multiple regression model showed an improvement in volume prediction (R^2 = 0.73, RMSE = 90 m^3/ha, and rRMSE = 22%) including a combination of a PVI type index and a band depth index (NBDI). The bootstrapping (**Table S3. 6**, Fig. S3. 8 and Fig. S3. 9) yielded similar results compared to cross validation approach, with a R^2 of 0.72 and a rRMSE of 22%.

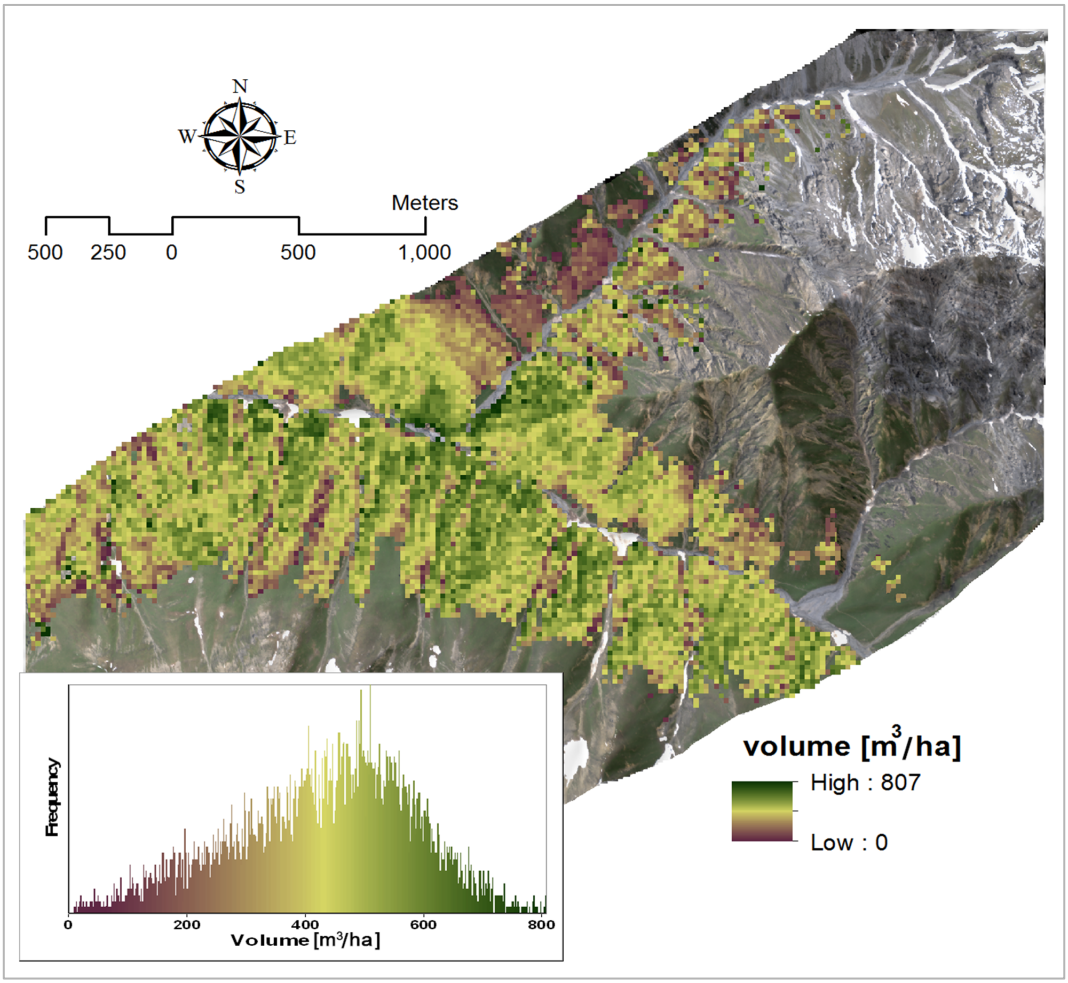

Fig. 3. 6. Map and frequency distribution of estimated forest volume in Val Trupchun; an APEX true color composite is used as background.

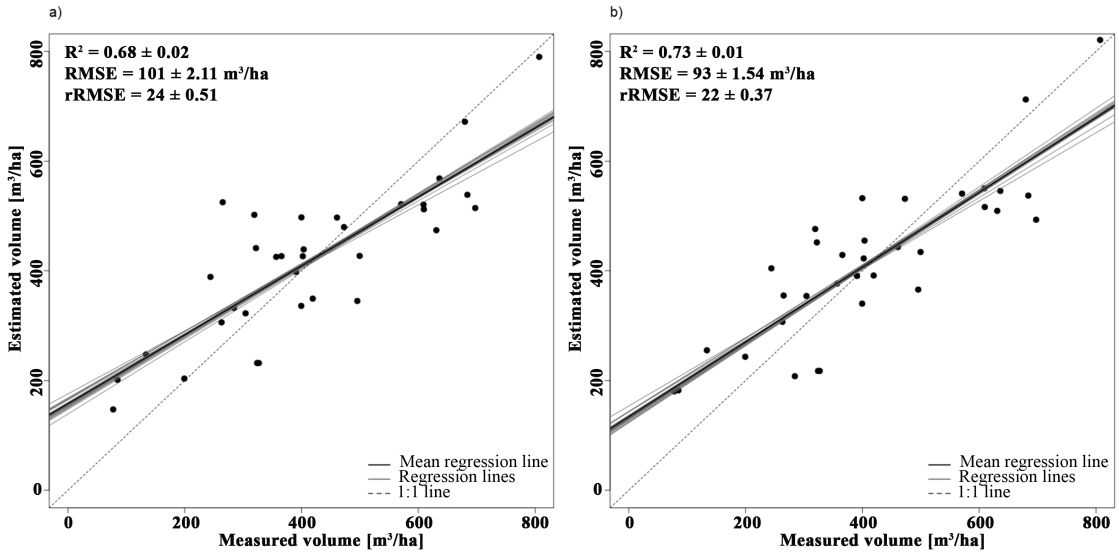

Fig. 3. 7. Agreement of estimated volume with is-situ data; (a) simple model based on a PVI index; (b) stepwise multiple regression model based on a combination of a band depth index and a PVI type index. The corresponding wavelengths of the indices are given in Table 3. 5. Coefficient of determination (R^2 ± SD), root mean square error (RMSE ± SD), and relative root mean square error of prediction (RMSE% ± SD) are shown.

3.4 Discussion

3.4.1 Reliability of structural parameter retrieval from APEX data

3.4.1.1 Canopy closure

Sensitive band combinations to predict canopy closure were selected from the red-edge, NIR, and SWIR part of the spectrum. These results are in line with previous studies suggesting optimal combinations for estimation of forest structural attributes in the red-edge region [62], [67], [98] and in the NIR and SWIR spectral regions [55], [58], [99]. Our canopy closure estimates are comparable or even higher than results reported elsewhere. For example, Schlerf et al. [61] employed a PVI index based on wavelengths at 885 nm and 954 nm with an R^2 of 0.79 to map crown volume in a relatively homogenous Norway spruce (*Picea abies*) stand. Although we assessed the capability of APEX IS data in a heterogeneous ecosystem with complicated stand structure and tree composition, our results are slightly higher than those reported in Schlerf et al. [61]. We conclude that heterogeneity helps to increase the spectral sensitivity required to infer forest structural variables due to increased contrast between canopy and background reflectance [100]. In other words, a highly dynamic spectral range, as found in heterogeneous areas, contributes to improved forest canopy closure estimations [101]. Reported accuracies for canopy closure estimates in previous studies utilizing multispectral [7], [102]–[104], hyperspectral [22], or a fusion of active and passive data [21], ranged between 0.50- 0.88 (R^2) and 15-30% (relative RMSE). The performances of our simple and stepwise multiple regression model lie in the reported accuracy ranges. However, the relative RMSE error of 10% indicates a remarkably higher accuracy of canopy closure estimation. It is worth to note that an acceptable level of error for operational forest inventory is 10% [105].

3.4.1.2 Basal area

The accuracy of the stepwise multiple regression to retrieve basal area is better than previously reported results that employed IS data to estimate basal area. Hyyppä et al. [15], for example, achieved an R^2 = 0.58 and a relative RMSE of 35% using data from an AISA sensor. Defibaugh y Chávez & Tullis [20] estimated the basal area with an R^2 less than 0.30 and a relative RMSE of 50%. Anderson et al. [106] reported an R^2 value of 0.40 for the basal area prediction using Airborne Visible/Infrared Imaging Sensor (AVIRIS) data. Lefsky et al. [25] predicted basal area with an R^2 value of 0.36 using AVIRIS data. However, our R^2 value was lower than the R^2 value of Welter et al. [102]. They used SPOT5 data to model the basal area. Literature reports R^2 and RMSE% for estimating basal area

between 0.20-0.75 and 20-50% [20], [102], [106]. The performance of our simple and stepwise multiple regression models lie in the accuracy range reported in previous studies.

3.4.1.3 Volume

Our two models tend to overestimate low values and underestimate high volume values (Fig. 3. 7), an effect known as 'local bias' [39]. Deviations between estimated and measured forest volume are largest for values around 300-500 m^3/ha, strongly affecting model accuracies. A possible explanation of this effect may be related to changes in composition and vertical structure of the respective forest stands. In general, they consist of a dominant tree (larch), which forms the upper tree story, and two associated species (i.e. Swiss stone pine and Norway spruce), which dominate the middle and lower parts of the canopy. As the upper part of the forest story is clearly seen by an imaging device, the underlying tree stories may be hidden. Therefore, the true spectral variation cannot be accurately modeled by a simple relationship [57], resulting in a poor relationship between measured and estimated forest volume. This problem might be partly solved, if a type specific calibration is applied or additional forest attributes (e.g., stand age, site index) are considered [17]. Nevertheless, the performance of our models is more accurate than what was achieved by previous studies that employed IS data to estimate forest volume. Hyyppä et al. [15] predicted forest volume with an R^2 of 0.55 and a relative RMSE of 45% using AISA IS data with 30 spectral bands (466-870 nm). In the case of APEX, the availability of a larger spectral range incorporating the SWIR region might explain why our models yielded a higher accuracy. Recently, Hill et al. [107] assessed the capability of LIDAR Canopy Height Models (CHM) and forest inventory data to map timber volume in a mountainous study site in Eastern Switzerland using a multiple linear regression model approach. They obtained an R^2 value of 0.64 and a RMSE of 123 m^3/ha (31% of the mean). Interestingly, both our simple and stepwise multiple regression model performed slightly better [107].

The relative error of volume estimation using optical remote sensing has been reported between 20-75% [63], [108], [109]. It should be mentioned that for operational forest management the acceptable level of estimation error is 15% at stand level [108]. Although APEX derived forest volume showed a significant improvement in estimation performance, the method is not yet accurate enough for operational forest management from an accuracy requirements point of view.

3.4.2 Reliability of empirical approaches to estimate canopy structural variables from IS data

Our results are in line with many other studies [39], [46], [47], [61] and clearly demonstrate that empirical-statistical methods allow relating spectroscopy measurements with forest structural variables and, thus, quantifying them. However, it is important to interpret such empirical results in the context of causality. Measurements of reflected radiance in the optical spectral domain are per se less or not sensitive for forest structural variables, particularly for the variables *basal area* or *timber volume*. In fact, optical measurements are mostly representative for the upper canopy part, and derived information tends, for example, to saturate with increasing canopy volume [40], [110], [111]. This indicates that results obtained in our study are likely based on secondary relationships. The explanation why we found significant correlations between IS data and forest structural variables is that certain forest structural variables (i.e., basal area, volume) are related to structural variables (i.e., canopy cover) directly affecting the radiative transfer of optical measurements. In fact, based on our field data we observed significant correlation between canopy cover and both volume ($r(35) = 0.62$, $p < 0.01$) and basal area ($r(35) = 0.74$, $p < 0.01$) (**Table S3. 7**). In addition, the combination of forest structural variables and sun illumination causes specific patterns of cast shadow. These illumination effects often persist after atmospheric compensation, particularly for heterogeneous surfaces measured in high spatial resolution [112]. These processing artifacts eventually translate into optical indices derived and allow relating them with canopy structural variables as shown with our results.

The contradiction between good empirical findings obtained and missing causality implies two things. First, it is possible to apply relatively simple methods to retrieve forest structural information from spectroscopy data, if extensive reference data are available and the empirical models are only applied to a specific canopy at particular time, observed with a specific sensor [41]. Second, obtained results must be interpreted very carefully: extreme values or observed anomalies are likely caused by the limited representativeness of underlying empirical models.

3.4.3 Strategies for improved simultaneous retrieval of biochemical and structural plant traits

The great advantage of optical RS data is that they allow retrieving various plant functional traits and these data are frequently used to estimate forest structural attributes. According to our discussion above, several problems are, however, related to the use of

optical RS data in combination with empirical approaches to retrieve structural variables. Particularly in closed dense forests with a complex and multi-layered canopy [25], [113], spectral signals and eventually derived empirical models saturate. Further, calculated surface reflectances are typically affected by shadowing and BRDF effects, contributions of the soil background, and atmospheric conditions. Active RS systems such as LiDAR are more suitable for capturing structural forest information, but also suffer from certain limitations (i.e., data are expensive, their availability is limited in coverage, they may be prone to low point density, algorithms to generate digital surface and terrain model suffer from shortcomings) and, importantly, do not allow obtaining functional or biochemical plant traits.

With increasing evidence it can be concluded that there is no single RS technology available to consistently retrieve forest structural attributes [20], [21], [114], [115]. The combination of both technologies is considered the most promising strategy to provide highly accurate estimates of forest structural attributes [66], [106], [116] and other plant traits [117], [118]. Future research attempts are needed to properly evaluate the capability of combined approaches and to tackle various technical issues such as the temporal and geometric integration of these complementary observational approaches.

3.5 Conclusion

We conclude that APEX data in combination with empirical-statistical approaches allow estimating forest structural attributes including canopy closure, basal area and volume in heterogeneous alpine ecosystems. The two tested *simple* and *stepwise multiple regression* models, applied to narrow-band indices and band depth indices, provide a relatively simple analytical framework for forest structural parameter retrievals but at the cost of causality between surface information and light interaction. Among the structural attributes, canopy closure was predicted more accurately than basal area and volume. The SWIR region of the reflectance spectrum was found to be particularly sensitive to forest structural attributes and could be used to predict relevant parameters. The availability of a high quality imaging spectrometer with high signal to noise ratio (SNR), especially in the SWIR region, is, thus, crucial for forest research. Once a simple model was applied, the use of a PVI type narrow-band index showed a strong correlation with canopy closure and volume. However, more variation was explained by using a SR type index to estimate basal area. Stepwise multiple regression models based on a combined use of narrow-band VIs and band depth indices provided improved estimates of forest structural attributes compared to simple models that apply only narrow-band type indices. We therefore

conclude that band depth indices generated from continuum removed spectra in combination with simple narrow-band indices can be used to predict forest structural variables, in particular for canopy closure assessment. This methodology, however, needs further investigation in different forest ecosystems with different structural and species compositions.

Considerable effort has been made by numerous researchers to successfully estimate forest structural attributes using empirical approaches [119]. However, results obtained from empirical approaches are limited in their representativeness and are only valid for specific vegetation types, phenological state, and sensors. Further, underlying empirical models rely on extensive in-situ data. Both aspects question the operational applicability of empirical approaches to retrieve complex surface information such as forest structural variables. Physically-based approaches may partly overcome these limitations but will still face the problem of a limited sensitivity of optical data for structural vegetation variables.

We suggest combining active and passive RS, two complementary techniques that provide optimal capability and sensitivity to characterize complex forest ecosystems. Active systems are the preferred solution to obtain various structural information, while optical systems can provide complementary information about other important plant functional traits.

Acknowledgements

This work was funded by the University of Kurdistan. We are grateful to Mahtab Pir Bavaghar, Naghi Shaebanian, Hedayat Ghazanfari, and Zahed Shakeri for their support at the Forestry Department, University of Kurdistan. We would like to thank Daniel Henke and Damien Markulin for their help with the field data collection, and the Swiss National Park staff for providing logistic support during field campaigns. The contribution of M.E.S. is supported by the University Research Priority Program on “Global Change and Biodiversity” (URPP GCB) of the University of Zurich. The authors would like to thank four anonymous reviewers for their valuable comments on the manuscript.

Author contributions

Parviz Fatehi designed the research and analyzed the data with scientific advice of Alexander Damm, Mathias Kneubühler, and Michael E. Schaepman. Parviz Fatehi wrote the manuscript and all co-authors thoroughly reviewed and edited the manuscript.

Conflicts of interest

The authors declare no conflict of interest.

Support Information

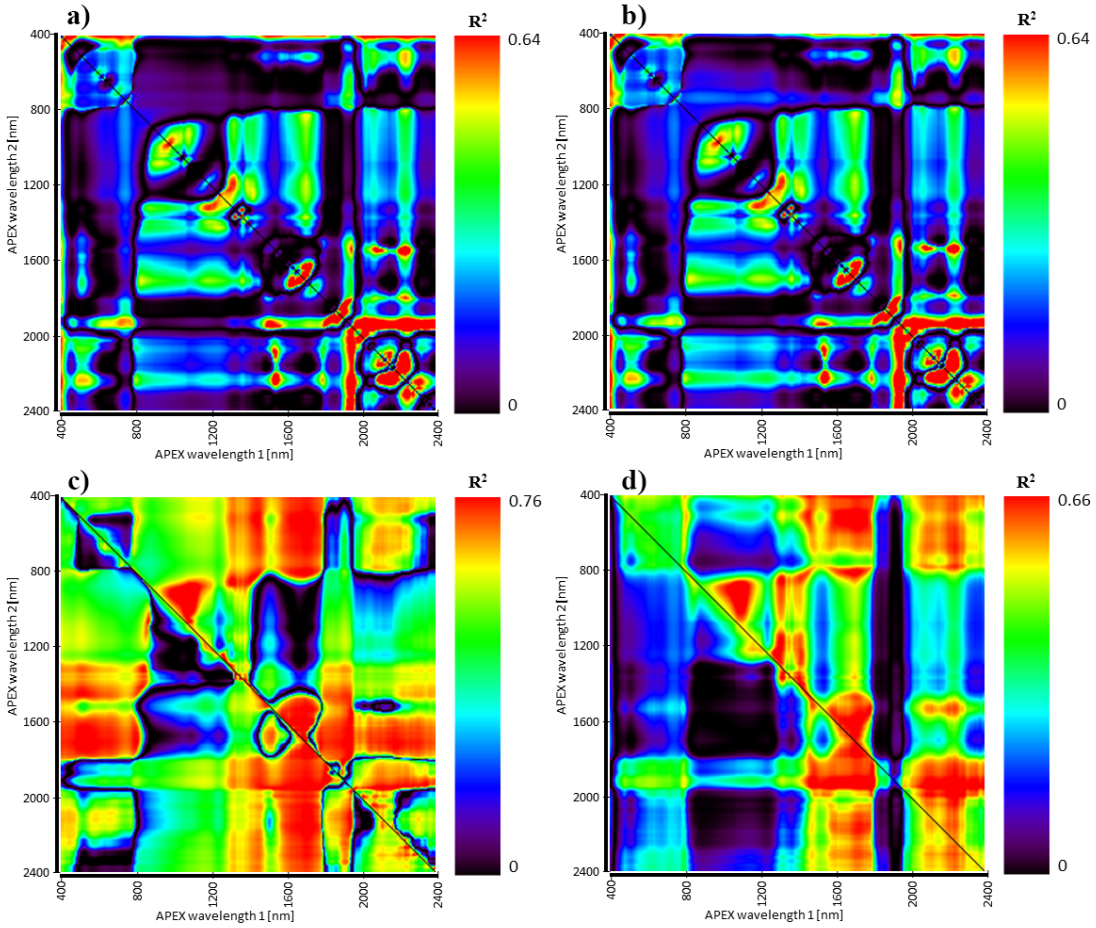

Fig. S3. 1. Correlograms showing the coefficients of determination (R^2) between VIs for all two-band combinations and forest canopy cover. (a) simple ratio (SR) type; (b) NDVI type ; (c) PVI type; (d) SAVI2 type.

Table S3. 1

Best narrow-band VIs derived from 2D correlograms to estimate canopy cover.

Vegetation index	ρ_1(nm)	ρ_2(nm)	R^2
SR Type	2326	1993	0.58
	2404	1993	0.61
	2267	1993	0.51
	2253	2204	0.62
	2204	2253	0.61
NDVI Type	2204	2253	0.61
	1993	2273	0.51
	1993	2326	0.54
	1993	2391	0.53
PVI Type	1716	553	0.54
	1707	586	0.53
	883	**763**	**0.76**
	1654	1545	0.52
	1724	1554	0.55

	1698	1654	0.62
	569	1689	0.53
	1698	1776	0.52
	2162	1993	0.56
	1636	1993	0.52
	1716	2155	0.52
	1716	2232	0.52
	895	754	0.65
	2162	1993	0.55
SAVI2 Type	2239	1993	0.55
	2287	1993	0.57
	2385	1993	0.61

Table S3. 2

Bootstrap results for the best simple and the best stepwise multiple regression model to estimate canopy closure.

Feature	Bootstrap R^2		Bootstrap RMSE (%)		Bootstrap rRMSE (%)	
	Mean	SD	Mean	SD	Mean	SD
Simple Regression	0.60	0.14	9.26	1.35	14.90	2.38
Multiple Regression	0.82	0.07	6.22	0.78	10.01	1.34

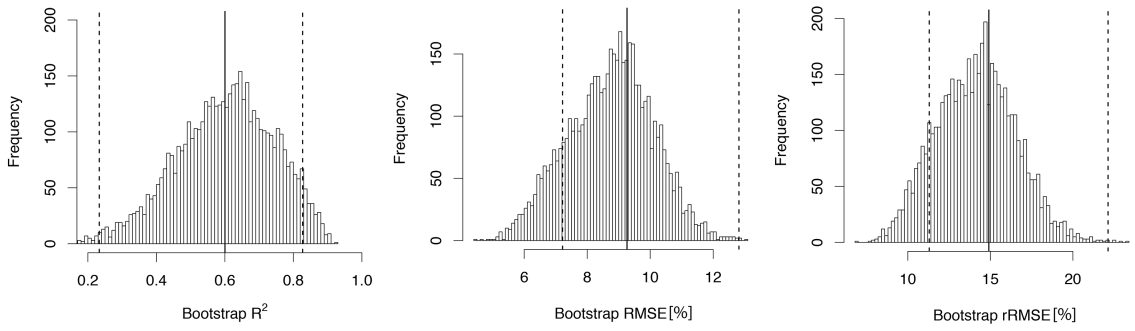

Fig. S3. 2. Histogram of R^2, RMSE, and rRMSE as obtained from the bootstrapping for the best simple regression model to estimate canopy closure. The solid line represents the mean value, both dashed lines indicate he upper and lower bounds for the 95 percent confidence.

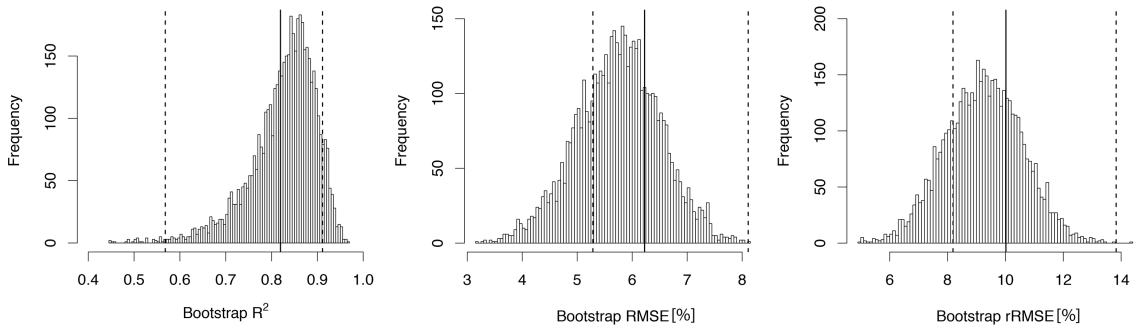

Fig. S3. 3. Histogram of R2, RMSE, and rRMSE as obtained from the bootstrapping for the best multiple regression model to estimate canopy closure. The solid line represents the mean value, both dashed lines indicate he upper and lower bounds for the 95 percent confidence.

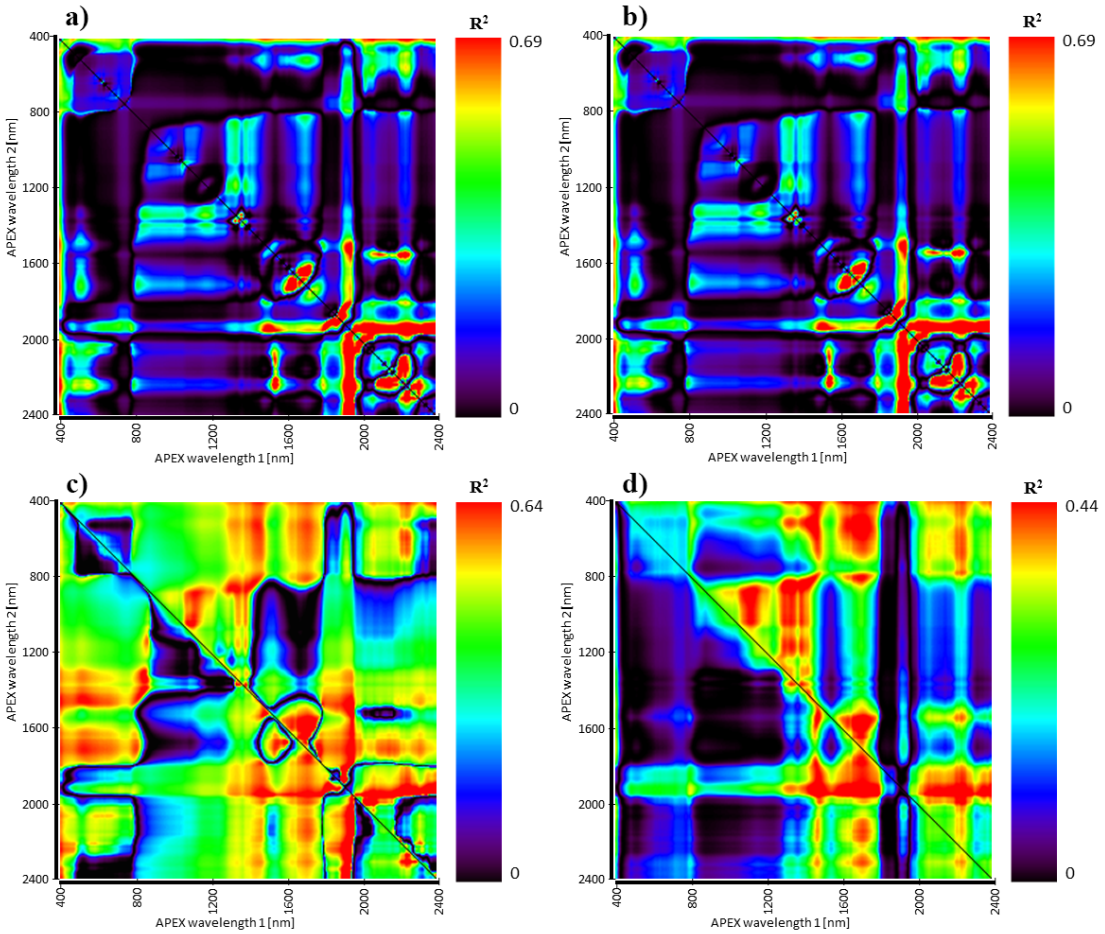

Fig. S3. 4. Correlograms showing the coefficients of determination (R^2) between VIs for all two-band combinations and basal area. (a) simple ratio (SR) type; (b) NDVI type; (c) PVI type; (d) SAVI2 type.

Table S3. 3

Best narrow-band VIs derived from 2D-correlograms to estimate basal area.

Vegetation Index	ρ_1(nm)	ρ_2(nm)	R^2
SR Type	1618	1724	0.58
	2112	1993	0.51
	2293	1993	0.53
	2385	**1993**	**0.63**
	1993	2300	0.50
	1993	2385	0.61
NDVI Type	1618	1724	0.58
	1993	2293	0.52
	1993	2391	0.62
PVI Type	1993	2112	0.55
	1993	2211	0.50
SAVI2 Type	1716	1993	0.42

Table S3. 4

Bootstrap results for the best simple and the best stepwise multiple regression model to estimate basal area.

Feature	Bootstrap R^2		Bootstrap RMSE (m^2/ha)		Bootstrap rRMSE (%)	
	Mean	SD	Mean	SD	Mean	SD
Simple regression	0.60	0.11	9.51	1.34	22.88	3.28
Multiple regression	0.68	0.07	8.50	1.01	20.45	2.47

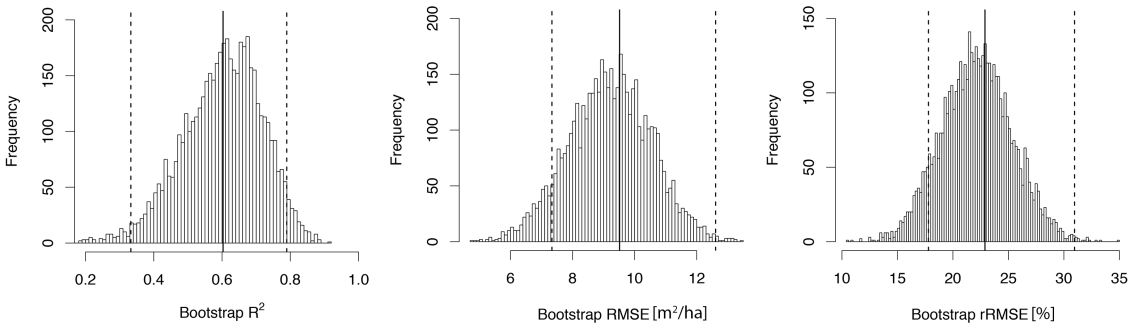

Fig. S3. 5. Histogram of R^2, RMSE, and rRMSE as obtained from the bootstrapping for the best simple regression model to estimate basal area. The solid line represents the mean value, both dashed lines indicate he upper and lower bounds for the 95 percent confidence.

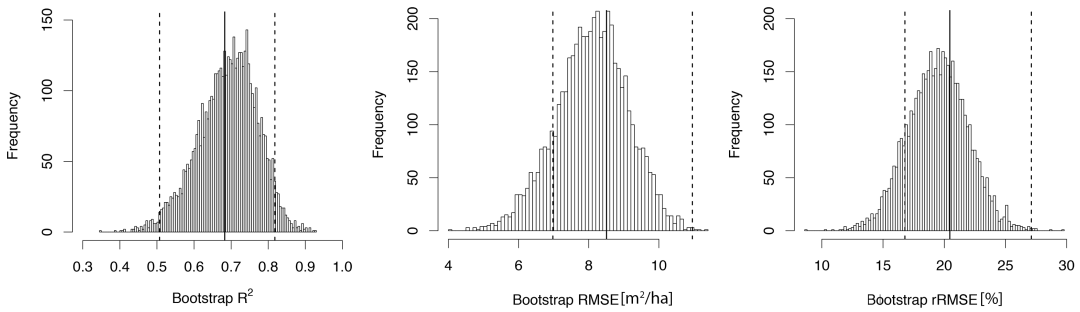

Fig. S3. 6. Histogram of R^2, RMSE, and rRMSE as obtained from the bootstrapping for the best multiple regression model to estimate basal area. The solid line shows the mean value and the dashed lines show he upper and lower bounds for the 95 percent confidence.

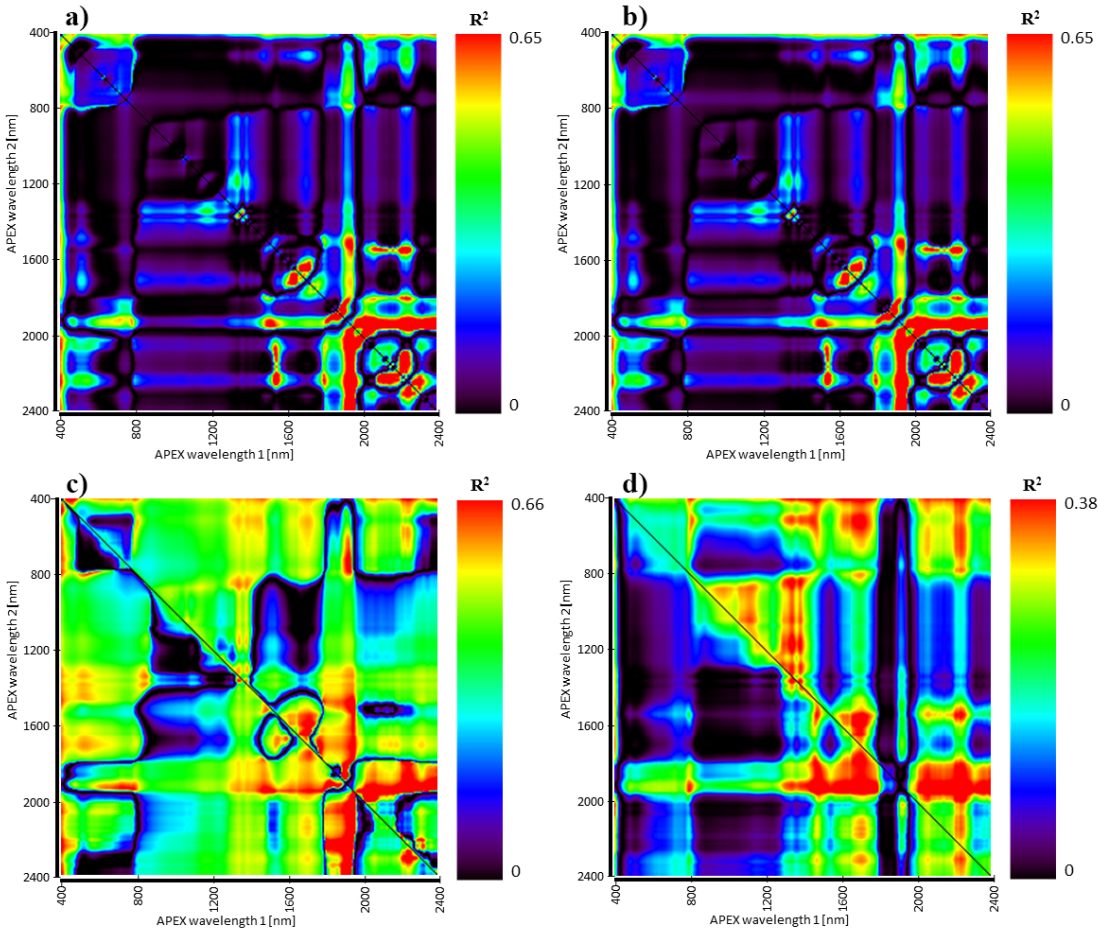

Fig. S3. 7. Correlograms showing the coefficients of determination (R^2) between VIs for all two-band combinations and timber volume. (a) simple ratio (SR) type; (b) NDVI type; (c) PVI type; (d) SAVI2 type.

Table S3. 5

Best narrow-band VIs derived from 2D-correlograms to estimate volume

Vegetation Index	ρ_1(nm)	ρ_2(nm)	R^2
SR Type	2293	1993	0.54
	2385	1993	0.61
	1993	2105	0.53
	1993	2300	0.55
	1993	2385	0.61
NDVI Type	1993	2098	0.53
	1993	2293	0.55
	1993	2385	0.61
PVI Type	2105	2001	0.56
	1993	**2091**	**0.64**
	1993	2155	0.54
SAVI2 Type	2287	1993	0.38

Table S3. 6

Bootstrap results for the simple and the best stepwise multiple regression model to estimate timber volume.

Feature	Bootstrap R^2		Bootstrap RMSE (m^3/ha)		Bootstrap rRMSE (%)	
	Mean	SD	Mean	SD	Mean	SD
Simple Regression	0.68	0.10	101.04	11.91	24.29	3.42
Multiple Regression	0.72	0.07	93.11	8.77	22.38	2.53

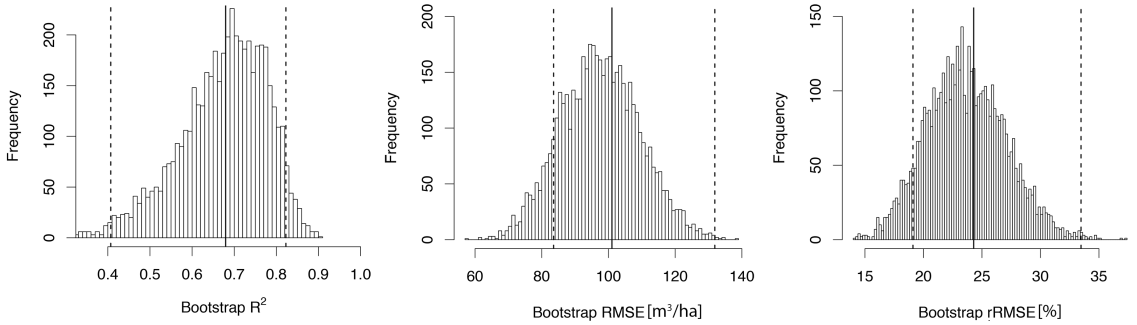

Fig. S3. 8. Histogram of R^2, RMSE, and rRMSE as obtained from the bootstrapping for the best simple regression model to estimate timber volume. The solid line represents the mean value, both dashed lines indicate he upper and lower bounds for the 95 percent confidence.

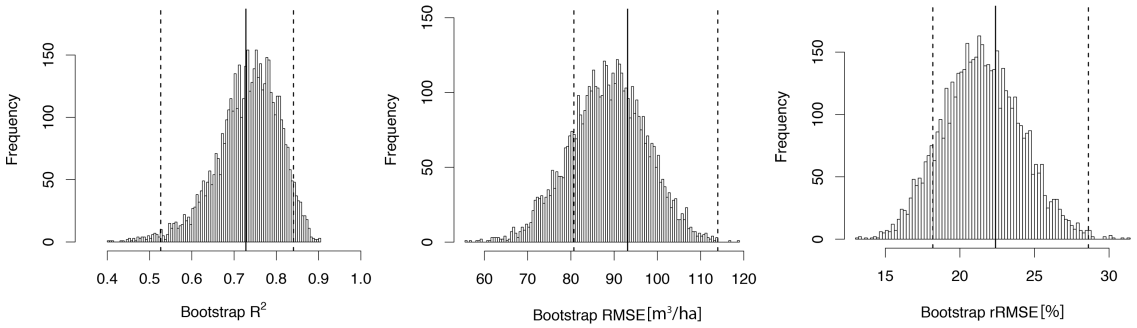

Fig. S3. 9. Histogram of R^2, RMSE, and rRMSE as obtained from the bootstrapping for the best multiple regression model to estimate timber volume. The solid line represents the mean value, both dashed lines indicate he upper and lower bounds for the 95 percent confidence.

Table S3. 7

. Correlation between measured basal area, forest volume and canopy closure (N = number of field plots, ** = correlation is significant at the *0.01* level, Sig. = indicates the *p-value* to check for significance).

		Canopy Closure	Basal Area	Volume
Canopy Closure	Pearson Correlation	1	0.741**	0.627**
	Sig.		0.000	0.000
	N	35	35	35
Basal Area	Pearson Correlation	**0.741****	1	0.946**
	Sig.	0.000		0.000
	N	35	35	35
Volume	Pearson Correlation	**0.627****	**0.946****	1
	Sig.	0.000	0.000	
	N	35	35	35

References

[1] A. Kangas and M. Maltamo, *Forest Inventory Methodology and Applications*. Springer,

2006.

[2] A. T. Hudak, N. L. Crookston, J. S. Evans, M. J. Falkowski, A. M. . Smith, P. E. Gessler, and P. Morgan, "Regression modeling and mapping of coniferous forest basal area and tree density from discrete-return lidar and multispectral satellite data," *Can. J. Remote Sens.*, vol. 32, no. 2, pp. 126–138, Apr. 2006.

[3] S. A. Soenen, D. R. Peddle, C. A. Coburn, R. J. Hall, and F. G. Hall, "Canopy Reflectance Model Inversion in Multiple For ward Mode : Forest Str uctural Information Retrieval fr om Solution Set Distributions," *Photogramm. Eng. Remote Sens.*, vol. 75, no. 4, pp. 361–374, 2009.

[4] IPCC, "Good practice guidance for land use, land-use change and forestry," Hayama, Japan, 2003.

[5] J. E. Luther, R. A. Fournier, D. E. Piercey, L. Guindon, and R. J. Hall, "Biomass mapping using forest type and structure derived from Landsat TM imagery," *Int. J. Appl. Earth Obs. Geoinf.*, vol. 8, no. 3, pp. 173–187, Sep. 2006.

[6] M. V. Gil, D. Blanco, M. T. Carballo, and L. F. Calvo, "Carbon stock estimates for forests in the Castilla y León region, Spain. A GIS based method for evaluating spatial distribution of residual biomass for bio-energy," *Biomass and Bioenergy*, vol. 35, no. 1, pp. 243–252, Jan. 2011.

[7] R. J. Hall, R. S. Skakun, E. J. Arsenault, and B. S. Case, "Modeling forest stand structure attributes using Landsat ETM+ data: Application to mapping of aboveground biomass and stand volume," *For. Ecol. Manage.*, vol. 225, no. 1–3, pp. 378–390, Apr. 2006.

[8] J. Cermák, N. Nadezhdina, M. Trcala, and J. Simon, "Open field-applicable instrumental methods for structural and functional assessment of whole trees and stands," *iForest - Biogeosciences For.*, vol. 40, no. 4, pp. 1–53, Sep. 2014.

[9] P. M. Treitz and P. J. Howarth, "Hyperspectral remote sensing for estimating biophysical parameters of forest ecosystems," *Prog. Phys. Geogr.*, vol. 23, no. 3, pp. 359–390, Jul. 1999.

[10] P. T. Wolter, P. a. Townsend, B. R. Sturtevant, and C. C. Kingdon, "Remote sensing of the distribution and abundance of host species for spruce budworm in Northern Minnesota and Ontario," *Remote Sens. Environ.*, vol. 112, pp. 3971–3982, 2008.

[11] M. E. Jakubauskas and K. P. Price, "Empirical Relationships between Structural and Spectral Factors of Yellowstone Lodgepole Pine Forests," *Photogramm. Eng. Remote Sens.*, vol. 63, no. 1, pp. 1375–1381, 1997.

[12] P. Hyde, R. Dubayah, W. Walker, J. B. Blair, M. Hofton, and C. Hunsaker, "Mapping forest structure for wildlife habitat analysis using multi-sensor (LiDAR, SAR/InSAR, ETM+, Quickbird) synergy," *Remote Sens. Environ.*, vol. 102, pp. 63–73, 2006.

[13] J. Schumacher and J. R. Christiansen, "Forest canopy water fluxes can be estimated using canopy structure metrics derived from airborne light detection and ranging (LiDAR)," *Agric. For. Meteorol.*, vol. 203, pp. 131–141, 2015.

[14] T. Ota, O. S. Ahmed, S. E. Franklin, M. A. Wulder, T. Kajisa, N. Mizoue, S. Yoshida, G. Takao, Y. Hirata, N. Furuya, T. Sano, S. Heng, and M. Vuthy, "Estimation of Airborne

Lidar-Derived Tropical Forest Canopy Height Using Landsat Time Series in Cambodia," *Remote Sens.*, vol. 6, no. 11, pp. 10750–10772, Nov. 2014.

[15] J. Hyyppä, H. Hyyppä, M. Inkinen, M. Engdahl, S. Linko, and Y.-H. Zhu, "Accuracy comparison of various remote sensing data sources in the retrieval of forest stand attributes," *For. Ecol. Manage.*, vol. 128, no. 1–2, pp. 109–120, Mar. 2000.

[16] D. Lu, "The potential and challenge of remote sensing-based biomass estimation," *Int. J. Remote Sens.*, vol. 27, no. 7, pp. 1297–1328, Apr. 2006.

[17] M. T. Gebreslasie, F. B. Ahmed, and J. a. N. van Aardt, "Predicting forest structural attributes using ancillary data and ASTER satellite data," *Int. J. Appl. Earth Obs. Geoinf.*, vol. 12, pp. S23–S26, Feb. 2010.

[18] K. T. Vashum and S. Jayakumar, "Methods to Estimate Above-Ground Biomass and Carbon Stock in Natural Forests - A Review," *J. Ecosyst. Ecography*, vol. 02, no. 04, pp. 1–7, 2012.

[19] R. Sivanpillai, C. T. Smith, R. Srinivasan, M. G. Messina, and X. B. Wu, "Estimation of managed loblolly pine stand age and density with Landsat ETM+ data," *For. Ecol. Manage.*, vol. 223, pp. 247–254, 2006.

[20] J. Defibaugh y Chávez and J. A. Tullis, "Deciduous Forest Structure Estimated with LIDAR-Optimized Spectral Remote Sensing," *Remote Sens.*, vol. 5, no. 1, pp. 155–182, Jan. 2013.

[21] D. Stojanova, P. Panov, V. Gjorgjioski, A. Kobler, and S. Džeroski, "Estimating vegetation height and canopy cover from remotely sensed data with machine learning," *Ecol. Inform.*, vol. 5, no. 4, pp. 256–266, Jul. 2010.

[22] R. Pu and P. Gong, "Wavelet transform applied to EO-1 hyperspectral data for forest LAI and crown closure mapping," *Remote Sens. Environ.*, vol. 91, pp. 212–224, 2004.

[23] J. Clevers, G. Van der Heijden, S. Verzakov, and M. E. Schaepman, "Estimating grassland biomass using SVM band shaving of hyperspectral data," *Photogramm. Eng. Remote Sens.*, vol. 73, no. 10, pp. 1141–1148, 2007.

[24] D. Lu, P. Mausel, E. Brondízio, and E. Moran, "Relationships between forest stand parameters and Landsat TM spectral responses in the Brazilian Amazon Basin," *For. Ecol. Manage.*, vol. 198, no. 1–3, pp. 149–167, Aug. 2004.

[25] M. A. Lefsky, W. B. Cohen, and T. A. Spies, "An evaluation of alternate remote sensing products for forest inventory, monitoring, and mapping of Douglas-fir forests in western Oregon," *Can. J. For. Res.*, vol. 31, no. 1, pp. 78–87, 2001.

[26] K. Lim, P. Treitz, M. A. Wulder, B. St-Onge, and M. Flood, "LiDAR remote sensing of forest structure," *Prog. Phys. Geogr.*, vol. 27, no. 1, pp. 88–106, Mar. 2003.

[27] E. Næsset, T. Gobakken, J. Holmgren, H. Hyyppä, J. Hyyppä, M. Maltamo, M. Nilsson, H. Olsson, Å. Persson, and U. Söderman, "Laser scanning of forest resources: the nordic experience," *Scand. J. For. Res.*, vol. 19, no. 6, pp. 482–499, Dec. 2004.

[28] J. Hyyppä, X. Yu, H. Hyyppä, M. Vastaranta, M. Holopainen, A. Kukko, H. Kaartinen, A. Jaakkola, M. Vaaja, J. Koskinen, and P. Alho, "Advances in Forest Inventory Using Airborne Laser Scanning," *Remote Sens.*, vol. 4, no. 12, pp. 1190–1207, May 2012.

[29] H. Latifi, A. Nothdurft, and B. Koch, "Non-parametric prediction and mapping of standing timber volume and biomass in a temperate forest: application of multiple optical/LiDAR-derived predictors," *Forestry*, vol. 83, no. 4, pp. 395–407, Jul. 2010.

[30] D. Riaño, E. Meier, B. Allgower, E. Chuvieco, and S. L. Ustin, "Modeling airborne laser scanning data for the spatial generation of critical forest parameters in fire behavior modeling," *Remote Sens. Environ.*, vol. 86, no. 2, pp. 177–186, Jul. 2003.

[31] A. Swatantran, R. Dubayah, D. Roberts, M. Hofton, and J. B. Blair, "Mapping biomass and stress in the Sierra Nevada using lidar and hyperspectral data fusion," *Remote Sens. Environ.*, vol. 115, no. 11, pp. 2917–2930, Nov. 2011.

[32] J. C. Suárez, C. Ontiveros, S. Smith, and S. Snape, "Use of airborne LiDAR and aerial photography in the estimation of individual tree heights in forestry," *Comput. Geosci.*, vol. 31, no. 2, pp. 253–262, Mar. 2005.

[33] H. K. Gibbs, S. Brown, J. O. Niles, and J. A. Foley, "Monitoring and estimating tropical forest carbon stocks: making REDD a reality," *Environ. Res. Lett.*, vol. 2, no. 4, p. 045023, Oct. 2007.

[34] T. Park, R. Kennedy, S. Choi, J. Wu, M. A. Lefsky, J. Bi, J. Mantooth, R. Myneni, and Y. Knyazikhin, "Application of Physically-Based Slope Correction for Maximum Forest Canopy Height Estimation Using Waveform Lidar across Different Footprint Sizes and Locations: Tests on LVIS and GLAS," *Remote Sens.*, vol. 6, no. 7, pp. 6566–6586, Jul. 2014.

[35] K. Lim, P. Treitz, K. Baldwin, I. Morrison, and J. Green, "Lidar remote sensing of biophysical properties of tolerant northern hardwood forests," *Can. J. Remote Sens.*, vol. 29, no. 5, pp. 658–678, Oct. 2003.

[36] M. A. Lefsky, W. B. Cohen, G. G. Parker, and D. J. Harding, "Lidar Remote Sensing for Ecosystem Studies," *Bioscience*, vol. 52, no. 1, p. 19, 2002.

[37] D. Gatziolis, J. S. Fried, and V. S. Monleon, "Challenges to estimating tree height via LiDAR in closed-canopy forests: A parable from Western Oregon," *For. Sci.*, vol. 56, no. 2, pp. 139–155, 2010.

[38] S. Tonolli, M. Dalponte, M. Neteler, M. Rodeghiero, L. Vescovo, and D. Gianelle, "Fusion of airborne LiDAR and satellite multispectral data for the estimation of timber volume in the Southern Alps," *Remote Sens. Environ.*, vol. 115, no. 10, pp. 2486–2498, Oct. 2011.

[39] M. A. Cho, A. K. Skidmore, and I. Sobhan, "Mapping beech (Fagus sylvatica L.) forest structure with airborne hyperspectral imagery," *Int. J. Appl. Earth Obs. Geoinf.*, vol. 11, no. 3, pp. 201–211, Jun. 2009.

[40] P. Fatehi, A. Damm, A. Schweiger, M. E. Schaepman, and M. Kneubühler, "Mapping Alpine Aboveground Biomass From Imaging Spectrometer Data : A Comparison of Two Approaches," *IEEE J. Sel. Top. Appl. Earth Obs. Remote Sens.*, vol. 8, no. 6, pp. 3123–3139, 2015.

[41] A. Schweiger, A. C. Risch, A. Damm, M. Kneubühler, R. Haller, M. E. Schaepman, and M. Schütz, "Using imaging spectroscopy to predict aboveground plant biomass in alpine grasslands grazed by large ungulates," *J. Veg. Sci.*, vol. 26, pp. 175–190, 2015.

[42] A. Damm, L. Guanter, E. Paul-Limoges, C. van der Tol, A. Hueni, N. Buchmann, W. Eugster, C. Ammann, and M. E. Schaepman, "Far-red sun-induced chlorophyll fluorescence shows ecosystem-specific relationships to gross primary production: An assessment based on observational and modeling approaches," *Remote Sens. Environ.*, vol. 166, pp. 91–105, Sep. 2015.

[43] M. E. Schaepman, M. Jehle, A. Hueni, P. D'Odorico, A. Damm, J. Weyermann, F. D. Schneider, V. Laurent, C. Popp, F. C. Seidel, K. Lenhard, P. Gege, C. Küchler, J. Brazile, P. Kohler, L. De Vos, K. Meuleman, R. Meynart, D. Schläpfer, M. Kneubühler, and K. I. Itten, "Advanced radiometry measurements and Earth science applications with the Airborne Prism Experiment (APEX)," *Remote Sens. Environ.*, vol. 158, pp. 207–219, 2015.

[44] V. C. E. Laurent, W. Verhoef, A. Damm, M. E. Schaepman, and J. G. P. W. Clevers, "A Bayesian object-based approach for estimating vegetation biophysical and biochemical variables from APEX at-sensor radiance data," *Remote Sens. Environ.*, vol. 139, pp. 6–17, Dec. 2013.

[45] V. C. E. Laurent, M. E. Schaepman, W. Verhoef, J. Weyermann, and R. O. Chávez, "Bayesian object-based estimation of LAI and chlorophyll from a simulated Sentinel-2 top-of-atmosphere radiance image," *Remote Sens. Environ.*, vol. 140, pp. 318–329, Jan. 2014.

[46] P. S. Thenkabail, E. A. Enclona, M. S. Ashton, and B. Van Der Meer, "Accuracy assessments of hyperspectral waveband performance for vegetation analysis applications," *Remote Sens. Environ.*, vol. 91, no. 3–4, pp. 354–376, Jun. 2004.

[47] P. S. Thenkabail, E. A. Enclona, M. S. Ashton, C. Legg, and M. J. De Dieu, "Hyperion, IKONOS, ALI, and ETM+ sensors in the study of African rainforests," *Remote Sens. Environ.*, vol. 90, no. 1, pp. 23–43, Mar. 2004.

[48] S. G. Zolkos, S. J. Goetz, and R. Dubayah, "A meta-analysis of terrestrial aboveground biomass estimation using lidar remote sensing," *Remote Sens. Environ.*, vol. 128, pp. 289–298, Jan. 2013.

[49] L. Ji, B. K. Wylie, D. R. Nossov, B. Peterson, M. P. Waldrop, J. W. McFarland, J. Rover, and T. N. Hollingsworth, "Estimating aboveground biomass in interior Alaska with Landsat data and field measurements," *Int. J. Appl. Earth Obs. Geoinf.*, vol. 18, pp. 451–461, Aug. 2012.

[50] J. Verrelst, M. E. Schaepman, B. Koetz, and M. Kneubühler, "Angular sensitivity analysis of vegetation indices derived from CHRIS/PROBA data," *Remote Sens. Environ.*, vol. 112, no. 5, pp. 2341–2353, May 2008.

[51] J. Weyermann, A. Damm, M. Kneubühler, and M. E. Schaepman, "Correction of reflectance anisotropy effects of vegetation on airborne spectroscopy data and derived products," *IEEE Trans. Geosci. Remote Sens. Remote Sens.*, vol. 52, no. January 2014, pp. 616–627, 2014.

[52] M. Schlerf, C. Atzberger, J. Hill, H. Buddenbaum, W. Werner, and G. Schüler, "Retrieval of chlorophyll and nitrogen in Norway spruce (Picea abies L. Karst.) using imaging spectroscopy," *Int. J. Appl. Earth Obs. Geoinf.*, vol. 12, no. 1, pp. 17–26, Feb. 2010.

[53] F. D. Schneider, R. Leiterer, F. Morsdorf, J. Gastellu-etchegorry, N. Lauret, N. Pfeifer, and M. E. Schaepman, "Simulating imaging spectrometer data: 3D forest modeling based on LiDAR and in situ data," *Remote Sens. Environ.*, vol. 152, pp. 235–250, Sep. 2014.

[54] A. Viña, A. A. Gitelson, A. L. Nguy-robertson, and Y. Peng, "Comparison of different vegetation indices for the remote assessment of green leaf area index of crops," *Remote Sens. Environ.*, vol. 115, no. 12, pp. 3468–3478, 2011.

[55] R. Darvishzadeh, C. Atzberger, A. Skidmore, and M. Schlerf, "Mapping grassland leaf area index with airborne hyperspectral imagery: A comparison study of statistical approaches and inversion of radiative transfer models," *ISPRS J. Photogramm. Remote Sens.*, vol. 66, no. 6, pp. 894–906, Nov. 2011.

[56] S. A. Soenen, D. R. Peddle, R. J. Hall, C. A. Coburn, and F. G. Hall, "Estimating aboveground forest biomass from canopy reflectance model inversion in mountainous terrain," *Remote Sens. Environ.*, vol. 114, no. 7, pp. 1325–1337, Jul. 2010.

[57] P. Holmgren and T. Thuresson, "Satellite remote sensing for forestry planning—A review," *Scand. J. For. Res.*, vol. 13, no. February 2015, pp. 90–110, 1998.

[58] A. Psomas, M. Kneubühler, S. Huber, and K. Itten, "Hyperspectral remote sensing for estimating aboveground biomass," *Int. J. Remote Sens.*, vol. 32, no. 24, pp. 9007–9031, 2011.

[59] G. Le Maire, C. Francois, K. Soudani, D. Berveiller, J. Pontailler, N. Breda, H. Genet, H. Davi, and E. Dufrene, "Calibration and validation of hyperspectral indices for the estimation of broadleaved forest leaf chlorophyll content, leaf mass per area, leaf area index and leaf canopy biomass," *Remote Sens. Environ.*, vol. 112, no. 10, pp. 3846–3864, Oct. 2008.

[60] M. A. Cho and A. K. Skidmore, "Hyperspectral predictors for monitoring biomass production in Mediterranean mountain grasslands: Majella National Park, Italy," *Int. J. Remote Sens.*, vol. 30, no. 2, pp. 499–515, Jan. 2009.

[61] M. Schlerf, C. Atzberger, and J. Hill, "Remote sensing of forest biophysical variables using HyMap imaging spectrometer data," *Remote Sens. Environ.*, vol. 95, no. 2, pp. 177–194, Mar. 2005.

[62] O. Mutanga and A. K. Skidmore, "Hyperspectral band depth analysis for a better estimation of grass biomass (Cenchrus ciliaris) measured under controlled laboratory conditions," *Int. J. Appl. Earth Obs. Geoinf.*, vol. 5, no. 2, pp. 87–96, May 2004.

[63] H. Franco-Lopez, A. R. Ek, and M. E. Bauer, "Estimation and mapping of forest stand density, volume, and cover type using the k-nearest neighbors method," *Remote Sens. Environ.*, vol. 77, pp. 251–274, 2001.

[64] L. Ghahramany, P. Fatehi, and H. Ghazanfari, "Estimation of Basal Area in West Oak Forests of Iran Using Remote Sensing Imagery," *Int. J. Geosci.*, vol. 03, no. 02, pp. 398–403, 2012.

[65] S. R. Freitas, M. C. S. Mello, and C. B. M. Cruz, "Relationships between forest

structure and vegetation indices in Atlantic Rainforest," *For. Ecol. Manage.*, vol. 218, no. 1–3, pp. 353–362, Oct. 2005.

[66] H. Latifi, F. Fassnacht, and B. Koch, "Forest structure modeling with combined airborne hyperspectral and LiDAR data," *Remote Sens. Environ.*, vol. 121, pp. 10–25, Jun. 2012.

[67] O. Mutanga and A. K. Skidmore, "Narrow band vegetation indices overcome the saturation problem in biomass estimation," *Int. J. Remote Sens.*, vol. 25, no. 19, pp. 3999–4014, Oct. 2004.

[68] R. F. Kokaly and R. N. Clark, "Spectroscopic Determination of Leaf Biochemistry Using Band-Depth Analysis of Absorption Features and Stepwise Multiple Linear Regression," *Remote Sens. Environ.*, vol. 67, no. 3, pp. 267–287, Mar. 1999.

[69] M. A. Cho, A. K. Skidmore, F. Corsi, S. E. van Wieren, and I. Sobhan, "Estimation of green grass/herb biomass from airborne hyperspectral imagery using spectral indices and partial least squares regression," *Int. J. Appl. Earth Obs. Geoinf.*, vol. 9, no. 4, pp. 414–424, Dec. 2007.

[70] S. Ullah, Y. Si, M. Schlerf, A. K. Skidmore, M. Shafique, and I. A. Iqbal, "Estimation of grassland biomass and nitrogen using MERIS data," *Int. J. Appl. Earth Obs. Geoinf.*, vol. 19, pp. 196–204, Oct. 2012.

[71] J. Chen, S. Gu, M. Shen, Y. Tang, and B. Matsushita, "Estimating aboveground biomass of grassland having a high canopy cover: an exploratory analysis of in situ hyperspectral data," *Int. J. Remote Sens.*, vol. 30, no. 24, pp. 6497–6517, 2009.

[72] A. K. Schweiger, M. Schütz, P. Anderwald, M. E. Schaepman, M. Kneubühler, R. Haller, and A. C. Risch, "Foraging ecology of three sympatric ungulate species – behavioural and resource maps indicate differences between chamois, ibex and red deer," *Mov. Ecol.*, vol. 3, no. 6, pp. 1–12, Mar. 2015.

[73] MeteoSwiss, "IDAweb. The data portal of MeteoSwiss for research and teaching.," *http://www.meteoschweiz.admin.ch/web/de/services/datenportal/idaweb.html. accessed*, 2013. .

[74] A. C. Risch, L. M. Nagel, S. Martin, B. O. KrÜsi, F. Kienast, and H. Bugmman, "Structure and Long-Term Development of Subalpine Pinus montana Miller and Pinus cembra L. Forests in the Central European Alps," *Forstwissenschaftliches Cent.*, vol. 122, no. 4, pp. 219–230, 2003.

[75] A. Leboeuf, A. Beaudoin, R. A. Fournier, L. Guindon, J. Luther, and M. Lambert, "A shadow fraction method for mapping biomass of northern boreal black spruce forests using QuickBird imagery," *Remote Sens. Environ.*, vol. 110, no. 4, pp. 488–500, Oct. 2007.

[76] G. G. Moisen, E. a. Freeman, J. a. Blackard, T. S. Frescino, N. E. Zimmermann, and T. C. Edwards, "Predicting tree species presence and basal area in Utah: A comparison of stochastic gradient boosting, generalized additive models, and tree-based methods," *Ecol. Modell.*, vol. 199, no. 2, pp. 176–187, Nov. 2006.

[77] S. Huang, S. J. Titus, and D. P. Wiens, "Comparison of nonlinear height-diameter functions for major Alberta tree species," *Can. J. For. Res.*, vol. 22, pp. 1297–1304,

1992.

[78] E. Rötheli, C. Heiri, and C. Bigler, "Effects of growth rates, tree morphology and site conditions on longevity of Norway spruce in the northern Swiss Alps," *Eur. J. For. Res.*, vol. 131, pp. 1117–1125, 2012.

[79] D. Schläpfer and R. Richter, "Geo-atmospheric processing of airborne imaging spectrometry data. Part 1: Parametric orthorectification," *Int. J. Remote Sens.*, vol. 23, no. 13, pp. 2609–2630, Jan. 2002.

[80] R. Richter and D. Schläpfer, "Geo-atmospheric processing of airborne imaging spectrometry data. Part 2: Atmospheric/topographic correction," *Int. J. Remote Sens.*, vol. 23, no. 13, pp. 2631–2649, Jan. 2002.

[81] A. Berk, G. P. Anderson, P. K. Acharya, L. S. Bernstein, L. Muratov, J. Lee, M. J. Fox, S. M. Alder-Golden, J. H. Chetwynd, M. L. Hoke, R. B. Lockwood, T. W. Cooley, and J. A. Gardner, "MODTRAN5: a reformulated atmospheric band model with auxiliary species and practical multiple scattering options," in *Proceedings of the Society of Photo-Optical Instrumentation Engineer*, 2005, pp. 662–667.

[82] G. Schaepman-Strub, M. E. Schaepman, T. H. Painter, S. Dangel, and J. V. Martonchik, "Reflectance quantities in optical remote sensing—definitions and case studies," *Remote Sens. Environ.*, vol. 103, no. 1, pp. 27–42, Jul. 2006.

[83] G. M. Devagiri, S. Money, S. Singh, V. K. Dadhawal, P. Patil, A. Khaple, A. S. Devakumar, and S. Hubballi, "Assessment of above ground biomass and carbon pool in different vegetation types of south western part of Karnataka, India using spectral modeling," *Trop. Ecol.*, vol. 54, no. 2, pp. 149–165, 2013.

[84] V. Torontow and D. King, "Forest complexity modelling and mapping with remote sensing and topographic data: a comparison of three methods," *Can. J. Remote Sens.*, vol. 37, no. 4, pp. 387–402, 2011.

[85] M. Poulain, M. Peña, A. Schmidt, H. Schmidt, and A. Schulte, "Relationships between forest variables and remote sensing data in a Nothofagus pumilio forest," *Geocarto Int.*, vol. 25, no. 1, pp. 25–43, Feb. 2010.

[86] R. L. Pearson and L. D. Miller, "Remote mapping of standing crop biomass for estimation of the productivity of the shortgrass prairie," *Remote Sens. Environ. VIII*, vol. 1, pp. 1357–1381, 1972.

[87] J. W. Rouse, R. H. Hass, J. A. Schell, D. W. Deering, and J. C. Harlan, "Monitoring the vernal advancements and retrogradation of natural vegetation," Greenbelt, MD, USA, 1974.

[88] A. J. Richardson and C. L. Wiegand, "Distinguishing vegetation from soil background information," *Photogramm. Eng. Remote Sensing*, vol. 43, no. 12, pp. 1541–1552, 1977.

[89] D. J. Major, F. Baret, and G. Guyot, "A ratio vegetation index adjusted for soil brightness," *Int. J. Remote Sens.*, vol. 11, no. 5, pp. 727–740, 1990.

[90] Z. Malenovský, L. Homolová, R. Zurita-Milla, P. Lukeš, V. Kaplan, J. Hanuš, J.-P. Gastellu-Etchegorry, and M. E. Schaepman, "Retrieval of spruce leaf chlorophyll content from airborne image data using continuum removal and radiative transfer,"

Remote Sens. Environ., vol. 131, pp. 85–102, Apr. 2013.

[91] A. Viña and A. A. Gitelson, "Sensitivity to foliar anthocyanin content of vegetation indices using green reflectance," *Geosci. Remote Sens. Lett.*, vol. 8, no. 3, pp. 463–467, 2011.

[92] J. C. Ingram, T. P. Dawson, and R. J. Whittaker, "Mapping tropical forest structure in southeastern Madagascar using remote sensing and artificial neural networks," *Remote Sens. Environ.*, vol. 94, no. 4, pp. 491–507, Feb. 2005.

[93] R. F. Kokaly, G. P. Asner, S. V. Ollinger, M. E. Martin, and C. A. Wessman, "Characterizing canopy biochemistry from imaging spectroscopy and its application to ecosystem studies," *Remote Sens. Environ.*, vol. 113, pp. S78–S91, Sep. 2009.

[94] P. Roy and S. A. Ravan, "Biomass estimation using satellite remote sensing data — An investigation on possible approaches for natural forest," *J. Biosci.*, vol. 21, no. 4, pp. 535–561, 1996.

[95] O. Mutanga, A. K. Skidmore, and H. H. T. Prins, "Discriminating sodium concentration in a mixed grass species environment of the Kruger National Park using field spectrometry," *Int. J. Remote Sens.*, vol. 25, no. 20, pp. 4191–4201, Oct. 2004.

[96] H. Ren and G. Zhou, "Estimating senesced biomass of desert steppe in Inner Mongolia using field spectrometric data," *Agric. For. Meteorol.*, vol. 161, pp. 66–71, Aug. 2012.

[97] R. D. Jackson and A. R. Huete, "interpreting vegetation indices," *Prev. Vet. Med.*, vol. 11, pp. 185–200, 1991.

[98] P. M. Hansen and J. K. Schjoerring, "Reflectance measurement of canopy biomass and nitrogen status in wheat crops using normalized difference vegetation indices and partial least squares regression," *Remote Sens. Environ.*, vol. 86, no. 4, pp. 542–553, Aug. 2003.

[99] R. Geerken, N. Batikha, D. Celis, and E. DePauw, "Differentiation of rangeland vegetation and assessment of its status: field investigations and MODIS and SPOT VEGETATION data analyses," *Int. J. Remote Sens.*, vol. 26, no. 20, pp. 4499–4526, Oct. 2005.

[100] J. Heiskanen, "Estimating aboveground tree biomass and leaf area index in a mountain birch forest using ASTER satellite data," *Int. J. Remote Sens.*, vol. 27, no. 6, pp. 1135–1158, Mar. 2006.

[101] C. M. Trotter, J. R. Dymond, and C. J. Goulding, "Estimation of timber volume in a coniferous plantation forest using Landsat TM," *Int. J. Remote Sens.*, vol. 18, no. 10, pp. 2209–2223, Jul. 1997.

[102] P. T. Wolter, P. a. Townsend, and B. R. Sturtevant, "Estimation of forest structural parameters using 5 and 10 meter SPOT-5 satellite data," *Remote Sens. Environ.*, vol. 113, no. 9, pp. 2019–2036, Sep. 2009.

[103] T. Calvão and J. M. Palmeirim, "A comparative evaluation of spectral vegetation indices for the estimation of biophysical characteristics of Mediterranean semi-deciduous shrub communities," *Int. J. Remote Sens.*, vol. 32, no. 8, pp. 2275–2296,

Mar. 2011.

[104] W. B. Cohen, T. K. Maiersperger, S. T. Gower, and D. P. Turner, "An improved strategy for regression of biophysical variables and Landsat ETM+ data," *Remote Sens. Environ.*, vol. 84, pp. 561–571, 2003.

[105] P. E. Waggoner, "Forest inventories: discrepancies and uncertainties," Washington, DC, 2009.

[106] J. Anderson, L. Plourde, M. Martin, B. Braswell, M. Smith, R. Dubayah, M. Hofton, and J. Blair, "Integrating waveform lidar with hyperspectral imagery for inventory of a northern temperate forest," *Remote Sens. Environ.*, vol. 112, no. 4, pp. 1856–1870, Apr. 2008.

[107] A. Hill, J. Breschan, and D. Mandallaz, "Accuracy Assessment of Timber Volume Maps Using Forest Inventory Data and LiDAR Canopy Height Models," *Forests*, pp. 2253–2275, 2014.

[108] H. J. Hyyppä, and J. M. Hyyppä, "Effects of Stand Size on the Accuracy of Remote Sensing-Based Forest Inventory," *IEEE Trans. Geosci. Remote Sens.*, vol. 39, no. 12, pp. 2613–2621, 2001.

[109] H. Mäkelä and A. Pekkarinen, "Estimation of forest stand volumes by Landsat TM imagery and stand-level field-inventory data," *For. Ecol. Manage.*, vol. 196, no. 2–3, pp. 245–255, Jul. 2004.

[110] A. A. Gitelson, "Wide Dynamic Range Vegetation Index for remote quantification of biophysical characteristics of vegetation.," *J. Plant Physiol.*, vol. 161, no. 2, pp. 165–73, Feb. 2004.

[111] M. Maltamo, K. Eerikäinen, J. Pitkänen, J. Hyyppä, and M. Vehmas, "Estimation of timber volume and stem density based on scanning laser altimetry and expected tree size distribution functions," *Remote Sens. Environ.*, vol. 90, no. 3, pp. 319–330, Apr. 2004.

[112] A. Damm, L. Guanter, W. Verhoef, D. Schläpfer, S. Garbari, and M. E. Schaepman, "Impact of varying irradiance on vegetation indices and chlorophyll fluorescence derived from spectroscopy data," *Remote Sens. Environ.*, vol. 156, pp. 202–215, Jan. 2015.

[113] H. Suganuma, Y. Abe, M. Taniguchi, H. Tanouchi, H. Utsugi, T. Kojima, and K. Yamada, "Stand biomass estimation method by canopy coverage for application to remote sensing in an arid area of Western Australia," *For. Ecol. Manage.*, vol. 222, no. 1–3, pp. 75–87, Feb. 2006.

[114] H. Torabzadeh, F. Morsdorf, and M. E. Schaepman, "Fusion of imaging spectroscopy and airborne laser scanning data for characterization of forest ecosystems – A review," *ISPRS J. Photogramm. Remote Sens.*, vol. 97, pp. 25–35, Nov. 2014.

[115] D. Leckie, F. Gougeon, D. Hill, R. Quinn, L. Armstrong, and R. Shreenan, "Combined high-density lidar and multispectral imagery for individual tree crown analysis," *Can. J. Remote Sens.*, vol. 29, no. 5, pp. 633–649, Jun. 2003.

[116] M. Dalponte, L. Bruzzone, and D. Gianelle, "A System for the Estimation of Single-Tree Stem Diameter and Volume Using Multireturn LIDAR Data," *IEEE Trans. Geosci.*

Remote Sens., vol. 49, no. 7, pp. 2479–2490, Jul. 2011.

[117] M. A. Higgins, G. P. Asner, R. E. Martin, D. E. Knapp, C. Anderson, T. Kennedy-Bowdoin, R. Saenz, A. Aguilar, and S. Joseph Wright, "Linking imaging spectroscopy and LiDAR with floristic composition and forest structure in Panama," *Remote Sens. Environ.*, vol. 154, pp. 358–367, May 2014.

[118] V. Thomas, P. Treitz, J. H. Mccaughey, T. Noland, and L. Rich, "Canopy chlorophyll concentration estimation using hyperspectral and lidar data for a boreal mixedwood forest in northern Ontario, Canada," *Int. J. Remote Sens.*, vol. 29, no. 4, pp. 1029–1052, Feb. 2008.

[119] F. E. Fassnacht, F. Hartig, H. Latifi, C. Berger, J. Hernández, P. Corvalán, and B. Koch, "Importance of sample size , data type and prediction method for remote sensing-based estimations of aboveground forest biomass," *Remote Sens. Environ.*, vol. 154, pp. 102–114, 2014.

4

Tree Density and Forest Productivity in a Heterogeneous Alpine Environment: Insights from Airborne Laser Scanning and Imaging Spectroscopy

This chapter is based on:

Fatehi, P., Damm, A., Leiterer, R., Bavaghar, M.P., Schaepman, M.E., & Kneubühler, M. (2016). Tree Density and Forest Productivity in a Heterogeneous Alpine Environment: Insights from Airborne Laser Scanning and Imaging Spectroscopy. To be submitted to Forest Ecology and Management Journal.

Abstract

Tree density (TD) and forest productivity (FP) are important forest variables, fundamental to forest management and planning, and crucial to understand feedbacks of forest ecosystems to environmental change. Since TD and FP are sensitive to resource gradients, both variables are interrelated and vary with abiotic factors such as topography, moisture and nutrient regimes. Reliable information about spatial-temporal variability of TD and FP across ecological scales is essential for ecosystem research. However, conventional inventory approaches are challenged, particularly in remote and structurally complex landscapes, and new monitoring approaches are urgently required. We consequently outline an approach combining Airborne Laser Scanning (ALS) and Imaging spectroscopy (IS) to quantify and assess patterns of TD and FP in a protected heterogeneous alpine forest in the Swiss National Park (SNP). We use ALS data and a local maximum (LM) approach to calculate TD, as well as imaging spectrometer data (Airborne Prism Experiment - APEX) and a simple empirical model to estimate FP. We investigate the dependency of TD and FP on site related factors, in particular on surface exposition and elevation. Based on reference data (i.e., 1,598 trees measured in 35 field plots), we observed an underestimation of ALS-based TD estimates of 40% that is even more pronounced for small trees (70%). Our results suggest a limited sensitivity of the ALS approach to small trees as well as a dependency of TD estimates on canopy heterogeneity, structure, and species composition. We found a weak to moderate relationship between surface elevation and TD (R^2 = 0.18-0.69) and a less pronounced trend with FP (R^2 = 0.0-0.56), suggesting that both variables depend on gradients of resource availability. Beside faced limitations in the sensitivity of applied approaches, we conclude that the combined application of ALS and IS data renders an efficient alternative to provide relevant information to gain understanding on relationships between TD and FP in complex structured landscapes across ecological scales.

Authors' contributions: PF, AD, MES, MK designed the study and developed the methodology. PF collected the data. PF, AD, RL, MB performed the analysis. All authors wrote the manuscript.

4.1 Introduction

Tree density (TD) and forest productivity (PF) are important structural and functional variables of forest ecosystems. TD, defined as the number of trees per unit area [1], is along with other structural information (e.g., species composition, canopy closure, tree height, and timber volume), fundamental for forest management planning [2]. TD provides information on stand basal area, timber volume [3], and aboveground carbon storage [4]. In managed forest ecosystems, TD information allows indicating essential treatments such as thinning, or to develop strategies to increase regeneration rates if the number of trees is too small [5]. Particularly in unmanaged and protected forests, TD is crucial to determine forest succession dynamics [6], and assess spatio-temporal patterns in tree mortality [7]. Gross primary production (GPP), defined as the capacity of a forest to gain carbon through photosynthesis over a given time period, has been widely used to quantify FP [8], [9]. FP is important to understand feedbacks of forests to climate change (i.e., rising atmospheric CO_2 concentrations [10]) and other natural disturbances such as insect and pathogen attacks [11]. Further, FP information facilitates the design of optimal silvicultural guidelines [12] and multi-temporal assessments of FP have shown a great potential to assess growth patterns of different forest types including virgin, natural or managed forests [13].

TD and FP balance each other by both determining the availability of resources, are complementary information variables to characterize forest ecosystems, and are valuable input for broad-scale modeling of biological and biogeochemical processes [14]. Understanding the relationship between FP and TD is important for ecologists and forest managers [15]. However, only few studies exploited inter-dependencies at larger ecosystem scales so far [4]. Further, ecologists are interested in abiotic components such as topography that often has a strong influence on structure, composition, and function of forest ecosystems [16]. Topography (i.e., elevation) has been identified as an easy proxy for resource availability and spatial pattern of ecosystem properties [17]. Changes in elevation can open up major changes in community-averaged leaf traits [18], which in turn may affect FP. Asner et al. (2016) [19] emphasized the lack of knowledge about the contribution of elevation on plant functional traits at different scales. Such information would allow modeling and predicting spatial variation in ecosystem processes at any given point along elevation gradients. In addition, the interrelation between FP and TD with elevation also can provide crucial information to determine tree-line elevation [20].

Nevertheless, the assessment of such relations between forest functional and structural attributes remains largely underrepresented at ecosystem scale.

Field surveys are still the most accurate approach to collect structural forest attributes [21], [22]. The advantage of the high accuracy achievable is often counterbalanced by substantial costs and difficulties to obtain information for large, remote, and structurally complex forest areas [3]. Further, providing continuous information of forest attributes typically requires additional interpolation approaches that are prone to errors [22]. With the launch of the first Earth observation (EO) satellites in the 1970's, substantial efforts have been conducted to find alternatives to traditional field surveys. Nowadays, the use of EO data and information extraction approaches are an important alternative to complement mapping forest attributes, particularly for large areas [23]–[25].

Estimates of TD from both active and passive EO systems has been widely demonstrated [25], [26], [27], [28]. In particular Airborne Laser Scanning (ALS) holds a large potential to accurately measure the three-dimensional distribution of forest structural components [29]–[31] and has become an essential component to operationalise forest inventories in various countries [32], [33]. Estimates of TD from ALS data can be obtained either from area-based approaches (ABAs) or individual tree detection approaches (ITD) [34]. Although ABAs are commonly applied in operational forestry applications [35], they show several limitations (i.e., dependent on extensive in situ data [36], [37],site specific [38], limited sensitivity to TD [39]). In contrast, ITD based approaches utilize either ALS point cloud data or canopy height models (CHM) to identify individual trees [34], [35], [40]. Plot or stand estimates are afterwards obtained by summing up identified trees. Kaartinen et al. [41] indicate that ITD approaches provide true stem distribution series and require less in situ data compared to ABAs. ITD approaches are, however, currently under development and have not yet been widely applied in practice and across forests heterogeneity in terms of structural complexity, species composition, and silvicultural treatments [35], [41].

FP can be approximated with GPP, which itself can stem from various approaches ranging from empirical to process-based modeling approaches. Empirical approaches based on optical EO data are simple to implement but rely on extensive in situ data and are thus site and ecosystem specific. A frequently used approach to map FP exploits optical EO data in combination with Monteith's light use efficiency model [42] [20], [43]. Both terms in Monteith's equation, absorbed photosynthetic active radiation (APAR) and light use efficiency (LUE) are typically parameterized with greenness based indices and semi-empirical modeling. Assumptions inherent to this approach (i.e., approximation of

potential rather actual photosynthesis), however, limit the representativeness of obtained GPP values [44] across ecosystems (cf., Turner et al. [45] for an assessment of the MODIS-GPP product (MOD17) or Coops et al. [46] for an evaluation of few other satellite based approaches). A recent achievement in optical remote sensing is the measurement of sun-induced chlorophyll fluorescence (SIF). SIF is the most direct measurement of plant photosynthesis and opens new perspectives to constrain estimates of GPP across ecosystems [47], [48]. Although this new EO approach is already well matured, certain components remain to be fully developed to operationally apply SIF measurements, i.e., the integration of SIF in photosynthesis models. The use of process based models renders the most mechanistic approach but requires precise and detailed information on soil, climate, and additional forest properties that are often lacking or are inaccurate [43].

The above argumentation yields two research needs that are addressed in this study, including i) the evaluation of pragmatic and less data driven ALS and imaging spectroscopy (IS) based approaches to obtain TD and FP in heterogeneous forest environments and ii) the exploitation of the interrelation between TD and FP with surface elevation. We particularly estimate TD using an ITD approach and ALS data in a heterogeneous mountain forest and validate results with in situ data. We map FP using an empirical greenness based approach in combination with data of the imaging spectrometer Airborne Prism Experiment (APEX). Further, we investigate the relationship between TD and FP and evaluate the impact of topography (i.e., surface exposition and elevation) on both forest variables.

4.2 Study area and data

4.2.1 Study area

The study area Trupchun valley (Val Trupchun) extends over a 22 km^2 area within the Swiss National Park (SNP), located in the southeast of Switzerland (Fig. 4. 1). The region is a heterogeneous alpine landscape with a dry and harsh climate. The mean annual precipitation totals 744 mm and the average annual temperature is 0.9 °C [49]. The study area is characterized by rough topography and steep slopes [50] with an elevation range between 1775 to 3145 meter above sea level (a.s.l.) [51]. The forest is classified as boreal-type forest, dominated by European larch (*Larix decidua L.*), with a changing proportion of Norway spruce (*Picea abies (L.) Karst*) and Swiss stone pine (*Pinus cembra L.*) (associated

species). Norway spruce trees dominate at lower altitudes, whereas Swiss stone pines are present in the high altitudes [2]. The trees are up to 250 years old and the forest ecosystem has been protected and unmanaged since 1914 [52].

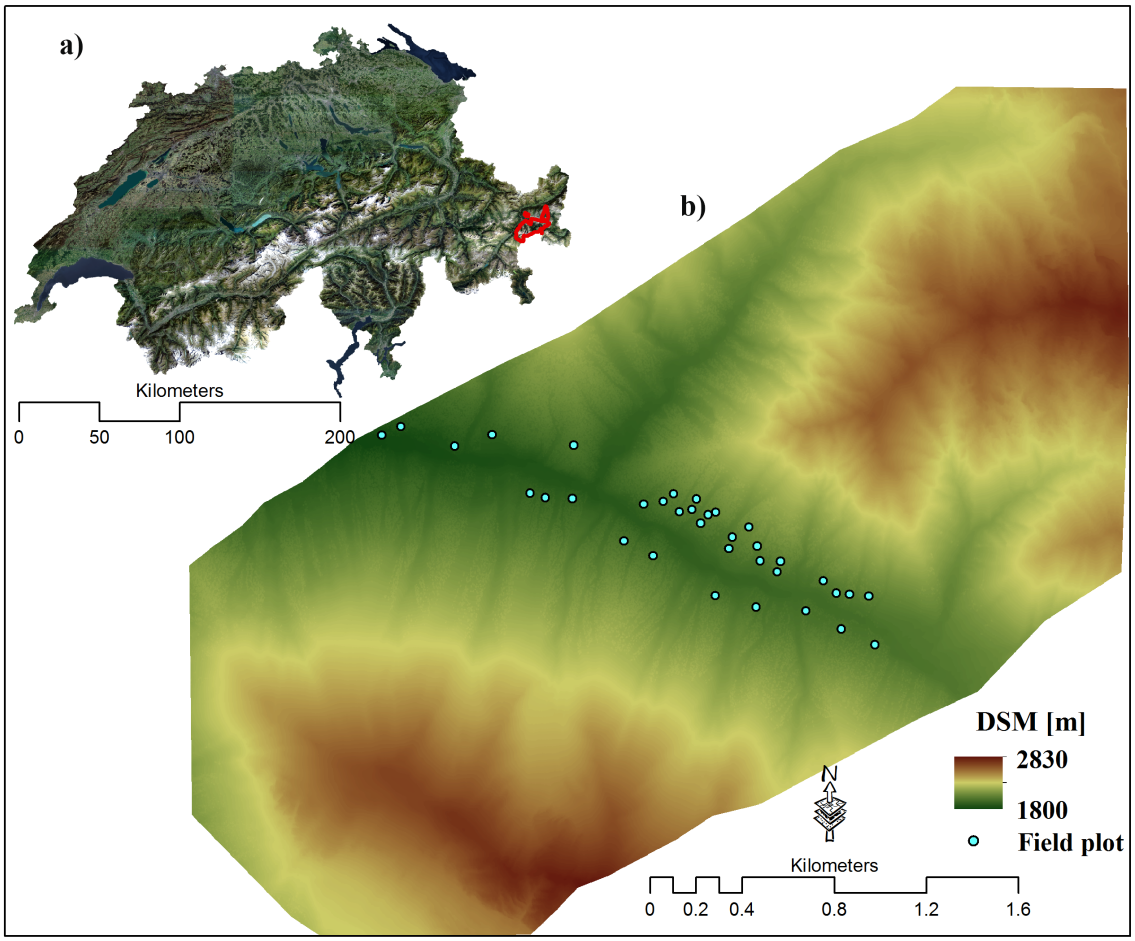

Fig. 4. 1. Study area and location of field plots. a): location of the SNP in Switzerland (red polygon) with a true color ortho image as background (source: swisstopo). b): location of field plots in Val Trupchun. A digital surface mode (DSM) generated from ALS data is used as background.

4.2.2 Field data

A stratified random sampling approach was established in summer 2012 (June and July) to collect ground information describing the forest ecosystem (Fig. 4. 1). A total of 35 squared field plots with a size of 30 m x 30 m were inventoried. Prior to field data collection, a slope correction factor depending on the slope angle was applied to convert the plot size into its equivalent on a horizontal plane [53]. The slope angle was measured by a SUUNTO clinometer device [54]. Identified plots represent most of the present tree species and their properties, i.e., canopy cover, density, and species composition. The geographical position of each field plot was recorded using a differential global positioning system (DGPS). In each plot, all trees having a diameter at breast height (DBH) larger than

5 cm were counted, corresponding DBHs and species types were recorded as well [3]. The selection of the 5 cm DBH threshold is justified by common practice in forest inventory [55]. TD was calculated as the number of tree per hectare by summing up all measured trees in each field plot [5].

In total 1598 trees were counted in all plots, while European larch species compose 718 trees (45%), Swiss stone pine 602 trees (38%), and Norway spruce 278 trees (17%). Considering the basal area per plot, European larches account for 59%, followed by Swiss stone pines (29%), and Norway spruce trees (12%). Descriptive statistics of TD obtained from all field plots for the Val Trupchun area can be found in **Table 4. 1**. The mean TD found amounts to 507 trees per ha. This is in line with findings by Risch et al. [56] who reported a value of 473 ± 90 trees per ha for this study area. We implemented various DBH thresholds to calculate the corresponding number of trees per ha. Due to different environmental factors for north-facing and south-facing slopes (i.e., solar radiation, water and soil nutrient availability) [12], we classified our field plots into north- and south-facing plots.

Table 4. 1

Tree density (TD) statistics for field plots in Val Trupchun.

Parameter	DBH > 5 cm	DBH > 12 cm	DBH > 20 cm	DBH > 30 cm	South-facing	North-facing
Number of plots [-]	35	35	35	35	25	10
Number of trees [-]	1598	1360	1103	691	1314	284
Tree density [N / ha]						
Mean	507	432	350	219	584	316
Minimum	122	122	89	56	122	122
Maximum	1067	755	600	456	1067	644
Standard deviation	249	189	141	96	238	161

Table 4. 1 shows large differences of TD's for south- and north-facing field plots. Results of an independent samples *t-test* [57] prove that this difference is statistically significant ($t(33) = 3.269,\ p = 0.003$). Mainly environmental factors, natural disturbances, and historical human activity before 1914 (i.e., charcoal production, timber harvesting) are reasons for these differences: multiple-stemmed trees frequently exist on south-facing areas, while high self-thinning due to light competition among trees causes the smaller TD on north-facing areas.

4.2.3 Airborne imaging spectroscopy data

APEX is an airborne imaging spectrometer measuring radiation in the spectral range between 350 nm and 2500 nm in 284 contiguous spectral bands [58]. It was operated at

an altitude of 6500 m a.s.l. over the study area on July 12, 2013, around 11:30 A.M. local time. The solar zenith angle and the solar azimuth angle were 28.1° and 139.1°. Surface height differences and slope changes cause a varying ground sampling distance across the flight line (i.e., between 1.5-3.0 m) and data was resampled to a 2 m pixel grid.

APEX data were geometrically corrected using a parametric geocoding approach (PARGE) [59]. Based on 15 ground control points well representing topographic diversity, a root mean square error (RMSE) of 3.2 m ± 1.4 m was calculated, indicating an acceptable geometric accuracy considering the availability of a coarse 25 m resolution digital elevation model only in combination with the complex topography. The atmospheric correction software (ATCOR-4) was used to compensate for atmospheric effects, to minimize illumination changes due to topography, and to eventually retrieve top-of-canopy hemispherical conical reflectance factor (HCRF) data [60] (for terminology see [61]). ATCOR-4 used look-up-tables (LUT) of atmospheric functions (i.e., up and down welling transmittances, path scattered radiance, spherical albedo), pre-calculated with the atmospheric radiative transfer code MODTRAN-5 [62]. We assumed a mid-latitude summer atmosphere type and a rural aerosol model and estimated water vapor as well as aerosol load pixel-wise to select LUT entries for subsequent compensation of atmospheric absorption and scattering effects. We further applied the ATCOR-4 supported correction of illumination changes due to topography using a coarse resolution (i.e., 25 m spatial resolution) digital elevation model.

4.2.4 Airborne laser scanning data

ALS data were acquired by Vermessung AVT ZT-GmbH, Imst, Austria (http://www.avt.at/home.html) in August 2011 using a double-scanner setup (LMS-Q560, RIEGL Laser Measurements Systems GmbH, Austria) mounted on a helicopter. Details of the sensor are discussed in Wagner et al. [63] and given in the technical sensor documentation provided by RIEGL [64]. Multiple returns were recorded for each emitted pulse and converted into a three-dimensional point cloud composed of planimetric coordinates (x and y) and ellipsoidal heights (z) [65]. The data cover an area of approximately 140 km^2 with an average point density of >5 pts/m^2. The point cloud was classified into soil, vegetation, water, and buildings using the TerraScan software (http://www.terrasolid.com/products/terrascanpage.php). Based on this classification, a digital terrain model (DTM) and a digital surface model (DSM) with a spatial resolution of 1x1 m were processed using SCOP++ (http://photo.geo.tuwien.ac.at/software/scop/). The

canopy height model (CHM) was subsequently calculated by subtracting the DTM from the DSM. A forest map was derived by applying a threshold to the CHM. The minimum tree height threshold was set to 3 m as utilized in the Swiss National Forest Inventory [66].

4.3 Methods

4.3.1 *Local Maxima approach to estimate tree density using ALS data*

The initial step to estimate TD using an ITD approach is the detection of individual trees. For this purpose, we used a CHM [40] that was smoothed with a Gaussian smoothing (function value of 0.7) to remove small variations in the canopy surface [67]. The local maxima (LM) approach is the most widely used approach for CHM-based tree detection among various methods available (e.g., valley-following [68], multiple scale edge [69], watershed segmentation [70], and local maxima finding [71], [72]). The relatively simple LM approach is fast and easy to implement [3], [41] and identifies the top of a tree crown as pixel containing the highest value above ground compared to all pixels in a specific neighborhood [23], [71]. We applied the LM-approach with variable spatial resolutions of the CHM (i.e., 1m x 1 m and 2 m x 2 m grid-cell resolution) and a moving window size of 3 x 3 pixel. A narrow-band NDVI (Normalized Differenced Vegetation Index) product obtained from APEX data (spectral bands at 665 and 831 nm) was calculated to remove falsely detected trees resulting from the complex terrain in the study area (cf. Khosravipour et al. 2015 [73]). On very steep slopes, for example, ALS echoes from grassland can have a range in altitude of larger than 3 m within the target grid-cell size of 1 m for the DEM/DSM generation, resulting in CHM values of >3 m. The identified treetops were afterwards summed up to calculate the TD per plot.

4.3.2 Spatial modeling of forest productivity using APEX data

Forest GPP was estimated to approximate forest productivity [74] by applying a simple global calibration equation as introduced by Hashimoto et al. (2012) [75]. Their results indicate that an empirical approach involving the Enhanced Vegetation Index (EVI) is a viable method for estimating GPP. The EVI was calculated according to Huete et al. (2002) [76] as:

$$EVI = G \frac{\rho_{NIR} - \rho_{red}}{\rho_{NIR} + C_1 \times \rho_{red} - C_2 \times \rho_{blue} + L} \quad (1)$$

where ρ indicates the surface HCRF for the near infrared (NIR), red and blue band, and L (1) is a canopy background adjustment. G (2.5) is the gain factor and C_1 (6) and C_2 (7.5) are band-specific atmospheric resistance correction coefficients. All values and the coefficients have been adapted for the MODIS EVI product [76]. Many studies have shown that these values are still valid to generate EVI index for higher spatial resolution [77]–[79]. We are aware of difficulties in using EVI to estimate GPP since it is representative for potential rather than actual photosynthetic activity. However, the study area is highly complex in terms of topography and we lack reliable data to facilitate new approaches (i.e., SIF based GPP estimates (Damm et al. 2015) [48]). We consequently applied a greenness-based approach to obtain first limited insights into GPP distribution in alpine environments.

Since the chosen calibration model was originally developed for MODIS data, APEX HCRF data were spectrally convolved to the respective MODIS bands. The convolution was carried out in the ENVI (Environment for Visualizing Images, Research System, Inc.) software using MODIS spectral response functions. Further, differences in spatial resolution (i.e., 2 m of APEX vs. 500 m of MODIS) require certain considerations as well: The high spatial resolution of APEX yields detailed measurements of forest ecosystems, including shaded and illuminated parts of tree crowns. These illumination patterns are primarily caused by geometric optical scattering and complicate the description of the radiative transfer particularly in shaded canopy areas, eventually impacting the accuracy of retrieved vegetation indices [80] and estimated GPP. Geometric-optical scattering scales with spatial resolution and its impact decreases with increasing ground-sampling distances. We consequently masked shade pixels using an empirical threshold approach to compare measurements of the differently resolved MODIS and APEX data. FP, the carbon uptake by all trees of a specific forested area, was eventually obtained by averaging resulting GPP values of tree crowns for a 30 m grid cell and normalizing for tree fractional cover in the respective area. Fractional cover of the 30 m grid cell was estimated from the ALS based CHM.

4.3.3 Validation

The accuracy of ALS based TD estimates was assessed using field measurements at plot level. The validation procedure was applied to all field plots and individually to those located on south-facing and north-facing slopes. The agreement was assessed by calculating the coefficient of determination (R^2), the root mean square error (RMSE), and

the relative RMSE (RMSE%). A quantitative validation of FP was not possible due to the lack of adequate data. Instead, we used in situ measurements of annual GPP of a close-by forest ecosystem similar to the one of our study site and assumed consistency of the algorithm performance across these two test sites.

4.4 Results

4.4.1 Airborne Laser Scanning based tree density estimation

An example result of the LM based tree detection is shown in Fig. 4. 2. The overall accuracy was calculated to validate ITD and relates the proportion of detected trees to the number of trees measured in the field. The validation shows an overall accuracy of 36%, whereby accuracies ranged between 43% to 85% considering the different DBH categories (cf., Section 2.2) (**Table 4. 2**).

Table 4. 2

Overall accuracy of individual tree detections (ITD) for three diameters at breast height (DBH) categories considering two canopy height model (CHM) resolutions.

		Overall accuracy [%]			
Measured trees	Detected trees	All DBH's	DBH>12	DBH>20	DBH>30
1598	581	36	43	53	84

Results of the ITD were used to calculate the TD per plot, expressed in trees/ha. Considering all trees and DBH classes, TD estimation shows a moderate accuracy with R^2 = 0.39 and RMSE = 389 [N/ha]. The accuracy increases by excluding small trees (i.e., DBH > 30 cm) to R^2 = 0.35 RMSE = 87 [N/ha] (**Table 4. 3**). If reference plots are stratified in north- and south-facing plots, the accuracy of TD estimates increases for north-facing plots (R^2 = 0.68, RMSE = 176 [N/ha]) and remains at a low to moderate level for south-facing plots (R^2 = 0.52, RMSE = 447 [N/ha]).

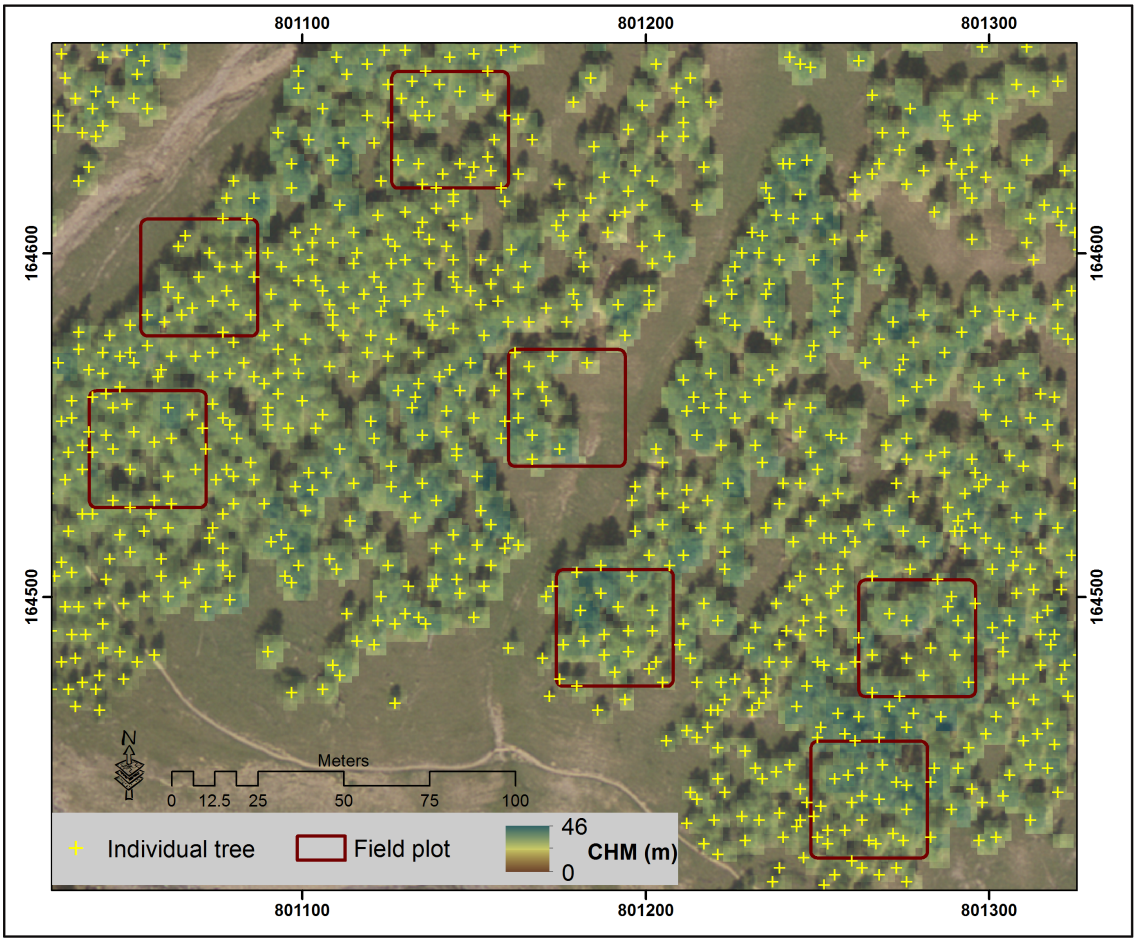

Fig. 4. 2. Result of individual tree detection (ITD) based on ALS data in combination with the local maxima approach. The yellow crosses mark the individual trees. A canopy height model (CHM) and a true color ortho image (© swisstopo) are used as background.

Table 4. 3

Agreement of measured and ALS-based tree density estimation. Statistical assessment is based on the RMSE in trees ha^{-1} and the coefficient of determination (R^2).

Plots	All trees		DBH>12		DBH>20		DBH>30	
	R^2	RMSE	R^2	RMSE	R^2	RMSE	R^2	RMSE
All (n=35)	0.39	389	0.40	294	0.42	201	0.35	87
North-facing (n=10)	0.68	176	0.68	124	0.74	101	0.80	68
South-facing (n=25)	0.52	447	0.58	339	0.53	229	0.27	93

The relationship between measured and estimated TD considering all plots and trees is shown in Fig. 4. 3a. We observe a general underestimation of TD estimates in particular with increasing amount of trees/ha that is associated with an increasing number of small trees. Even if only large trees are considered (i.e., DBH > 30 cm), there is a tendency for an underestimation of TD in dense canopies (Fig. 4. 3b).

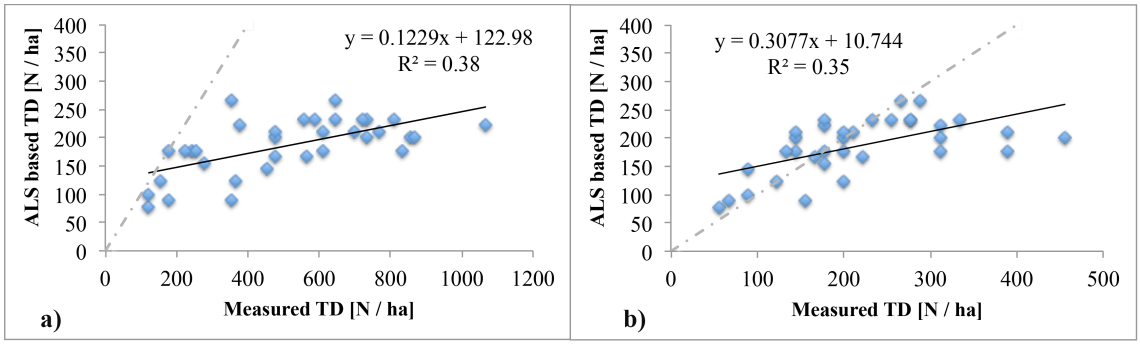

Fig. 4. 3. Relationship of ALS derived tree density (TD) and measured tree density for all trees (a) and for trees with a DBH > 30 cm (b). The dashed line indicates the 1:1 line.

The effect of species composition on TD estimates was assessed by stratifying field plots into four classes according to their dominant species. Plots showing individual proportions less than 60% across all species were considered as mixed [81]. In result, 18 mixed plots, 10 Larch plots, six Swiss stone pine plots, and one Norway spruce plot were classified. We observe a strong relationship between the amount of trees per ha and the TD estimation error (i.e., the difference between measured trees in the field and estimated trees from ALS data) across species composition (i.e., R^2 = 0.68 for mixed plots, R^2 = 0.97 for larch, and R^2 = 0.90 for Swiss stone pine plots) (Fig. 4. 4a). If only large trees are considered (DBH > 30 cm), the TD error tends to be less dependent on TD but seems to be species specific (i.e., R^2 = 0.59 for mixed plots, R^2 = 0.04 for larch, and R^2 = 0.69 for Swiss stone pine plots) (Fig. 4. 4b).

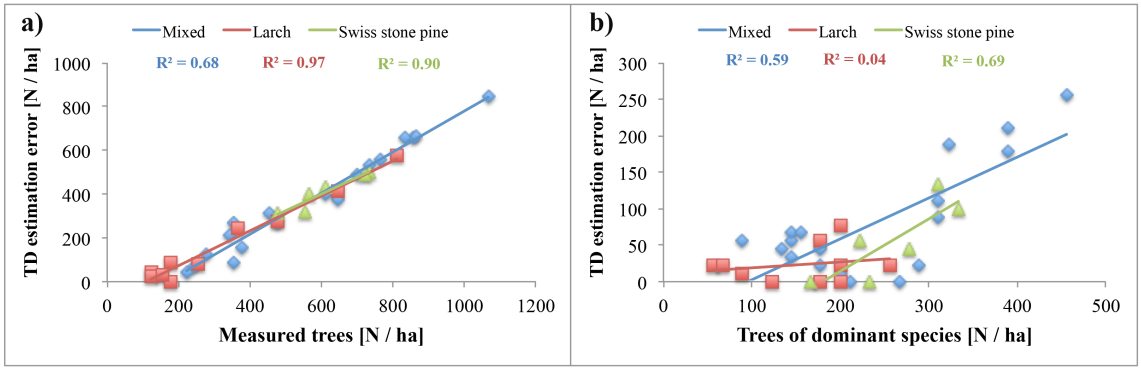

Fig. 4. 4. Relationship of tree species abundance and tree density estimation error for mixed plots, Larch, and Swiss stone pine dominated plots. a): all trees, b) trees with DBH >30 cm.

4.4.2 Spatial distribution of tree density

Identified trees were spatially counted considering a 30 m grid to eventually obtain a thematic TD map of the study area (Fig. 4. 5). The average TD estimated from ALS data is

184 +/- 50 [N/ha], differing by 64% from the average value obtained from field surveys (i.e., 507 [N/ha]).

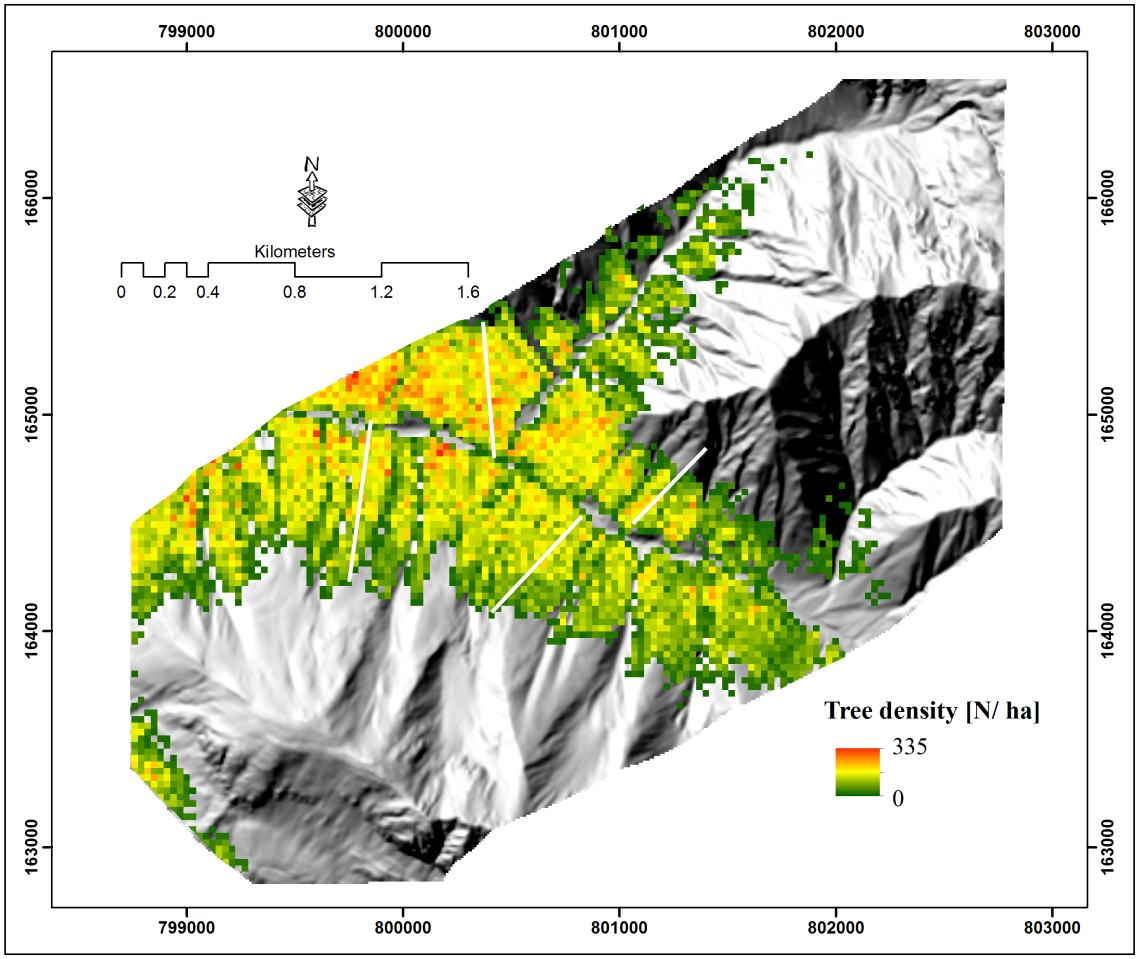

Fig. 4. 5. Spatial distribution of tree density (TD) at 30 m spatial resolution. Tree density was estimated from ALS data using a local maximum approach. White lines indicate the location of four vertical transects.

The TD map depicts high TD values at low elevations and a decreasing TD with increasing elevation. This negative relationship between TD and surface elevation can be confirmed by the field data (**Fig. 4. 6**a) and by evaluating ALS based TD values at plot scale (**Fig. 4. 6**b). The assessment of four slope-line parallel transects shows a negative relationship between TD and surface elevation as well (R^2 = 0.4) (Fig. 4. 7). Further, in situ and ALS based TD estimates depict that negative relationships are stronger for north-facing (R^2 = 0.66, R^2 = 0.69) than for south-facing plots (R^2 = 0.33, R^2 = 0.18) (**Fig. 4. 6**).

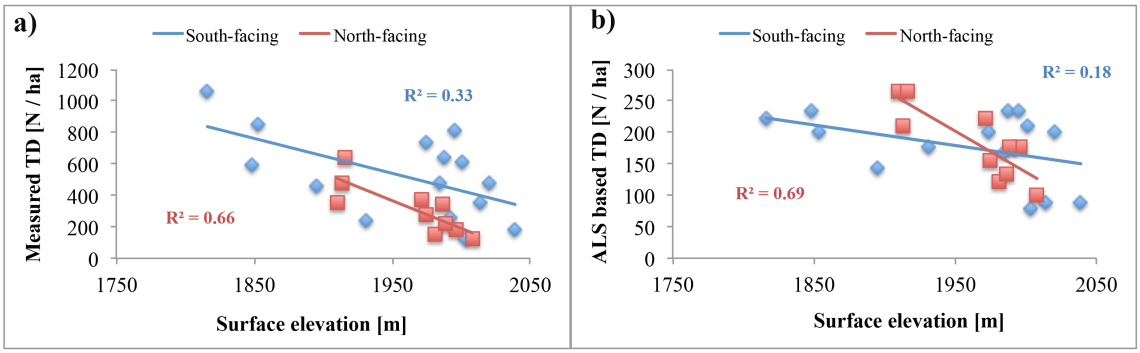

Fig. 4. 6. Dependency of tree density (TD) and surface elevation. a): In situ measured tree density. b) ALS based tree density estimates.

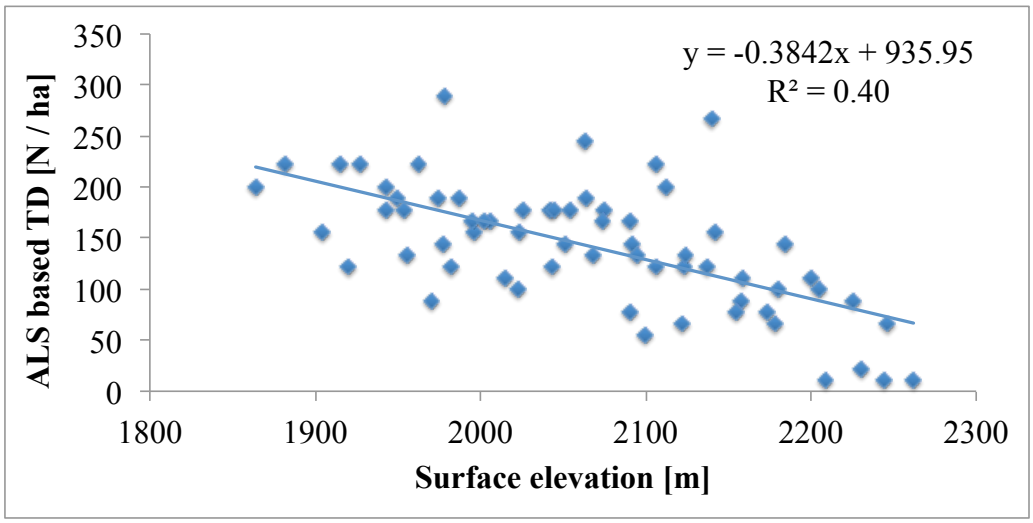

Fig. 4. 7. Dependency of tree density (TD) on surface elevation along four slope-line parallel transects.

4.4.3 Spatial distribution of forest productivity

A *forest productivity* map was calculated by aggregating GPP of sunlit tree crowns to a 30 m grid and normalizing for tree fractional cover (Fig. 4. 8). A notable range of forest productivity values is depicted in the map, ranging between 0 to 2920 g C m^{-2} $year^{-1}$. The average forest productivity is 1255 +/- 342 g C m^{-2} $year^{-1}$. The map depicts a height gradient of forest productivity with largest productivity values at low elevations and vice versa. However, low forest productivity values frequently occur in vicinity of a river at the valley bottom.

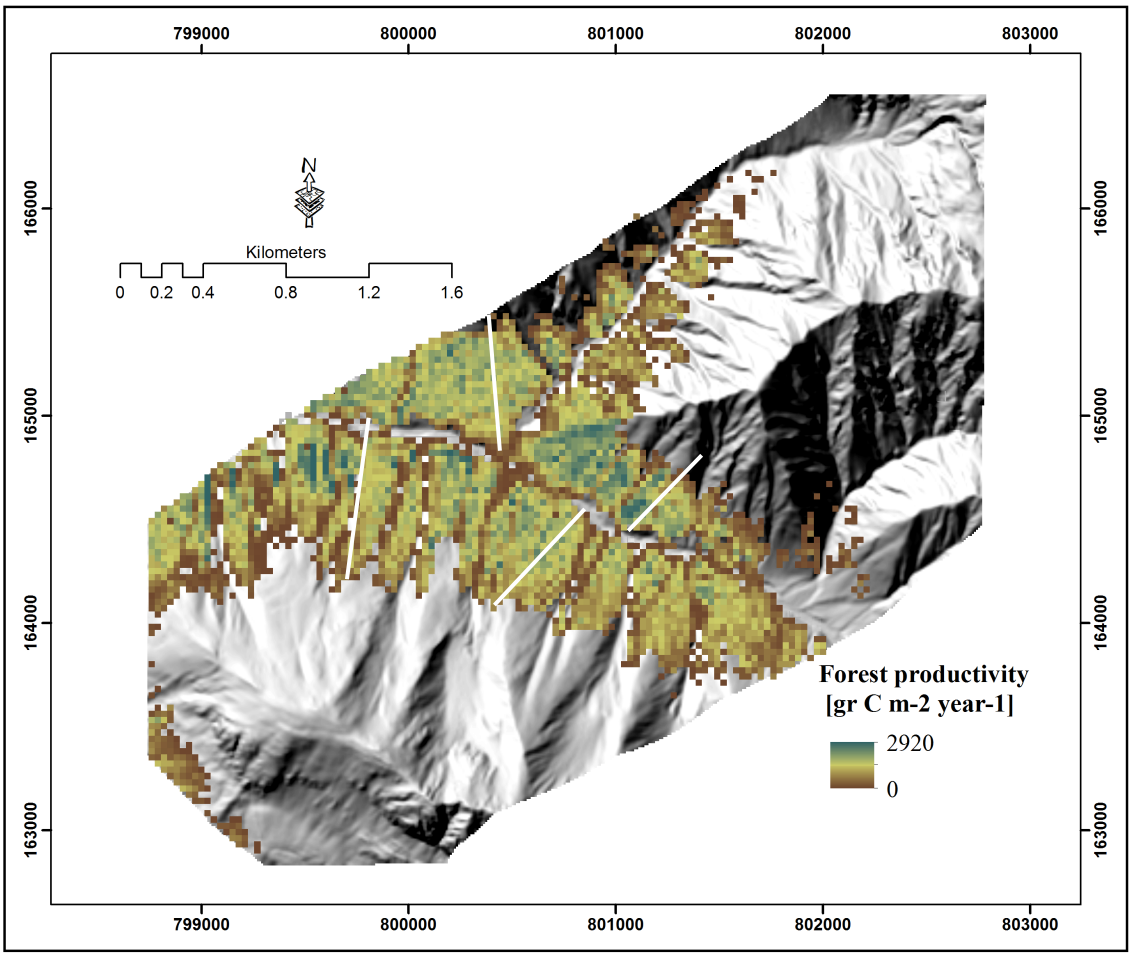

Fig. 4. 8. Forest productivity with 30 m spatial resolution obtained from Enhanced Vegetation Index (EVI) based gross primary production (GPP) estimates using APEX data. White lines indicate slope-line perpendicular transects used for further analysis.

The relationship between FP and surface elevation was assessed. FP, shows a low negative relationship with surface elevation for north-facing plots (R^2 = 0.31) while no relationship was found for south-facing plots. The analysis at landscape level considering four slope-line parallel transects revealed a more general view on the relationship between FP and surface elevation (see white lines in Fig. 4. 8). In general, findings confirm the plot scale analysis for north-facing slopes: we observe a negative relationship (R^2 = 0.12) (Fig. 4. 9) with increasing surface elevation. It must be noted that FP generally shows a moderate negative relationship with surface elevation. The lower FP close to a river at the valley bottom, however, determines a bell shaped relationship with surface elevation and causes the relatively low R^2 if a linear relationship is considered.

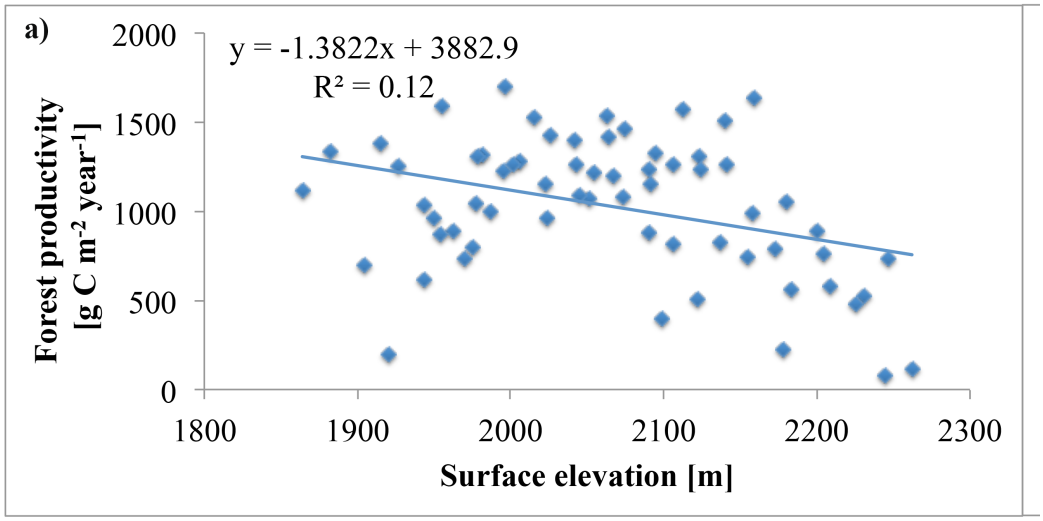

Fig. 4. 9. Dependency of forest productivity on surface elevation along four slope-line parallel transects.

4.4.4 Relationship of tree density with tree and forest productivity

The relationship between TD and FP from spatially aggregated APEX data at plot level is shown in Fig. 4. 10. The relationships are moderate and positive across exposition (i.e., north- and south-facing slopes) and ITD estimation methods (i.e., field and ALS based) (R^2 between 0.21, R^2 = 0.67). Plot level results are confirmed at landscape level while we found a positive relationship between TD and FP of R^2 = 0.38 (Fig. 4. 11).

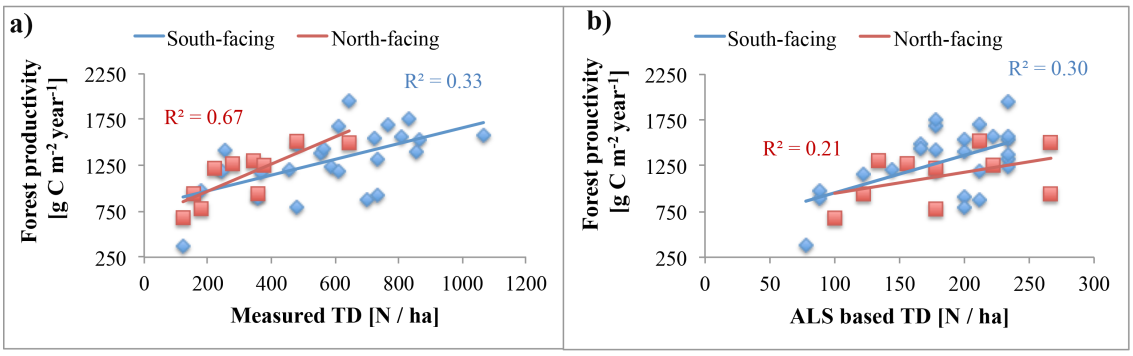

Fig. 4. 10. Relationship between tree density (TD) and forest productivity for north- and south-facing plots. a) In situ measured TD. b) ALS estimated TD.

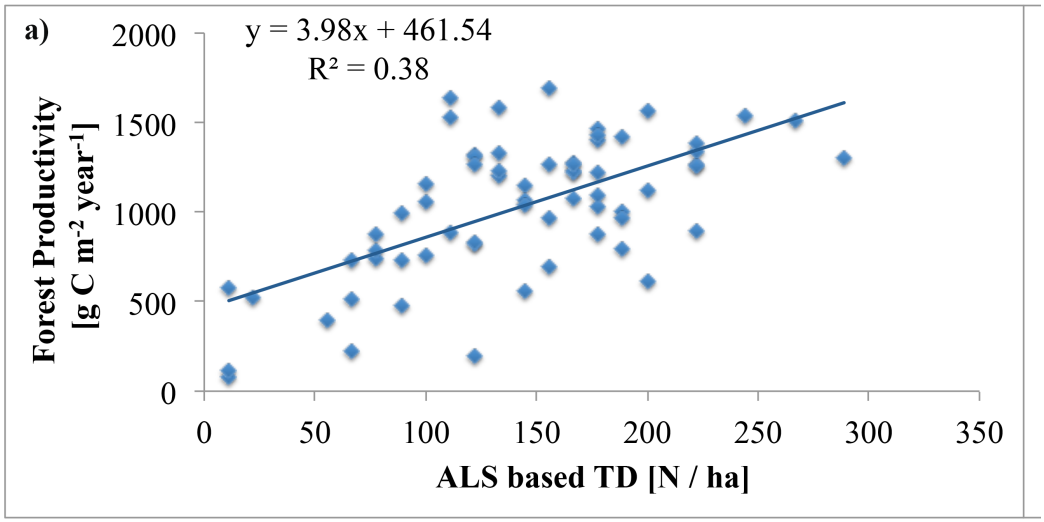

Fig. 4. 11. Relationship between tree density (TD) and forest productivity (a) and tree productivity (b) along four slope-line parallel transects.

4.5 Discussion

4.5.1 Reliability of tree density retrieval

We assessed a LM based approach in combination with ALS data to estimate TD in a heterogeneous alpine forest. Considering all trees with a DBH threshold > 5 cm, a moderate accuracy (i.e. R^2 of 0.39) with a substantial underestimation (RMSE of 389 trees per ha = 70 %) was achieved in the heterogeneous alpine environment. This result is in agreement with Næsset & Bjerknes [5], who found a relationship between estimated and reference TD of R^2 = 0.40 in a coniferous forest in Norway. Yet other studies evaluating the TD estimation accuracy report R^2 values that range from 0.40 to 0.85 [5], [24], [29], [40], [71], [82]. Jaskierniak et al. [83] indicate TD estimation accuracies ranging between 40 and 70% considering several studies carried out in Scandinavian and European forests.

The consideration of trees with larger DBHs decreases uncertainties in estimated TD (i.e., R^2 increases up to 0.80, RMSE decreases to 68 trees per ha = 40 %). This finding corresponds to results documented by Lefsky et al. [29], who found a strong relationship for ALS based TD estimates considering DBH>100 cm (R^2 = 0.85). Casas et al. [84] report a TD estimation accuracy of 87% for trees with a DBH > 30 cm. The dependency of the TD estimation accuracy on DBH indicates a sensitivity issue of the applied ALS-LM approach, while mainly small trees cannot be differentiated and reliably identified. In fact, we observe better TD estimates using a CHM with higher resolution, which is in agreement with Tesfamichael et al. [3].

Our results suggest that forest structure and species composition affect the TD retrieval accuracy. Indeed, crown shape and canopy density determine the success of the LM approach that basically exploits the morphology of ALS derived CHM's [40], [72]. If tree crowns are flat or show multiple main branches, the LM approach is likely to fail. Several studies demonstrated that forest structure strongly affects the capability of ALS data to characterize forest properties [39], [40], [85], [86]. In particular the occurrence of multi-stemmed trees, caused by a complex mix of environmental factors, disturbances and historical management [87] impacts the detection of individual trees [25], [86], [88], [89]. Further, in presence of steep slopes, a spatial misplacement between crown top and stem position on ground is likely and additionally affects the accuracy of ITD's [90], [91].

Structural effects obviously cause ITD and eventually TD estimates to be dependent on actual species. Physiological considerations add another complication and cause TD estimates to be dependent on species composition, in particular in multi-layered heterogeneous forests. European larch, for example, is largely abundant in our study site and a shade intolerant and fast growing species. Therefore, larch trees form and dominate the upper forest canopy layer [52], covering other more shade tolerant and slow growing species underneath, i.e., Swiss stone pine and Norway spruce. The multi-layering hides trees and thus impacts the TD estimation accuracy. We observed a dependency of TD estimates on surfaces orientation, i.e., north- and south-facing. TD estimates were less accurate for south-facing slopes compared to those on north-facing slopes. Since south-facing areas are characterized by a higher TD and the occurrence of multiple-stemmed trees, the lower TD estimation accuracy can be attributed to structural aspects.

Optimized ALS data acquisition allows overcoming certain issues discussed above, eventually yielding in improved ITD and TD estimates. One option would be the use of multi-temporal ALS data (i.e., leaf-on and leaf-off) [92]. Since Larch is a deciduous conifer tree, leaf-off data would allow improving the detection of trees present in lower canopy layers. Further, employing ALS data with higher point density can increase the chance to capture more echo returns vertically across the forest canopy. Vauhkonen et al. [40], for example, found that an ITD approach performs best with a dense point density (5-10 pts/m^2) or by using full waveform data [23], [92]. Further, a stratified field sampling as implemented in our study is important as well to facilitate the data analysis. Besides distributing potential reference plots along elevation gradients, a stratification for exposition, tree age and size [5], tree species, and species composition [86] has been found to be crucial to provide a representative set of reference data for remote sensing based

analysis. Such considerations are also recommended to optimize forest inventories if time-consuming field surveys are needed.

4.5.2 Reliability of forest productivity retrievals

We approximated FP with GPP. Estimates of GPP from optical EO data are typically based on two approaches: using vegetation greenness to indicate potential photosynthetic activity or measurements directly related to actual photosynthesis such as SIF. The use of SIF would be the preferred option, but the resolution of APEX is not optimized for SIF retrievals. Although SIF retrievals from APEX have been successfully demonstrated (Damm et al., 2015 [48]), retrievals in topographically complex environments are likely to be uncertain. We hence applied a greenness-based approach in this study. Such simple empirical approaches are frequently used to estimate forest GPP with optical remote sensing data. The approach by Hashimoto et al. [75] as applied in this study, relies on the EVI to constrain estimates of GPP. Previous studies have demonstrated that the sole use of the EVI can predict GPP as accurate as the current version of the MOD17 algorithm [93], [94]. Comparisons of modeled GPP and the MOD17 GPP product indicate an agreement of both products in terms of their predicated GPP range. The mean modeled GPP, however, was 26% lower compared to the MOD17 GPP product. Further, Heinsch et al. [95] report that the MOD17 GPP product tends to overestimate flux tower-based GPP by 20%-30%. Such uncertainties can be attributed to the fact that all these approaches rely on vegetation indices representing the greenness of vegetation, thus, potential rather than actual photosynthetic activity. Further, we took a single observation in time in combination with the empirical model from Hashimoto to obtain annual GPP. Since the forest ecosystem shows a pronounced phenological cycle, estimated GPP are likely to be overestimated. In fact, Zielis et al. [96] and Wolf et al. [97] report maximum GPP values of 5 g C m^{-2} day^{-1} for a Norway spruce forest close to Davos, Switzerland, that is comparable to our investigated forest. Scaling their flux tower based GPP estimates to annual values results in roughly 1000 g C m^{-2} $year^{-1}$, while we observed average values of 1255 +/- 342 g C m^{-2} $year^{-1}$, confirming the expected overestimation of GPP using the EVI approach. Use of time series of the new EO approach SIF allows overcoming such limitations since SIF is the most direct measurement of photosynthetic activity. The measurement of SIF can be considered mature but the use of SIF to constrain estimates of GPP still requires further attention. Nevertheless, first studies demonstrate and suggest improved SIF based GPP

estimates across scales, i.e., field scale [98], regional scale [48], [99], and global scale [100]–[102], as well as theoretically [103].

4.5.3 Topography effects on tree density and forest productivity

We observed a negative relationship between TD and surface elevation. This trend is coherent across used TD estimates (i.e., ALS or in situ based) and scales (i.e., plot, landscape) and is in line with results documented in literature [104]. The decreasing TD with increasing surface elevation can be associated to the availability of resources (i.e., temperature, water, nutrients) and the competition among trees for them. Also mechanical pressure (e.g., storm damages) in combination with slow growing rates can explain the topography impact on TD. Our results show stronger negative trends for north-facing slopes (i.e., $R^2 \sim 0.6$) compared to south-facing slopes (i.e., $R^2 \sim 0.2$-0.3). This finding suggests and provides further evidence that resource availability strongly determines TD, since north-facing slopes are generally colder and thus show even larger temperature gradients that are less favorable for tree growth.

TD and FP are positively related across scales. This finding is expected since a co-variance of both variables with height dependent gradients of growth limiting factors and eventually canopy density exists: The more trees, the higher the total productivity of a forested area and vice versa. Associated to this is the negative relationship between FP and surface elevation. This finding is in line with an early and often-cited study by Whittaker et al. [105] and other studies [104], [106], [105],[107]. As for TD, the negative relationship is plausible for the investigated alpine environment since surface elevation dependent gradients of growth limiting factors (e.g., nutrients, temperature, water) are likely to affect tree growth. Paulsen et al. [104], for example, conclude that a reduction of tree productivity towards the upper tree line is directly associated to decreasing temperature. We also observed a strong decline of FP in lower elevations in the vicinity of a river in the valley bottom. Causes for the reduced productivity are related to steep terrain and unfortunate soil conditions (rock, nutrient limitation) due to flooding events of the river.

However, it must be noted that the use of simple vegetation indices as proxy for GPP in combination with difficulties in describing the radiative transfer of complex canopies (i.e., the fractions of direct and diffuse irradiance components) [80] likely contributes to uncertainty in the FP estimates. Further analyses considering larger elevation gradients and more suited remote sensing approaches (i.e., SIF) are suggested to yield a more

general view on forest growth patterns in alpine environments and underlying causes such as resource limitations.

4.6 Conclusion

We conclude that estimates of TD in heterogeneous alpine landscapes challenge current technology and analytical approaches. Mainly tree and canopy structure determine the success of TD estimates, being in addition dependent on forest type and canopy species composition. ALS based approaches show limited sensitivity limit for small trees. Specific sampling schemes, e.g., multi-temporal ALS data acquisition with high point density, will partly allow increasing TD estimation sensitivity and accuracy. Further, simple empirical approaches provide sufficient accuracy to reveal first insights in interrelationships between FP and topography effects. More sophisticated and mechanistic approaches are, however, required to yield in depth knowledge. We conclude that Airborne laser scanning and imaging spectroscopy and their combination provide crucial technology to assess TD and FP at relevant ecological scales.

We can confirm existing theory that heterogeneous alpine forests are characterized by positive relationships between FP and TD, mainly due to a significant co-variance of both variables with elevation dependent gradients of growth limiting factors. We suggest extending this analysis by considering a wider range of forest types, landscape heterogeneity, topography and resource gradients. This ultimately allows gaining deeper understanding on the TD and FP variability and interrelationships across landscapes.

Acknowledgements

We sincerely appreciate the logistic support during the fieldwork and the permission to use ALS data provided by the Swiss National Park. This research was supported by the University of Kurdistan. We are grateful to Naghi Shaebanian, Hedayat Ghazanfari, Loghman Ghahramani, and Zahed Shakeri for their support at the Forestry Department, University of Kurdistan. We would like to thank Daniel Henke and Damien Markulin for their help with the field data collection. The contribution of A.D. was supported by a grant of the Swiss University Conference and ETH-Board in frame of the Swiss Earth Observatory Network (SEON) project, the contribution of M.E.S. is supported by the University of Zurich Research Priority Program on ‘Global Change and Biodiversity’.

References

[1] P. E. Johnson, S. R. Shifley, and R. Rogers, The ecology and silviculture of oaks. CABI, 2009.

[2] P. Fatehi, A. Damm, M. E. Schaepman, and M. Kneubühler, "Estimation of alpine forest structural variables from imaging spectrometer data," *Remote Sens.*, vol. 7, no. 12, pp. 16315–16338, 2015.

[3] S. G. Tesfamichael, F. Ahmed, J. a. N. van Aardt, and F. Blakeway, "A semi-variogram approach for estimating stems per hectare in Eucalyptus grandis plantations using discrete-return lidar height data," *For. Ecol. Manage.*, vol. 258, no. 7, pp. 1188–1199, Sep. 2009.

[4] D. K. Bolton, N. C. Coops, and M. A. Wulder, "Measuring forest structure along productivity gradients in the Canadian boreal with small-footprint Lidar," *Environ. Monit. Assess.*, vol. 185, pp. 6617–6634, 2013.

[5] E. Næsset and K.-O. Bjerknes, "Estimating tree heights and number of stems in young forest stands using airborne laser scanner data," *Remote Sens. Environ.*, vol. 78, no. 3, pp. 328–340, Dec. 2001.

[6] R. S. Capers, R. L. Chazdon, A. R. Brenes, and B. V. Alvarado, "Successional dynamics of woody seedling communities in wet tropical secondary forests," *J. Ecol.*, vol. 93, no. 6, pp. 1071–1084, 2005.

[7] G. J. Sproull, M. Adamus, M. Bukowski, T. Krzyżanowski, J. Szewczyk, J. Statwick, and J. Szwagrzyk, "Tree and stand-level patterns and predictors of Norway spruce mortality caused by bark beetle infestation in the Tatra Mountains," *For. Ecol. Manage.*, vol. 354, pp. 261–271, 2015.

[8] H. Pretzsch, *Forest dynamics, growth, and yield*. Berlin: Springer Berlin Heidelberg, 2009.

[9] J. P. Skovsgaard and J. K. Vanclay, "Forest site productivity: A review of the evolution of dendrometric concepts for even-aged stands," *Forestry*, vol. 81, no. 1, pp. 13–31, 2008.

[10] M. G. Rayan, D. Binkley, and J. H. Fownes, "Age-Related Decline in Forest Productivity : Pattern and Process," *Adv. Ecol. Res.*, vol. 27, pp. 213–262, 1997.

[11] S. J. Goetz and S. D. Prince, "Remote sensing of net primary production in boreal forest stands," *Agric. For. Meteorol.*, vol. 78, no. 3–4, pp. 149–179, Feb. 1996.

[12] J.-D. Bontemps and O. Bouriaud, "Predictive approaches to forest site productivity: recent trends, challenges and future perspectives," *Forestry*, vol. 87, no. 1, pp. 109–128, Nov. 2013.

[13] F. Maselli, D. Papale, N. Puletti, G. Chirici, and P. Corona, "Combining remote sensing and ancillary data to monitor the gross productivity of water-limited forest ecosystems," *Remote Sens. Environ.*, vol. 113, no. 3, pp. 657–667, Mar. 2009.

[14] T. W. Crowther, H. B. Glick, K. R. Covey, C. Bettigole, D. S. Maynard, S. M. Thomas, J. R. Smith, G. Hintler, M. C. Duguid, G. Amatulli, M.-N. Tuanmu, W. Jetz, C. Salas, C. Stam, D. Piotto, R. Tavani, S. Green, G. Bruce, S. J. Williams, S. K. Wiser, M. O. Huber, G. M. Hengeveld, G.-J. Nabuurs, E. Tikhonova, P. Borchardt, C.-F. Li, L. W. Powrie, M. Fischer, A. Hemp, J. Homeier, P. Cho, A. C. Vibrans, P. M. Umunay, S. L. Piao, C. W.

Rowe, M. S. Ashton, P. R. Crane, and M. A. Bradford, “Mapping tree density at a global scale,” *Nature*, Sep. 2015.

[15] R. T. Belote, S. Prisley, R. H. Jones, M. Fitzpatrick, and K. de Beurs, “Forest productivity and tree diversity relationships depend on ecological context within mid-Atlantic and Appalachian forests (USA),” *For. Ecol. Manage.*, vol. 261, no. 7, pp. 1315–1324, Apr. 2011.

[16] M. A. Lefsky, W. B. Cohen, G. G. Parker, and D. J. Harding, “Lidar Remote Sensing for Ecosystem Studies,” *Bioscience*, vol. 52, no. 1, p. 19, 2002.

[17] J. Liu, T. Yunhong, and J. W. F. Slik, “Topography related habitat associations of tree species traits, composition and diversity in a Chinese tropical forest,” *For. Ecol. Manage.*, vol. 330, pp. 75–81, 2014.

[18] C. Körner, G. D. Farquhar, and Z. Roksandic, “A global Survey of carbon Isotope Discrimination in Plants from High Altitude,” *Oecologia*, vol. 74, no. 4, pp. 623–632, 2009.

[19] G. P. Asner, R. E. Martin, C. B. Anderson, K. Kryston, N. Vaughn, D. E. Knapp, L. P. Bentley, A. Shenkin, N. Salinas, F. Sinca, R. Tupayachi, K. Quispe Huaypar, M. Montoya Pillco, F. D. Ccori Álvarez, S. Díaz, B. Enquist, and Y. Malhi, “Scale dependence of canopy trait distributions along a tropical forest elevation gradient,” *New Phytol.*, 2016.

[20] N. C. Coops, F. Morsdorf, M. E. Schaepman, and N. E. Zimmermann, “Characterization of an alpine tree line using airborne LiDAR data and physiological modeling.,” *Glob. Chang. Biol.*, vol. 19, pp. 3808–3821, Jul. 2013.

[21] J. Hyyppä, H. Hyyppä, M. Inkinen, M. Engdahl, S. Linko, and Y.-H. Zhu, “Accuracy comparison of various remote sensing data sources in the retrieval of forest stand attributes,” *For. Ecol. Manage.*, vol. 128, no. 1–2, pp. 109–120, Mar. 2000.

[22] F. Maselli, M. Chiesi, M. Mura, M. Marchetti, P. Corona, and G. Chirici, “Combination of optical and LiDAR satellite imagery with forest inventory data to improve wall-to-wall assessment of growing stock in Italy,” *Int. J. Appl. Earth Obs. Geoinf.*, vol. 26, pp. 377–386, Feb. 2014.

[23] B. Koch, U. Heyder, and H. Weinacker, “Detection of Individual Tree Crowns in Airborne Lidar Data,” *Photogramm. Eng. Remote Sens.*, vol. 72, no. 4, pp. 357–363, Apr. 2006.

[24] S. A. Hall, I. C. Burke, D. O. Box, M. R. Kaufmann, and J. M. Stoker, “Estimating stand structure using discrete-return lidar: an example from low density, fire prone ponderosa pine forests,” *For. Ecol. Manage.*, vol. 208, no. 1–3, pp. 189–209, Apr. 2005.

[25] M. Maltamo, K. Eerikäinen, J. Pitkänen, J. Hyyppä, and M. Vehmas, “Estimation of timber volume and stem density based on scanning laser altimetry and expected tree size distribution functions,” *Remote Sens. Environ.*, vol. 90, no. 3, pp. 319–330, Apr. 2004.

[26] A. T. Hudak, N. L. Crookston, J. S. Evans, M. J. Falkowski, A. M. . Smith, P. E. Gessler, and P. Morgan, “Regression modeling and mapping of coniferous forest basal area

and tree density from discrete-return lidar and multispectral satellite data," *Can. J. Remote Sens.*, vol. 32, no. 2, pp. 126–138, Apr. 2006.

[27] R. Sivanpillai, C. T. Smith, R. Srinivasan, M. G. Messina, and X. B. Wu, "Estimation of managed loblolly pine stand age and density with Landsat ETM+ data," *For. Ecol. Manage.*, vol. 223, pp. 247–254, 2006.

[28] M. A. Cho, A. K. Skidmore, and I. Sobhan, "Mapping beech (Fagus sylvatica L.) forest structure with airborne hyperspectral imagery," *Int. J. Appl. Earth Obs. Geoinf.*, vol. 11, no. 3, pp. 201–211, Jun. 2009.

[29] M. A. Lefsky, W. B. Cohen, S. A. Acker, G. G. Parker, T. A. Spies, and D. Harding, "Lidar Remote Sensing of the Canopy Structure and Biophysical Properties of Douglas-Fir Western Hemlock Forests," *Remote Sens. Environ.*, vol. 70, no. 3, pp. 339–361, Dec. 1999.

[30] K. D. Brosofske, R. E. Froese, M. J. Falkowski, and A. Banskota, "A Review of Methods for Mapping and Prediction of Inventory Attributes for Operational Forest Management," *For. Sci.*, vol. 60, no. 4, pp. 733–756, 2014.

[31] R. Leiterer, W. Mücke, F. Morsdorf, M. Hollaus, N. Pfeifer, and M. E. Schapeman, "Operational forest structure monitoring using airborne laser scanning," *Photogramm. Fernerkundung, Geoinf.*, vol. 3, pp. 173–184, 2013.

[32] M. Maltamo, E. Næsset, and J. Vauhkonen, *Forestry applications of airborne laser scanning: concepts and case studies*. Dordrecht: Springer, 2014.

[33] M. A. Wulder, N. C. Coops, A. T. Hudak, F. Morsdorf, R. Nelson, G. Newnham, and M. Vastaranta, "Status and prospects for LiDAR remote sensing of forested ecosystems," *Can. J. Remote Sens.*, vol. 39, no. S1, pp. 1–5, 2013.

[34] J. Hyyppä, X. Yu, H. Hyyppä, M. Vastaranta, M. Holopainen, A. Kukko, H. Kaartinen, A. Jaakkola, M. Vaaja, J. Koskinen, and P. Alho, "Advances in Forest Inventory Using Airborne Laser Scanning," *Remote Sens.*, vol. 4, no. 12, pp. 1190–1207, May 2012.

[35] P. Tompalski, N. C. Coops, J. C. White, and M. A. Wulder, "Enriching ALS-Derived Area-Based Estimates of Volume through Tree-Level Downscaling," *Forests*, vol. 6, no. 8, pp. 2608–2630, 2015.

[36] E. Næsset, "Determination of mean tree height of forest stands using airborne laser scanner data," *ISPRS J. Photogramm. Remote Sens.*, vol. 52, no. 2, pp. 49–56, 1997.

[37] J. C. White, M. a. Wulder, A. Varhola, M. Vastaranta, N. C. Coops, B. D. Cook, D. Pitt, and M. Woods, "A best practices guide for generating forest inventory attributes from airborne laser scanning data using an area-based approach," *For. Chron.*, vol. 89, no. 6, pp. 722–723, 2013.

[38] S. D. Roberts, T. J. Dean, D. L. Evans, J. W. McCombs, R. L. Harrington, and P. a. Glass, "Estimating individual tree leaf area in loblolly pine plantations using LiDAR-derived measurements of height and crown dimensions," *For. Ecol. Manage.*, vol. 213, no. 1–3, pp. 54–70, 2005.

[39] M. Vastaranta, N. Saarinen, V. Kankare, M. Holopainen, H. Kaartinen, J. Hyyppä, and H. Hyyppä, "Multisource Single-Tree Inventory in the Prediction of Tree Quality Variables and Logging Recoveries," *Remote Sens.*, vol. 6, no. 4, pp. 3475–3491, 2014.

[40] J. Vauhkonen, L. Ene, S. Gupta, J. Heinzel, J. Holmgren, J. Pitkanen, S. Solberg, Y. Wang, H. Weinacker, K. M. Hauglin, V. Lien, P. Packalen, T. Gobakken, B. Koch, E. Naesset, T. Tokola, and M. Maltamo, "Comparative testing of single-tree detection algorithms under different types of forest," *Forestry*, vol. 85, no. 1, pp. 27–40, 2012.

[41] H. Kaartinen, J. Hyyppä, X. Yu, M. Vastaranta, H. Hyyppä, A. Kukko, M. Holopainen, C. Heipke, M. Hirschmugl, F. Morsdorf, E. Næsset, J. Pitkänen, S. C. Popescu, S. Solberg, B. M. Wolf, and J.-C. Wu, "An International Comparison of Individual Tree Detection and Extraction Using Airborne Laser Scanning," *Remote Sens.*, vol. 4, no. 12, pp. 950–974, Mar. 2012.

[42] J. L. Monteith and C. J. Moss, "Climate and the efficiency of crop production in Britain [and discussion]," *Philos. Trans. R. Soc. London B Biol. Sci.*, vol. 281, no. 980, pp. 227–294, 1977.

[43] R. H. Waring, N. C. Coops, W. Fan, and J. M. Nightingale, "MODIS enhanced vegetation index predicts tree species richness across forested ecoregions in the contiguous U.S.A.," *Remote Sens. Environ.*, vol. 103, no. 2, pp. 218–226, 2006.

[44] T. Hilker, N. C. Coops, M. A. Wulder, T. A. Black, and R. D. Guy, "The use of remote sensing in light use efficiency based models of gross primary production: a review of current status and future requirements," *Sci. Total Environ.*, vol. 404, no. 2–3, pp. 411–23, Oct. 2008.

[45] D. P. Turner, W. D. Ritts, W. B. Cohen, T. K. Maeirsperger, S. T. Gower, A. A. Kirschbaum, S. W. Running, M. Zhao, S. C. Wofsy, A. L. Dunn, B. E. Law, J. L. Campbell, W. C. Oechel, H. J. Kwon, T. P. Meyers, E. E. Small, S. A. Kurc, and J. A. Gamon, "Site-level evaluation of satellite-based global terrestrial gross primary production and net primary production monitoring," *Glob. Chang. Biol.*, vol. 11, no. 4, pp. 666–684, 2005.

[46] N. C. Coops, C. J. Ferster, R. H. Waring, and J. Nightingale, "Comparison of three models for predicting gross primary production across and within forested ecoregions in the contiguous United States," *Remote Sens. Environ.*, vol. 113, no. 3, pp. 680–690, 2009.

[47] D. Schimel, R. Pavlick, J. B. Fisher, G. P. Asner, S. Saatchi, P. A. Townsend, C. Miller, C. Frankenberg, K. Hibbard, and P. Cox, "Observing terrestrial ecosystems and the carbon cycle from space," *Glob. Chang. Biol.*, vol. 21, no. 5, pp. 1762–1776, 2015.

[48] A. Damm, L. Guanter, E. Paul-Limoges, C. van der Tol, A. Hueni, N. Buchmann, W. Eugster, C. Ammann, and M. E. Schaepman, "Far-red sun-induced chlorophyll fluorescence shows ecosystem-specific relationships to gross primary production: An assessment based on observational and modeling approaches," *Remote Sens. Environ.*, vol. 166, pp. 91–105, Sep. 2015.

[49] MeteoSwiss, "IDAweb. The data portal of MeteoSwiss for research and teaching.," *http://www.meteoschweiz.admin.ch/web/de/services/datenportal/idaweb.html. accessed*, 2013. .

[50] A. Hill, J. Breschan, and D. Mandallaz, "Accuracy Assessment of Timber Volume Maps Using Forest Inventory Data and LiDAR Canopy Height Models," *Forests*, pp. 2253–2275, 2014.

[51] A. K. Schweiger, M. Schütz, P. Anderwald, M. E. Schaepman, M. Kneubühler, R. Haller, and A. C. Risch, "Foraging ecology of three sympatric ungulate species – behavioural and resource maps indicate differences between chamois, ibex and red deer," *Mov. Ecol.*, vol. 3, no. 6, pp. 1–12, Mar. 2015.

[52] A. C. Risch, L. M. Nagel, S. Martin, B. O. KrÜsi, F. Kienast, and H. Bugmman, "Structure and Long-Term Development of Subalpine Pinus montana Miller and Pinus cembra L. Forests in the Central European Alps," *Forstwissenschaftliches Cent.*, vol. 122, no. 4, pp. 219–230, 2003.

[53] A. Kangas and M. Maltamo, *Forest Inventory Methodology and Applications*. Springer, 2006.

[54] T. A. da Cunha, C. A. G. Finger, and H. Hasenauer, "Tree basal area increment models for Cedrela, Amburana, Copaifera and Swietenia growing in the Amazon rain forests," *For. Ecol. Manage.*, vol. 365, pp. 174–183, 2016.

[55] A. Leboeuf, A. Beaudoin, R. A. Fournier, L. Guindon, J. Luther, and M. Lambert, "A shadow fraction method for mapping biomass of northern boreal black spruce forests using QuickBird imagery," *Remote Sens. Environ.*, vol. 110, no. 4, pp. 488–500, Oct. 2007.

[56] A. C. Risch, M. F. Jurgensen, D. S. Page-Dumroese, O. Wildi, and M. Schütz, "Long-term development of above-and below-ground carbon stocks following land-use change in subalpine ecosystems of the Swiss National Park," *J. For.*, vol. 1602, pp. 1590–1602, 2008.

[57] H. Pretzsch, "Canopy space filling and tree crown morphology in mixed-species stands compared with monocultures," *For. Ecol. Manage.*, vol. 327, pp. 251–264, Sep. 2014.

[58] M. E. Schaepman, M. Jehle, A. Hueni, P. D'Odorico, A. Damm, J. Weyermann, F. D. Schneider, V. Laurent, C. Popp, F. C. Seidel, K. Lenhard, P. Gege, C. Küchler, J. Brazile, P. Kohler, L. De Vos, K. Meuleman, R. Meynart, D. Schläpfer, M. Kneubühler, and K. I. Itten, "Advanced radiometry measurements and Earth science applications with the Airborne Prism Experiment (APEX)," *Remote Sens. Environ.*, vol. 158, pp. 207–219, 2015.

[59] D. Schläpfer and R. Richter, "Geo-atmospheric processing of airborne imaging spectrometry data. Part 1: Parametric orthorectification," *Int. J. Remote Sens.*, vol. 23, no. 13, pp. 2609–2630, Jan. 2002.

[60] R. Richter and D. Schläpfer, "Geo-atmospheric processing of airborne imaging spectrometry data. Part 2: Atmospheric/topographic correction," *Int. J. Remote Sens.*, vol. 23, no. 13, pp. 2631–2649, Jan. 2002.

[61] G. Schaepman-Strub, M. E. Schaepman, T. H. Painter, S. Dangel, and J. V. Martonchik, "Reflectance quantities in optical remote sensing—definitions and case studies," *Remote Sens. Environ.*, vol. 103, no. 1, pp. 27–42, Jul. 2006.

[62] A. Berk, G. P. Anderson, P. K. Acharya, L. S. Bernstein, L. Muratov, J. Lee, M. J. Fox, S. M. Alder-Golden, J. H. Chetwynd, M. L. Hoke, R. B. Lockwood, T. W. Cooley, and J. A. Gardner, "MODTRAN5: a reformulated atmospheric band model with auxiliary species and practical multiple scattering options," in *Proceedings of the Society of*

Photo-Optical Instrumentation Engineer, 2005, pp. 662–667.

[63] W. Wagner, M. Hollaus, C. Briese, and V. Ducic, "3D vegetation mapping using small-footprint full-waveform airborne laser scanners," *Int. J. Remote Sens.*, vol. 29, no. 5, pp. 1433–1452, 2008.

[64] RIEGL, "Products. Airborne Scanning. Datasheets," 2015. [Online]. Available: www.riegl.com. [Accessed: 04-Jun-2015].

[65] C. Mallet and F. Bretar, "Full-waveform topographic lidar: State-of-the-art," *ISPRS J. Photogramm. Remote Sens.*, vol. 64, no. 1, pp. 1–16, 2009.

[66] P. Brassel and H. Lischke, "Swiss national forest inventory: methods and models of the second assessment," Birmensdorf, Switzerland, 2001.

[67] V. Kankare, M. Vastaranta, M. Holopainen, M. Räty, X. Yu, J. Hyyppä, H. Hyyppä, P. Alho, and R. Viitala, "Retrieval of Forest Aboveground Biomass and Stem Volume with Airborne Scanning LiDAR," *Remote Sens.*, vol. 5, no. 5, pp. 2257–2274, May 2013.

[68] D. Leckie, "Stand delineation and composition estimation using semi-automated individual tree crown analysis," *Remote Sens. Environ.*, vol. 85, no. 3, pp. 355–369, May 2003.

[69] M. Katoh and F. a. Gougeon, "Improving the Precision of Tree Counting by Combining Tree Detection with Crown Delineation and Classification on Homogeneity Guided Smoothed High Resolution (50 cm) Multispectral Airborne Digital Data," *Remote Sens.*, vol. 4, no. 12, pp. 1411–1424, May 2012.

[70] E. Lindberg, J. Holmgren, K. Olofsson, J. Wallerman, and H. Olsson, "Estimation of Tree Lists from Airborne Laser Scanning Using Tree Model Clustering and k-MSN Imputation," *Remote Sens.*, vol. 5, no. 4, pp. 1932–1955, Apr. 2013.

[71] M. Wulder, K. O. Niemann, and D. G. Goodenough, "Local Maximum Filtering for the Extraction of Tree Locations and Basal Area from High Spatial Resolution Imagery," *Remote Sens. Environ.*, vol. 73, no. 1, pp. 103–114, Jul. 2000.

[72] D.-A. Kwak, W.-K. Lee, J.-H. Lee, G. S. Biging, and P. Gong, "Detection of individual trees and estimation of tree height using LiDAR data," *J. For. Res.*, vol. 12, no. 6, pp. 425–434, Oct. 2007.

[73] A. Khosravipour, A. K. Skidmore, T. Wang, M. Isenburg, and K. Khoshelham, "Effect of slope on treetop detection using a LiDAR Canopy Height Model," *ISPRS J. Photogramm. Remote Sens.*, vol. 104, pp. 44– 52, 2015.

[74] J. M. Nightingale, W. Fan, N. C. Coops, and R. H. Waring, "Predicting tree diversity across the United States as a function of modeled gross primary production," *Ecol. Appl.*, vol. 18, no. 1, pp. 93–103, 2008.

[75] H. Hashimoto, W. Wang, C. Milesi, M. a. White, S. Ganguly, M. Gamo, R. Hirata, R. B. Myneni, and R. R. Nemani, "Exploring Simple Algorithms for Estimating Gross Primary Production in Forested Areas from Satellite Data," *Remote Sens.*, vol. 4, no. 12, pp. 303–326, 2012.

[76] A. Huete, K. Didan, T. Miura, E. P. Rodriguez, X. Gao, and L. G. Ferreira, "Overview of

the radiometric and biophysical performance of the MODIS vegetation indices," *Remote Sens. Environ.*, vol. 83, pp. 195–213, 2002.

[77] N. Huang, Z. Niu, Y. Zhan, S. Xu, M. C. Tappert, C. Wu, W. Huang, S. Gao, X. Hou, and D. Cai, "Relationships between soil respiration and photosynthesis-related spectral vegetation indices in two cropland ecosystems," *Agric. For. Meteorol.*, vol. 160, pp. 80–89, Jul. 2012.

[78] X. Li, X. Liu, M. Liu, C. Wang, and X. Xia, "A hyperspectral index sensitive to subtle changes in the canopy chlorophyll content under arsenic stress," *Int. J. Appl. Earth Obs. Geoinf.*, vol. 36, pp. 41–53, Apr. 2015.

[79] T. Wang, A. K. Skidmore, A. G. Toxopeus, and X. Liu, "Understory Bamboo Discrimination Using a Winter Image," *Photogramm. Eng. Remote Sens.*, vol. 75, no. 1, pp. 37–47, 2009.

[80] A. Damm, L. Guanter, W. Verhoef, D. Schläpfer, S. Garbari, and M. E. Schaepman, "Impact of varying irradiance on vegetation indices and chlorophyll fluorescence derived from spectroscopy data," *Remote Sens. Environ.*, vol. 156, pp. 202–215, Jan. 2015.

[81] M. García, D. Riaño, E. Chuvieco, and F. M. Danson, "Estimating biomass carbon stocks for a Mediterranean forest in central Spain using LiDAR height and intensity data," *Remote Sens. Environ.*, vol. 114, no. 4, pp. 816–830, Apr. 2010.

[82] J. Pitkänen, M. Maltamo, J. Hyyppä, and X. Yu, "Adaptive Methods for Individual Tree Detection on Airborne Laser Based Canopy Height Model," in *Proceedings of ISPRS Workshop Laser-Scanners for Forest and Landscape Assessment*, 2004, pp. 187–191.

[83] D. Jaskierniak, G. Kuczera, R. Benyon, and L. Wallace, "Using tree detection algorithms to predict stand sapwood area, basal area and stocking density in Eucalyptus regnans forest," *Remote Sens.*, vol. 7, no. 6, pp. 7298–7323, 2015.

[84] Á. Casas, M. García, R. B. Siegel, A. Koltunov, C. Ramírez, and S. Ustin, "Burned forest characterization at single-tree level with airborne laser scanning for assessing wildlife habitat," *Remote Sens. Environ.*, vol. 175, pp. 231–241, 2016.

[85] D. Leckie, F. Gougeon, D. Hill, R. Quinn, L. Armstrong, and R. Shreenan, "Combined high-density lidar and multispectral imagery for individual tree crown analysis," *Can. J. Remote Sens.*, vol. 29, no. 5, pp. 633–649, Jun. 2003.

[86] M. Heurich, "Automatic recognition and measurement of single trees based on data from airborne laser scanning over the richly structured natural forests of the Bavarian Forest National Park," *For. Ecol. Manage.*, vol. 255, no. 7, pp. 2416–2433, Apr. 2008.

[87] S. R. Freitas, M. C. S. Mello, and C. B. M. Cruz, "Relationships between forest structure and vegetation indices in Atlantic Rainforest," *For. Ecol. Manage.*, vol. 218, no. 1–3, pp. 353–362, Oct. 2005.

[88] E. Næsset, T. Gobakken, J. Holmgren, H. Hyyppä, J. Hyyppä, M. Maltamo, M. Nilsson, H. Olsson, Å. Persson, and U. Söderman, "Laser scanning of forest resources: the nordic experience," *Scand. J. For. Res.*, vol. 19, no. 6, pp. 482–499, Dec. 2004.

[89] M. J. Falkowski, A. M. S. Smith, P. E. Gessler, A. T. Hudak, L. A. Vierling, and J. S.

Evans, "The influence of conifer forest canopy cover on the accuracy of two individual tree measurement algorithms using lidar data.," *Can. J. Remote Sens.*, vol. 34, no. Supplement 2, pp. 338–350, 2008.

[90] H. Torabzadeh, F. Morsdorf, R. Leiterer, and M. E. Schaepman, "Fusing imaging spectrometry and airborne laser scanner data for tree species discrimination," in *International Geoscience and Remote Sensing Symposium (IGARSS)*, 2014, pp. 1253–1256.

[91] D. Gatziolis, J. S. Fried, and V. S. Monleon, "Challenges to estimating tree height via LiDAR in closed-canopy forests: A parable from Western Oregon," *For. Sci.*, vol. 56, no. 2, pp. 139–155, 2010.

[92] X. Yu, P. Litkey, J. Hyyppä, M. Holopainen, and M. Vastaranta, "Assessment of Low Density Full-Waveform Airborne Laser Scanning for Individual Tree Detection and Tree Species Classification," *Forests*, vol. 5, no. 5, pp. 1011–1031, 2014.

[93] D. A. Sims, A. F. Rahman, V. D. Cordova, B. Z. El-Masri, D. D. Baldocchi, L. B. Flanagan, A. H. Goldstein, D. Y. Hollinger, L. Misson, R. K. Monson, W. C. Oechel, H. P. Schmid, S. C. Wofsy, and L. Xu, "On the use of MODIS EVI to assess gross primary productivity of North American ecosystems," *J. Geophys. Res. Biogeosciences*, vol. 111, no. 4, pp. 1–16, 2006.

[94] N. Jahan and T. Y. Gan, "Developing a gross primary production model for coniferous forests of northeastern USA from MODIS data," *Int. J. Appl. Earth Obs. Geoinf.*, vol. 25, pp. 11–20, Dec. 2013.

[95] F. A. Heinsch, M. Zhao, S. W. Running, J. S. Kimball, R. R. Nemani, K. J. Davis, P. V. Bolstad, B. D. Cook, A. R. Desai, D. M. Ricciuto, B. E. Law, W. C. Oechel, H. Kwon, H. Luo, S. C. Wofsy, A. L. Dunn, J. W. Munger, D. D. Baldocchi, L. Xu, D. Y. Hollinger, A. D. Richardson, P. C. Stoy, M. B. S. Siqueira, R. K. Monson, S. P. Burns, and L. B. Flanagan, "Evaluation of remote sensing based terrestrial productivity from MODIS using regional tower eddy flux network observations," *IEEE Trans. Geosci. Remote Sens.*, vol. 44, no. 7, pp. 1908–1923, 2006.

[96] S. Zielis, S. Etzold, R. Zweifel, W. Eugster, M. Haeni, and N. Buchmann, "NEP of a Swiss subalpine forest is significantly driven not only by current but also by previous year's weather," *Biogeosciences*, vol. 11, no. 6, pp. 1627–1635, 2014.

[97] S. Wolf, W. Eugster, C. Ammann, M. Häni, S. Zielis, R. Hiller, J. Stieger, D. Imer, L. Merbold, and N. Buchmann, "Contrasting response of grassland versus forest carbon and water fluxes to spring drought in Switzerland," *Environ. Res. Lett.*, vol. 8, no. 3, p. 035007, 2013.

[98] A. Damm, J. Elber, A. Erler, B. eniamino Gioli, K. Hamdi, R. Hutjes, M. Kosvancova, M. Meroni, F. Miglietta, A. Moersch, J. Moreno, A. Schickling, R. Sonnenschein, T. Udelhoven, S. van der Linden, P. Hostert, and U. Rascher, "Remote sensing of sun-induced fluorescence to improve modeling of diurnal courses of gross primary production (GPP)," *Glob. Chang. Biol.*, vol. 16, no. 1, pp. 171–186, 2010.

[99] X. Yang, J. Tang, J. F. Mustard, J. E. Lee, M. Rossini, J. Joiner, J. W. Munger, A. Kornfeld, and A. D. Richardson, "Solar-induced chlorophyll fluorescence that correlates with canopy photosynthesis on diurnal and seasonal scales in a temperate deciduous forest," *Geophys. Res. Lett.*, vol. 42, no. 8, pp. 2977–2987, 2015.

[100] J.-E. Lee, J. a. Berry, C. van der Tol, X. Yang, L. Guanter, A. Damm, I. Baker, and C. Frankenberg, "Simulations of chlorophyll fluorescence incorporated into the Community Land Model version 4," *Glob. Chang. Biol.*, vol. 21, no. 9, pp. 3469–3477, 2015.

[101] N. C. Parazoo, K. Bowman, J. B. Fisher, C. Frankenberg, D. B. A. Jones, A. Cescatti, Ó. Pérez-Priego, G. Wohlfahrt, and L. Montagnani, "Terrestrial gross primary production inferred from satellite fluorescence and vegetation models," *Glob. Chang. Biol.*, vol. 20, no. 10, pp. 3103–3121, 2014.

[102] L. Guanter, Y. Zhang, M. Jung, J. Joiner, M. Voigt, J. a Berry, C. Frankenberg, A. R. Huete, P. Zarco-Tejada, J.-E. Lee, M. S. Moran, G. Ponce-Campos, C. Beer, G. Camps-Valls, N. Buchmann, D. Gianelle, K. Klumpp, A. Cescatti, J. M. Baker, and T. J. Griffis, "Global and time-resolved monitoring of crop photosynthesis with chlorophyll fluorescence.," *Proc. Natl. Acad. Sci. U. S. A.*, vol. 111, no. 14, pp. E1327–33, 2014.

[103] J. Verrelst, C. van der Tol, F. Magnani, N. Sabater, J. P. Rivera, G. Mohammed, and J. Moreno, "Evaluating the predictive power of sun-induced chlorophyll fluorescence to estimate net photosynthesis of vegetation canopies: A SCOPE modeling study," *Remote Sens. Environ.*, vol. 176, pp. 139–151, 2016.

[104] J. Paulsen, U. M. Weber, and C. Körner, "Tree growth near treeline: Abrupt or gradual reduction with altitude?," *Arctic, Antarct. Alp. Res.*, vol. 32, no. 1, pp. 14–20, 2000.

[105] R. H. Whittaker, F. H. Bormann, and G. E. Likens, "The Hubbard Brook ecosystem study: forest biomass and production," *Ecol. Monogr.*, vol. 44, no. 2, pp. 233–254, 1974.

[106] R. Tateno and H. Takeda, "Forest structure and tree species distribution in relation to topography-mediated heterogeneity of soil nitrogen and light at the forest floor," *Ecol. Res.*, vol. 18, no. 5, pp. 559–571, 2003.

[107] B. D. Pinno, D. Paré, L. Guindon, and N. Bélanger, "Predicting productivity of trembling aspen in the Boreal Shield ecozone of Quebec using different sources of soil and site information," *For. Ecol. Manage.*, vol. 257, no. 3, pp. 782–789, 2009.

5

Synthesis

5.1 Main findings

The main achievements of this dissertation are structured according to the research questions detailed in section 1.4 and the respective publications (chapter 2-4).

5.1.1 How can remotely sensed data capture the heterogeneity of an alpine ecosystem and what are the accuracies of retrieved ecosystem variables?

This research question was addressed in chapter 2. The aim of this chapter was to test two approaches that allow representing environmental variables across various land cover types (LCTs) in a heterogeneous alpine environment. The discrete and continuous field (CF) approaches were applied to retrieve vegetation (i.e., grassland and forest) aboveground biomass (AGB).

First, narrow-band vegetation indices (VIs), i.e., simple ratio (SR) and normalized difference vegetation index (NDVI), coupled with in-situ AGB measurements were used to generate calibration models to predict, separately, grassland and forest AGB from APEX data. Relevant and sensitive band combinations and final calibration models were selected based on the correlograms, R^2, RMSE, and variance inflation factor (VIF). For the estimation of grassland AGB, we found an SR index including a spectral band in the shortwave infrared (SWIR) at 1689 nm and a spectral band from near infrared (NIR) at 851 nm as best performing index. The final calibration model for forest AGB estimation was an SR employing spectral bands in the SWIR region at 1498 nm and 2112 nm. We found that the SWIR part of the spectrum is crucial for vegetation AGB estimation.

Second, we implemented a Boolean logic to classify grassland, forest, rock/soil, and snow LCTs from an APEX dataset on a per-pixel basis. In fact, this approach produces a classification map with hard boundaries between LCTs. Subsequently, a discrete vegetation AGB map was produced as a function of grassland and forest calibration models, and relevant LCTs maps. In contrast, the CF approach, the proposed approach in this paper, needs several steps to produce an AGB map. A linear spectral mixture (LSM) algorithm was applied to generate sub-pixel abundances of each LCT in the study area. The LCT abundance values were scaled between 0 and 1. The grassland and forest AGB thematic maps were generated by employing the relevant calibration models coupled with the APEX dataset. Then, the rescaled abundance maps were multiplied with the corresponding thematic maps to generate the final vegetation AGB CF map. The proposed

approach can cope with frequently occurring mixed pixels, highly challenging the capability of remote sensing (RS) data in heterogeneous environments.

The performance of the two approaches was assessed using independent field plots. Regardless of the implemented approach, we found a higher performance for grassland AGB estimation compared to forest AGB. The CF approach predicted grassland AGB (rRMSE = 15%) more accurately than the discrete approach (rRMSE = 26%). Furthermore, the discrete approach showed also an overestimation for low AGB values, while high AGB values were underestimated. For forest AGB, the discrete approach predicted biomass with an rRMSE of 25%. The CF mapping approach again improved the performance with decreasing rRMSE to 21%. In light of these results, we conclude that both approaches are generally capable to map grassland and forest AGB. However, the CF mapping approach shows several advantages including better capability to incorporate heterogeneity effects caused by changing understory or varying soil background. Further, the results of this study provide evidence that the concept of continuous fields allows successful representations of ecosystem parameters in complex environments.

5.1.2 Can forest structural attributes be estimated based on IS data in a heterogeneous, alpine forest area?

This research question was addressed in chapter 3. In this chapter we evaluated the capability of APEX data for estimating forest structural attributes including canopy cover, basal area, and timber volume in a heterogeneous alpine ecosystem, i.e., the Swiss National Park (SNP). The estimation of forest structural attributes using optical RS is based on determining a link between spectral information contained in a dataset and vegetation metrics of interest. The hypothesis is that the variations in forest attributes affect the spectral reflectance of a given forest and can be modelled by an empirical approach. We applied a parametric regression model (i.e., simple and stepwise multiple regression) to predict forest structural attributes of interest (dependent variables) from narrowband VIs, (i.e., SR, NDVI, second soil-adjusted vegetation index (SAVI2), perpendicular vegetation index (PVI), and band depth indices).

The performance of these empirical approaches was evaluated by computing the agreement of estimated values with *in-situ* data. For *canopy closure*, we found that a simple regression model based on a PVI can explain 60% of variance with an rRMSE of 15%. However, the stepwise multiple regression (SMR) employing band depth indices and an SR index obtained higher accuracy (R^2 = 0.81, and rRMSE = 10%). An ANOVA test showed a

statistically significant difference (*p = 0.0005*) between the two models at 5% significance level. This result is promising since the required relative RMSE for operational forest inventory is commonly referred to be lower than 15% at stand scale [1]. The SMR estimated *basal area* (R^2 = 0.68, and rRMSE = 20%) proved to be more precise than in the case of the simple regression (R^2 value of 0.60 and rRMSE of 23%). An ANOVA test *(p = 0.017*) confirmed that the two models are statistically significant. For *timber volume* estimation, the simple regression explained 68% of variability with an rRMSE of 24%. SMR, again, showed a statistical (*p = 0.024*) improvement in timber volume estimation (R^2 = 0.73, and rRMSE = 22%).

Our results showed that among the investigated forest structural attributes, unsurprisingly, canopy closure was estimated more precisely than basal area and timber volume. Canopy closure is an attribute that has a direct control on the canopy spectral reflectance, and thus, can be predicted with potentially higher accuracy. The predicting models for both basal area and especially timber volume tend to marginally overestimate low values and underestimate high values, an effect known as "local bias" [2]. This constraint has also been reported by Nink et al. [3], who predicted timber volume using simulated EnMAP and Sentinel-2 images with different approaches (i.e., a parametric Partial Least Squares (PLS) regression and a non-parametric K-Nearest Neighbours (k-NN) algorithm). It is important to note that VI wavelengths originating from the SWIR region were chosen more frequently than wavelengths from other parts of the electromagnetic spectrum in all regression models. Therefore, our findings confirm that the SWIR region significantly contributes to the estimation of forest structural attributes. Further, Hyyppä et al. [4] predicted forest volume with an R^2 of 0.55 and a relative RMSE of 45% using AISA imaging spectrometer data with 30 spectral bands (466-870 nm). The availability of a larger spectral range (400-2500 nm) using the APEX sensor in comparison to AISA highlighted the importance of capturing the full spectrum, and incorporating the SWIR region for forest structural assessment. This can explain why our models yielded a higher accuracy. Our results revealed that a combination of narrowband VIs (i.e., SR, and PVI) and band depth indices generated from continuum removed reflectance data improved the predictive power of fitted models for estimating all forest structural attributes. It is important to note that some forest structural attributes, such as LAI or canopy closure, directly affect the canopy reflectance behaviour. In contrast, structural attributes like basal area, timber volume, and tree diameter have no direct control on canopy reflectance properties. Therefore, the successful estimation of these attributes using optical data highly depends on their correlation with attributes that directly affect forest canopy

reflectance properties [2],[5]. In our study, for example, we observed significant correlations between canopy cover and both basal area ($r(n=35) = 0.75$, $p < 0.01$), and timber volume ($r(n=35) = 0.62$, $p < 0.01$).

5.1.3 What is the potential capability of ALS and IS data integration to map *structural and functional properties* in a heterogeneous, alpine forest area?

This research question was addressed in chapter 4. This chapter presents a framework methodology to integrate airborne laser scanning (ALS) and imaging spectroscopy (IS) data with the aim to quantify an alpine forest structurally (i.e., tree density (TD)) and functionally (i.e., forest productivity (FP)) at plot scale. To take advantage of actively sensed data that allow a 3D surface representation of individual trees [6], we used ALS data in combination with a local maxima (LM) approach to estimate TD and compared it with reference data. Variable window sizes coupled with different pixel sizes of a canopy height model (CHM) were applied. A narrow-band NDVI product generated from APEX data was used to eliminate falsely detected trees resulting from the complex terrain in the study area (i.e., very steep slopes) [7]. The independent validation showed an underestimation of TD (rRMSE = 77%). However, a significant improvement in TD estimation was observed for a class of large trees, i.e., trees with a diameter larger than 30 cm (rRMSE = 40%). The obtained results were different for field plots located on north-facing slopes (rRMSE = 33%) and south-facing slopes (rRMSE = 42%). Obtaining lower accuracies in south-facing plots may be due to the presence of significantly higher number of trees, in addition to the occurrence of multiple-stemmed trees. Tanhuapää et al. (2016) [8] have highlighted that plots with higher numbers of trees caused an increasing TD estimation error. The assessment of the role of species composition on the TD estimation revealed that TD error tends to be species specific. The lowest error was found in Larch–dominated plots, while the highest error occurs in mixed plots. It is important to keep in mind that Larch (*Larix decidua*) trees were present, indeed with varying proportion, in all field plots. Larix occupies the upper forest canopy layer because of its faster growing properties. Swiss stone pine (*Pinus cembra*) and Norway spruce (*Picea abies*), on the contrary, were observed less distributed and they mainly contributed to form the lower part of the canopy layer [5]. Therefore, they are often not detectable by ALS data [9]. We found that the variability of TD estimation errors was related to the proportion of Swiss stone pine and Norway spruce. The issue of undetected trees might be improved by i) the use of multi-temporal ALS data (i.e. leaf-on and leaf-off) [10], and ii) acquiring ALS data

with a dense point density as indicated by Vauhkonen et al. [11], mentioning that an individual tree detection (ITD) approach performs best with a dense point density (5-10 pts/m^2).

We further applied an empirical approach to map Gross Primary Production (GPP), as an approximation of forest productivity, using APEX data of the study area. The combination of optical reflectance data and ALS data allowed to generate a GPP map and to subsequently modify it by identifying shaded pixels and normalizing for tree fraction cover in the respective area. We found an agreement between the modelled GPP and the well-documented MOD17 GPP product. However, we observed a 20% overestimation compared to a flux tower-based GPP range reported for a close-by forested area in Davos, Switzerland. The observed overestimation may be due to the fact that i) the greenness-based approach to model GPP is reflecting the potential, rather than the actual photosynthetic activity, or ii) modelling annual GPP using a single observation in time introduces uncertainty as the forest phenological cycle plays an important role in annual GPP, which can only be captured by multi-temporal data acquisition. Our findings regarding the interrelationship between forest productivity, TD, and surface elevation showed that surface elevation constrains both forest productivity and TD. In other words, there is a decline in estimated TD and forest productivity with increasing elevation. Also, a positive relationship between forest productivity and TD was observed. It is important to note that the trends obtained from remote sensing-based estimates agree with field-based measurements at both plot and landscape scales. This may be particularly promising for further assessment of changes in forest productivity, TD, and tree mortality caused by an increasing number of environmental drivers across diverse gradients (e.g. elevation, climate, soils), as emphasized recently by Asner et al. (2016) [12].

5.2 Conclusions

In this thesis, a remote sensing-based approach was implemented to map forest structural and functional attributes in a heterogeneous alpine environment. Based on the main findings detailed in section 5.1, the following conclusions can be drawn:

Firstly, this thesis emphasizes that attention should be paid to choose an appropriate approach to map ecosystem parameters in a heterogeneous landscape. It provides quantitative evidence that the continuous field (CF) mapping approach is a powerful concept and offers the capability to estimate and map continuous ecological parameters such as vegetation AGB [13], water content [14], or wetland types [15]. It highlights the

sensitivity of the CF approach to correctly account for natural gradients in surface characteristics by considering sub-pixel information when heterogeneity is high. The findings reveal significant improvements in vegetation AGB estimation using the CF approach compared to a traditional approach (i.e., the discrete approach).

Secondly, this thesis underpins that optical remote sensing data, i.e., APEX data in combination with an empirical approach, allow providing spatially explicit information on the distribution of forest structural attributes including canopy closure, basal area, and timber volume at a satisfactory level of accuracy (i.e., rRMSE less than 30% [16]). The results underline the important role of the SWIR spectral region to estimate forest structural attributes. These findings further emphasize the need for high quality optical data with high signal-to-noise (SNR) ratio, especially in the SWIR region. In the absence of ALS data, which is the case for many areas on Earth, free access to optical data is important, and the application of relatively simple empirical approaches to estimate ecosystem variables in general, and forest attributes in particular, is strongly suggested.

Thirdly and finally, this thesis provides an investigation and related accuracy assessment of how active and passive remote sensing data can be combined to assess structural and functional attributes of a heterogeneously forested area. Chapter 4 shows that the estimation of TD in a heterogeneous alpine forest environment is a challenge given current technology and analytical approaches. More precisely, the findings show an acceptable accuracy of ALS data to capture information on large and tall trees at the upper layer of a canopy, whereas co-dominant and covered trees at lower canopy levels can hardly be detected using ALS data. Overall, this thesis contributes to understand the interrelationships among measured and estimated TD, topography, and modelled forest productivity, and provides a report of achieved accuracies using RS approaches.

This thesis improved and developed methods for providing spatially explicit predictions of a number of forest structural attributes such as biomass, canopy closure, basal area, timber volume, tree density, and a functional attribute, i.e., forest productivity. These attributes are the important key features often used to characterize forests in support of forest inventories, management strategies and conservation activities [17]. In commercial forests, for example, the primary objective of most forest inventories is to estimate standing basal area and timber volume. Remote sensing-based products can help managing forest resources, i.e. when selecting harvest hot-spot locations in a forested area during a specific period [18]. A tree density map can be of use to indicate essential silvicultural treatments, such as reduction of TD by thinning if TD is too high, or definition of a proper strategy to increase regeneration rate if TD is low [19]. Canopy closure is used

as an important criterion to identify a specific area as forest (forest definition) and, finally, to generate forest cover maps in many countries. In Switzerland, for example, the minimum canopy closure of a forest is defined to be at least 20% [20]. The promising results obtained in chapter 3 with mapping canopy closure may contribute to produce accurate forest cover maps. Canopy closure metrics also provide important information regarding forest functions and for quantifying mass, energy, and gas exchange between a forest ecosystem and the atmosphere [21]. The estimated structural attributes in this thesis may be especially useful for site quality assessment. At a given age, for example, a lower number of trees with higher basal area/volume indicates a good site productivity index [22] .

5.3 Study limitations and outlook

This thesis investigated the capability of an empirical approach in combination with imaging spectroscopy data to map AGB (chapter 2), canopy closure, basal area and timber volume (chapter 3), as well as forest productivity (Chapter 4). The results show that the empirical approach is able to estimate structural/functional forest attributes with reasonable accuracy. However, some limitations of optical remote sensing data have effects on the estimation performance. In chapter 2, for example, a comparison of hemispherical conical reflectance factor (HCRF) spectra of corresponding pixels located in the overlapping area of two adjacent APEX flight-lines showed differences in HCRF measured values. These differences can be contributed to surface anisotropy, commonly described as bi-directional reflectance distribution function (BRDF) [23], and remaining topographic effects after the atmospheric correction implementation. These uncertainties may afterwards be transferred into derived ecosystem products [24]. Hence, special effort is needed to apply appropriate approaches in order to reduce the BRDF and topographic effects especially in rugged terrain areas [25]–[27].

The key to success in CF mapping is to precisely model the resulting abundance maps. In this thesis a linear spectral mixture (LSM) algorithm was applied to estimate the proportion of each land cover type using selected pure spectra called *end-members* [13]. The LSM assumes that in mixed pixels the reflected spectrum collected by an optical system (i.e., spectrometer) is a linear combination of end-members weighted by their corresponding abundances. In fact, it assumes that no multiple scattering or secondary reflectance happens in reflected radiation before being collected by a spectrometer [28], [29]. This assumption forces the LSM algorithm to model abundance fractions of present

LCTs in a natural complex landscape that are prone to multiple scattering [30]. Therefore, non-linear spectral mixture may yield better results once there is a complex and multiple interaction between radiation and components of a given pixel [31].

In remote sensing for forest assessment the collection of field data plays an important role [32]. A sufficient number of field plots, measurement consistency, a suitable sampling approach (i.e., simple random, systematic, or clustered), and the appropriate time for field data collection are all critical to obtain reliable field reference data. It is essential to select an optimum number of plots in a way that the sampling scheme covers the entire range of attributes of interest (such as AGB, canopy closure etc.,) [33]. Further, it is important to collect the field data at the same time or as close as possible to remote sensing data acquisition [32], because time differences may impact model prediction performance. In this thesis, grassland field data and APEX data were acquired at the same day in June 2010. However, there was a two-year time lag between forest field data collection and APEX data acquisition. Since the SNP is a protected area, it was assumed that forest structural attributes remained relatively constant during this period. Nevertheless, this assumption introduces some uncertainty in forest structure estimation. Multi-temporal acquisition of both RS data and field measurements is crucial to cope with seasonal and phenological dependencies of structural attributes. In other words, the prediction power of structural attributes (especially for grassland biomass which shows strong seasonal variation) can be improved by taking into account the possibility of collecting a richer temporal data set and type-specific calibration models [13], [34].

Empirical approaches are comparably easy to implement, and often yield accurate results in the specific study area and at the spatial scale they were calibrated for [35], [36]. Therefore, these approaches have been more widely used for predicting vegetation attributes (i.e., biochemical, and structural attributes) [37], [38] than physical-based approaches. Their biggest issue, however, is the transferability of a calibrated model to other locations and dates [39]. More precisely, models are i) sensor specific, ii) specific to the dataset used for calibration, and iii) dependent on extensive *in-situ* data [40]. In this context, physical-based approaches can, theoretically, overcome these limitations since their main advantage is their general applicability to different sites and sampling conditions [41]. It is important to note that the retrieval capacity of physical-based approaches is limited to a few forest attributes, such as leaf area index [40], chlorophyll content [42], water content [43] and canopy closure [44]. Therefore, an additional empirical approach is needed to establish a relationship between a parameter predicted by a physical-based approach and the parameters of interest such as biomass [45].

The leave-one-out validation procedure showed that for forest AGB estimation (Fig. 2. 11), basal area estimation (Fig. 3.5) and timber volume estimation (Fig. 3.7) the maximum variation and highest scattering between estimated and measured variables were observed in their mid range values. This pattern shows that using only spectral reflectance data is not sensitive enough to estimate structural attributes covering these ranges. The same issue has been reported by Nink et al. (2015) [3]. In future studies, a combination of spectral data with ancillary data (i.e., stand age, site index, elevation, slope and mean annual temperature) may improve the prediction power [46], [47].

Predicting tree density in a structurally heterogeneous forested area with multi-stemmed trees using an ITD approach in combination with relatively low point density (less than 5 pts/m^2) proved to be a difficult task. Applying an Area-Based Approach (ABA) using a nonparametric regression in such a forest may help to improve the prediction power.

The use of simple vegetation indices as a proxy for GPP in combination with difficulties in describing the radiative transfer of complex canopies (i.e., the fractions of direct and diffuse irradiance components) likely contributes to uncertainty in the forest productivity estimates [26]. Further analyses that consider larger elevation gradients and more sophisticated remote sensing approaches (i.e., sun-induced chlorophyll fluorescence) may yield a more general view on forest growth patterns in alpine environments and underlying causes such as resource limitations.

References

[1] H. J. Hyyppä, and J. M. Hyyppä, "Effects of Stand Size on the Accuracy of Remote Sensing-Based Forest Inventory," *IEEE Trans. Geosci. Remote Sens.*, vol. 39, no. 12, pp. 2613–2621, 2001.

[2] M. A. Cho, A. K. Skidmore, and I. Sobhan, "Mapping beech (Fagus sylvatica L.) forest structure with airborne hyperspectral imagery," *Int. J. Appl. Earth Obs. Geoinf.*, vol. 11, no. 3, pp. 201–211, Jun. 2009.

[3] S. Nink, J. Hill, H. Buddenbaum, J. Stoffels, T. Sachtleber, and J. Langshausen, "Assessing the suitability of future multi- and hyperspectral satellite systems for mapping the spatial distribution of norway spruce timber volume," *Remote Sens.*, vol. 7, no. 9, pp. 12009–12040, 2015.

[4] J. Hyyppä, H. Hyyppä, M. Inkinen, M. Engdahl, S. Linko, and Y.-H. Zhu, "Accuracy comparison of various remote sensing data sources in the retrieval of forest stand attributes," *For. Ecol. Manage.*, vol. 128, no. 1–2, pp. 109–120, Mar. 2000.

[5] P. Fatehi, A. Damm, M. E. Schaepman, and M. Kneubühler, “Estimation of alpine forest structural variables from imaging spectrometer data,” *Remote Sens.*, vol. 7, no. 12, pp. 16315–16338, 2015.

[6] S. C. Popescu and R. H. Wynne, “Seeing the Trees in the Forest : Using Lidar and Multispectral Data Fusion with Local Filtering and Variable Window Size for Estimating Tree Height,” *Photogramm. Eng. Remote Sensing*, vol. 70, no. 5, pp. 589–604, 2004.

[7] A. Khosravipour, A. K. Skidmore, T. Wang, M. Isenburg, and K. Khoshelham, “Effect of slope on treetop detection using a LiDAR Canopy Height Model,” *ISPRS J. Photogramm. Remote Sens.*, vol. 104, pp. 44– 52, 2015.

[8] T. Tanhuanpää, N. Saarinen, V. Kankare, and K. Nurminen, “Evaluating the Performance of High-Altitude Aerial Image-Based Digital Surface Models in Detecting Individual Tree Crowns in Mature Boreal Forests,” *Forests*, vol. 7, no. 143, pp. 1–17, 2016.

[9] Á. Casas, M. García, R. B. Siegel, A. Koltunov, C. Ramírez, and S. Ustin, “Burned forest characterization at single-tree level with airborne laser scanning for assessing wildlife habitat,” *Remote Sens. Environ.*, vol. 175, pp. 231–241, 2016.

[10] X. Yu, P. Litkey, J. Hyyppä, M. Holopainen, and M. Vastaranta, “Assessment of Low Density Full-Waveform Airborne Laser Scanning for Individual Tree Detection and Tree Species Classification,” *Forests*, vol. 5, no. 5, pp. 1011–1031, 2014.

[11] J. Vauhkonen, L. Ene, S. Gupta, J. Heinzel, J. Holmgren, J. Pitkanen, S. Solberg, Y. Wang, H. Weinacker, K. M. Hauglin, V. Lien, P. Packalen, T. Gobakken, B. Koch, E. Naesset, T. Tokola, and M. Maltamo, “Comparative testing of single-tree detection algorithms under different types of forest,” *Forestry*, vol. 85, no. 1, pp. 27–40, 2012.

[12] G. P. Asner, R. E. Martin, C. B. Anderson, K. Kryston, N. Vaughn, D. E. Knapp, L. P. Bentley, A. Shenkin, N. Salinas, F. Sinca, R. Tupayachi, K. Quispe Huaypar, M. Montoya Pillco, F. D. Ccori Álvarez, S. Díaz, B. Enquist, and Y. Malhi, “Scale dependence of canopy trait distributions along a tropical forest elevation gradient,” *New Phytol.*, 2016.

[13] P. Fatehi, A. Damm, A. Schweiger, M. E. Schaepman, and M. Kneubühler, “Mapping Alpine Aboveground Biomass From Imaging Spectrometer Data : A Comparison of Two Approaches,” *IEEE J. Sel. Top. Appl. Earth Obs. Remote Sens.*, vol. 8, no. 6, pp. 3123–3139, 2015.

[14] M. Kneubühler, A. Damm, A. Schweiger, A. C. Risch, M. Schütz, and M. E. Schaepman, “Continuous Fields From Imaging Spectrometer Data for Ecosystem Parameter Mapping and Their Potential for Animal Habitat Assessment in Alpine Regions,” *IEEE J. Sel. Top. Appl. Earth Obs. Remote Sens.*, vol. 7, no. 6, pp. 2600–2610, 2014.

[15] J. Reschke and C. Hüttich, “Continuous field mapping of Mediterranean wetlands

using sub-pixel spectral signatures and multi-temporal Landsat data," *Int. J. Appl. Earth Obs. Geoinf.*, vol. 28, no. 1, pp. 220–229, 2014.

[16] M. Maltamo, K. Eerikäinen, J. Pitkänen, J. Hyyppä, and M. Vehmas, "Estimation of timber volume and stem density based on scanning laser altimetry and expected tree size distribution functions," *Remote Sens. Environ.*, vol. 90, no. 3, pp. 319–330, Apr. 2004.

[17] A. C. Lee and R. M. Lucas, "A LiDAR-derived canopy density model for tree stem and crown mapping in Australian forests," *Remote Sens. Environ.*, vol. 111, no. 4, pp. 493–518, Dec. 2007.

[18] M. S. Williams, P. L. Patterson, and H. T. Mowrer, "Comparison of Ground Sampling Methods for Estimating Canopy Cover," *For. Sci.*, vol. 49, no. 2, pp. 235–246, 2003.

[19] E. Næsset and K.-O. Bjerknes, "Estimating tree heights and number of stems in young forest stands using airborne laser scanner data," *Remote Sens. Environ.*, vol. 78, no. 3, pp. 328–340, Dec. 2001.

[20] L. T. Waser, C. Fischer, Z. Wang, and C. Ginzler, "Wall-to-Wall Forest Mapping Based on Digital Surface Models from Image-Based Point Clouds and a NFI Forest Definition," *Forests*, vol. 6, no. 12. Multidisciplinary Digital Publishing Institute, pp. 4510–4528, 11-Dec-2015.

[21] J. L. R. Jensen, K. S. Humes, L. a. Vierling, and A. T. Hudak, "Discrete return lidar-based prediction of leaf area index in two conifer forests," *Remote Sens. Environ.*, vol. 112, no. 10, pp. 3947–3957, 2008.

[22] P. E. Johnson, S. R. Shifley, and R. Rogers, *The ecology and silviculture of oaks*. CABI, 2009.

[23] F. Gao, "Detecting vegetation structure using a kernel-based BRDF model," *Remote Sens. Environ.*, vol. 86, no. 2, pp. 198–205, Jul. 2003.

[24] J. Weyermann, A. Damm, M. Kneubühler, and M. E. Schaepman, "Correction of reflectance anisotropy effects of vegetation on airborne spectroscopy data and derived products," *IEEE Trans. Geosci. Remote Sens. Remote Sens.*, vol. 52, no. January 2014, pp. 616–627, 2014.

[25] L. Homolová, M. E. Schaepman, P. Lamarque, J. G. P. W. Clevers, F. De Bello, W. THuiller, and S. Lavorel, "Comparison of remote sensing and plant trait-based modelling to predict ecosystem services in subalpine grasslands," *Echosphere*, vol. 5, no. 8, p. art1000, 2014.

[26] A. Damm, L. Guanter, W. Verhoef, D. Schläpfer, S. Garbari, and M. E. Schaepman, "Impact of varying irradiance on vegetation indices and chlorophyll fluorescence derived from spectroscopy data," *Remote Sens. Environ.*, vol. 156, pp. 202–215, Jan. 2015.

[27] H. Yuan, R. Ma, C. Atzberger, F. Li, S. Loiselle, and J. Luo, "Estimating Forest fAPAR from Multispectral Landsat-8 Data Using the Invertible Forest Reflectance Model INFORM," *Remote Sens.*, vol. 7, no. 6, pp. 7425–7446, 2015.

[28] G. S. Okin, D. A. Roberts, B. Murray, and W. J. Okin, "Practical limits on hyperspectral vegetation discrimination in arid and semiarid environments," *Remote Sens. Environ.*, vol. 77, no. 2, pp. 212–225, Aug. 2001.

[29] C. Wu, "Normalized spectral mixture analysis for monitoring urban composition using ETM+ imagery," *Remote Sens. Environ.*, vol. 93, no. 4, pp. 480–492, Dec. 2004.

[30] M. A. Gilabert, F. J. Garcia-Haro, and J. Melià, "A Mixture Modeling Approach to Estimate Vegetation Parameters for Heterogeneous Canopies in Remote Sensing," *Remote Sens. Environ.*, vol. 72, pp. 328–345, 2000.

[31] R. Heylen, M. Parente, and P. Gader, "A review of nonlinear hyperspectral unmixing methods," *IEEE J. Sel. Top. Appl. Earth Obs. Remote Sens.*, vol. 7, no. 6, pp. 1844–1868, 2014.

[32] S. E. Franklin, *Remote Sensing for Sustainable Forest Management*. Boca Raton, Florida, USA: Lewis Publishers, 2001.

[33] M. Köhl, S. Magnussen, and M. Marchetti, *Sampling Methods, Remote Sensing and GIS Multiresource Forest Inventory*. Springer Berlin Heidelberg, 2006.

[34] M. E. Jakubauskas and K. P. Price, "Empirical Relationships between Structural and Spectral Factors of Yellowstone Lodgepole Pine Forests," *Photogramm. Eng. Remote Sens.*, vol. 63, no. 1, pp. 1375–1381, 1997.

[35] C. Eisfelder, C. Kuenzer, and S. Dech, "Derivation of biomass information for semi-arid areas using remote-sensing data," *Int. J. Remote Sens.*, vol. 33, no. February 2015, pp. 2937–2984, 2012.

[36] A. Schweiger, A. C. Risch, A. Damm, M. Kneubühler, R. Haller, M. E. Schaepman, and M. Schütz, "Using imaging spectroscopy to predict aboveground plant biomass in alpine grasslands grazed by large ungulates," *J. Veg. Sci.*, vol. 26, pp. 175–190, 2015.

[37] A. Viña and A. A. Gitelson, "Sensitivity to foliar anthocyanin content of vegetation indices using green reflectance," *Geosci. Remote Sens. Lett.*, vol. 8, no. 3, pp. 463–467, 2011.

[38] F. E. Fassnacht, F. Hartig, H. Latifi, C. Berger, J. Hernández, P. Corvalán, and B. Koch, "Importance of sample size , data type and prediction method for remote sensing-based estimations of aboveground forest biomass," *Remote Sens. Environ.*, vol. 154, pp. 102–114, 2014.

[39] G. M. Foody, D. S. Boyd, and M. E. J. Cutler, "Predictive relations of tropical forest biomass from Landsat TM data and their transferability between regions," *Remote Sens. Environ.*, vol. 85, no. 4, pp. 463–474, Jun. 2003.

[40] M. Schlerf and C. Atzberger, "Vegetation Structure Retrieval in Beech and Spruce Forests Using Spectrodirectional Satellite Data," *IEEE J. Sel. Top. Appl. Earth Obs. Remote Sens.*, vol. 5, no. 1, pp. 8–17, Feb. 2012.

[41] M. Schlerf and C. Atzberger, "Inversion of a forest reflectance model to estimate structural canopy variables from hyperspectral remote sensing data," *Remote Sens. Environ.*, vol. 100, no. 3, pp. 281–294, Feb. 2006.

[42] F. Gascon, J.-P. Gastellu-Etchegorry, M.-J. Lefevre-Fonollosa, and E. Dufrene, "Retrieval of forest biophysical variables by inverting a 3-D radiative transfer model and using high and very high resolution imagery," *Int. J. Remote Sens.*, vol. 25, no. 24, pp. 5601–5616, Dec. 2004.

[43] R. Colombo, M. Mmeroni, A. Marchesi, L. Busetto, M. Rossini, C. Giardino, and C. Panigada, "Estimation of leaf and canopy water content in poplar plantations by means of hyperspectral indices and inverse modeling," *Remote Sens. Environ.*, vol. 112, no. 4, pp. 1820–1834, Apr. 2008.

[44] Y. Zeng, M. E. Schaepman, B. Wu, J. G. P. W. Clevers, and A. K. Bregt, "Scaling-based forest structural change detection using an inverted geometric-optical model in the Three Gorges region of China," *Remote Sens. Environ.*, vol. 112, no. 12, pp. 4261–4271, 2008.

[45] S. A. Soenen, D. R. Peddle, R. J. Hall, C. A. Coburn, and F. G. Hall, "Estimating aboveground forest biomass from canopy reflectance model inversion in mountainous terrain," *Remote Sens. Environ.*, vol. 114, no. 7, pp. 1325–1337, Jul. 2010.

[46] M. González-Roglich and J. J. Swenson, "Tree cover and carbon mapping of Argentine savannas: Scaling from field to region," *Remote Sens. Environ.*, vol. 172, pp. 139–147, Jan. 2016.

[47] M. T. Gebreslasie, F. B. Ahmed, and J. a. N. van Aardt, "Predicting forest structural attributes using ancillary data and ASTER satellite data," *Int. J. Appl. Earth Obs. Geoinf.*, vol. 12, pp. S23–S26, Feb. 2010.

Curriculum vitae

Academic education

2010-2016	Ph.D. Department of Geography, Remote Sensing Laboratories, University of Zurich (Switzerland). Thesis: Remote Sensing of Alpine Forest Structural Attributes.
2001-2004	M.Sc. in Forestry, Department of Forestry and Forest Economy, University of Tehran (Iran). Thesis: *Demonstration of an applicable forest territorial organization in Northern Zagros Forests*.
1997-2001	B.Sc. in Forestry, Department of Forestry and Forest Economy, University of Tehran (Iran). Thesis: *Gorazbon Forest management plan*.

Professional experience

2005-2010	Research assistant, Agriculture and Natural Resources Research Center, Sanandaj (Iran).
2004-2005	Research assistant, GIS & Remote Sensing Lab, Department of Forestry and Forest Economy, University of Tehran (Iran).
2002-2003	Student assistant, GIS & Remote Sensing Lab, Department of Forestry and Forest Economy, University of Tehran (Iran).

Teaching and supervision

2005-2010	Lecture (Interpretation of Aerial Photograph in Forestry), Department of Forestry, University of Kurdistan (Iran).

Graduate courses and professional training

- PhD Seminar I
- PhD Seminar II
- Principles and Theories in Geography
- Retreat Seminar
- Scientific writing in the Sciences and Medicine
- Data analysis with R; R for spatial data analysis and visualization
- Project management
- Time and self management
- Voice training and presentation skills
- Understanding lectures & participating in discussion B2

- Workshops
  - 4th advanced training course in land remote sensing
  - Uncertainty in decision making in a changing climate

Peer-reviewed Journal papers

Fatehi, P., Damm, A., Schaepman, M. E., and Kneudbühler, M. (2015). Estimation of alpine forest structural variables from imaging spectrometer data. *Remote Sensing (MDPI)*. vol. 7, no. 12, pp. 16315–16338.

Fatehi, P., Damm, A., Schweiger, A., Schaepman, M. E., and Kneudbühler, M. (2015). Mapping Alpine Aboveground Biomass From Imaging Spectrometer Data : A Comparison of Two Approaches. *Journal of Selected Topics in Applied Earth Observations and Remote Sensing.* vol. 8, no. 6, pp. 3123–3139.

Ghahramany, L., **Fatehi, P**., and Ghazanfari, H. (2012). Estimation of basal area in West Oak forests of Iran using remote sensing imagery. *International Journal of Geosciences.* Vol. 3, pp. 398-403.

Shahvali Koohshor, A., Bavaghar, M., and **Fatehi, P**. (2012). Forest canopy density mapping in spare and semi dense forests using forest canopy density model (Case study: Marivan forests). *Journal of Applied RS&GIS in Natural Resources Science.* Vol. 13, no. 3, pp. 73-83.

Bavaghar, M., Ghahramani, L., and **Fatehi, P**. (2011). Evaluation of the capability of SPOT5-HRG data for predicting tree density in the northern Zagros forests. *Iranian Journal of Forest and Poplar Research.* vol. 19, no. 2, pp. 242–253.

Fatehi, P., Namiranian, M., Darvishsefat, A. A., and Fattahi, M. (2010). The study of suitable forest territorial organization in the northern Zagros forests. *Journal of Forest and Wood Products (JFWP), Iranian Journal of Natural Resources,* Vol. 62, no. 4. pp.417-428.

Azizi, S., Najafi, A., **Fatehi, P.,** and Bavaghar, M. (2010). Extraction of forest roads network map by Fuzzy theory and mathematical algorithms. *Journal of Forest and Wood Products (JFWP), Iranian Journal of Natural Resources,* Vol. 62, no. 4, pp.371-379.

Mohammadi, F., Shabanian, N., Pourhashemi, M., and **Fatehi, P.** (2010). Risk zone mapping of forest fire using GIS and AHP in a part of Pavaeh forests. *Iranian Journal of Forest and Poplar Research*, Vol. 18, no. 4, pp. 569- 586

Azizi, S., Najafi, A., **Fatehi, P.,** and Bavaghar, M. (2010). Forest Stand volume estimation using IRS_P6 imagery. *Iranian Journal of Forest and Poplar Research*, Vol. 18, no. 1, pp. 144-152.

Moradi, A., Oladi, J., Fallah, A., and **Fatehi, P**.(2009). Evaluating the capacity of IRS- LISS III & SPOT- HRG Data for identification and separation of Pollarding Forest Areas of Northern Zagros, *Iranian Journal of Forest and Poplar Research*, Vol. 17, no. 3, pp. 450-463.

Acknowledgments